PRMT5 inhibition as a strategy to induce immunogenicity in pancreatic ductal adenocarcinoma

Denise Reyna Jeldes

Reuben College

University of Oxford

A thesis submitted for the degree of

Doctor of Philosophy in Oncology

Trinity 2026

¿Qué diría la gente, recortada y vacía,
si en un día fortuito, por ultrafantasía,
me tiñera el cabello de plateado y violeta,
usara peplo griego, cambiara la peineta
por cintillo de flores: miosotis o jazmines,
cantara por las calles al compás de violines,
o dijera mis versos recorriendo las plazas,
libertado mi gusto de vulgares mordazas?

¿Irían a mirarme cubriendo las aceras?
¿Me quemarían como quemaron hechiceras?
¿Campanas tocarían para llamar a misa?

En verdad que pensarlo me da un poco de risa.

(Alfonsina Storni, El Dulce Daño, 1918)

Acknowledgements

The following work would not have been possible without the guidance of Professor Nicholas La Thangue. This academic experience was undoubtedly a turbulent flow of personal challenges thanks to his insight. I also extend my deepest gratitude to Professor Pawel Swietach, for his kind will to collaborate and help me through all the sections of my thesis related with pH dynamics. I also thank Dr Alzbeta Hulikova for helping me with all the technical aspects of pH imaging during the last stage of this work.

A big 'thank you' goes to Dr Wojciech Barczak, for all his advice in the initial parts of my research, and for supporting my irrational ideas when nobody did. However, these initial thoughts would never have flourished without the knowledge and constant support of Dr Wiktoria Blaszczak. Thank you, Wiktoria, for all your help, good conversations, podcast suggestions, teachings, and thorough corrections. In the latter subject, I would also like to thank Dr Garret Rochford, whose writing suggestions and perspectives were always valuable for this work. I wish you the best in this lovely new chapter of your family life, Garret! My deepest gratitude also goes to Dr Laurel Bate-Eya, Dr Simon Carr, and Dr Geng Liu. Your help throughout these years has been key to my learning process.

The journey inside this house of trees and its branches was a tough experience in many aspects. However, if there was an instant when I really found a path in the wind, that was the time that I shared with Chuyue Zhang. Dear *Par de Patos* (I know the nickname doesn't apply anymore, but I like it, it has... history), thanks for our chats, for always being available to share a couple of random thoughts. All for the sake of joyful exploration. For the reckless sake of imagining possibilities, of escaping paradigms for a while. You were the very first friend who listened to my dreams of cotton smiles, cherry blossoms, and blue skies. Thanks for your friendship. I can't wait to hear your new stories.

Despite the challenges of this trip, Oxford has also given me beautiful memories and experiences beyond the realm of Science. If I've ever came close to

the concept of chosen family, Oxford was the place where I found it. But that's not entirely true. It was the other way around. Someone found me. After a very insightful workshop, Sasha gave the initial spark to a lovely friendship that gave me the opportunity to open up and meet a group of phenomenal humans with whom I've been able to achieve things more relevant for my life than any line in a CV. Thanks, dear Sasha, for our meaningful conversations, for your guitar strumming, your intricate jokes that I get two months later, and for being the perfect representation of the poster you gifted me: "Give me your hand. Tell me your name." As I promised, I'll hang it proudly in any future office that I have, not just because I agree with those ideals, but because I had the wonderful opportunity to meet a nice friend who applied those principles with a sister in need.

I can't continue without thanking you, Katharine, for all your help and support. Your drawings and words have been the seed of hope in moments of absolute despair. When I thought that my flame couldn't provide any warmth, it was your company and kindness the reason to keep up believing and fighting for better things. Maybe not for us, but for the ones to come. Thanks for making me part of some of your activities and passions. Now I can't see a concert of choral music without thinking about you. Thanks for all what you taught me about life, about hope, about myself by just being the exceptional person you are. Hope that knitted jumper of yours protects you from all kinds of winter. It contains the love of a mother and a friend in every thread. Thanks to you, I can proudly say that the best *brazo de reina* I've ever tasted was made in Britain, with *manjar* of remarkable quality and ineffable amounts of love. Someday, if you and Sasha decide to do a trip to that faraway place that I call home, be absolutely sure that I would love to have you as my guests and guide you through some of the landscapes that you have drawn for me.

Dear Jon, oh mighty Xir Joncelot! The best hugger in all Britain and an amazing friend. Please keep working in your writing! Your letters are full of beauty and skilful wordplay. They are a kind invitation to the landscapes of your inner world. Lately I've been taking your hope pills practically twice a day, and I've found many flowers, many reasons to keep the inspiration going. Thank you so much for your

wise prescription. Oh, and thanks for your clever humour! One day I'll try to surpass it... I can't lie to you about my chances, but... I have your sympathies, right? ;).

To the rest of my lovely queer family: thanks Rachel, for our instants of literature, philosophy, humour, and professional soul care; you are someone who I really enjoy listening, like Ravel in the form of dialogue. Thanks, Cesca, for your beautiful writing and passionate ideas; hope your travels bring you someday to Chile, I'd love to share a good glass with you and have one of those irate and loud talks that we both enjoy so much. Thank you, Kate, for your delicate but significant expressions of care; I really hope we can share more occasions to do music together! My gratitude to you Jak for being always so open to listen to my crazy ramblings; for being so supportive with my artistic being and guiding me to different artistic platforms so I could show a snippet of the ideas behind this colourful bouquet of contradictions called Denise. I don't have the magical, culinary, and performative talents that you have, dear Sofía, but I can definitely conjure all my gratitude to you, for your efforts binding our Community in the shape of cupcakes, movie nights, Chappell Roan and protest chants in the name of fairness and what needs to be done. Thank you, Rosemary, for your kindness, wisdom and lovely anecdotes; the lovely beauty of your drawings has taught me how to be more aware and grateful of those little sparks of grace in our daily lives. Thank you, Kim, for your listening ear, your tender expressions of care, and your empathy as a colleague in cellular and molecular biology. My biggest gratitude to you, Karin, for our musical gatherings, for introducing me to Matthew Halsall, for our meaningful conversations; thanks for sharing with me your passion for Music, writing, and reflection; the things that I learned from you are the essence of why I'm (surprisingly) alive. Lastly, my thanks to Alba, Ziggy, the Kidlington Tiger, and The Boy. A human life would never learn how to flow without the wisdom and swag of our furry friends.

A kiss to my harbour in the storm, to that space of love and support called Oxford Proud Voices. Since the moment I joined, when the Choir was just a rainbow cotyledon, the feelings of being part of a beautiful and joyful community never faded. As my lovely friend Katharine taught me, you never skip Choir rehearsals, because singing with all of you is a soothing breeze, a reminder that any tonic for the

soul contains a little bit of music as top note. My gratitude goes to all the lovely humans who helped me rediscover my love for Music, but specially to Debbie, Ben, Hannah, Charlotte, Matt, Ross, Cookie, June, Ella, Rowena, Vera, Luis, Rafael and Sara. Thanks for your kindness. All of you are the loving proof of the saying *quien canta sus males espanta*.

Y bueno, querides angloparlantes, comienza ahora el segmento en español. Sabrán perdonar, pero este instante son escamas arcoíris en la cintura de un mar de brea, extractos de Fantasía en Mi bemol Mayor. Este instante sabe al mote con huesillos que nunca preparé y a la botella de pisco que me robaron. Tintura de *chuchás* que quise blandir y nunca lancé. Este documento será trompeta en el Club Silencio tras un estridente "¡No hay banda!". *Senza sordino*, sin embargo, porque si Serrat ilustró que el amor puede surgir hasta del cartón piedra, imbuiré vida a la palabra para agradecer a todas las hermosas personas que estuvieron junto a mí en estos cuatro años de soledad pendular. Ese distante solaz ante una ausencia que se sintió como cuando descubrí que la joya del Gabito quedó abandonada en lo alto de un mueble, destinada al polvo y la indiferencia, al mismo olvido que asoló a los habitantes de Macondo. Frente a esa situación, habló la Violeta: "No tuve nada. Lo di todo. Quise dar, no encontré quien recibiera". Sin embargo, con ustedes y mis verdaderas amistades en Reino Unido, logré mantener la esperanza para seguir dando el corazón y no sucumbir a la ponzoña del cinismo.

Un horizonte al medio es patológicamente fome, y al igual que don Ata, no engraso los ejes porque el sonido soy yo. No me gusta el sendero donde no crece el pasto. Mi martillo seguirá en la mano, un clavo a la vez. Si la perfección nos come las patas, transformando todo lo humano en procedimiento, moriré hecha nitrocelulosa, papel de revista, bakelita. Esta es la forma de inclinarme en gratitud a la Filosofía y así sentirme un poco más digna del grado a adquirir.

Infinito amor a mi madre, Betty Jeldes Pizarro -la *Soa Betty*- y a mi padre, Ernesto Reyna Huerta. Les agradezco juntitos porque no quiero que compitan sobre a quién quiero más. Siempre he dicho que yo no soy más que ustedes con defectos añadidos, que mi vida no ha sido más que un intento por honrar su sacrificio y su lucha constante, porque si hay algo que me conmueve en esta vida es pensar en su

entrega, en la visión de su proyecto de familia, en una semilla que hoy es árbol, esa que ha aguantado literales y metafóricos terremotos para estar donde está. ¡Y vaya hermosos frutos que ha dado! ¡Mírenla a una! (*Eeeeeella)*. Si tanto aquí como en Chile he firmado con mis dos apellidos, llegando al punto de unirlos con un guion para que no los omitan o crean que Reyna es mi segundo nombre, es porque no me gusta olvidar mis raíces. Porque la humilde pero amorosa casita de Blanco Viel, *La Banda del Cabe'* y aquella horrible foto de la fiesta de Navidad de Cambiasso donde todos salimos hilarantemente mal siguen en mi corazón. No importa cuánto cosmético y cuánta seda me eche encima, esta mona como mona se queda. Sin embargo, soy una mona orgullosa. Orgullosa de las enseñanzas vuestras, de su amor constante e incondicional. Gracias, de verdad. Por todo. Por absolutamente todo. Los amo a ustedes y a nuestra familia en su imperfecta humanidad. Por ustedes soy Denise.

Gracias infinitas, Mariola, Niko e Izan. Querides que supieron de mi alita rota mucho antes que yo misma, que aceptaron a esta loca sin rechistar y le dieron el amor que sólo puede venir cuando Comunidad y familia se unen. Gracias a ustedes, hoy camino sin avergonzarme de mis colores, pues antes siquiera de haber vuelto al hogar, ya estuvieron ustedes preparando el nido al cual volvería. Agradecida estaré siempre de ustedes, de que siempre me contacten y pregunten cómo estoy, y por saber que siempre podré contar con su apoyo. Sea lo que sea. En el pan y la cebolla. Saben que este sentir es absolutamente recíproco, que estoy con ustedes para lo que haga falta, que les apoyaré en su andar, aunque sea desde la lejanía.

Sigo contigo, Yeyita, porque es imposible enumerar todo lo que has significado para mí en esta vida. Como amigos, matrimonio y mejores amigas para toda la vida, siempre has sido complicidad en los ratos de humor y consejo en mis momentos de incertidumbre. Gracias a ti, vivo en la satisfacción de saber que juntas plantamos un árbol y desafiamos la tempestad y las cejas arqueadas del mundo para demostrarnos una forma de amor que trasciende lógicas. Porque este cariño no es caldo de entendimiento, sino la resonancia de trinos que supieron hallarse en vuelo, almas que se abrazaron en la honestidad de las heridas.

Agradezco que me permitas seguir siendo parte de tu vida y que me hayas visto en diáfana claridad mucho antes de que yo lo hiciese, de que seas la espiga de lavanda de la que germinó mi vida. Para una existencia tan acaecida como la mía, el que nos hallamos encontrado y amparado es prueba de que, a veces, soy increíblemente afortunada. Infinitas gracias por desafiar los cánones del amor y la amistad, por haber aguantado el ser la villana cuando la gente no entendía tu infinita bondad. Tal nivel de amorosa entrega sólo la puedo comparar con mi madre. Tengo muchas ganas de saber qué nos deparará la vida. Sea lo que sea, sabes que estaré allí para ti, para una risa, un momento de descompresión o una palabra de aliento (de las de verdad eso sí, no las del Mentira Martínez).

Querida Caroline, las palabras se intimidan cuando se trata de hablar de ti. Trémulas tratan de describir la inmensidad de todo lo que hemos vivido en conjunto. Se hacen chiquititas tratando de expresar toda mi gratitud hacia tu visión. Como bordada por Gabriela misma, me bridaste tu cariñoso apoyo desde muy temprana edad en mi desarrollo profesional, siendo maestra, consejera, jefa, colega, madre y amiga. Tal como Carlos, mi padre adoptivo, en su admirable y taciturna rebeldía, han amparado mi corazón de tal forma que me es imposible separar la Ciencia de nuestra naturaleza. Con ustedes aprendí que un número sin poesía es mera tecnocracia, belleza sin gracia, pétrea sintonía. Gracias por tanto amor y sabiduría.

Besitos miles para mi hermosa familia nuclear y extendida. Para ti Nadia, Ernesto, Italy, Ayelen, Daniel, Aylin, Thais, Nahuel, abuelita Silvia, señora Ceci y don Toño, señora Mona, Alejandra, Antonia, Danilu, Jerusa, Diego, Rubencito y Teté. No saben cuánto los amo. Muchas veces me he dejado comer por la rutina y no he podido ser tan constante con mis gestos de cariño hacia ustedes, pero como dice la canción, ustedes son más verdad que el pan y la tierra. Lo que disfruto de la vida es porque lo celebro y comparto con ustedes, porque ustedes me recuerdan quien soy mejor que nadie, porque son la luz amiga en los instantes en que no me encuentro ni en el reflejo. Gracias infinitas por el apoyo, por las risas, por existir.

Agradezco a la gente de mi país que, a través de la Agencia Nacional de Investigación y Desarrollo y el programa Becas Chile, me permitió vivir esta

experiencia de agraz dulce, dulce agraz y agraz agraz. Vuelvo hermosa y vuelvo tierna, vuelvo para sembrar, para que otres sueñen más allá de lo que puedo vislumbrar, para que otres sean mejores que yo, para que el celeste no le cueste tanto a los mismos de siempre. Me gusta el circo de Chamorro. Extraño el atar con alambres, las pequeñas victorias que se tienen desde lo que Galeano llamó la mesa de los perdedores. No es romanticismo. Es compasión (gracias a Simone Weil por tan hermoso concepto). Es mi genuino amor por lo falible, terrenal e imperfecto de mi ser y mi gente. La misma que se levanta tras el desastre natural de cada año. La misma que manda el tieso labio superior a la cresta y vive con intensidad. La misma que ríe y llora en absoluto desparpajo. La misma que, por el simple hecho de creer en la justicia social, permitió que pudiese nacer, acceder a una educación que jamás habríamos podido pagar, vivir de acuerdo con mi identidad de género, y finalmente, tener esta experiencia que jamás hubiera podido soñar. Tras este inmenso regalo, mi retribución no es reglamento, sino respiración. Es la forma de decir gracias a Chile por la única cerilla que me dio para hacer esta fogata. Hoy deseo que mi llama sea hogar en otras casas. Sí. Vuelvo hermosa y vuelvo tierna. Vuelvo para dejar de perseguir la gloria y empezar a invitarla a tomar desayunito, porque quiero seguir aprendiendo, pero de otra forma. Con fruta, pan y café, como mi gente lo sabe escribir, cantar y hacer.

Termino contigo, paciente persona que leyó estas palabras. Si fuiste capaz de leer todo esto, realmente lo agradezco. El sereno gesto de querer conocer un poco a la persona detrás de todo lo que sigue es de un respeto inenarrable. Una joya extraña entre tanto plazo vencido. Gracias por ello, y perdón si me pierdo en las secciones venideras. Esa prosa es nada más que mi final de la Quinta de Shostakovich. Te deseo lo mejor y que en la menguante naturaleza estas páginas puedas encontrar algo útil para tus futuros viajes.

Abstract

Pancreatic ductal adenocarcinoma (PDAC) is a disease with high mortality rates where conventional chemotherapeutics have shown limited efficacy. Mutation of key driver genes and the presence of a highly acidic tumour microenvironment generate a permanent state of low antigenicity and sustained immunosuppression that is at the core of PDAC therapeutic failure. Here is shown that PRMT5 inhibition is a promising pharmacological approach to enhance PDAC immunogenicity and improve its microenvironmental conditions. Results reveal that PDAC cells under PRMT5 inhibition are capable to slightly activate T and NK cells in tumour sites and induce the expression and translation of immunogenic lncRNA-derived peptides that are capable to reduce tumour growth *in vivo*. PRMT5 inhibition also alters pH dynamics in a bicarbonate-dependent fashion by promoting the skipping of exon 25 of the sodium/bicarbonate co-transporter SLC4A7. These findings highlight the potential of PRMT5 inhibition as a dual immunosensitizing strategy for PDAC treatment, which can provide a platform for future studies involving combinatorial treatments or deeper mechanistic understanding.

Statement of authorship

The work shown in this thesis was performed by the author, except for the following cases explicitly stated in this document that include:

- Library preparation and RNA sequencing were outsourced to Genewiz (Azenta Life Sciences, Leipzig, Germany)
- MATLAB codes used for data and image analysis were written by Professor Pawel Swietach (Department of Physiology, Anatomy and Genetics, University of Oxford)
- Animal experiments to evaluate the effects of PRMT5 inhibition were outsourced to Charles River Laboratories (Freiburg, Germany)
- Manufacturing of the ChAdOx1-PepLncP2 vaccine was outsourced to the Viral Vector Core Facility (Pandemic Sciences Institute, University of Oxford)
- Cryosection and mounting of tumour samples stained with FITC-pHLIP were outsourced to the Histology Facility (Department of Physiology, Anatomy and Genetics, University of Oxford)
- Whole-slide scanning was outsourced to the Translational Histopathology Lab (Department of Oncology, University of Oxford)

In addition, the *in vivo* experiments detailed in Chapter 5, Sections 5.2.1 and 5.2.3, were performed entirely by Dr. Wiktoria Blaszczak.

Table of contents

List of figures

List of tables

List of abbreviations:

|log2FC|: Absolute value of the base-2 logarithm of fold change

2'-OMePS: 2'-O-methyl-modified ribose with phosphorothioate backbone

A3SS: Alternative 3' splice site

A5SS: Alternative 5' splice site

AS: Alternative splicing

ASO: Antisense oligonucleotide

BAM: Binary alignment map

BP: Biological processes

CA19-9: Cancer antigen 19-9

CAF: Cancer-associated fibroblast

CAR-T: Chimeric antigen receptor T cell

Cas9: Empty pSpCas9(BB)-2A-Puro (PX459) V2.0 backbone transfection control

CDKN2A: Cyclin dependent kinase inhibitor 2A

ChIP: Chromatin immunoprecipitation

ChIPseq: Chromatin immunoprecipitation sequencing

CHX: Cycloheximide

CisP: Cisplatin

CRC: Colorectal cancer

CTLA4: Cytotoxic T-lymphocyte-associated protein 4

CTO: Cell Tracker Orange

DAB: Diaminobenzidine

DBD: DNA binding-domain

DC: Dendritic cells

DE: Differentially expressed

DEG: Differentially expressed genes

Dox: Doxorubicin

DP: Dimerization partner

E2F1Cr: E2F1 CRISPR knockout

ECM: Extracellular matrix

EGFR: Epidermal growth factor receptor

FBS: Foetal bovine serum

FDR: False discovery rate

FFPE: Formalin-fixed paraffin-embedded

FITC-pHLIP: FITC-conjugated pH-low insertion peptide

FOLFIRINOX: Folinic acid, 5-fluorouracil, irinotecan and oxaliplatin

GM-CSF: Granulocyte-macrophage colony stimulating factor

GO: Gene ontology

GZMB: Granzyme B

HLA: Human leukocyte antigen

HPTS: 8-Hydroxypyrene-1,3,6-trisulfonic acid

IC_{50}: Median inhibitory concentration

IFNγ: Interferon γ

KRAS: Kirsten rat sarcoma viral oncogene homologue

MCT: Monocarboxylate transporter

MDSC: Myeloid-derived suppressor cell

MFI: Mean fluorescent intensity

MHC-I: Major histocompatibility complex class I

MTA: 2-methylthioadenosine

MTAP: Methylthioadenosine phosphorylase

MXE: Mutually exclusive exons

NALIRIFOX: Folinic acid, liposomal irinotecan, 5-fluorouracil and oxaliplatin

NBCn1 / SLC4A7: Electroneutral sodium bicarbonate cotransporter 1

NK: Natural killer

NVB: Non-volatile buffering

OCT: Optimal cutting temperature

ORF: Open reading frame

OXPHOS: Oxidative phosphorylation

P/S: Penicillin/Streptomycin

PanIN: Pancreatic intraepithelial neoplasia

PARP: Poly (ADP-ribose) polymerase

PBS-T: PBS + 0.1% v/v Tween 20

PDAC: Pancreatic ductal adenocarcinoma

PD-L1: Programmed death-ligand 1

PHA: Phytohemagglutinin-L

pH_e: Extracellular pH

pH_i: Intracellular pH

PI: Propidium iodide

PRMT5: Protein arginine methyltransferase 5

PSC: Pancreatic stellate cell

PSI: Proportion spliced-in

RBD: Randomized blocks design

RI: Retained intron

Ribo-seq: Ribosome sequencing

RNAseq: RNA sequencing

RNY1: Non-coding Y RNA 1

RuBPY: Tris(2,2'-bipyridyl)dichlororuthenium(II)

SAM: S-adenosylmethionine

SDMe: Symmetric dimethylation

sDMEM: Supplemented DMEM

SE: Skipped exon

sgRNA: Single guide RNA

SLC: Solute carrier

TAM: Tumour-associated macrophage

TCR: T cell receptor

TGF-β: Transforming growth factor β

TME: Tumour microenvironment

TPM: Transcripts per million

WT: Wild type

Δ25 ASO: SLC4A7 exon 25-skipping ASO

λ_{em}: Emission wavelength

λ_{ex}: Excitation wavelength

Chapter 1 : Introduction

1.1. Pancreatic ductal adenocarcinoma: characteristics and therapeutic challenges

1.1.1. Epidemiology and clinical aspects

Pancreatic cancer is a global concern in human health that despite having the twelfth highest incidence among all cancers worldwide (510,992 new cases/year) (Bray et al., 2024), it is associated with a concerning global death rate of 467,409 deaths/year (Bray et al., 2024). This makes pancreatic cancer the eighth cause of cancer-related deaths worldwide (Bray et al., 2024; Hayat et al., 2025) and the third in Europe and the United States (Ilic and Ilic, 2022; Siegel et al., 2019).

Among all types of pancreatic cancer, pancreatic ductal adenocarcinoma (PDAC), affecting the exocrine portion of this organ, is the most common case of pancreatic malignancies (≈90%) (Halbrook et al., 2023; Orth et al., 2019; Rozengurt and Eibl, 2026; Sarantis et al., 2020). Other less frequent types of pancreatic cancer are neuroendocrine tumours, like insulinomas, glucagonomas and gastrinomas, which arise from islet cells and represent less than 2% of all pancreatic cancer cases (Sonbol et al., 2022); acinar carcinoma, affecting the homonymous cells and accounting 0.2-4.3% of all cases (Ikezawa et al., 2024); and pancreatoblastoma, a rare condition in adults but more frequent in children (<1% and 25% of pancreatic cancer cases, respectively) that affects the pancreatic exocrine epithelia (Sheng et al., 2022; Yuan et al., 2024).

Modifiable risk factors of PDAC include alcohol consumption, smoking, obesity and exposure to metalworking byproducts, pesticides, polychlorinated biphenyls and particulate air pollutants (Bogumil et al., 2021; Michalak and Małecka-Wojciesko, 2023; Rawla et al., 2019; Ushio et al., 2021). In the case of genetic-based comorbidities, patients with hereditary breast and ovarian cancer syndrome (associated with pathogenic variants in BRCA1 and BRCA2 genes), Lynch syndrome (in the particular cases of loss-of-functions mutations in MLH1, MSH2, MSH6 and EPCAM) and familial atypical multiple mole melanoma syndrome (linked to a deregulated function of CDKN2A) are associated with increased PDAC risk (Jacobs and Stoffel, 2024; Peduzzi et al., 2025; Rawla et al., 2019). Despite this landscape, PDAC is characterized by a largely unspecific (*e.g.* weight loss, fatigue, nausea and vomiting, jaundice, epigastric pain, anorexia and back pain) or totally absent symptomatology that poses a challenge to differential diagnosis (Hayat et al., 2025; Sarantis et al., 2020; Takikawa et al., 2022).

Regarding PDAC diagnostics, computed tomography scanning appears as the preferred imaging technique, followed by magnetic resonance imaging and endoscopic ultrasound, because of its wide availability, suitable sensitivity (89-97%) and its relevance in PDAC staging and treatment response evaluation (Bilreiro et al., 2024; Miller et al., 2023). Despite their performance, the use of these methods normally occurs at advanced stages of PDAC development, when symptoms are more apparent to the patient and clinicians. This situation stimulates the search for novel biomarkers that could be used for PDAC screening.

However, many of the efforts focused on finding specific biomarkers for early-stage detection of PDAC, like the assessment of cancer antigen 19-9 (CA19-9) and glypican-1, have failed in terms of achieving suitable sensitivity and specificity to be used in routine analysis (Chen et al., 2025; Force, 2019). Despite this situation, initiatives to improve PDAC diagnostics are still ongoing. Some examples of this are the implementation of natural language processing algorithms to analyse patient's health records for early detection (Chen et al., 2025), the identification and validation of a panel of circular RNAs associated with PDAC onset (Xu et al., 2024), and the use of microRNA-196 and microRNA-423 as biomarkers to be integrated with CA19-9 assessment to increase its sensitivity and specificity detecting PDAC, and discriminate between this malignancy and chronic pancreatitis (Škrha et al., 2025).

The unspecific nature of PDAC symptomatology, along with a lack of reliable biomarkers, severely limits early-stage diagnosis. Because of this, the majority of PDAC cases (≈ 80%) are identified when tumours have reached its metastatic phase, when 5-year overall survival rates are lower than 14% and therapeutic efficacy is limited (Blackford et al., 2024; Hayat et al., 2025; Takikawa et al., 2022). Given this adverse landscape of late-stage diagnosis and poor prognosis, many studies have focused to understand the cellular and molecular basis of PDAC as away to draw new perspectives in diagnostics and therapeutics.

1.1.2. Characteristics of PDAC at cellular level

In terms of its cellular origin, PDAC cells arise from the cells located in the exocrine pancreas, namely ductal and acinar cells, which function involves the secretion of bicarbonate ions and digestive enzymes and their transport into the duodenum, a significant part of the postprandial response within the gastrointestinal tract (Hu et al., 2025; Pian et al., 2025).

In PDAC progression, different stages of cellular or inflammatory damage, known as pancreatic intraepithelial neoplasia (PanIN), can develop from an early reversible pathophysiological event called acinar-to-ductal metaplasia, where acinar cells lose their physiological functions and differentiate to ductal-like cells (Hendi et al., 2025; Marstrand-Daucé et al., 2023). Depending on the level of atrophy and changes in the architecture, and the nuclear integrity of these cells, PanINs are classified intro three categories ranging from papillary lesions with columnar epithelia and basal nuclei (PanIN 1) to cellular swelling and nuclear dysplasia (PanIN 2) and severe intraluminal outgrowth and loss of nuclear polarity (PanIN 3) (Musiu et al., 2024; Park et al., 2021; Pian et al., 2025).

The acquisition and progression of these lesions is largely based on the mutational background of the affected cells, which lead to PDAC development and the establishment of a tumour microenvironment (TME) that sustains tumour survival, immune evasion and resistance to treatment (Cao et al., 2021; Musiu et al., 2024). Both factors, the mutational burden of PDAC cells and the characteristics of its TME will be discussed in the following sections.

1.1.2.1. Mutational landscape

The onset of PDAC tumorigenesis is associated with a complex network of different genomic alterations affecting PanINs. From these somatic mutations, Kirsten rat sarcoma viral oncogene homologue (KRAS), TP53, SMAD4 and cyclin dependent kinase inhibitor 2A (CDKN2A) are considered to be the key targets of oncogenic events that lead to PDAC development and progression (Cao et al., 2021; Sivapalan et al., 2022).

KRAS gain-of-function mutations are the most present in PDAC, occurring in about 90% of cases (Scarlato et al., 2025). Some of the identified oncogenic mutations and their respective frequencies in PDAC are: KRAS G12D (39.9%), G12V (28.6%), G12R (14.6%), Q61H (4.2%) and G12C (1.7%) (Pant et al., 2025). These mutations are associated with conformational changes in the GTP-binding site of KRAS, which leads to a reduced interaction of this GTPase with RAS GTPase-activating proteins and a subsequent reduction of GTP hydrolysis rate that results in KRAS mutants being in a continuous GTP-bound conformation (Drizyte-Miller et al., 2025b; Moghadamchargari et al., 2019; Zhang et al., 2023b). This state is capable to activate downstream signalling pathways such as PI3K/AKT/mTOR, RAF/MEK/ERK, RALGDS and PLC, or downregulate tumour-suppressor mediators like SIRT3, which are largely associated with cell survival, metabolism, proliferation and differentiation (Mai et al., 2026; Uniyal et al., 2025; Zhang et al., 2023b). In terms of clinical outcomes, reports state that patients with KRAS G12D, Q61H and G12V mutants have worse prognosis in terms of overall survival when compared to patients carrying KRAS G12R mutations (Norton et al., 2025; Yousef et al., 2024).

The tumour suppressor gene TP53, and some of its hyperactive variants, like p53[53,54], have been associated with dampening of KRAS signalling and restricting of acinar-to-ductal metaplasia in PanINs (Mello et al., 2023). However, 50–90% of PDAC cases have a type of TP53 mutation. These could be cases of loss-of-function mutations, which compromise the DNA binding-domain (DBD) of p53, whether by reducing its capacity to bind to its canonical motifs or inducing structural changes (Mahat et al., 2025; Stefanoudakis et al., 2024). TP53 mutations are also associated with oncogenic gain-of-function activities, which are mostly associated with transcription modulation by interfering with different protein-protein interactions, including transcription factors (Maddalena et al., 2021; Mahat et al., 2025). From all of these cases, the gain-of-function mutation TP53 R175H (being R172H its equivalent in mice) is one of the most studied mutations, and its presence altogether with KRAS G12D on *in vivo* human pancreatic cancer models has been associated with escape from cell cycle arrest and metastasis progression (Morton et al., 2010). Another report using *in vitro* and *in vivo* models of PDAC indicates that TP53 R172H promoted PDAC tumour growth and, at the same time, contributed to generate an immunosuppressive TME by reducing the infiltration of CD4 and CD8 cells, promoting the recruitment of anti-inflammatory myeloid-derived suppressor cells (MDSCs) while inducing the expression of immunosuppressive cytokine CXCL1 (Mahat et al., 2025).

Occurring in 50-55% of patients, and frequently found in PanIN 2 and PanIN 3 lesions, SMAD4 missense mutations include non-functional variants (*e.g.* A406T, K428T and R515T), which impair the activity of this protein as a transcription factor, and structural alterations (*e.g.* P130S and A351H) that promote its phosphorylation

by GSK3 and subsequent proteasomal degradation (Yao et al., 2024). In a physiological context, SMAD4 is a relevant tumour suppressor that regulates cell cycle by inducing G1-phase arrest via activation of p21 and p15, and participates as a transcription factor in transforming growth factor β (TGF-β) signalling, which can have anti- or pro-tumour effects depending on context (Tsanov et al., 2025; Yao et al., 2024).

In PDAC, SMAD4 inactivation is normally associated with tumour progression, metastasis and the establishment of an immunosuppressive TME by reducing T cell infiltration and interferon γ (IFNγ) release (Murimwa et al., 2025; Principe et al., 2022). However, the aforementioned effects of SMAD4 inactivation are mostly applicable to primary tumours, because recent studies using genetically engineered mouse models have shown that SMAD4 mutations have different roles in the viability of metastatic sites by showing that SMAD4 inactivation exacerbates pro-tumoral signalling in liver metastases, but induced the opposite effect in lung metastases (Tsanov et al., 2025).

CDKN2A is a tumour suppressor gene that encodes the proteins $p16^{INK4a}$ and $p14^{ARF}$ proteins, which are normally linked to CDK4/6 inhibition leading to G1 cell cycle arrest and MDM2 inhibition that results in p53 induction (Kimura et al., 2021). In cancer, high CDKN2A expression levels are associated with higher infiltration and activation of CD4, CD8 and natural killer (NK) cells (Chen et al., 2021b). In the case of pancreatic cancer, CDKN2A inactivation is present in PanIN 1 and PanIN 2 lesions and 75-95% of PDAC cases and its caused by homozygous deletions or promoter region hypermethylation (Hayashi et al., 2021; Stefanoudakis et al., 2024), which,

altogether with KRAS and TP53 mutations, stimulate cell cycle progression, tumour growth, angiogenesis and metabolism (Wu et al., 2020a). Deletion of CDK2A occurs with the loss of methylthioadenosine phosphorylase (MTAP) in 30.2% pancreatic adenocarcinomas and it has been associated with poor prognosis (Kryukov et al., 2016; Lyu et al., 2026).

Altogether, the mutations detailed in this section are a core element of PDAC survival and progression. However, microenvironmental conditions also need to be considered to understand the cellular conditions that lead to poor prognosis and therapeutic failure in PDAC.

1.1.2.2. Tumour microenvironment

Aside from the mutational burden found in PDAC cells, another essential component in PDAC pathogenesis is its TME. PDAC TME emerges from the complex interaction between its cellular (*e.g.* cancer cells, pancreatic stellate cells -PSCs-, cancer-associated fibroblasts -CAFs- and immune cells) and non-cellular (*e.g.* growth factors, cytokines and extracellular matrix -ECM- components) elements (Kane et al., 2020). This microenvironment is characterized by a dense desmoplastic stroma with intense immunosuppression and elevated acidosis, which create favourable conditions for PDAC progression and resistance to treatment and immune recognition (Byeon et al., 2023; Kane et al., 2020).

PDAC dense ECM is generated by the activation of CAFs and PSCs induced by tumour cells, which results in production of high levels of collagen, fibronectin, laminin, hyaluronic acid and other proteoglycans and polysaccharides (Glapiński

et al., 2025). This process, known as desmoplasia, not only increases ECM rigidity and generates a barrier around tumour cells, protecting them from immune recognition and therapeutic agents, but also collapses blood vessels, which has an impact on oxygen distribution, thus promoting metabolic reprogramming in PDAC cells (Henke et al., 2019; Ho et al., 2020). However, ECM density is a dynamic process, with CAFs and PSCs being also capable to remodel the ECM by synthetizing the proteolytic matrix metalloproteinases 2, 3, 9 and 13, which not only are essential for tumour metastasis and invasion, but also induce shifts in the metabolic profile of PDAC cells by providing alternative substrates derived from ECM degradation, like hyaluronic acid (which is processed through the hexosamine biosynthetic pathway) and proline derived from collagen (used as a tricarboxylic acid cycle substrate) (Efthymiou et al., 2025; Glapiński et al., 2025; Ho et al., 2020).

Another feature of PDAC TME is its marked immunosuppression, which is characterized by disrupted antigen presentation by PDAC cells, the presence of immunosuppressive chemokines (*e.g.* CXCL12) and cytokines (*e.g.* IL-1, IL-10, IL-12, TGF-β and TNF-α) (Karamitopoulou, 2019), and increased surface expression of proteins associated with immune cell inactivation (*e.g.* programmed death-ligand 1 -PD-L1- and cytotoxic T-lymphocyte-associated protein 4 -CTLA4-) (Sherman and Beatty, 2023). PDAC TME impairs the activity of cytotoxic T cells and NK cells, and restrict the infiltration of dendritic cells (DCs) while promoting the activity of pro-inflammatory neutrophils and macrophages, regulatory T cells and MDSCs (Bräutigam et al., 2025; Karamitopoulou, 2019; Sherman and Beatty, 2023).

Both ECM remodelling and immunosuppression are favoured by an acidic TME generated by an unrestricted PDAC cell proliferation, impaired perfusion and increased metabolic acid production (Rolver et al., 2025). Regarding the latter, metabolic reprogramming in PDAC cells is a dynamic process that is influenced by key gene mutations (such as KRAS G12D and TP53 R273H) and substrate exposure, that allow PDAC cells adaptive shifts between glycolysis, oxidative phosphorylation (OXPHOS), fatty acid β-oxidation and amino acids metabolism (Boedtkjer and Pedersen, 2020; Gong et al., 2023; Rolver et al., 2025; Stigliani et al., 2024). This flexibility explains the metabolic heterogeneity observed within PDAC tumours, where is possible to find near-neutral pH aeras (pH ≈ 7.0), more reliant in OXPHOS, adjacent to highly glycolytic areas ($5.6 \leq pH < 7.0$), where H^+ and lactate extrusion is enhanced (Boedtkjer and Pedersen, 2020; Chianese et al., 2026; Swietach et al., 2023; Xu et al., 2022).

Key to this metabolic adaptability is the capacity of PDAC cells to alter pH dynamics, a process that is achieved by modifying the expression and activity of different acid/base or metabolite transporters, such as HCO_3^- importers (*e.g.* SLC4A4 and SLC4A7), H^+ extruders (*e.g.* NHE1) and H^+/lactate transporters (*e.g.* MCT1 and MCT4) (Blaszczak et al., 2022; Czaplinska et al., 2023; Hosonuma and Yoshimura, 2023; Kay and Zanivan, 2023; Sniegowski et al., 2023). The activity of these transporters is summarised in Figure 1.1.

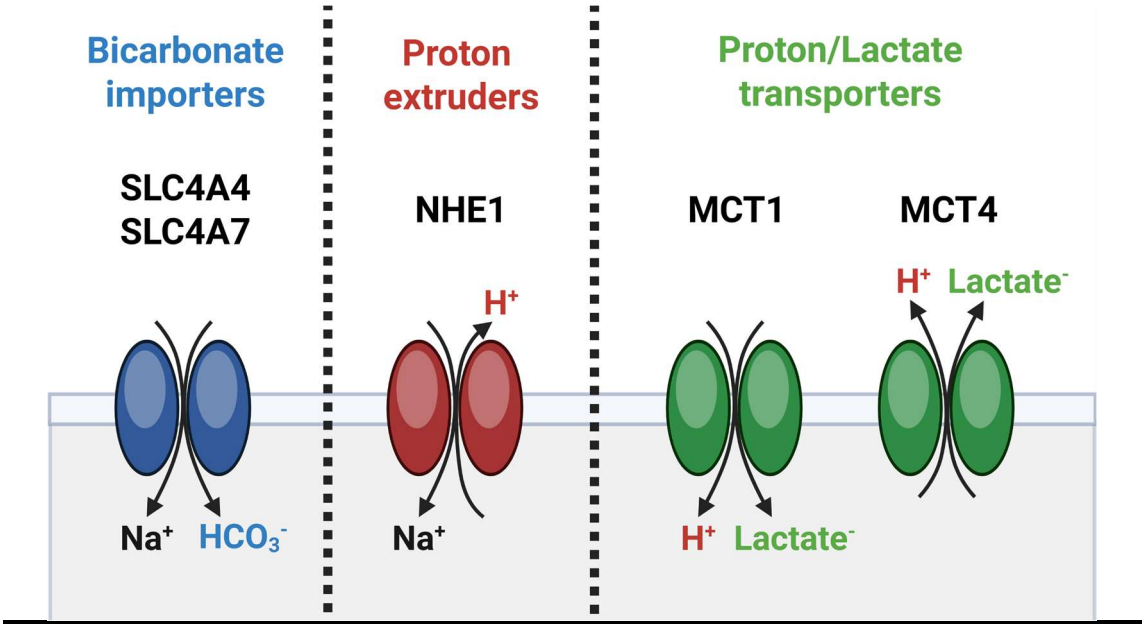

Figure 1.1. Relevant transporters in PDAC metabolic adaptation.
Examples of bicarbonate, proton and metabolite exchangers that PDAC cells use to alter pH dynamics to promote their survival . Figure created in https://BioRender.com.

PDAC cells can induce these alterations to increase intracellular pH (pH_i), enhance the activity of glycolytic enzymes like hexokinase, phosphofructokinase and lactate dehydrogenase (Cappellesso et al., 2022), thus increasing their glycolytic rate and H^+/lactate extrusion, which leads to extracellular acidification that impairs the activity of DCs, and hinders the activity of glycolytic effector T cells (Kay and Zanivan, 2023; Wu et al., 2020b; Zhang et al., 2024).

As evidenced in this section, PDAC TME conditions (*i.e.* a highly acidic and immunosuppressive microenvironment with a dense ECM) are fundamental to understand PDAC tumours aggressiveness and the challenges that therapies must overcome in order to be effective against this malignancy (Andersen et al., 2021).

1.1.3. PDAC therapeutics

1.1.3.1. Conventional approaches

As first lines of treatment, surgery is the only treatment option that can potentially cure PDAC, being applicable only to patients with localized PDAC (15-20% of cases). Unfortunately, this approach is associated with morbidity rates between 22-40%, tumour recurrence rates ranging between 60-90% (Lockie et al., 2025; Rozengurt and Eibl, 2026; Taieb et al., 2020), and 10-year overall survival rates after resection of 5.3%, according to a nationwide study performed in the Netherlands (Verkolf et al., 2025).

On the other hand, the use of radiotherapy in PDAC has been a topic of controversy, with clinical studies showing inconsistent efficacy. However, novel initiatives based on the technical improvements of the field have proposed the use of radiotherapy as neoadjuvant or adjuvant treatment in patients receiving/not receiving chemotherapy (Dardare et al., 2026; Xiao et al., 2025).

In the case of patients with late-stage or metastatic PDAC (80-85%), chemotherapy is the first-line treatment (Debiais et al., 2026). Gemcitabine, a nucleoside analogue, was the first agent to demonstrate efficacy against metastatic PDAC in 1997 (Debiais et al., 2026) and it is still used until this day. However, current standards of care recommend three possible combinatorial treatments as first-line therapy: gemcitabine combined with albumin-bound paclitaxel (nab-paclitaxel), and the quadruplets folinic acid, 5-fluorouracil, irinotecan and oxaliplatin (FOLFIRINOX) and folinic acid, liposomal irinotecan, 5-fluorouracil and oxaliplatin (NALIRIFOX), each one with median overall survival of 8.5, 11.1 and 11.1 months,

respectively (Jia et al., 2025; Taieb et al., 2020; Wainberg et al., 2023). In addition, safety concerns around the severity of their adverse events (*e.g.* severe anaemia, neutropenia, thrombocytopenia, and nausea) makes FOLFIRINOX and NALIRINOX the preferred options only for patients who can tolerate these side effects (Kang et al., 2024; Mastrantoni et al., 2024).

Additional pharmacological approaches, such as gemcitabine + nab-paclitaxel, 5-fluorouracil/folinic acid + oxaliplatin, liposomal irinotecan + 5-fluorouracil/folinic acid, and gemcitabine single treatments have been suggested, but none of these approaches have supposed any further improvements in terms of overall survival of patients when compared with regimes that only considered first-line agents (Dayyani et al., 2023; Fukahori et al., 2023; Trovato et al., 2025).

This scenario of unsatisfactory safety and efficacy for conventional chemotherapeutics is mostly based on PDAC cells heterogeneity and their TME conditions. For this reason, targeted therapies and immune-based approaches appear as a suitable strategy to improve clinical outcomes by considering these features.

1.1.3.2. Targeted agents and immunotherapy

Unlike systemic chemotherapy, targeted therapies are characterized by a high selectivity, focused on inhibiting specific proteins or signalling pathways that contribute to PDAC progression. A widespread example of the former is the case of KRAS inhibitors, being sotorasib, a KRAS G12C inhibitor, the first agent to receive FDA approval to treat non-small cell lung carcinoma (Nakajima et al., 2022). In the

particular case of PDAC, KRAS G12C inhibitors like ASR-853 and ASR-1620 have not shown any benefits *in vivo*, and sotorasib showed limited applicability, because this mutation is only present in 1% of patients with metastatic PDAC (Li et al., 2024; Xie et al., 2025). Despite this, the results of ongoing clinical trials focused on describing the safety and efficacy of other KRAS G12C inhibitors, like adagrasib, divarasib, glecirasib and garsorasib, will determine if this particular mutation is a relevant target in PDAC (Drizyte-Miller et al., 2025b; Malla et al., 2025). Regarding KRAS G12D inhibitors, MRTX-1133 showed potent and highly selective anti-cancer effects on preclinical models, but failed at phase I trials due to complications In its pharmaceutical formulation (Hallin et al., 2022; Malla et al., 2025). However, early clinical trials using zoldonrasib (also known as RMC-9805) in single and combination treatments have shown promising results in terms of toxicity and efficacy against PDAC (Drizyte-Miller et al., 2025b; Li et al., 2024). To date, *pan*-KRAS inhibitors, such BGB-53038, and RMC-6236, are under clinical evaluation, but, as non-selective agents, their use raises safety concerns (Li et al., 2024; Reiss et al., 2025).

Recently, the results of the phase III clinical trial RASolute 302 showed remarkable results for the multiselective RASON inhibitor daraxonrasib (RMC6236), capable to inhibit G12, G13 and Q61 mutated variants of KRAS, NRAS and HRAS, in patients with previously-treated metastatic PDAC. Patients treated with orally-administered daraxonrasib exhibited longer overall survival and progression-free survival when compared with groups of patients that received gemcitabine + nab-paclitaxel, liposomal irinotecan + 5-FU + folinic acid, FOLFOX and modified FOLFIRINOX (O'Reilly et al., 2026).

Some examples of agents targeting signalling pathways relevant for PDAC progression are poly (ADP-ribose) polymerase (PARP) inhibitors, like olaparib, veliparib and niraparib, which have shown increased progression-free survival, but no major impact on overall survival in patients with BRCA1/2 mutations (Fang et al., 2023; Malla et al., 2025; Xie et al., 2025); epidermal growth factor receptor (EGFR) inhibitors, like erlotinib, which improved survival in patients with advanced PDAC when combined with gemcitabine (Moore et al., 2023); vascular endothelial growth factor receptor inhibitors, like bevacizumab, which showed no efficacy both in single and combinatorial approaches (Dittrich et al., 2019; Kindler et al., 2010); or multi-targeting initiatives using RMC-6236 plus the EGFR inhibitor afatinib and the STAT3 inhibitor SD36, which recently showed promising efficacy and tolerance in patient-derived xenografts and murine PDAC models (Liaki et al., 2025).

In addition to these agents, many immune-based approaches for PDAC treatment have been evaluated. From these strategies, immune checkpoint inhibitors, such as anti-PD1, anti-PD-L1 or anti-CTLA4 drugs, have shown limited or no efficacy both as single or combined treatments with chemotherapy (*e.g.* FOLFIRINOX and gemcitabine/nab-paclitaxel) (Farhangnia et al., 2024; Timmer et al., 2021). Associated with this, a randomized phase II study using FOLFIRINOX plus the anti-PD1 monoclonal antibody pembrolizumab as neoadjuvant therapy showed a modest improvement of response when compared with standard FOLFIRINOX (Chen et al., 2022). This example highlights the contrast between PDAC and other malignancies with higher immunogenicity, where neoadjuvant approaches using immune checkpoint inhibitors could lead to pathological responses > 70% (Chick and Pawlik, 2024). Conversely, when the macrophage activator sotigalimab, an anti-

CD40 monoclonal antibody, was used on *in vivo* PDAC models, contradictory results were reported, and phase II clinical trials failed to improve the condition of PDAC patients (Farhangnia et al., 2024; Ju et al., 2024). A similar situation was observed for CSF-1R blockers, which achieved promising results in syngeneic orthotopic PDAC tumours, but only yielded modest results when the anti-CSF-1R monoclonal antibody cabiralizumab was used with anti-PD1 (Maldonado et al., 2023; Zhu et al., 2014).

Other immune-based approaches, like oncolytic viruses, cancer vaccines and adoptive cell therapies, have been evaluated in PDAC with mixed results. Treatment with oncolytic viruses like ONYX-015, an adenovirus designed to be replicated inside of cells with impaired p53 function because of its E1B deletion (Bischoff et al., 1996), and VCN-01, another adenovirus which uses E2F1 promoters in the E1B site to promote its replication inside of cells with deregulated pRb function (Bazan-Peregrino et al., 2021), had shown promising results preclinical studies and early-phase clinical trials (Garcia-Carbonero et al., 2022). However, impairments in viral replicability, reduced efficiency and safety because of the activation of systemic immune response in the host and reduced penetration to tumour sites because of PDAC TME conditions are challenges that need to be covered in order to improve their applicability (Taylor and Lopez, 2023).

Regarding cancer vaccines used in PDAC, GVAX, a genetically-engineered vaccine designed to induce the secretion of granulocyte-macrophage colony stimulating factor (GM-CSF), was capable to achieve complete pathologic response in 35% of the patients when used as a neoadjuvant agent with nivolumab

and stereotactic body radiation therapy in patients with borderline resectable PDAC (Agarwal et al., 2023). Another report of the use of cancer vaccines in PDAC is the one regarding autogene cevumeran, a personalized mRNA vaccine, which, in combination with the anti-PD-L1 monoclonal antibody atezolizumab and modified FOLFIRINOX, was capable to induce neoantigen-specific T cell response in half of the patients who received the treatment and increased their recurrence-free survival when the response of the patients was evaluated 18 months later (Rojas et al., 2023).

When adoptive cell therapies in PDAC are considered, tumour-infiltrating lymphocyte therapy, T cell receptor (TCR) engineering, chimeric antigen receptor T cells (CAR-T) are approaches which are in different stages of preliminary clinical evaluation (Chick and Pawlik, 2024; Sherpally and Manne, 2025). As a recent example, *ex vivo*-expanded T helper cells targeting the tumour-associated antigens MAGEA4, NY-ESO-1, PRAME, survivin and SSX2 were administered to PDAC patients sensitive and resistant to first-line treatments, resulting in disease control rates of 84.6 and 25.0%, respectively (Musher et al., 2026).

Despite the wide variety of signalling pathways that has been described in this section as pharmacological targets, the search for pathophysiologically-relevant candidates is a matter of permanent interest for PDAC therapeutics. In the next section, the role of protein arginine methyltransferase 5 (PRMT5) and its applicability as a target for cancer treatment will be discussed.

1.2. PRMT5 and its role in cancer

1.2.1. General features of PRMT5 and its relevance in tumour biology

Among the events comprised as post-translational modifications, arginine methylation is an ubiquitous process that can take place at both nuclear and cytoplasmic level by members of PRMT family (Motolani et al., 2021). These enzymes use S-adenosylmethionine (SAM) to catalyse the transfer of a methyl group to the ω-guanidino nitrogen of arginine residues (Antonysamy et al., 2012; Motolani et al., 2021). In humans, 9 members have been identified in the PRMT family, which have been classified according to their catalytic activity as Type I (PRMT1-4, PRMT6 and PRMT8, which are capable to induce arginine monomethylation and asymmetric dimethylation), Type II (PRMT5 and PRMT9, that promote monomethylation and symmetric dimethylation) and Type III (PRMT7, which is the only member with exclusive monomethyl transferase activity) (Gu et al., 2025; Kim and Ronai, 2020).

In terms of its structure, PRMT5 is a 637 amino acids long protein which contains an N-terminal TIM barrel domain, a middle Rossman fold domain and a C-terminal β-barrel domain (Motolani et al., 2021). In humans, PRMT5 assembles as a hetero-octamer with MEP50 (forming a 435 kDa complex). This association is structured by two inner PRMT5 dimers assembled by their β-barrel domain and four PRMT5:MEP50 complexes bound by the TIM barrel domain of PRMT5 (Antonysamy et al., 2012; Gu et al., 2025; Kim and Ronai, 2020).

PRMT5 is capable to symmetrically dimethylate both histone (Histone H2A, H3 and H4 specifically) and non-histone targets (*e.g.* p53, CASP4, SRSF1, RAF-1, AKT1, E2F1, NF-κB/p65, etc), exerting a regulatory role in cellular processes such as gene transcription, gene splicing, cell cycle progression, apoptosis and differentiation (Chen et al., 2021a; Gillespie et al., 2025; Gu et al., 2025; Liang et al., 2021; Radzisheuskaya et al., 2019). Because of its involvement in a wide array of functions essential for cell survival (summarised in Figure 1.2), PRMT5 is frequently upregulated in lung cancer, colorectal cancer (CRC), breast cancer, glioblastoma, ovarian cancer and PDAC (Abe et al., 2024; Abe et al., 2023; Banasavadi-Siddegowda et al., 2018; Barczak et al., 2020; Chen et al., 2021a; Ozturk et al., 2025; Qin et al., 2019).

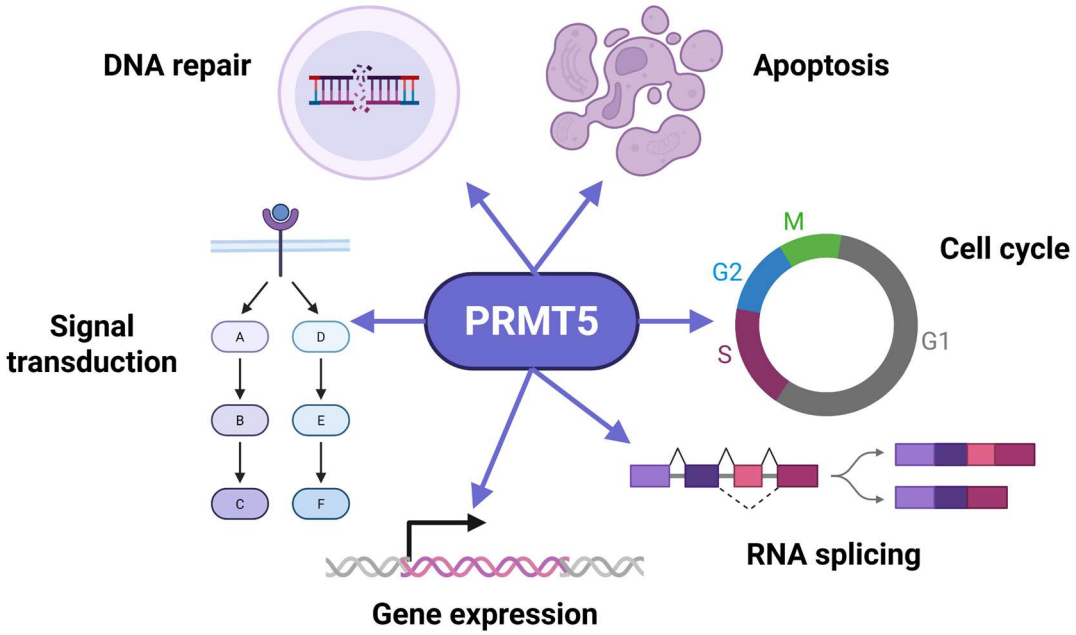

Figure 1.2. Cellular processes regulated by PRMT5 activity.
Summary of the biological functions controlled by PRMT5 which are important for tumour progression. Figure created in https://BioRender.com.

In the particular context of PDAC, PRMT5 overexpression is associated with higher aggressiveness (Schneider et al., 2025). These features are explained, in part, by the capacity of PRMT5 to interact with different protein targets like MYC, which has been associated with a higher reliance on PRMT5 activity to preserve splicing fidelity and promote glycolysis and proliferation (Orben et al., 2022; Qin et al., 2019; Schneider et al., 2025), and Hippo, where PRMT5 inhibition has been associated with a reactivation of Hippo signalling and a reduction of tumour growth on immunodeficient mice bearing Panc-1 xenografts (Sun et al., 2023).

Another target of PRMT5 that is relevant for cancer progression is the transcription factor E2F1. The characteristics of this interaction and its relevance for cancer survival are topics that will be discussed in the following section.

1.2.2. PRMT5-E2F1 interaction and its association with cancer progression

The transcription factor family E2F is integrated by 8 members with relevant regulation roles in DNA damage repair, cell cycle progression, apoptosis, differentiation, angiogenesis and metabolism (Xie et al., 2021). According to their transcriptional function and role in cell cycle, E2F members are classified as activators (E2F1-3), canonical repressors (E2F4-6) and atypical repressors (E2F7 and E2F8) (Li et al., 2023; Xie et al., 2021).

From the activator isoforms, E2F1 overexpression in cancer is frequent and it has been associated with reduced overall survival and disease-free survival (Li et al., 2023). E2F1 activates gene transcription by binding to E2 recognition sites (canonically 5'-TTTCGCGC-3´) in the DNA and associating with dimerization

partner (DP) proteins (Fang et al., 2020). Regarding its function in the cell cycle, E2F1 is inactivated by forming complexes with the tumour suppressor protein pRb (a frequently-deregulated target in cancer). During G1 phase, an enhanced cyclinD-CDK4/6 activity phosphorylates pRb and releases E2F1, which drives the transcription of relevant genes for G1 to S phase transition (Manickavinayaham et al., 2020; Stevens and La Thangue, 2003).

E2F1 activity can be regulated via post-translational modifications such as phosphorylation, acetylation, ubiquitination, SUMOylation and methylation (Graves et al., 2020; Marzio et al., 2000; Sun et al., 2024; Tang et al., 2023). Regarding the later, PRMT5 is capable to symmetrically dimethylate E2F1 at the RGRGR motifs present at its R111 and R113 residues, and PRMT1 methylates E2F1 at R109 (Cho et al., 2012). The activity of these enzymes is mutually exclusive and regulate opposing cellular responses (*e.g.* R109 methylation promotes apoptosis and inhibits cell growth, while R111/R113 methylation exerts contrasting effects) associated with cell fate (Cho et al., 2012; Zheng et al., 2013). In addition, R111/R113 methylation induced by PRMT5 promotes the interaction between E2F1 and p100/TSN, an RNA binding protein which has activation roles in gene transcription, alternative splicing (AS) and cell proliferation (Roworth et al., 2019; Saarikettu et al., 2023; Zheng et al., 2013).

All the biological effects, plus the described interaction of PRMT5 with other cancer-relevant targets like E2F1, portray PRMT5 inhibition as a promising pharmacological strategy in cancer.

1.2.3. PRMT5 inhibition as a pharmacological approach in cancer

From a pharmacological perspective, PRMT5 contains two orthosteric sites, namely its SAM-binding site and substrate-binding site at its Rossman fold domain (Hu and Chen, 2024; Sun et al., 2011). Additionally, other pharmacologically-relevant sites for PRMT5 inhibition include an allosteric binding site between the Rossman fold and β-barrel domains and a PRMT5/MEP50 dimerization site at is Tim barrel domain (Hu and Chen, 2024). Based on these structural elements, PRMT5 inhibitors can be classified as: (i) SAM inhibitors, which exert its activity by interacting with a SAM-binding site in a cooperative (*e.g.* GSK-3326595 and SCR-6920) or competitive (*e.g.* JNJ-64619178, PF-06939999 and PRT811) fashion; (ii) cooperative inhibitors of the endogenous inhibitor 2-methylthioadenosine (MTA), which binds to PRMT5 substrate site (*e.g.* AMG-193, AZD3470 and MRTX-1719); (iii) allosteric inhibitors (*e.g.* compound 1a); and (iv) PRMT5-substrate adaptor interactor inhibitors, which bind to the PRMT5/MEP50 dimerization site (*e.g.* BRD-6988 and BRD-0639) (Lee et al., 2025; Palte et al., 2020; Shen et al., 2020; Shen and Li, 2025).

Preclinical studies using PRMT5 inhibitors have shown promising effects in lymphoma, NSCLC, breast cancer, melanoma, glioblastoma and leukaemia, by regulating apoptosis, cell cycle, gene expression and splicing, cell proliferation, epithelial-mesenchymal transition and metastasis (Lee et al., 2025; Song and Yang, 2026). As examples of this, previous work from our research group with the selective PRMT5 substrate inhibitor T1-44 have shown that this drug is capable to inhibit CRC migration and invasion by interfering with the expression of the E2F1 target cortactin

(Barczak et al., 2020), trigger apoptosis in neuroblastoma by recovering the splicing fidelity of DIABLO (Bate-Eya et al., 2025), and enhance the immunogenicity of CRC by inducing the expression and presentation of lncRNA-derived peptides (Barczak et al., 2023). In the context of CDK2A/MTAP co-deleted malignancies, the use of PRMT5 inhibitors, like MRTX1719 and IDE892, is showing signs of efficacy in early-stage clinical trials of tumours including non-small cell lung cancer and PDAC (IDEAYA-Biosciences, 2026; Mulvaney, 2023)

Considering the pressing need for therapeutic alternatives that can increase PDAC responsiveness to treatment, the relevance of the PRMT5/E2F1 interaction in several aspects of tumour survival, and the promising effects that PRMT5 inhibition had shown in several types of cancer, the aim of following thesis has been focused on exploring the potential of PRMT5 inhibition as a pharmacological tool to enhance PDAC immunosensitivity.

1.3. Research hypothesis

PRMT5 inhibition is capable to increase the immunogenicity of PDAC cell lines due to its effects on gene expression and alternative splicing.

1.4. Research objectives

- To characterize the effects of PRMT5 inhibition on the proliferation of PDAC cell lines.

- To assess the role of PRMT5 inhibition modifying lncRNA expression and regulating alternative splicing, and its subsequent impact on pH_i/pH_e dynamics in PDAC cellular and animal models.
- To establish if the effects of PRMT5 inhibition on pH dynamics and lncRNA expression and alternative splicing can be used as a potential immunosensitizing strategy for PDAC *in vivo*.

Chapter 2 : Materials and Methods

2.1. Cell culture, stable transfections, and compound treatments

Human and murine PDAC cell lines Panc-1 and Panc02, respectively, were kindly provided by IngenOx Therapeutics (Oxford, UK), authenticated via short tandem repeats (STR) profiling (Panc-1: Nortgene, C-33674-6. Panc02: ATCC, MUSA3601) and cultured in DMEM (Gibco) supplemented (sDMEM) with 10% foetal bovine serum (FBS; Thermo Fisher Scientific), and 1% of a penicillin/streptomycin antibiotic solution (P/S; Gibco). Cultures were grown and maintained up to passage 30 in a humidified incubator at 37°C + 5.0 % CO_2, and MycoSensor qPCR Assay Kit (Agilent) was used to verify that all cell models were Mycoplasma-free. The mutational profile of these cell lines is detailed in Table 1.

Table 1. Mutational profile of PDAC cell lines

Cell line	TP53	KRAS	SMAD4	CDKN2A
Panc-1	R273H	G12A	WT	WT
Panc02	WT	WT	E174stop	WT

E2F1 CRISPR knockout (E2F1Cr) cell lines were generated via stable transfection with GeneJuice (Sigma-Aldrich) for 48 h following the protocol described by Ran *et al.* (Ran et al., 2013). For this purpose, a pSpCas9(BB)-2A-Puro (PX459) V2.0 vector (Addgene plasmid #62988) that includes a single guide RNA (sgRNA) sequence that targets exon 2 of both human and murine E2F1 (5'-AAACTGACCATCAGTACC-3') was used to generate E2F1Cr cells. In addition, a control condition transfected with the empty backbone (Cas9) was included for

each cell line. After transfection, puromycin selection and expansion processes, knockouts were validated by immunoblotting.

T1-44 (IngenOx Therapeutics) was used as selective PRMT5 inhibitor (Barczak et al., 2020) in concentrations and incubation times depending on the experiment. To account for the inherent measurement variability associated with the location of wells, seeding and treatment conditions, a randomized blocks design (RBD; examples illustrated in Figure 2.1) was used for performing assays that involved the use of 96-well plates (Festing, 2020; Karp and Fry, 2021). Randomization was made using Excel 365 (Microsoft Corporation) at the day of each experiment.

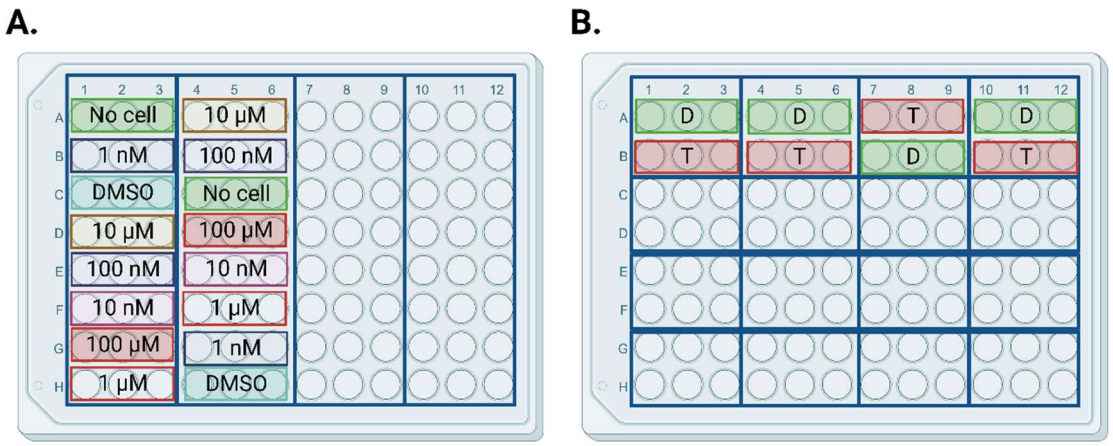

Figure 2.1. Representative examples of the randomized blocks design strategy used for 96-well plates-based experiments.

A. *RBD strategy used for T1-44 MTT assays. The four blue rectangles represent each one of the incubation time blocks to be randomized (2, 3, 4 or 5 d). On each incubation time block, triplicates of each treatment condition (no-cell control, DMSO, 1 nM - 100 µM T1-44) were also allocated randomly as treatment blocks.* ***B.*** *RBD model used for RT-qPCR experiments using T1-44 treatment. Here, each one of the 16 blue rectangles represents a block with a different gene to be randomized. The position of each treatment triplicate (DMSO or 1.0 µM T1-44) was also assigned randomly for every gene block. Figure created in https://BioRender.com.*

2.2. Antisense oligonucleotides (ASO) design and transfections

Design and validation of 2'-O-methyl-modified ribose with phosphorothioate backbone (2'-OMePS) ASOs was performed following specific guidelines (Aartsma-Rus et al., 2022; Aung-Htut et al., 2019), using eSkip-Finder (Chiba et al., 2021) as *in silico* platform to identify potential ASO candidates to induce both human and murine SLC4A7 exon 25 skipping (Δ25 ASO). An additional scrambled non-targeting ASO was designed as negative control with the same number of nucleotides and GC% as the SLC4A7-targeting ASO. *In silico* specificity was checked for every ASO using NCBI BLAST (https://blast.ncbi.nlm.nih.gov/Blast.cgi) using both human and murine RefSeq Genome databases. With this information, the chosen ASO sequences detailed in Table 2 were synthesized by Integrated DNA Technologies (Coralville, IA, USA).

Table 2. List of 2'OMe-PS ASO for SLC4A7 exon 25 skipping

Target	Species	Sequence (5'-3')
SLC4A7 H/M25A (+27+48)	Human/ Mouse	GCAGUUUUGGCCAUUUCAUCUG
Scrambled SLC4A7 H/M25A (+27+48)	Human/ Mouse	AGUUGCCGUUAGUCUAUGCUCU

ASO transfections were performed for 48 h using Lipofectamine 3000 (Invitrogen) according to the manufacturer's guidelines, with 200 nM as final ASO concentration. ASO products and performance were validated via RT-qPCR by establishing SLC4A7 exon 25 inclusion/exclusion ratio, and PCR by comparing the pixel density ratio between spliced-in and spliced-out PCR products and subsequent sequencing those amplicons (performed by Source BioScience, Cambridge, UK). Chosen Δ25 ASO validation primers are described in Table 3.

Table 3. List of primers for ASO products validation

Target	Species	Forward sequence (5'-3')	Reverse sequence (5'-3')
SLC4A7 Ex23-26 validation PCR primers			
SLC4A7 Ex23-26	Human	TTGTGCGCAAACTCATGGAC	CTATAATGAAGTTTCAGCATCCACG
Slc4a7 Ex23-26	Mouse	GTCTTTGTGCGCAAGCTCAT	GTCACACTCACAGGCTTTTCA
SLC4A7 splicing RT-qPCR primers			
SLC4A7 SE Ex24-25	Human	AAGGCCCTAAAATATAGTGTT GATCCC	AGCATCCACGTATTTCTTTCTTGGTT
SLC4A7 SE Ex24-26	Human	CCCTAAAATATAGTCCTGATAA ACCTGTGA	AGCATCCACGTATTTCTTTCTTGGTT
Slc4a7 SE Ex24-25	Mouse	TATCAGATGAAATGGCCAAAA CTGC	TACAATGAAGTTTCAGCATCCATGT ATTT
Slc4a7 SE Ex24-26	Mouse	AAAATATAGCCCTGAAAAGCC TGTGA	TACAATGAAGTTTCAGCATCCATGT ATTT

2.3. Cell proliferation

To establish cell growth under different treatment conditions, parental, Cas9 and E2F1Cr Panc-1 and Panc02 cells were seeded in 6-well plates (Greiner Bio-One) at a density of 50,000 cells/well. After an overnight incubation, treatment or transfection conditions were added, using DMSO or non-ASO-containing transfection wells as control treatments, respectively. Every 2 days, cells were collected and cell number was determined using a Luna-II Automated Cell Counter (Logos Biosystems), performing last measurements on day 8.

2.4. MTT assay

Parental, Cas9 and E2F1Cr Panc-1 and Panc02 cells were seeded on 96-well plates (Greiner Bio-One) in density of 2,000-5,000 cells/well to achieve 40–50% confluence the next day. After adhesion, cells were treated with T1-44 dilutions in sDMEM (concentration range: 1 nM - 100 µM) for 2 to 5 days. On each plate, DMSO-

treated cells and a background condition without cells were included. After incubation, a 1 mM MTT (ApexBio) in sDMEM solution was added to cells according to previous reports (Kumar et al., 2018). Absorbance measurements were performed using a Sunrise® microplate reader (Tecan) at 570 nm corrected with 650 nm. For data analysis, cell survival percentages were obtained by deducting the cell-free background signal and then comparing the DMSO-treated measurements with those acquired for T1-44 treatment. Median inhibitory concentrations (IC_{50}) were calculated for each condition by adjusting curves to an exponential fit using Prism 10.4.1 software (GraphPad).

2.5. Cell cycle analysis

First, cells were seeded on 100 mm dishes to achieve a 60-70% confluence after an overnight incubation. Then, plates were treated for 48 h with 0, 0.1, 1.0 and 10.0 µM T1-44, and 100 nM doxorubicin (Dox, which was used as positive control based on previous reports for Panc-1 and Panc02 cells (Barros et al., 2018; Yagublu et al., 2013)) for 48 h. After treatment, cells were trypsinized, washed with PBS, and centrifuged for 3 min at 300 *g* at 4°C. Supernatants were discarded and cell pellets were fixed using cold 70% v/v ethanol added dropwise while vortexing and incubated for 30 min on ice. Fixed samples were washed twice with PBS and then treated with 100 µg/mL propidium iodide (PI; Sigma-Aldrich) and 200 µg/mL RNAse A (Sigma-Aldrich) and incubated for 25 min at RT. Cell cycle profiles were obtained on an Accuri C6 flow cytometer (Beckton Dickinson), acquiring a minimum of

30,000 events per sample. Data were depicted as graphs showing the mean ± SD of Sub-G_1 phase percentages.

2.6. Annexin V/PI staining

To establish the effects of T1-44 on apoptosis, PDAC cells were seeded on 100 mm dishes and treated as stated in section 2.5 (*Cell cycle analysis*). Staining was conducted by using the FITC Annexin V Apoptosis Detection Kit I (BD Pharmigen) according to the manufacturer's guidelines. 10,000 events per sample were collected using an Accuri C6 flow cytometer (Beckton Dickinson), and FL1 and FL3 channels were chosen to obtain Annexin V and PI fluorometric measurements, respectively. To illustrate results, comparisons were made using the overall percentage of apoptotic cells obtained after each treatment.

2.7. Western blot

Cells cultured on 100 mm dishes were trypsinized, pelleted, washed with PBS and lysed using modified RIPA buffer (50 mM Tris-HCl pH 7.4, 1% v/v IGEPAL CA-630, 150 mM NaCl, 1 mM EDTA, 1 mM NaF, 1 mM Na_3VO_4, 1 mM AEBSF supplemented with protease inhibitor cocktail) for 30 min on ice. Then, samples were centrifuged for 10 min at 12,000 rpm at 4°C, supernatants were collected, and total protein amount was quantified using the Bradford method (Sigma-Aldrich). The samples were resolved by SDS-PAGE using extemporarily-prepared 8-15% poly-acrylamide gels and transferred onto membranes in a semi-dry transfer system (Trans-Blot Turbo System with 0.2 µm nitrocellulose transfer packs (Bio-Rad) at 25

V, 1.0 A for 30 min). 5% w/v skimmed milk (Sigma-Aldrich) solution in PBS + 0.1% v/v Tween 20 (PBS-T) was used for blocking (30 min at room temperature), and blocked membranes were incubated overnight at 4°C using 1:1,000 dilutions of primary antibodies (detailed in Table 4). After incubation, membranes were washed with PBS-T and treated for 1 h at RT with suitable HRP-conjugated secondary antibodies (1:10,000 dilution). Membranes were washed with PBS-T and bands were visualised using Clarity Western ECL Substrate solutions (Bio-Rad) and X-ray films (Fujifilm).

Table 4. List of primary antibodies used for immunoblotting

Target	Catalogue number	Manufacturer
E2F1	3742S	Cell Signalling Technologies
PRMT5	79998S	Cell Signalling Technologies
Symmetric Dimethyl Arginine motif (SDMe)	13222S	Cell Signalling Technologies
NBCn1/SLC4A7	PA5-104154	Invitrogen
Histone H4	ab174628	Abcam
Symmetric Dimethyl R3 Histone H4	ab5823	Abcam
FLAG	F1804	Merck Millipore
GAPDH	MAB374	Merck Millipore

2.8. RT-qPCR

With the purpose of harmonizing both terminologies and reproducibility, these experiments were performed following the Minimum Information for Publication of Quantitative Real-Time PCR Experiments (MIQE) guidelines when suitable (Bustin et al., 2025). Total RNA extraction was performed using TriZol (Thermo Fisher Scientific) following the manufacturer's protocol, and subsequent reverse transcription of 1.0 µg total RNA was performed using an oligo(dT)20 primer (Invitrogen) and SuperScript III reverse transcriptase (Invitrogen) according to the supplier's instructions. RT-qPCR reactions were conducted in an AriaMx Real-Time PCR System (Agilent), the Brilliant III Ultra-Fast SYBR® Green qPCR Master Mix

(Agilent) with 20 ng cDNA and the reaction formulations and thermal protocols recommended by the manufacturer. Relative expression values were calculated using the $2^{\Delta\Delta Cq}$ method (Livak and Schmittgen, 2001) with GAPDH as reference gene for both species, and DMSO-treated condition as basal expression control when compared to other treatments. Specific primer pairs for these experiments (detailed in Table 5) were designed using Primer-BLAST (https://www.ncbi.nlm.nih.gov/tools/primer-blast/), choosing pairs that generate a 50-200 bp PCR product size, an 60ºC annealing/extension temperature, and a GC content between 40-60%.

Table 5. List of RT-qPCR primers used in this study

Gene	Species	Forward sequence (5'-3')	Reverse sequence (5'-3')
		lncRNA primers	
PYDC2-AS1-212	Human	GGAGTCCTTCATCCGAATGGTAAA	TTAGCTCCCCCTTGTTAGTGTG
SNHG1-258	Human	AACCAATAACCTGCTTGGCTCA	GTTTTCCTCAAACTCCTCTTGGG
DIO3OS-225	Human	GTGTACGGAGAGAGCTCGGA	AAGGGTCCTCTTGCAGGCAT
DANCR	Human	CTTCATGTTCACCTTTTCAACC	CAGAGTATTCAGGGTAAGGGTC
MALAT1	Human	GTCGGCAATATGTTGTTTTTC	CCTGAAAAAGAGAAACCTACAAC
BX322557.10	Human	CGTTTCTGGTCTTTGAAAGAC	GCTGGCTACCATCTTTATGTC
CCDC183-AS1-201	Human	GCTGTGCAGGTTCCTCCC	GACAGACATGCTGGCTGACA
NEAT1-201	Human	ACCAAGGGCTGTGAACCC	CACTGCCACCACCCTGG
MAP3K2-DT-208	Human	GCATACGCACCTGGGTTGT	CCAAGAAGAAGCTTTTCACGGGAT
Gm6093-201	Mouse	GTTGCAAGTTCTCTTCATCACACA	GCCAGCCTGCTTCCATGAAC
Gm43085-201	Mouse	TCTAGGTTAGTGGGCTCAGGAAA	ATCCTCAAAGTCCACTCCTGTG
Snhg3-204	Mouse	AAGGTATAAATATGGCTGCGTCG	GACCGGGTCAAGAACAAGCA
Gm37494-201	Mouse	TCAAATACCTGAAAGGGCTCG	ACTGAATATTGCACCACATTGC
Gm15635-201	Mouse	TGGAGGCCTATGAATCTGAGGG	GATGTCTTCCGTGTGCCTGAG
Gm37855-201	Mouse	GGAAAACTGAAAGGTCCTGAGC	AGAACGGCCAGTGTCAGAGA
A830082K12Rik-210	Mouse	TTGGCATAGAGAGAAGAGCAGTTA	CATTCCATGGCCACAATATACATGTTC
C430049B03Rik-201	Mouse	GCCATGGTAACCCTAAAGTATTGATTC	TCGATGGTCACGAAAAGAGAGC
Gm35940-201	Mouse	ACATGCAACTAGTGGAGACAACA	TGGGATGTGTCCACCTCCATT
		SLC gene family primers	
SLC4A4	Human	CAGGAGGATGGAGGATGAAGC	ATGGTATGGTGGCCTTCTACT
SLC4A7	Human	TTGCTTGAAAGGAATGGGGAAGG	CAAGGAAAGGTTTGAGGCAGA
SLC5A1	Human	ATCTGTGGGGTGCACTACTT	ACACAGACGGTAGAGATGCACA
SLC5A2	Human	GTGCCTGAGGTGTGCAGG	CCGCGCAGACCGTTGG
Slc4a4	Mouse	TCAAACCCCTCATCTCCCCG	AGAAGCTCATCGAGTTCCGTG
Slc4a7	Mouse	AGGGCACAAACATCACCACC	CGATGGCGTGTCATAAGAAGGA

Slc5a1	Mouse	ACATTGGAAGTGGTCACTTTGTG	AAAACCAAGGCGTTCCATTCAAAG
Slc5a2	Mouse	GGCACTGATGTACACAGACACT	CATGGAAAGCATAACCAGTGAGG
		SLC4A7 skipped exon 25 event primers	
SLC4A7 SE Ex24-25	Human	AAGGCCCTAAAATATAGTGTTGATCCC	AGCATCCACGTATTTCTTTCTTGGTT
SLC4A7 SE Ex24-26	Human	CCCTAAAATATAGTCCTGATAAACCTGTGA	AGCATCCACGTATTTCTTTCTTGGTT
Slc4a7 SE Ex24-25	Mouse	TATCAGATGAAATGGCCAAAACTGC	TACAATGAAGTTTCAGCATCCATGTATTT
Slc4a7 SE Ex24-26	Mouse	AAAATATAGCCCTGAAAAGCCTGTGA	TACAATGAAGTTTCAGCATCCATGTATTT
		Reference gene for relative quantification	
GAPDH	Human/ Mouse	TTCATTGACCTCAACTACAT	GTGGCAGTGATGGCATGGAA

2.9. RNA sequencing (RNAseq) and splicing analysis

Panc-1 and Panc02 cells were treated with DMSO and 1.0 μM T1-44 for 48 h. RNA was extracted using the Direct-zol RNA Mini Prep Plus (Zymo Research) kit following the supplier's instructions. Samples with total RNA concentration ≥10 ng/μL and 260/280 and 260/230 absorbance ratios ≈2.0 were sent to Genewiz (Azenta Life Sciences, Leipzig, Germany), who performed quality control, library preparation, and sequencing. For RNAseq analysis, resulting FASTQ files were uploaded to Galaxy platform global server (https://usegalaxy.org/) (Community, 2022), adapter removal was verified using Cutadapt v.4.4, and quality control of the reads was checked by FastQC v.0.12.1. For differentially expressed gene (DEG) analysis, initial sequence mapping was performed using STAR (v.2.7.10b), using a 100-bp read length, and h19/GRCh38.p14 and mm10/GRCm39 as reference genomes and GENCODE gene annotation versions in Panc-1 and Panc02 samples, respectively. The binary alignment map (BAM) files were used to obtain normalized gene counts with featureCounts v.2.0.3, and these counts files were then used for differential gene expression analysis with DESeq2 v.1.40.2, using a false discovery

rate (FDR) < 0.01 as significance threshold. Heatmaps were generated using Z-scores on normalized counts, and volcano plots were made considering adjusted *p* value < 0.01 and absolute value of the base-2 logarithm of fold change ($|\log_2 FC|$) > 0.58 as cutoffs. Additionally, $\log_2 FC$ results of significant DEGs were used for Gene Ontology (GO) analysis with Goseq v.1.26.0 considering $p < 0.05$ as cutoff for significant terms.

For lncRNA transcript analysis, Kallisto v.0.48.0 was run on FASTQ files, using human GRCh38.p14 and mouse GRCm39 GENCODE reference transcriptomes. Significant transcripts were identified using the tximport v1.28.0 package to process transcripts per million (TPM) values on DESeq2 v.1.40.2 with FDR < 0.01 as significance threshold. LncRNA transcript heatmaps were generated using Z-scores on TPM, and top 20 up- and downregulated lncRNA transcripts were identified for both cell lines using FDR < 0.01 and $|\log_2 FC| > 1.0$ as cutoffs.

To analyse the effects of T1-44 on alternative splicing (AS), rMATS turbo v.4.1.2 algorithm was applied using human GRCh37.p14 and murine GRCm38 as GENCODE referential annotations. Identified AS events included skipped exons (SE), retained introns (RI), mutually exclusive exons (MXE), and alternative 5' and 3' splicing sites (A5SS and A3SS, respectively). Events were considered significant when FDR < 0.05 and $\Delta\Psi > 0.05$.

2.10. lncRNA promoter analysis

Differentially expressed (DE) lncRNA gene promoters were checked for E2F1 binding using chromatin immunoprecipitation sequencing (ChIPseq) track sets available on UCSC Genome Browser (https://genome.ucsc.edu/) (Kent et al., 2002). GRCh37/h19 assembly was used for human genes, and *in silico* predicted E2F1 binding sites were identified using the E2F1 ChIPseq tracks (obtained for HeLa-S3, MCF-7 and K562 cells) available on ENCODE and ConTraV3 (http://bioit2.irc.ugent.be/contra/v3/#/step/1) platforms (Kreft et al., 2017). For murine genes, GRCm39/mm39 assembly was chosen, and JASPAR Core 2022 and ReMap Atlas of Regulatory Regions ChIPseq data tracks (obtained for CH12 and MEL cells) were used for E2F1 binding predictions.

lncRNA genes were classified as direct E2F1 binders, associated to other E2F1 target, or non-binders whenever was possible to recognize E2F1 binding sites 500 bp at either side of the transcription start site, if this site was shared with another E2F1 target, or no E2F1 binding sites were found around this area, respectively.

2.11. Polysome profiling, ribosome sequencing (Ribo-seq) and polysome enrichment analysis

To evaluate whether T1-44-regulated lncRNAs are capable to be translated, Panc02 cells were seeded on 100 mm dishes and treated with DMSO and 1.0 μM T1-44 for 48 h. After this, cultures were treated with 100 μg/mL cycloheximide (CHX; Santa Cruz Biotechnology) for 10 min at 37°C + 5.0 % CO_2, trypsinized, washed with

cold PBS + 100 µg/mL CHX and resuspended in polysome extraction buffer (PEB; 20 mM Tris-HCl pH 7.4, 50 mM KCl, 10 mM $MgCl_2$, 1 mM DTT, 100 µg/mL CHX, 200 µg/mL heparin, 1x protease inhibitors (VWR), 1x RiboLock RNAse inhibitor (Thermo Fisher Scientific) and 1% Triton X-100). Tubes with PEB were maintained on ice for 10 min with frequent mixing by careful inversion and then centrifuged at 12,000 *g* for 10 min at 4°C. Total RNA amounts were quantified for each crude cytoplasmic lysate using a Nanodrop 2000 spectrophotometer (Thermo Fisher Scientific). Sucrose gradients were prepared the day before the experiments by gently overlaying 2 mL of 10-50% sucrose dilutions and allowed to linearize overnight at 4°C. Next, cytoplasmic lysates containing 300 µg RNA were added on top of the linearized gradients and fractionation was performed by ultracentrifugation using a SW40Ti rotor at 190,000 *g* for 1.5 h at 4°C (Optima XE-90 ultracentrifuge, Beckman Coulter). After this, twelve fractions were collected manually, and 254 nm absorbance was measured. RNA from each fraction was extracted using the Direct-zol RNA Mini Prep Plus (Zymo Research) kit according to the protocol provided by the manufacturer.

Then, RNA extracts from the sucrose fractions corresponding to polysomes (fractions 8 to 12) were combined together and sent to Genewiz for RNAseq. The obtained FASTQ files were uploaded to the Galaxy Europe (https://usegalaxy.eu/) server (Community, 2022), adapter removal was done using Cutadapt v.4.4 and reads quality was checked by FastQC v.0.12.1. For DEG analysis, initial mapping was performed by using STAR (v.2.7.10b), setting a 150-bp read length, and mm10 and GRCm39 as reference genome and GENCODE gene annotation versions, respectively. Normalized gene counts were obtained using featureCounts v.2.0.3 on the BAM files, and DESeq2 v.1.40.2 was used afterwards for DEG identification, with

an FDR < 0.01 as significance threshold. Heatmaps were generated using Z-scores on normalized counts, and volcano plots were made with adjusted *p* value < 0.01 and $|\log_2 FC| > 1.0$ as thresholds. DEG data were used for Gene Ontology (GO) analysis with Goseq v.1.26.0 considering $p < 0.05$ as significance cutoff.

DE lncRNA transcripts were identified using two approaches. First, Kallisto v.0.48.0 was used on FASTQ files, using GRCm39 as reference transcriptome, and transcripts were identified using the tximport v1.28.0 package on DESeq2 v.1.40.2 with FDR < 0.01 as significance threshold. In addition to the Kallisto/DESeq2 workflow, a second approach was performed using RNA STAR. Mapped data was assembled into transcripts using StringTie v2.2.3 with GRCm39 as reference transcriptome. Afterwards, assemblies were merged using GENCODE M32 as reference lncRNA annotation, gene counts were obtained using featureCounts v.2.0.3, and DESeq2 v.1.40.2 was performed establishing FDR < 0.01 as significance threshold for DE lncRNA transcripts. Results with the StringTie/FeatureCounts/DESeq2 workflow were used to generate lncRNA transcript heatmaps using Z-scores on TPM values, and top 20 up- and downregulated lncRNA transcripts were identified with FDR < 0.01 and $|\log_2 FC| > 1.0$ as cutoffs. For subsequent analysis, only the overlapping DE lncRNA transcripts between the Kallisto/DESeq2 and StringTie/FeatureCounts/DESeq2 approaches were used. These findings were validated *in vitro* by performing polysome enrichment analysis following the protocol described by Han *et al*., 2021 (Han et al., 2022) and the RT-qPCR protocols described in section 2.8 (*RT-qPCR*). Briefly, a list of overlapping DE lncRNA were chosen and their polysome enrichment profile (via % RNA) was established by performing RT-qPCR (primer sequences detailed in

Table 6) reactions on cDNA samples derived from the RNA extracts of each sucrose fraction. GAPDH and non-coding Y RNA 1 (RNY1) were used as positive and negative controls for polysomal enrichment, respectively.

Table 6. List of RT-qPCR primers used polysome enrichment analysis

Gene	Forward sequence (5'-3')	Reverse sequence (5'-3')
1700018L02Rik-201	CCAAAGAAACTGAAAACTGTGGGT	GGCGGGTGTATAGCTAGTTTCT
Gm42549-201	GCGAGAAGCAACCCCACTAT	AACAGGCAGTGTTAGCCTCC
ENSMUST00000203403.3	CGGTGGTACCGGGTGAAGA	ATCTTGGGGTTCATCTTGCTCT
D5Ertd615e-201	AACCTCTCAAGAAATCCTGAAGCA	AGAAGGCAGCACCAGGC
GAPDH	TTCATTGACCTCAACTACAT	GTGGCAGTGATGGCATGGAA
hY1	GGCTGGTCCGAAGGTAGTGA	GCAGTAGTGAGAAGGGGGGA

2.12. *In silico* lncRNA-derived peptides database creation and MHC-I binding prediction

Using the overlapping DE lncRNA transcripts from Ribo-seq analysis as starting point, complete cDNA sequences were obtained with Ensembl BioMart using GRCm39 dataset, and open reading frames (ORF) annotation was made using ORF Finder (https://www.ncbi.nlm.nih.gov/orffinder/) (Rombel et al., 2002), setting a minimal ORF of 75 nucleotides, standard genetic code and detection of both canonical (*i.e.* ATG) and alternative (*i.e.* CTG and TTG) ORF start codons. Once the sequences of standard and nested ORFs were obtained, datasets for lncRNA-derived peptides were created using EMBOSS Transeq for *in silico* translation (Madeira et al., 2022). Afterwards, the binding affinity of these predicted lncRNA-derived peptides to the major histocompatibility complex class I (MHC-I) haplotypes of C57BL/6 mice (H-2Kb and H-2Db) was assessed using NetMHCpan 4.1a (Reynisson et al., 2020). The resulting list of strong H-2Db/Kb binders was used for the design of a cancer vaccine prototype.

2.13. lncRNA ORF cloning

To determine whether *in silico*-predicted lncRNA-derived ORFs can be translated, the sequence of a representative lncRNA transcript, 1700018L02Rik-201, was amplified using Phusion High Fidelity DNA Polymerase (New England Biolabs) with suitable PCR primers (forward primer: 5'-ACTGACGAATTCCAGAGGTCAAACATACTAGCTCC-3'; reverse primer: 5'-ACTGACCTCGAGAAAAGCCTTACTTCCACCCCT-3') that covered the ORF sequence plus 30-bp of the upstream region (to include any potential ribosome binding sites), and *EcoRI*/*XhoI* restriction sites. This insert was cloned into the C-terminus FLAG-tagged vector pSF-CMVNEO-COOH-3xFLAG (OxGene) as previously described (Barczak et al., 2023). After cloning was confirmed by sequencing, Panc02 cells were transfected with the generated construct for 48 h, after which total protein was extracted and FLAG was detected by immunoblotting (F1804, 1:1000 dilution, Merck Millipore). A previously described E2F1-FLAG construct (Barczak et al., 2023) was used as positive control.

2.14. ChAdOx1 vaccine manufacturing

Once the translation potential and the binding to H-2Db and H-2Kb was confirmed, a list of lncRNA-derived candidate peptides was chosen for vaccine design. The poly-antigenic cassette was created by combining the lncRNA-derived peptide sequences with their 4 flanking amino acids into one string with Kozak,

codon start and tPA sequences added at its 5' end. This cassette, named PepLncP2, consisted of 28 T1-44-induced lncRNA-derived peptides plus a double stop codon. The complete cassette, each of the lncRNA-derived 9-mers, their bridging sequences, and bridges plus following 9-mer sequences were crossed-referenced against both human and murine UniProtKB/Swiss-Prot databases using NCBI BLAST to validate that no homology with other protein-coding sequences was found.

The complete cassette was optimised using GeneArt (Thermo Fisher Scientific) by Viral Vector Core Facility (Pandemic Sciences Institute, University of Oxford), to enhance translatability and prevent recombination before starting the synthesis and cloning process into the replication-deficient chimpanzee adenovirus vector ChAdOx1. Briefly, the transgene was cloned into pC1936 24ADUFVD_3931316 plasmid, and this construct and the entry vector p1990 were digested with *KpnI/NotI* to obtain the insert sequence and its corresponding backbone, respectively. After agarose gel electrophoresis and gel DNA extraction, the sequences were ligated and transformed into DH10b chemically competent *E. coli* cells (Thermo Fisher Scientific). After colony selection using kanamycin and subsequent DNA extraction, the obtained clone of the pC1937 pENTR4LPTOS-PepLncP2 plasmid was cloned into the destination vector ChAdOx1 (p2563) using LR clonase II (Thermo Fisher Scientific). This product was used for DH10b transformation, plating, kanamycin + chloramphenicol selection and colony PCR to choose a single clone to be used to prepare the BAC vector pC1938 pChAdOx1-PepLncP2. The resulting DNA was sequenced before proceeding with *PmeI* digestion and linearisation. After confirmation, linearised pChAdOx1-PepLncP2

was transfected into T-REx™-293 cells (Thermo Fisher Scientific) for virus production. Integrity of the virus expansion and recovery was checked for sterility and infectious units (IU) quantification via immunostaining. The presence of the PepLncP2 antigen was confirmed by identity PCR, and Flank-Flank PCR was used to check the integrity of the antigenic DNA sequence and the absence of any other contaminating Adenovirus. A diagram of this vaccine and the details of its DNA and peptide sequence are detailed in Appendix II. ChAdOx1-GFP was used as control condition for any subsequent experiment using the ChAdOx1-PepLncP2 vaccine.

2.15. Intracellular pH measurements

All experiments related to pH regulation and O_2 consumption were performed at the Laboratory of Proton Dynamics in collaboration with Professor Pawel Swietach (Department of Physiology, Anatomy and Genetics, University of Oxford). These experiments were performed according to the guidelines for pH control in live cell cultures (Michl et al., 2019). Briefly, Panc-1 and Panc02 cells were seeded in triplicate (Panc-1: 10,000 cells/well; Panc02: 5,000 cells/well) in clear bottom black 96-well µ-plates (Ibidi) and left to attach overnight. Then, cells were treated with T1-44 (1.0 and 5.0 µM), Δ25 ASO (200 nM) and a combination of 1.0 µM T1-44 and 200 nM Δ25 ASO for 48 h. DMSO, 2.5 µM CisP (as reported previously for pH_i measurements in the literature (Shirmanova et al., 2017)) and 200 nM scrambled ASO were used as controls for treatment, mechanism of action and ASO transfection, respectively. On the day of imaging, cells were labelled for 15 min with a sDMEM solution containing 5 µg/mL cSNARF-1 AM (Invitrogen) and 1.0 µg/mL

Hoechst 33342 (Invitrogen). Then, loading medium was discarded and wells were washed twice with pre-equilibrated phenol-red free DMEM (Sigma-Aldrich) with varying sodium bicarbonate (Sigma-Aldrich) concentrations corresponding to different pH points at 37ºC and 5.0% CO_2. The formulation of these physiologically-buffered (HCO_3^-/CO_2) media is detailed in Table 7. After washing, media was added to the wells for a third time and plates were imaged in a Cytation 5 (Biotek) plate reader.

For imaging, bicarbonate-buffered plates were set up at 37°C and 5.0% CO_2, delaying imagining by 30 min to allow for media to equilibrate. Fluorescence images (10x) of each well were acquired using the appropriate excitation (λ_{ex}) and emission (λ_{em}) wavelengths for each dye, specifically cSNARF-1, λ_{ex} = 531 nm and λ_{em} = 590 and 640 nm, and Hoechst 33342, λ_{ex} = 377 nm and λ_{em} = 447 nm.

To assess that the T1-44 regulation of pH_i was bicarbonate-dependent, pH imaging was performed using media containing a non-volatile buffering (NVB) system composed of 10 mM HEPES (Sigma-Aldrich) and 10 mM MES (Sigma-Aldrich) followed by pH adjustments at 37°C (pH points used are detailed in Table 7). For these experiments, imaging was done in a CO_2-free atmosphere.

Image analysis, cSNARF-1 fluorescence ratios, conversion to pH_i and pH_i distribution adjusted to cell number was performed using MATLAB scripts written by Prof. Swietach (Blaszczak et al., 2022; Michl et al., 2023).

Table 7. sDMEM formulations used to prepare pH-adjusted media

General components		
Reagent	**Concentration**	**Manufacturer**
Glucose	25 Mm	Sigma-Aldrich
FBS	10%	Thermo Fisher Scientific
Glutamine	2 mM	Gibco
Sodium pyruvate	1 mM	Gibco
Penicillin/Streptomycin solution	1%	Gibco
Formulations for $NaHCO_3$ / 5.0% CO_2 buffering		
$NaHCO_3$ concentration (mM)	**NaCl concentration (mM)**	**pH (37ºC + 5.0% CO_2)**
44.00	0.00	7.71
22.00	22.00	7.41
11.00	33.00	7.11
5.50	38.50	6.81
2.75	41.25	6.51
0.00	44.00	6.20
Formulations for HEPES / MES buffering		
HEPES concentration (mM)	**MES concentration (mM)**	**Adjusted pH (37ºC)**
10.00	10.00	8.05 7.89 7.43 7.07 6.52 6.02

2.16. Extracellular pH (pH_e) and O_2 consumption measurements

The effect of T1-44 and Δ25 ASO on H^+ production (associated with pH_e) and O_2 consumption was established using a surrogate protocol described previously for glycolytic and oxidative metabolism measurements (Blaszczak et al., 2021). This protocol uses the combination of the ratiometric fluorescent pH sensor 8-hydroxypyrene-1,3,6-trisulfonic acid (HPTS, Sigma-Aldrich), and the O_2-quenched fluorophore tris(2,2'-bipyridyl)dichlororuthenium(II) (RuBPY, Sigma-Aldrich) to report extracellular pH and O_2 levels. In addition, CellTracker Orange (CTO; Invitrogen) was included for cell number normalization. Black 96-well plates (Greiner) were seeded with Panc-1 and Panc02 cells following a RBD performed at the same day of the experiment, and after an overnight incubation, cells were

treated with T1-44 and Δ25 ASO as previously described (Section 2.15, *Intracellular pH (pH_i) measurements*). To perform the assessments, cells were loaded with 25 μM CTO for 15 min. Then, loading medium was discarded and the plates were washed with low-buffering medium (sDMEM containing 2.9 mM $NaHCO_3$/41 mM NaCl or 2 mM HEPES/2 mM MES for physiological and NVB, respectively). Next, a labelling solution consisting of 2 μM HPTS/50 μM RuBPY in low-buffering medium was added onto the plate and sealed by adding mineral oil (Sigma-Aldrich) to control O_2 diffusion. Then, plates were put in a Cytation 5 (Biotek) plate reader and fluorescence readings were collected every 10 min for 17 h at five $\lambda_{ex}/\lambda_{em}$ channels (Ch1: 540/580 nm for CTO; Ch2: 400/510 nm and Ch3: 460/510 nm for HPTS; and Ch4: 416/510 nm and Ch5: 450/620 nm for RuBPY). The set-up conditions for the plate reader were 37ºC, 21% O_2, and 0.0% or 0.5% CO_2 for NVB and HCO_3^-/CO_2 buffering conditions, respectively.

pH_e, O_2 percentage, and cumulative H^+ production and O_2 consumption data were calculated based on fluorometric measurements using MATLAB macros described in previous reports (Blaszczak et al., 2021; Blaszczak et al., 2024; Michl et al., 2022).

2.17. Lipid peroxidation assay

To evaluate if the effects of T1-44 and Δ25 ASO on pH_i/pH_e dynamics have functional implications on the activity of other drugs, PDAC cells were seeded on 100 mm dishes following the protocol stated in section 2.5 (*Cell cycle analysis*). After attachment, culture medium was replaced with physiological low-buffering

sDMEM prepared as described in section 2.16 (*Extracellular pH (pH_e) and O_2 consumption measurements*) and cells were treated for 48 h with different combinations of T1-44 and Δ25 ASO, and Dox, a weakly basic drug (pK_a = 8.2) (Yamada, 2020). Lipid peroxidation, a well-known cellular effect of Dox associated with its pro-oxidative mechanism of action (Alhowail et al., 2019), was measured by using the Lipid Peroxidation Assay Kit (Abcam). The assay detects non-peroxidised (PE) and peroxidised (FITC) lipids by staining with a proprietary ratiometric dye. After treatment, cells were harvested via trypsinization and stained with the lipid peroxidation sensor for 30 min. Next, cells were washed and FITC and PE mean fluorescent intensity (MFI) was acquired using an Accuri C6 flow cytometer (Beckton Dickinson). Lipid peroxidation was established by calculating the PE/FITC ratio of each experimental condition. As a positive control, cells were treated with 250 μM H_2O_2 for 30 min.

2.18. *In vivo* immunogenicity testing

Two groups of five 8-weeks-old female C57BL/6 mice (Charles River Laboratories) were intravenously vaccinated with a single 1.25 x 10^8 IU dose of ChAdOx1-PepLncP2 suspended in 100 μL PBS, and ChAdOx1-GFP, which was used as control carrying an irrelevant antigen (GFP). At 10 days post-vaccination, animals were culled and their spleens were collected. Animals were housed at the Biomedical Sciences Building, University of Oxford under pathogen-free conditions, and experiments were performed by Dr Wiktoria Blaszczak under the UK Home

Office licence PP6528177 in agreement with the UK Animal (Scientific Procedures) Act 1986.

One day before the endpoint, multiscreen 96-well plates with hydrophobic PVDF membranes (Merck Millipore) were incubated overnight at 4ºC with anti-mouse IFNγ capture antibody (clone AN18, 3321-3-1000, 1:200 dilution, MabTech) solution in PBS. After incubation, wells were washed four times with PBS and blocked with R10 solution (RPMI medium supplemented with 10% FBS and 1% P/S) for 2 h at 37ºC. For splenocyte extraction, the organs were passed through a 70 µm cell strainer (Merck Millipore) using sterile syringe plungers, the filters were washed with PBS, and the obtained single-cell suspensions were pelleted by centrifugation. To remove red blood cells, pellets were vigorously resuspended with ACK lysing buffer (Gibco), and reaction was stopped after 1 min by adding R10 followed by a 400 *g* for 4 min centrifugation at room temperature. Cell pellets were resuspended again in R10, counted, and the cell concentration was adjusted to 3 x 10^6 cells/mL, and 50 µL of cell suspension (1.5 x 10^5 cells) was added to each well. Cells were stimulated with a pool of the 28 PepLncP2 peptides (synthetised by GeneScript, each peptide at a 10 µg/mL final concentration), and DMSO and phytohemagglutinin-L (PHA; Roche) dilutions were used as negative and positive controls, respectively. The cells were incubated overnight at 37ºC + 5.0% CO_2, then contents were discarded, wells were washed 7 times with PBS and treated for 4 h at room temperature with a biotin-conjugated anti-mouse IFNγ detection antibody (clone R4-6A2-Biotin, 3321-6-1000, 1:2000 dilution, MabTech) resuspended in 2.5% BSA in PBS solution. After this, wells were washed 4 times with PBS and then treated for 2 h at RT with an alkaline phosphatase-conjugated anti-biotin secondary

antibody (SP-3020, 1:1000 dilution, Vector Labs) in 2.5% BSA in PBS solution. To develop the reaction, wells were washed 4 times with PBS and then treated for 15 min at RT with 50 µL of a BCIP/NBT substrate solution (Thermo Fisher Scientific) per well. Colour development was stopped by discarding the BCIP/NBT solution and washing the plate 3 times with tap water. Then, the rubber bottom of the plate was removed, and the plate was air dried overnight. Spots were quantified using an S6 Universal M2 ELISpot scanner (ImmunoSpot. Cellular Technology Limited).

2.19. Anticancer effects of PRMT5 inhibition *in vivo*

These experiments were outsourced to Charles River Laboratories (Freiburg, Germany) and were conducted under the approval of the Charles River Animal Care and Use Committee in accordance with the German National Committee for the Protection of Animals Used for Scientific Purposes. To assess the effects of T1-44 in a syngeneic tumour model, 52 6-8-weeks-old female C57BL/6 mice were injected subcutaneously with 5×10^6 Panc02 cells suspended in 100 µL of a 1:1 Matrigel:PBS mixture. Once tumour volumes reached 50-150 mm^3, the mice were randomized to one of the following daily oral treatment groups (12 mice per group): 100 mg/Kg T1-44 dissolved in a 5.0% DMSO, 0.5% Tween 80 in water solution as vehicle, vehicle only, and vehicle plus *ad libitum* bicarbonate water (positive control designated to remove acidosis within the TME (Lin et al., 2024; Pilon-Thomas et al., 2016)).

Body weight and tumour volume measurements were taken twice per week. Ulceration, tumour volumes exceeding 1200 mm^3 and weight loss over 30% were causes of early termination. Within each group, four animals were treated until day 8, and 12 h after the final dosing, the animals were intravenously injected with FITC-

conjugated pH-low insertion peptide (FITC-pHLIP; MedChemExpress; 1 µmol/Kg, 200 µM in 2% DMSO in PBS) to stain acidic niches as reported previously (Michl et al., 2024; Reshetnyak et al., 2011). 20 minutes after injection, animals were sacrificed and their tumours harvested.

Tumours were snap frozen and used for RT-qPCR evaluation of SLC4A7 expression and exon 25 skipping, and for acidic niches imaging. The remaining animals were maintained until 16 days of treatment, tumour volume and body weight measurements were taken until this point, and four tumour formalin-fixed paraffin-embedded (FFPE) samples per group were collected for analysis of the TME.

2.20. Immunofluorescent detection of acidic niches

Snap-frozen tumour samples collected from animals injected with the FITC-pHLIP probe were processed in the Histology Facility of the Department of Physiology, Anatomy and Genetics, University of Oxford. Samples were embedded in optimal cutting temperature (OCT) sectioning medium (Thermo Fisher Scientific) and stored at -80ºC overnight. After this, 10-µm tissue sections were cut using a cryostat, mounted on gelatine-coated slides and post-fixed for 10 min with 4% paraformaldehyde (Sigma-Aldrich). Sections were mounted using antifade agent containing Hoechst 33342 (Thermo Fisher Scientific) and sealed with coverslips before imaging.

Images were acquired at the Laboratory of Proton Dynamics in collaboration with Professor Pawel Swietach (Department of Physiology, Anatomy and Genetics, University of Oxford) using a Zeiss LSM 700 confocal microscope with an EC Plan-Neofluar 40x/1.30 Oil M27 objective. All images were taken using the following settings, chosen from samples with positive acid niches staining: 8-bit, 1,024 x 1,024 pixels, averaging of 16 captures, pinhole between 3.90 and 3.95 Airy units, gain between 755 and 835 V, and laser power between 1.2 and 2.4%. Image export was made using ZEN 2.3 SP1 (Carl Zeiss) and figures were assembled using Adobe Photoshop CS5 (Adobe Systems). Image analysis was performed using a MATLAB macro written by Professor Swietach to assess the mean florescence of FITC normalised to cell number (based on the number of nuclei) between all treatment conditions and samples. In parallel, whole-slide scanning of the tumour samples was outsourced to the Translational Histopathology Lab, Department of Oncology, University of Oxford.

2.21. Immunohistochemical staining

Tumour FFPE samples were sectioned by the Translational Histopathology Lab (Department of Oncology, University of Oxford). Four-µm sections were washed three times for 5 min with HistoChoice (Sigma-Aldrich), followed by two 10-min washes with 100% ethanol, 95% ethanol and distilled water. Sections were incubated for 20 min at 99°C with a sodium citrate pH 6.0 or Tris-EDTA pH 9.0 buffer (Abcam) for antigen retrieval, then washed three times with distilled water for 5 min each, incubated for 10 min with a freshly-prepared 3% H_2O_2 solution, then washed

twice for 5 min with water and PBS-T. Non-specific binding was blocked by incubation with animal-free blocking solution (Cell Signalling Technologies) for 1 h at RT, and incubated overnight at 4°C with the following primary antibodies: CD4 (ab183685, 1:8,000 dilution, Abcam), CD8 (ab237723, 1:500 dilution, Abcam), granzyme B -GZMB- (46890S, 1:100 dilution, Cell Signalling Technologies), PRMT5 (79998S, 1:400 dilution, Cell Signalling Technologies) and SDMe (13222S, 1:5,000 dilution, Cell Signalling Technologies). As background signal control, sections were incubated with a rabbit IgG isotype control (3900S, Cell Signalling Technologies) using a similar concentration as the one used for primary antibodies (≈ 25 µg/mL).

After incubation, sections were washed three times for 5 min with PBS-T, incubated for 30 min at RT with HRP-conjugated secondary antibody (SignalStain Boost Detection Reagent Rabbit IgG, Cell Signalling Technologies). Sections were then washed three times for 5 min with PBS-T and incubated with diaminobenzidine (DAB) substrate solution (SignalStain DAB substrate kit, Cell Signalling Technologies) for 10 min. Slides were washed in distilled water and counterstained with a Haematoxylin solution (Sigma-Aldrich) for 60 seconds. After washing sections twice for 5 min with distilled water, the excess of liquid was gently dried, and samples were mounted with Aquatex (Sigma-Aldrich) and allowed to dry for at least 2 h before imaging. Image acquisition was performed using a Leica Mica widefield microhub using a Leica HC PL Fluotar L 40x/0.6 dry objective. Representative images from four different regions of each sample were taken. Image analysis was performed as described by Crowe and Yue (2019) using ImageJ 1.54d software (National Institutes of Health) with the Colour Deconvolution 2 plugin (Landini et al., 2020) to separate and analyse each staining independently.

Individual DAB and haematoxylin images were subsequently used to determine mean pixel density and nuclei count, respectively, and semi-quantitative results were shown as percentage of DAB pixel density/nuclei.

2.22. ChAdOx1-PepLncP2 tumour challenge

With the aim to evaluate the effects of ChAdOx1-PepLncP2 vaccination on tumour growth, two groups of ten 8-weeks-old female C57BL/6 mice received a single 1.25 x 10^8 IU dose of ChAdOx1-PepLncP2 or ChAdOx1-GFP (used as control condition). 13 days after vaccination, tumour implantation was performed by injecting animals with a subcutaneous dose of 5 x 10^5 Panc02 cells suspended in 100 µL of a 1:1 PBS:Vitrogel (TheWell Bioscience) mixture. After this, animals were maintained for 25 days, taking body weight and tumour volume measurements twice per week and collecting spleen samples for ELISpot evaluation. Animals were housed at the Biomedical Sciences Building, University of Oxford under pathogen-free conditions, and experiments were performed by Dr Wiktoria Blaszczak under the UK Home Office licence PP6528177 in agreement with the UK Animal (Scientific Procedures) Act 1986.

2.23. Statistical analysis

Analyses were performed and graphs made using GraphPad Prism version 10.4.1. Shapiro-Wilk and Bartlett tests were performed to confirm normal distribution and homoscedasticity, respectively. Parametric analysis was executed

by using two-tailed unpaired Student's t-test (or Mann–Whitney test as non-parametric alternative) for the comparison of two groups, and ANOVA or Kruskal-Wallis were used as parametric and non-parametric tests for multiple groups comparisons. For all these cases, data are presented as mean ± SD, unless stated otherwise. Level of significance was defined at $\alpha = 0.05$, and *p*-values were indicated on figures using asterisks as follows: (*) for $0.01 \leq p < 0.05$, (**) for $0.001 \leq p < 0.01$, (***) for $0.0001 \leq p < 0.001$, and (****) for $p < 0.00001$.

Chapter 3 : Effects of PRMT5 inhibition on PDAC cell proliferation and SDMe

3.1. Introduction

It has been proven that PRMT5 regulates gene expression, epigenetics, RNA splicing and the metabolic profile of cancer cells through its interaction with transcription factors which, like E2F1, are often deregulated in cancer (Barczak et al., 2020; Ge et al., 2020; Qin et al., 2019; Roworth et al., 2019). Among the transcriptional changes induced by PRMT5 inhibition, modifications in long non-coding RNA (lncRNA) expression appear as a promising target due to their involvement in different functions associated with PDAC survival. For example, LINC00673-derived protein RASON enhances oncogenic RAS signalling (Cheng et al., 2023), and the CF129-induced degradation of p53 (Liu et al., 2019). Additionally, it has been reported that resistance to gemcitabine mediated by PVT1-induced Wnt/β-catenin activation can be reversed using PRMT5 inhibitors (Wei et al., 2020; Zhou et al., 2020). Furthermore, the use of the selective PRMT5 inhibitor T1-44 and changes in E2F1 expression modified the transcriptional and translational profiles of lncRNA (Barczak et al., 2023). These changes induced a number of immunogenic lncRNA-derived peptides which, formulated in a poly-antigen cassette and included in an adenoviral vector, were capable to activate immune response and reduce tumour growth *in vivo* (Barczak et al., 2023). Considering these previous results in CRC, and the relevance of PRMT5 and E2F1 in various aspects of tumour survival, the following chapter is focused on characterizing the general effects of

PRMT5 inhibition in human and murine PDAC models and the involvement of E2F1 in these responses. This chapter describes a general landscape of T1-44-driven effects on PDAC cell lines.

3.2. Results

3.2.1. T1-44 supresses SDMe mark without compromising cell viability in PDAC cells

In previous work from our research group, T1-44 was shown to be an effective PRMT5 inhibitor capable to suppress SDMe in breast and CRC cell models (Barczak et al., 2023; Barczak et al., 2020). Using similar conditions to those studies, T1-44 suppressed SDMe signal after incubating both parental Panc-1 and Panc02 cells for 48 h with 1.0 and 5.0 μM T1-44 without altering E2F1 and PRMT5 immunodetection (Figure 3.1B). After this confirmation, T1-44 effects were evaluated using MTT assay, confirming that the chosen concentrations did not affect cell survival of Panc-1 (IC_{50} = 16.06 ± 3.44 μM) and Panc02 (IC_{50} = 14.24 ± 2.07 μM) cells (Figure 3.1A). These IC_{50} values declined progressively as incubation time increased. Later, effects on cell cycle and apoptosis were tested, finding that T1-44 treatment conditions did not induce any significant changes on these responses (Figure 3.1C).

To provide additional confirmation that 48-h T1-44 treatments did not induce any changes in cell viability, a set of growth curves were performed, finding that 48-h incubations with 1.0 μM T1-44 did not compromise the growth rate of any of the studied cell lines, but PRMT5 inhibition reduced cell growth when treatments extended from 4 to 8 days (Figure 3.1D).

Altogether, these results show that 48-h treatments with T1-44 at concentrations below 5.0 μM are capable to supress SDMe without affecting cell survival, growth, cell cycle, and apoptosis profiles of Panc-1 and Panc02 cells. In line with the main objective of this thesis, which aims to establish the use of T1-44 as a potential immunosensitising agent, but not as an antiproliferative drug *per se*, the aforementioned concentration range was considered to establish an optimal concentration to evaluate the effects of T1-44 in gene expression and splicing. Furthermore, the involvement of E2F1 in these biological responses is going to be described in the following subsection.

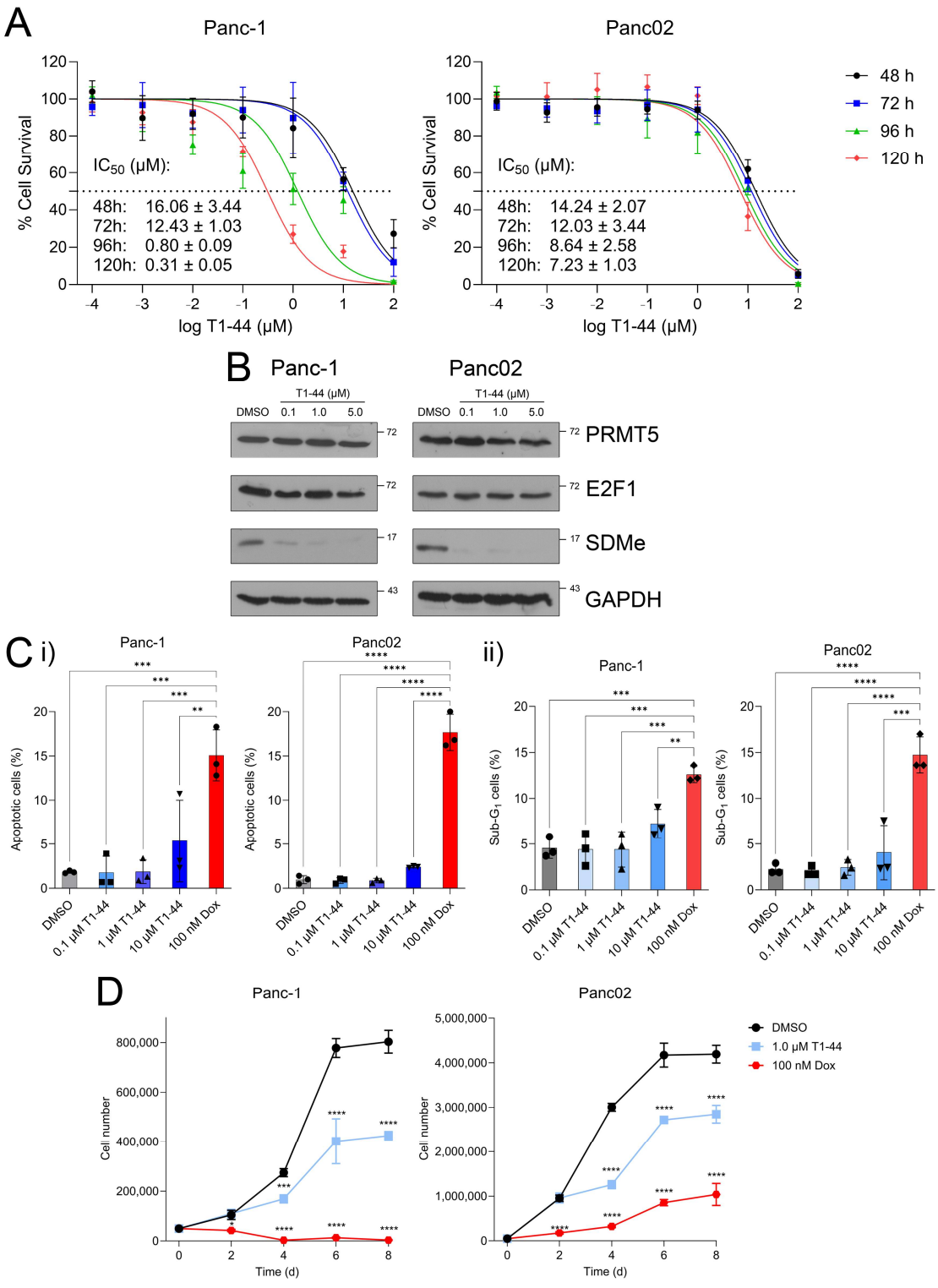
A
Panc-1
Panc02
% Cell Survival
log T1-44 (μM)
IC50 (μM):
48h: 16.06 ± 3.44
72h: 12.43 ± 1.03
96h: 0.80 ± 0.09
120h: 0.31 ± 0.05
48h: 14.24 ± 2.07
72h: 12.03 ± 3.44
96h: 8.64 ± 2.58
120h: 7.23 ± 1.03
48 h
72 h
96 h
120 h
B
Panc-1
Panc02
T1-44 (μM)
DMSO 0.1 1.0 5.0
PRMT5
E2F1
SDMe
GAPDH
C i)
Panc-1
Panc02
Apoptotic cells (%)
ii)
Sub-G1 cells (%)
DMSO
0.1 μM T1-44
1 μM T1-44
10 μM T1-44
100 nM Dox
D
Panc-1
Panc02
Cell number
Time (d)
DMSO
1.0 μM T1-44
100 nM Dox

Figure 3.1. Effects of PRMT5 inhibition in parental Panc-1 and Panc02 cells. ***A.*** *Median inhibitory concentrations obtained for parental Panc-1 (left) and Panc02 (right) cells treated with T1-44 for 48 to 120 h. Cell survival percentages are relative to the DMSO-treated control; n = 4 independent experiments performed in technical triplicates. Results are expressed as mean ± SD.* ***B.*** *Representative immunoblot for the same cellular models after treating cells with T1-44 for 48 h. SDMe was used as a general marker of T1-44 activity; n = 3 independent experiments.* ***C.*** *Percentage of apoptotic cells and sub-G1 cells obtained after annexin V/PI staining (i) and cell cycle profiling (ii) experiments for parental Panc-1 and Panc02 cells treated with T1-44 for 48 h. Doxorubicin was used as positive control for these experiments; n = 3 independent experiments performed in technical duplicates. Results are expressed as mean ± SD; one-way ANOVA with Tukey's multiple comparisons;* ** *p < 0.001,* *** *p < 0.0001,* **** *p < 0.00001.* ***D.*** *Proliferation curves representing T1-44 treatment of parental Panc-1 and Panc02 cells from 2 to 8 days. Doxorubicin was used as positive control for these experiments; n = 3 independent experiments performed in technical duplicates. Results are expressed as mean ± SD; one-way ANOVA with Tukey's multiple comparisons;* *** *p < 0.0001,* **** *p < 0.00001.*

3.2.2. Loss of E2F1 reduces PDAC cell sensitivity to PRMT5 inhibition

To evaluate the influence of E2F1 status in the response of Panc-1 and Panc02 cells to T1-44, Cas9 and E2F1Cr clones were generated. Loss of E2F1 was confirmed via Western blot (Figures 3.2B and 3.3B), and with the aim to find treatment conditions that do not impact cell proliferation, a range of T1-44 concentrations was assessed using MTT assay. Both Panc-1 and Panc02 E2F1Cr cells exhibited IC_{50} ≈ 2-fold higher than their Cas9 counterparts after a 48-h T1-44 treatment (Figure 3.2A and Figure 3.3A, respectively), maintaining this tendency when 72 h, 96 h and 120 h incubations were performed.

When the apoptotic response was analysed, it was found that there were no significant differences between the proportion of apoptotic cells obtained after treating Cas9 and E2F1Cr cells with DMSO or 1.0 μM T1-44 for 2, 4, 6 and 8 days (Figure 3.2Ci and Figure 3.3Ci). Conversely, when these treatment conditions were used for cell cycle profiling, an increase in the percentage of cells in Sub-G1 phase

after T1-44 treatment was observed for both Cas9 and E2F1Cr. Significant changes were observed for treatments lasting 4 days and longer in both Panc-1 Cas9 and E2F1Cr cells (Figure 3.2Cii), after 6 and 8 days for Panc02 Cas9, and only at 8 days of treatment for Panc02 E2F1Cr cells (Figure 3.3Cii). These results are in accordance with those obtained for growth curves, where 1.0 μM T1-44 reduced cell growth from 4-day incubations onwards in Cas9 Panc-1 and Panc02 cells. Conversely, the sensitivity to these effects was reduced in E2F1-knockout cells, observing a growth rate reduction in Panc-1 E2F1Cr and Panc02 E2F1Cr cells only after 6 and 8 days of T1-44 treatment, respectively (Figures 3.2D and Figure 3.3D).

In summary, these experiments show that, in the absence of E2F1, Panc-1 and Panc02 cells exhibit reduced sensitivity to PRMT5 inhibition, altering their cell proliferation, growth, cell cycle and apoptosis responses to T1-44 treatment.

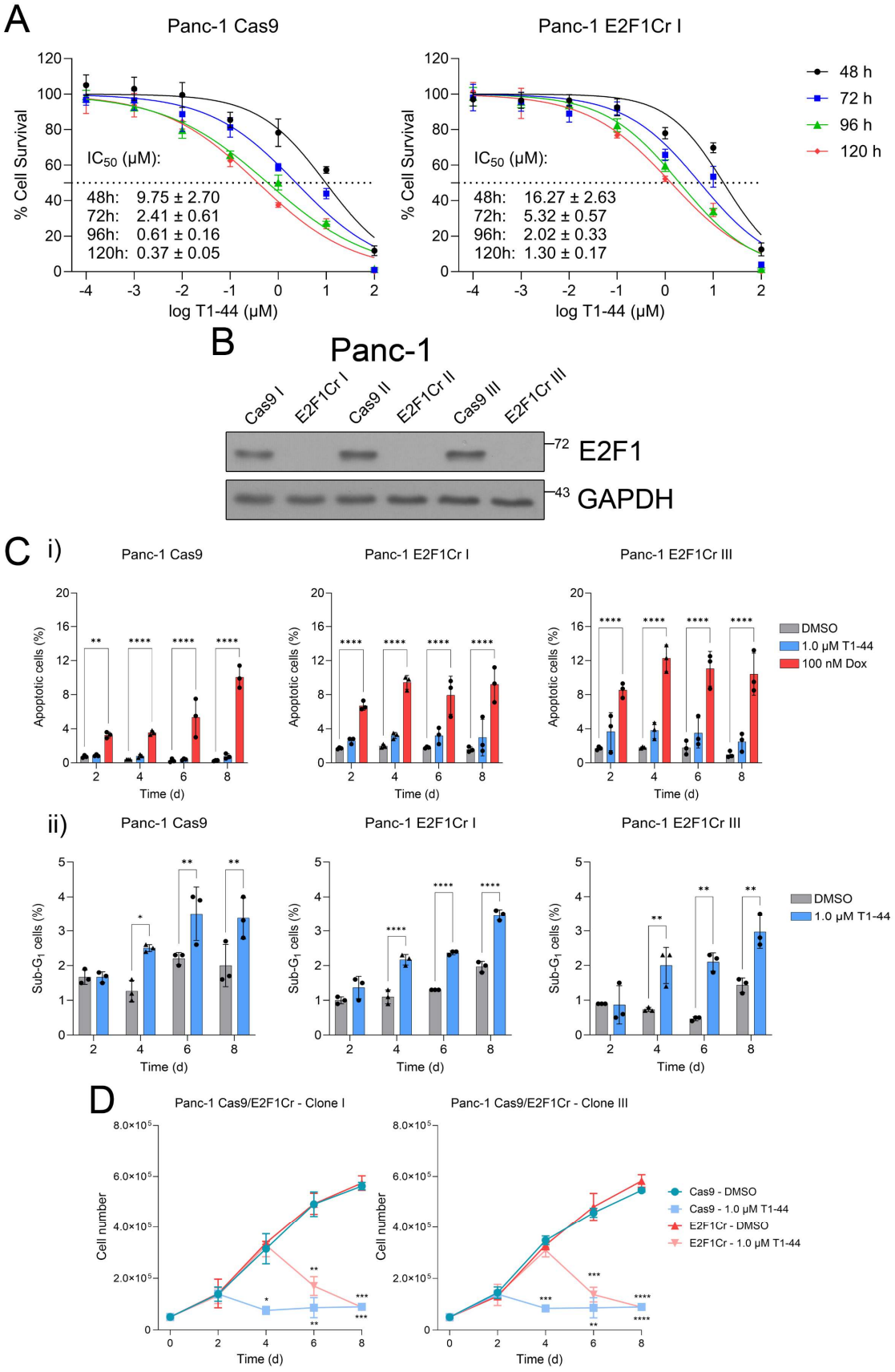
A
Panc-1 Cas9
Panc-1 E2F1Cr I
% Cell Survival
log T1-44 (μM)
IC50 (μM):
48h: 9.75 ± 2.70
72h: 2.41 ± 0.61
96h: 0.61 ± 0.16
120h: 0.37 ± 0.05
48h: 16.27 ± 2.63
72h: 5.32 ± 0.57
96h: 2.02 ± 0.33
120h: 1.30 ± 0.17
48 h
72 h
96 h
120 h
B
Panc-1
Cas9 I
E2F1Cr I
Cas9 II
E2F1Cr II
Cas9 III
E2F1Cr III
72
E2F1
43
GAPDH
C
i)
Panc-1 Cas9
Panc-1 E2F1Cr I
Panc-1 E2F1Cr III
Apoptotic cells (%)
Time (d)
DMSO
1.0 μM T1-44
100 nM Dox
ii)
Sub-G1 cells (%)
DMSO
1.0 μM T1-44
D
Panc-1 Cas9/E2F1Cr - Clone I
Panc-1 Cas9/E2F1Cr - Clone III
Cell number
Cas9 - DMSO
Cas9 - 1.0 μM T1-44
E2F1Cr - DMSO
E2F1Cr - 1.0 μM T1-44

Figure 3.2. Effects of PRMT5 inhibition in Cas9 and E2F1Cr Panc-1 cells.
A. *Median inhibitory concentrations obtained for a representative clone of Cas9 (left) and E2F1Cr (right) Panc-1 cells treated with T1-44 for 48 to 120 h. Cell survival percentages are relative to the DMSO-treated control; n = 4 independent experiments performed in technical triplicates. Results are expressed as mean ± SD.* ***B.*** *Representative immunoblots to evaluate the E2F1 signal of three stable Cas9 and E2F1Cr clones of Panc-1 cells; n = 3 independent experiments.* ***C.*** *Percentage of apoptotic cells and sub-G1 cells obtained after annexin V/PI staining (i) and cell cycle profiling (ii) experiments for Cas9, and two clones of E2F1Cr Panc-1 cells treated with T1-44 for 2 to 8 days. Doxorubicin was used as positive control for annexin V/PI experiments; n = 3 independent experiments performed in technical duplicates. Results are expressed as mean ± SD; one-way ANOVA with Tukey's multiple comparisons; * $p < 0.05$, ** $p < 0.001$, *** $p < 0.0001$, **** $p < 0.00001$.* ***D.*** *Proliferation curves representing T1-44 treatment of Cas9 and two clones of E2F1Cr Panc-1 from 2 to 8 days; n = 3 independent experiments performed in technical duplicates. Results are expressed as mean ± SD; one-way ANOVA with Tukey's multiple comparisons;* $^{*}p < 0.05$, $^{**}p < 0.001$, $^{***}p < 0.0001$, $^{****}p < 0.00001$.

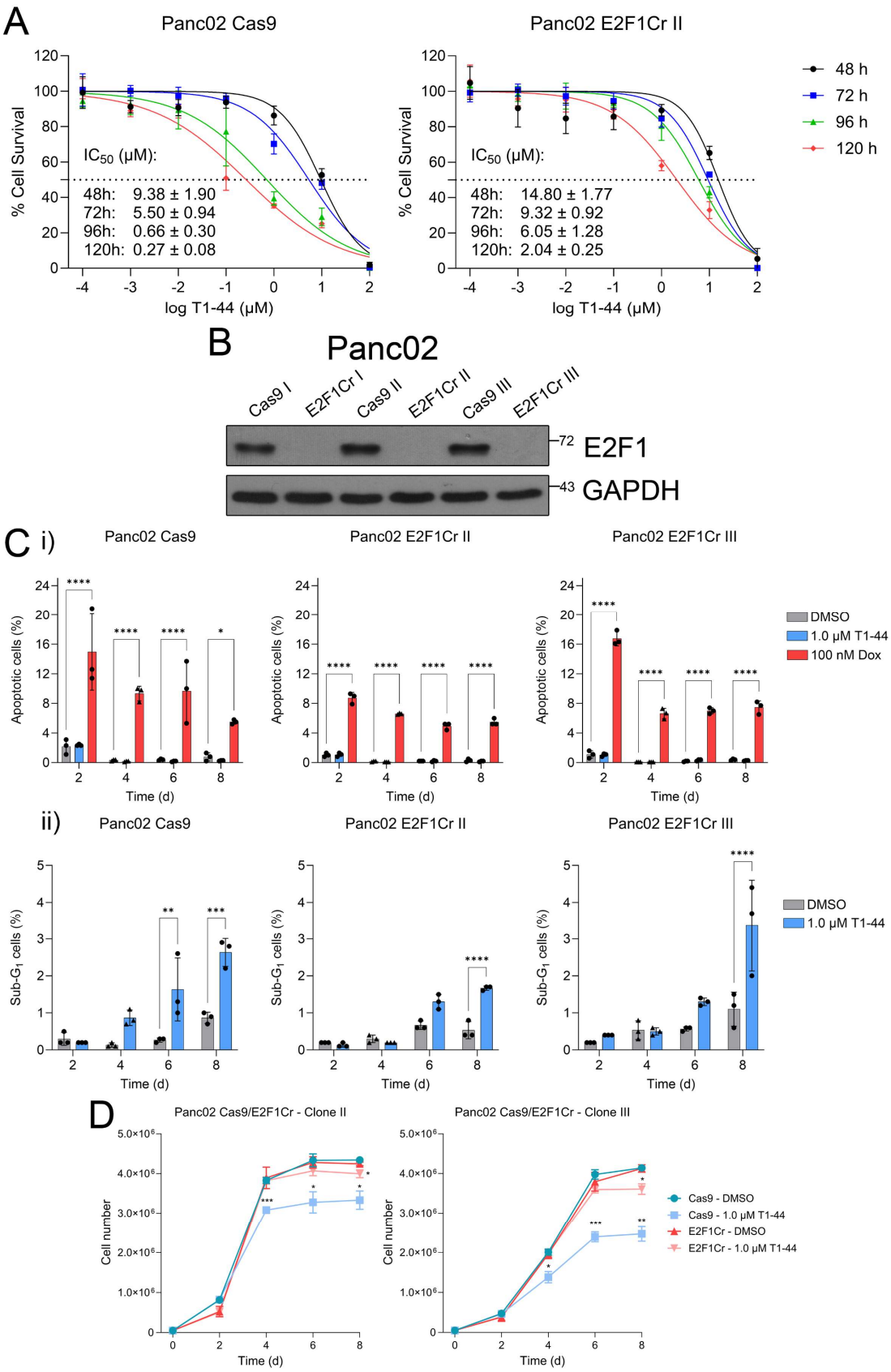
A
Panc02 Cas9
Panc02 E2F1Cr II
% Cell Survival
IC50 (μM):
48h: 9.38 ± 1.90
72h: 5.50 ± 0.94
96h: 0.66 ± 0.30
120h: 0.27 ± 0.08
48h: 14.80 ± 1.77
72h: 9.32 ± 0.92
96h: 6.05 ± 1.28
120h: 2.04 ± 0.25
log T1-44 (μM)
48 h
72 h
96 h
120 h
B
Panc02
Cas9 I
E2F1Cr I
Cas9 II
E2F1Cr II
Cas9 III
E2F1Cr III
72
E2F1
43
GAPDH
C i)
Panc02 Cas9
Panc02 E2F1Cr II
Panc02 E2F1Cr III
Apoptotic cells (%)
Time (d)
DMSO
1.0 μM T1-44
100 nM Dox
ii)
Sub-G1 cells (%)
DMSO
1.0 μM T1-44
D
Panc02 Cas9/E2F1Cr - Clone II
Panc02 Cas9/E2F1Cr - Clone III
Cell number
Cas9 - DMSO
Cas9 - 1.0 μM T1-44
E2F1Cr - DMSO
E2F1Cr - 1.0 μM T1-44

Figure 3.3. Effects of PRMT5 inhibition in Cas9 and E2F1Cr Panc02 cells.
A. *Median inhibitory concentrations obtained for a representative clone of Cas9 (left) and E2F1Cr (right) Panc02 cells treated with T1-44 for 48 to 120 h. Cell survival percentages are relative to the DMSO-treated control; n = 4 independent experiments performed in technical triplicates. Results are expressed as mean ± SD.* ***B.*** *Representative immunoblots to evaluate the E2F1 signal of three stable Cas9 and E2F1Cr clones of Panc02 cells; n = 3 independent experiments.* ***C.*** *Percentage of apoptotic cells and sub-G1 cells obtained after annexin V/PI staining (i) and cell cycle profiling (ii) experiments for Cas9 and two clones of E2F1Cr Panc02 cells treated with T1-44 for 2 to 8 days. Doxorubicin was used as positive control for annexin V/PI experiments; n = 3 independent experiments performed in technical duplicates. Results are expressed as mean ± SD; one-way ANOVA with Tukey's multiple comparisons; * $p < 0.05$, ** $p < 0.001$, *** $p < 0.0001$, **** $p < 0.00001$.* ***D.*** *Proliferation curves representing T1-44 treatment of Cas9 and two clones of E2F1Cr Panc02 from 2 to 8 days; n = 3 independent experiments performed in technical duplicates. Results are expressed as mean ± SD; one-way ANOVA with Tukey's multiple comparisons;* $^{*}p < 0.05$, $^{**}p < 0.001$, $^{***}p < 0.0001$.

3.3. Discussion

With the aim to provide the background for subsequent research, initial characterization experiments using parental human (Panc-1) and murine (Panc02) PDAC cell lines were performed. Concentrations up to 5.0 µM T1-44 for 48 h inhibited PRMT5 without altering cell survival, growth rates, and cell cycle and apoptotic profiles of these cells. All of these effects are in agreement with previous reports for the human CRC cell line HCT-116, where 48-h 1.0 µM T1-44 treatments did not affect cell proliferation nor cell cycle profile, but also showed an $IC_{50} \approx$ 2-fold higher (36.36 µM) (Barczak et al., 2020) than Panc-1 cells (16.06 µM). This difference could be explained due to the lower MTAP expression observed for Panc-1 when compared to HCT116 cells (Marjon et al., 2016). In PDAC, MTAP is frequently co-deleted with CDK2A, thus leading to the accumulation of the endogenous PRMT5 inhibitor MTA, therefore increasing Panc-1 sensitivity to T1-44 (Marjon et al., 2016; Ngoi et al., 2022; Orben et al., 2022). Similarly, comparable IC_{50} have been reported

when other agents with recognized PRMT5i activity, like the repurposed drugs candesartan and cloperastine, and the synthetic agent EZP015556, were used against the PDAC cell lines Panc-1, MiaPaCa2 and AsPC1, and PDAC patient-derived organoids, respectively (Driehuis et al., 2019; Prabhu et al., 2023). Generally, studies that propose PRMT5 inhibitors as anti-PDAC agents, used these drugs in combination with conventional PDAC chemotherapeutics (*e.g.* gemcitabine) (Wei et al., 2020), ionizing radiation (He et al., 2022) or targeted agents like vactosertib, an inhibitor of TGF-β_1 signalling (Hong et al., 2023). These combinatorial approaches were found capable to reduce tumour growth (He et al., 2022; Orben et al., 2022; Prabhu et al., 2023; Wei et al., 2020), alter cell cycle (He et al., 2022; Orben et al., 2022), induce apoptosis (Hong et al., 2023; Orben et al., 2022) and inhibit cell migration (Hong et al., 2023) in PDAC cell models.

When the role of E2F1 was analysed in some of these responses, a ≈ 2-fold reduction of the effect of T1-44 in cell proliferation was observed when comparing E2F1Cr cells with their Cas9 counterparts. These effects are consistent with previous reports in CRC (Barczak et al., 2020) and neuroblastoma cell lines (Bate-Eya et al., 2025), where a similar IC_{50} increase was observed upon E2F1 loss. These changes in the sensitivity to PRMT5 inhibition under the absence of E2F1 can be explained by the loss of the interaction between E2F1 and downstream targets involved with cell cycle progression (Pastore et al., 2020), or changes in the expression of PRMT5/E2F1-dependent pro-apoptotic mediators like DIABLO (Bate-Eya et al., 2025; Pastore et al., 2020).

Regarding other cell responses, the absence of E2F1 does not appear to induce apoptosis, which is also consistent with effects observed in Cas9 and E2F1Cr HCT116 cells (Barczak et al., 2020). This absence of apoptosis can be attributed to the redundancy of effects between the activator isoforms of E2F (*i.e.* E2F1, E2F2 and E2F3) (Julian et al., 2016; Kong et al., 2007), which could possibly provide when E2F1 is suppressed. Despite this, a potential E2F1-PRMT5 dependent effect could be observed for growth curves, where 1 μM T1-44 was capable to decrease growth rates after treating Panc-1 E2F1Cr and Panc02 E2F1Cr cells for 6 and 8 days, respectively. A potential explanation of these differences might be associated with the effects of PRMT5 inhibition at transcriptional level, which is a topic that will be developed in the following chapter.

Despite these effects of PRMT5 inhibition have been widely described in different types of tumours, this methyltransferase is also involved in other cell processes relevant to PDAC, like gene expression, metabolism and AS (Fedoriw et al., 2019; Mavrakis et al., 2016). The following chapters of this thesis aim to describe the effects of T1-44 not as an antiproliferative drug *per* se, but rather as a potential immunosensitizing agent in PDAC.

Chapter 4 : PRMT5 inhibition modifies alternative splicing, lncRNA expression and pH dynamics in PDAC cells

4.1. Introduction

It has been reported that PRMT5, in association with E2F1, modifies the expression of several transcripts associated with cancer cell survival, migration and the expression of lncRNA-derived peptides (Barczak et al., 2023; Barczak et al., 2020; Pastore et al., 2020). Similarly, but aside the conventional roles of E2F1 as a transcription factor, PRMT5 and E2F1 are also capable to regulate alternative splicing (Bate-Eya et al., 2025; Roworth et al., 2019). These effects highlight the potential of PRMT5 inhibition as an interesting approach to modify the gene expression and alternative splicing landscape of PDAC cells with the aim to alter their cellular functions, immunosensitivity and/or microenvironmental conditions. Recent reports show that the use of PRMT5 inhibitors, like JNJ-64619178, GSK-3326595, GSK-3368715 and BMS-986504, induced AS and suppressed the growth of MYC-amplified patient-derived PDAC organoids (Orben et al., 2022), and MTAP-deleted PDAC cells and xenografts when co-treated with $KRAS^{G12C}$ or $KRAS^{G12D}$ inhibitors (Drizyte-Miller et al., 2025a). Addition of PRMT5 inhibitors to therapeutic regimes improved the response of PDAC patient-derived xenografts to gemcitabine, and reduced the glycolytic rate of cancer cells (Feng et al., 2024; Wei et al., 2025). The effect on glycolysis impacts proton production, which mitigates extracellular

acidification and therefore alters PDAC microenvironmental conditions, improving their immune landscape and drug response (Pethő et al., 2023). With that in mind, the work in this chapter focused on describing the role of PRMT5 in regulating gene expression and alternative splicing, and the impact these changes have on cell metabolism and pH dynamics.

4.2. Results

4.2.1. PRMT5 and E2F1 modify the expression lncRNA transcripts

To establish the effects of T1-44 at whole-transcript level, RNAseq datasets of wild-type (WT) Panc-1 and Panc02 cells treated for 48 h with 1.0 μM T1-44 were analysed, finding 582 and 516 DEGs (adjusted *p* value < 0.01 and $|\log_2 FC| > 0.58$) for Panc-1 and Panc02 cells, respectively (Figure 4.1Ai). The full list of DEGs can be found in Appendix I. From these DEGs, 31 up-regulated and 74 down-regulated, and 48 up-regulated and 59 down-regulated lncRNA DEGs were identified for Panc-1 and Panc02. To differentiate which lncRNA transcripts are dependent of E2F1 activity, RNAseq analysis was performed on Cas9 and E2F1Cr Panc02 cells treated with for 1.0 μM T1-44 for 48 h. As results, 267 DEGs (adjusted *p* value < 0.01), 126 up- and 141 down-regulated genes (adjusted *p* value < 0.01 and $|\log_2 FC| > 1.00$), were found to be influenced by E2F1 status (Figure 4.1Aii). The presence of E2F1-binding sites in the promoter region of these lncRNA transcripts was checked using UCSC Genome Browser, finding that 64 (58.18%) and 72 (42.29%) of the DE lncRNA promoter sequences contained E2F1 binding sites for Panc-1 and Panc02 cells, respectively (Figure 4.1B). These findings were validated by comparing the

expression levels of selected lncRNA targets between Cas9 and E2F1Cr cells (Figure 4.2).

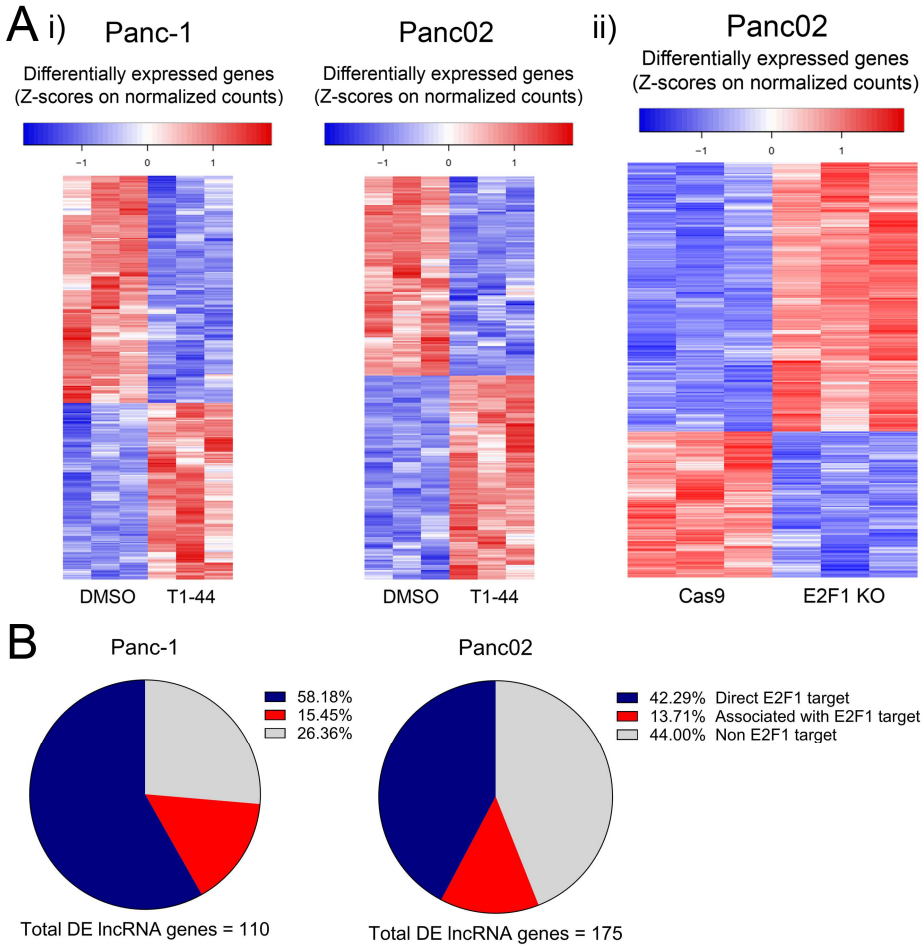

Figure 4.1. PRMT5 inhibition and E2F1 status influences lncRNA expression. ***A.*** *Changes in differential gene expression (q < 0.01) represented as Z-scores on the normalized counts obtained for (i) E2F1-expressing parental Panc-1 and Panc02 cells after a 48-treatment with 1.0 μM T1-44, and (ii) Panc02 cells expressing E2F1 (Cas9) versus E2F1 knockouts; n = 3 independent experiments.* ***B.*** *Proportion of lncRNA DEGs that has been previously recognized as E2F1 binders or associated to other known targets according to the information available in UCSC Genome Browser and ConTraV3 databases.*

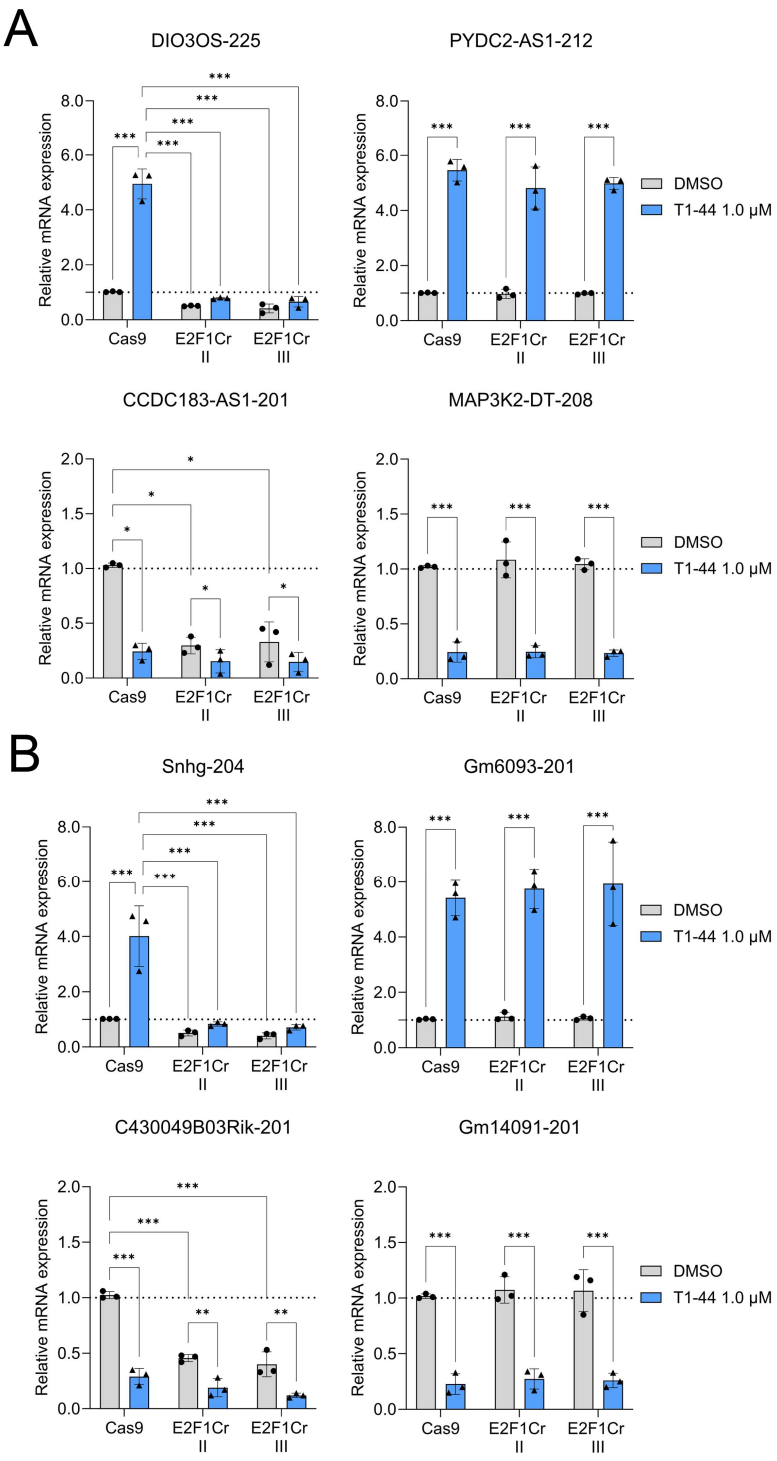

Figure 4.2. Validation of in silico-predicted E2F1 targets and their response to PRMT5 inhibition.

*qPCR of lncRNA DEGs obtained after treating Cas9 and E2F1Cr (**A**) Panc-1 and (**B**) Panc02 cells with T1-44. The genes used for this validation correspond in each case to: Up-regulated lncRNA predicted as E2F1 binder and non-binder (top left and right, respectively), and E2F1-binding and non-binding down-regulated lncRNA (bottom left and right, respectively); n = 3 independent experiments performed in technical triplicates. Results are expressed as mean ± SD; one-way ANOVA with Tukey's multiple comparisons; * p < 0.05, ** p < 0.001, *** p < 0.0001, **** p < 0.00001*

Despite the observed effects of PRMT5 inhibition and E2F1 status on lncRNA expression on Panc-1 and Panc02 cells, it was not clear whether these targets, derived from regions annotated as non-coding, could be translated into polypeptides. The capacity of T1-44-mediated lncRNAs to be translated was assessed by performing Ribo-seq on polysomal extracts. In Panc02 cells treated with T1-44, 259 up- and 386 down-regulated polysome-associated lncRNA transcripts were identified (adjusted p value < 0.01 and $|\log_2 FC| > 1.00$) when compared with the DMSO-treated condition (Figure 4.3A). These results were validated measuring the enrichment profile of three of the highest and one of the lowest-ranking DE lncRNAs in all 12 sucrose fractions used for polysome profiling. For these studies, fractions 1 to 4 were defined as free mRNA, 5 to 7 as monoribosomal, and 8 to 12 as polysomal fractions. Significant RNA enrichment in the polysomal fractions was found for all three up-regulated lncRNA targets (1700018L02Rik-201, Gm42549-201 and ENSMUST00000203403.3; Figure 4.3B, upper row), and the opposite trend was observed for the selected downregulated target (D5Ertd615e-201; Figure 4.3B, bottom left corner).

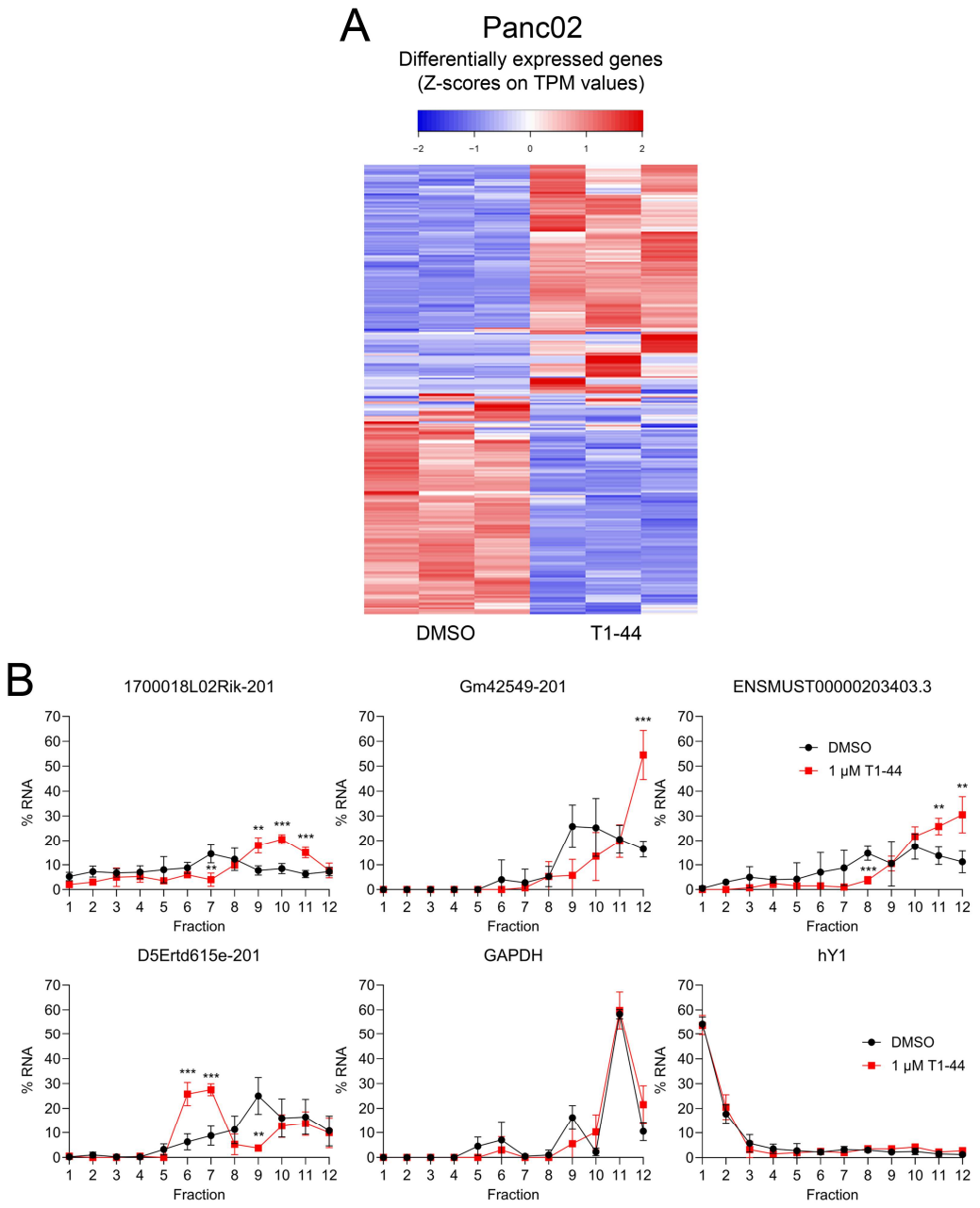

Figure 4.3. PRMT5 inhibition induces the expression of potentially-translatable lncRNA.

A. *Heatmap representing the changes in differential gene expression (q < 0.01) as Z-scores on the TPM values obtained for polysomal extracts of Panc02 cells treated with 1.0 μM T1-44 for 48 h; n = 3 independent experiments.* ***B.*** *Polysome enrichment graphs obtained for Panc02 cells treated for 48 h with DMSO (black lines and dots) and 1.0 μM T1-44 (red lines and squares). The represented genes correspond to the validation of upregulated (upper row) and downregulated (bottom left) lncRNA in the polysomal RNA fraction found in Ribo-seq. GAPDH and hY1 were used as technical controls for polysomal and cytoplasmic distribution; n = 4 independent experiments performed in technical triplicates. Results are expressed as mean ± SD; two-tailed Student's t-test; ** p < 0.001, *** p < 0.0001.*

Based on this data, 16 up-regulated lncRNA transcripts for which the association with polysomal fractions was confirmed were chosen for *in silico* ORF annotation using ORF Finder. 350 theoretical peptides longer than 75 nt were identified from predicted ATG and CTG ORFs. The MHC-I binding affinity to the C57BL/6 mice haplotype was evaluated using NetMHCpan 4.1. This way, a final list of 28 strong H2-Db and H2-Kb binding peptides was generated. To confirm that the *in silico*-predicted ORFs were functional and able to produce peptides, one 1700018L02Rik-201 ORF (encoding the peptide SAYCVPLYL) was cloned into the pSF-CMV-NEO-COOH-FLAG plasmid containing a FLAG tag. Immunoblotting of protein extracts derived from plasmid-transfected cells detected a ≈ 10 KDa band corresponding to 1700018L02Rik-201 (Figure 4.4), thus confirming the functionality of the tested ORF.

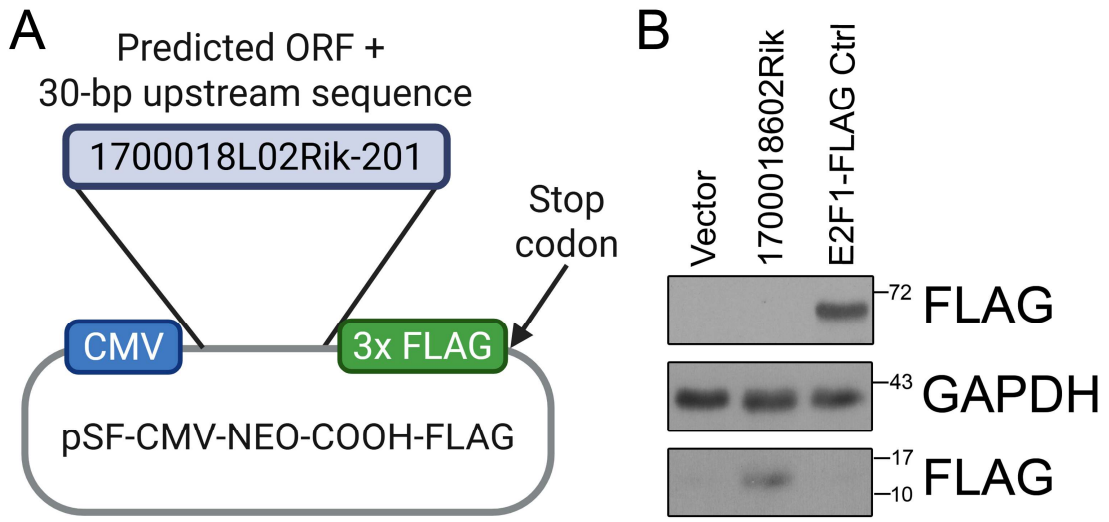

Figure 4.4. Translatability testing of a predicted lncRNA ORF.
A. *Diagram of lncRNA ORF cloning strategy. The in silico-predicted ORF sequence of one of the potentially-translatable lncRNA identified in the Ribo-seq data (1700018L02Rik-201), and its potential endogenous ribosome binding site (considered to be in the 30-bp upstream sequence), were inserted in the multicloning site of the 3xFLAG-tagged vector pSF-CMV-NEO-COOH-FLAG. Figure created in https://BioRender.com.* ***B.*** *Immunoblotting of Panc02 cells transfected with the FLAG-tagged predicted ORF plasmid (lower section). A construct made with the same FLAG-tagged vector but using an E2F1 insert as positive control condition (E2F1-FLAG Ctrl); n = 3 independent experiments.*

After the capacity to undergo translation was proven for the DE lncRNA 1700018L02Rik-201, the pipeline proposed by Barczak *et al.*, 2023 for the design of a ChAdOx1-based lncRNA-derived peptides vaccine was followed. This tool was capable to induce immunogenicity and reduce tumour growth on BALB/c mice bearing CT26 cells (Barczak et al., 2023). As an adaptation of this pipeline to design a potential vaccine against PDAC, a string containing 28 strong H-2Db/Kb binders (detailed in Table 8) was used to create the poly-antigenic cassette PepLncP2, which was included in the adenoviral vector ChAdOx1 to generate a prototype of cancer vaccine derived from *in silico*-predicted peptides. Details of the sequence of this vaccine are shown in Appendix II.

These results confirm that PRMT5 inhibition is capable to induce the expression of potentially translatable lncRNA. However, the immunogenic potential of these lncRNA-derived peptides will be discussed in *Chapter 5*.

Table 8. List of the 28 predicted lncRNA-derived used for PepLncP2 cassette design

Sequence	Accession (GRCm39)	Transcript name	NetMHCpan score H-2-Db	NetMHCpan score H-2-Kb
SAPLHPTPL	ENSMUST00000187897	1700018L02Rik-201	0.0055	0.1367
SAFSPVDNL	ENSMUST00000187897	1700018L02Rik-201	0.0634	0.2275
SAFSPHFLL	ENSMUST00000187897	1700018L02Rik-201	0.0991	0.1032
SAYCVPLYL	ENSMUST00000187897	1700018L02Rik-201	0.1478	0.3771
SGFGMLSHL	ENSMUST00000246336	C630043F03Rik-202	0.2205	0.0999
SSPEIWLSM	ENSMUST00000203403	ENSMUST00000203403.3	0.0504	0.1162
TIFGNFTII	ENSMUST00000203403	ENSMUST00000203403.3	0.1323	0.4808
TQYKIIHQI	ENSMUST00000203403	ENSMUST00000203403.3	0.2176	0.2883
STFQMFVLI	ENSMUST00000203403	ENSMUST00000203403.3	0.2811	0.1520
TSFHLNYTL	ENSMUST00000203403	ENSMUST00000203403.3	0.2889	0.2766
ASFDIGASL	ENSMUST00000203403	ENSMUST00000203403.3	0.3712	0.1147
ISLFLRQEL	ENSMUST00000203403	ENSMUST00000203403.3	0.3883	0.3133
SSGVLFNAL	ENSMUST00000203403	ENSMUST00000203403.3	0.4034	0.4238
VSPVVNILL	ENSMUST00000188891	Gm10634-202	0.3711	0.4447
SALEFCQKM	ENSMUST00000247121	Gm12999-202	0.3097	0.1029
SSGSFQTPL	ENSMUST00000199060	Gm17494-202	0.2341	0.4360
YSLKRFLNI	ENSMUST00000199060	Gm17494-202	0.4208	0.1485
SALSFSQSV	ENSMUST00000202392	Gm42549-201	0.1777	0.1231
ASLLLLSNL	ENSMUST00000202392	Gm42549-201	0.2675	0.2507
TAASHSHNL	ENSMUST00000202392	Gm42549-201	0.3509	0.4038
AIIHLHVTL	ENSMUST00000202392	Gm42549-201	0.3966	0.1377
VSPLHPILF	ENSMUST00000202392	Gm42549-201	0.4179	0.2260
VQPQFGAQL	ENSMUST00000201771	Gm42846-201	0.3755	0.1200
SSFSSWMHL	ENSMUST00000205219	Gm44199-201	0.0905	0.0420
ISLKLLASL	ENSMUST00000247510	Gm57457-201	0.2503	0.0922
SPLLILRL	ENSMUST00000247510	Gm57457-201	0.3245	0.1415
SSIWPFLHL	ENSMUST00000247510	Gm57457-201	0.3289	0.0482
VQLTLLSHF	ENSMUST00000247510	Gm57457-201	0.4774	0.4792

4.2.2. PRMT5 inhibition regulates the expression and alternative splicing of solute carriers associated with pH regulation

After DEG assessments, GO analysis was performed in WT Panc-1 and Panc02 cells treated with T1-44, showing that the top over-represented biological processes (BP) terms ($p < 0.05$) were mostly associated with cell metabolism in both cell lines (Figure 4.5A). These broad terms were subsequently mined in more depth, identifying enriched terms corresponding to OXPHOS, glycolysis, and ion/metabolite transmembrane transport. Considering the relevance of the later category in PDAC pathophysiology (Cappellesso et al., 2022; Cho et al., 2025; Zhou et al., 2026), this term was analysed even further, identifying solute carrier (SLC) family genes associated with Na^+/HCO_3^- (*e.g.*, SLC4A4, SLC4A7 and SLC26A11), Na^+/glucose (*e.g.*, SLC5A1 and SLC5A2), creatine (*e.g.*, SLC7A11) and amino-acid (*e.g.*, SLC6A8 and SLC38A5) transport. When the effects of T1-44 on the expression of these transporters were analysed, it was found that PRMT5 inhibition reduced (*e.g.*, SLC6A8, SLC7A11, SLC38A5), increased (*e.g.*, SLC26A11), and did not alter (*e.g.*, SLC4A4, SLC4A7, SLC5A1, SLC5A2) the expression of these transporters. Later, RNAseq results associated with Na^+/HCO_3^- (SLC4A4 and 4A7) and Na^+/glucose (SLC5A1 and 5A2) transport were validated via qPCR, confirming that T1-44 treatment did not alter the expression of these transporters in Panc-1 and Panc02 cells (Figure 4.6Ai).

After assessing the effects of T1-44 on gene expression, rMATS analysis was performed to evaluate the impact of PRMT5 inhibition on AS, revealing a total of 9,711 and 5,483 significant events (adjusted p value < 0.05) in Panc-1 and Panc02,

respectively. Out of these events, exon skipping was identified as the most frequent for both cell lines (64.6% in Panc-1 and 58.3% in Panc02; Figure 4.5Bi). The electroneutral sodium/bicarbonate co-transporter 1 (NBnC1/SLC4A7) was identified as one of the significant targets of exon skipping in both cell lines, with T1-44 inducing skipping of exon 12 ($\Delta\Psi$ = -5.6%, adjusted *p* value = 0.007) and exon 25 ($\Delta\Psi$ = -9.8%, adjusted p value = $3.2 \cdot 10^{-5}$) in Panc02, and only exon 25 ($\Delta\Psi$ = -9.0%, adjusted *p* value = 0.024) in Panc-1 (Figure 4.5Bii).

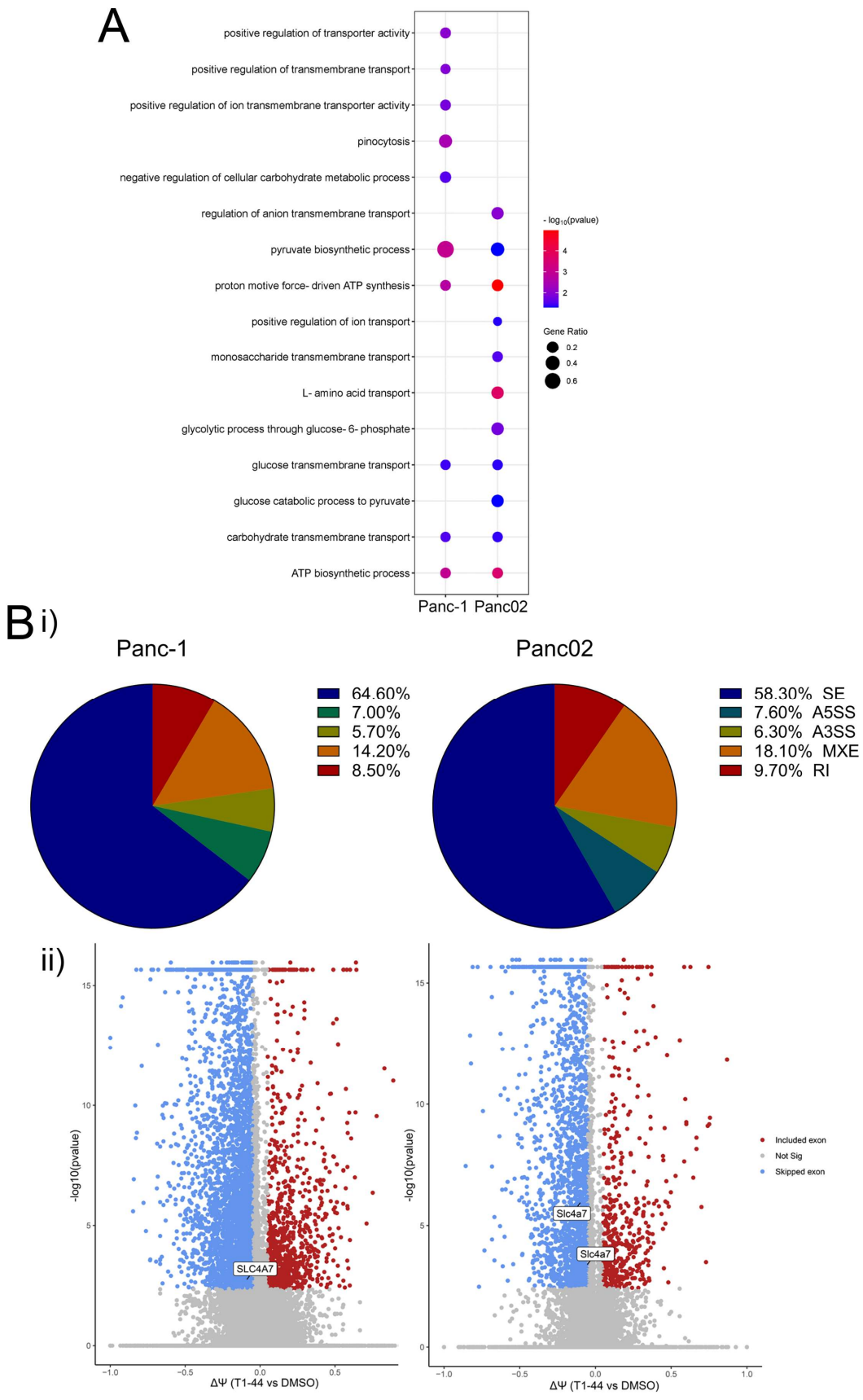
A
positive regulation of transporter activity
positive regulation of transmembrane transport
positive regulation of ion transmembrane transporter activity
pinocytosis
negative regulation of cellular carbohydrate metabolic process
regulation of anion transmembrane transport
pyruvate biosynthetic process
proton motive force- driven ATP synthesis
positive regulation of ion transport
monosaccharide transmembrane transport
L- amino acid transport
glycolytic process through glucose- 6- phosphate
glucose transmembrane transport
glucose catabolic process to pyruvate
carbohydrate transmembrane transport
ATP biosynthetic process
Panc-1 Panc02
- log10(pvalue)
Gene Ratio
0.2
0.4
0.6
B i)
Panc-1
Panc02
64.60%
7.00%
5.70%
14.20%
8.50%
58.30% SE
7.60% A5SS
6.30% A3SS
18.10% MXE
9.70% RI
ii)
-log10(pvalue)
SLC4A7
Slc4a7
ΔΨ (T1-44 vs DMSO)
Included exon
Not Sig
Skipped exon

Figure 4.5. PRMT5 inhibition alters the expression of transcripts associated with metabolism and modifies the alternative splicing profile of the sodium/bicarbonate cotransporter SLC4A7.

A. *Enrichment plots highlighting significant terms related with ion/metabolite transport, OXPHOS and glycolysis ($p < 0.05$) obtained for Panc-1 and Panc02 cells after PRMT5 inhibition; n = 3 independent experiments.* ***B.*** *(i) Pie charts illustrating the distribution of significant AS events (adjusted p value < 0.05) found for Panc-1 and Panc02 cells after T1-44 treatment; n = 3 independent experiments. (ii) Volcano plots showing the SE events obtained for Panc-1 and Panc02 cells treated with 1.0 μM T1-44 for 48 h, representing significant skipped and included exon events with blue and red dots, respectively (adjusted p value < 0.05 and $|\Delta\Psi| > 0.05$ were used as significance cutoffs). SLC4A7 splicing events were labelled for both cell lines; n = 3 independent experiments.*

When qPCR validation of the SLC4A7 exon 25 skipping event was performed, a 5-10-fold decrease in the normalized proportion spliced-in (PSI) was found for both cell lines after T1-44 treatment (Figure 4.6Aii). To verify if T1-44 was capable to alter the protein levels of NBCn1 (protein encoded by the SLC4A7 gene), immunoblotting was performed, finding no significant differences between treated and untreated cells (Figure 4.6B).

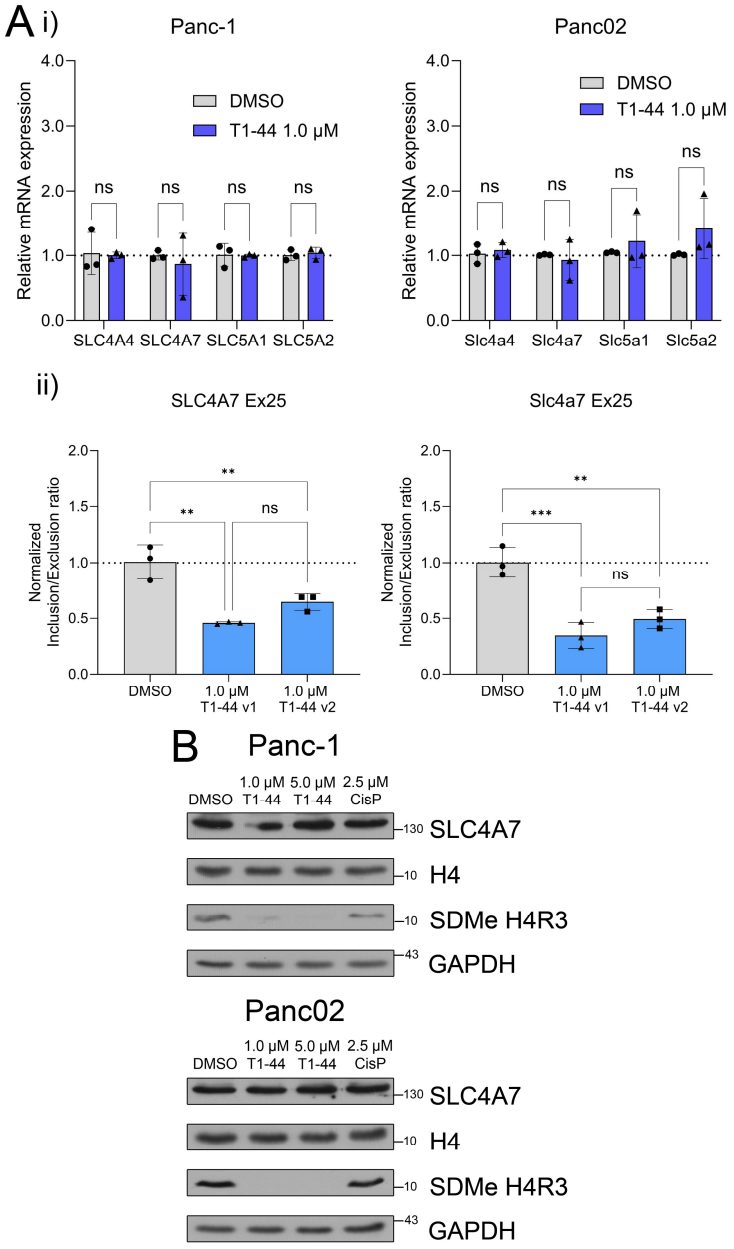

Figure 4.6. PRMT5 inhibition modifies the skipping of SLC4A7 exon 25 without compromising its protein levels.

A. *(i) qPCR validation of relevant SLC family genes identified in Panc-1 and Panc02 RNAseq results. Relative expression was calculated considering the DMSO-treated condition as basal expression; n = 3 independent experiments performed in technical triplicates. Results are expressed as mean ± SD; two-tailed Student's t-tests were performed between the T1-44 and DMSO-treated groups for each gene; ns $p > 0.05$. (ii) qPCR validation of the SLC4A7 exon 25 skipping event found in silico for Panc-1 (left) and Panc02 (right) cells treated with 1.0 µM T1-44 for 48 h using two different sets of primers (namely v1 and v2); n = 3 independent experiments performed in technical triplicates. Results are expressed as mean ± SD; one-way ANOVA with Tukey's multiple comparisons; ns $p > 0.05$, ** $p < 0.001$, *** $p < 0.0001$.* ***B.*** *Immunoblots representing the effect of 48-h T1-44 treatments in terms of NBCn1/SLC4A7 protein levels in WT Panc-1 and Panc02 cells. H4 and SDMe H4R3 were added as conditions to establish T1-44 activity, and CisP was included as non-PRMT5 targeting control; n = 3 independent experiments.*

Overall, these results highlight that T1-44 promotes the AS of NBnC1/SLC4A7, a solute carrier involved in pH_e and pH_i regulation (Figure 4.7). The functional implications that PRMT5 inhibition might have in pH dynamics and oxygen consumption will be described in the following section.

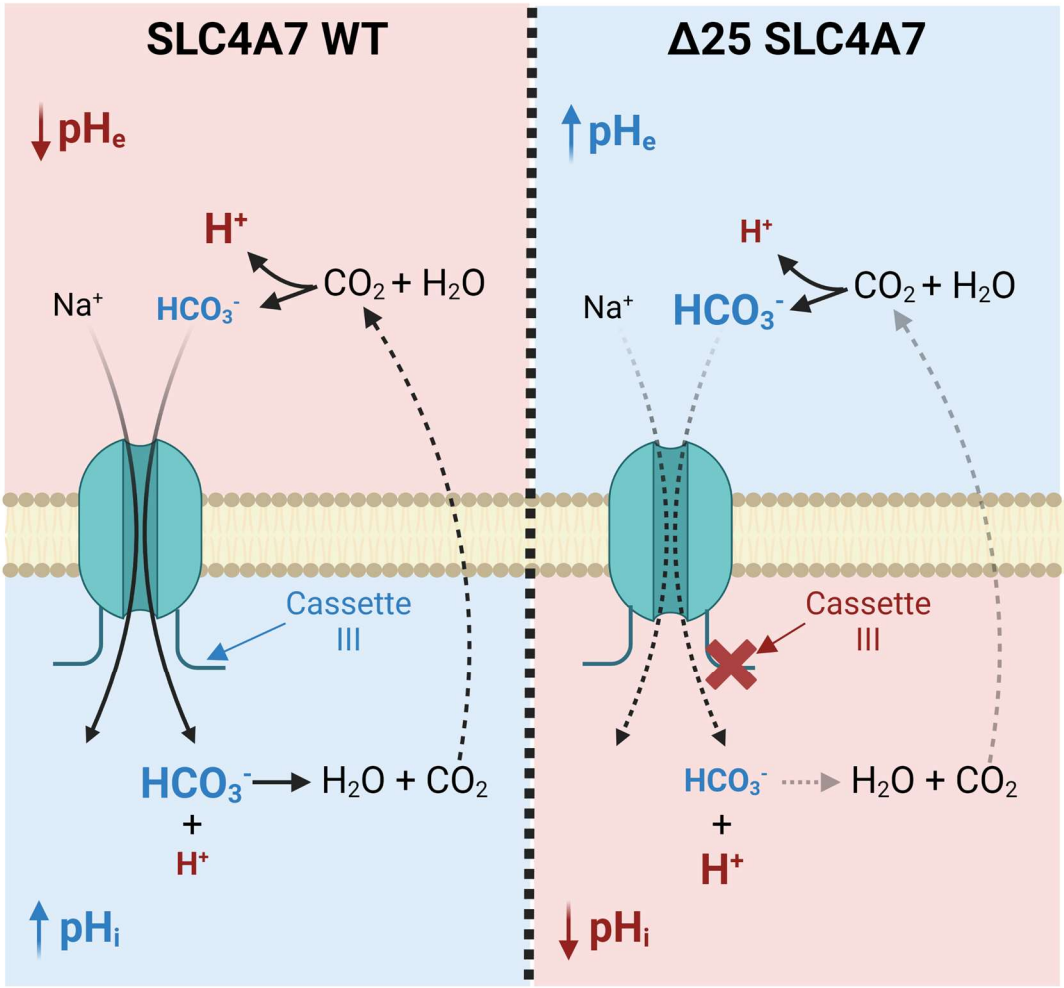

Figure 4.7. Functional effects of altering SLC4A7 exon 25 skipping on intra- and extracellular pH balance.

Diagram representing the theoretical implications that the absence of SLC4A7 exon 25 (cassette III) can drive in terms of pH dynamics. Figure created in https://BioRender.com.

4.2.3. T1-44 alters pH dynamics and reduces oxygen consumption

With the aim to establish if the transcriptional effects of PRMT5 inhibition on metabolism and ion transport have a functional impact, pH_i/pH_e and O_2 consumption measurements were performed on WT Panc-1 and Panc02 cells. In general, 48-h T1-44 treatments reduced pH_i under physiological (CO_2/HCO_3^-) buffering when compared to the DMSO condition in both Panc-1 (Figure 4.8A, left graph) and Panc02 (Figure 4.9A, left graph) cells. Conversely, these effects were lost when non-volatile buffering (NVB) conditions were used in both Panc-1 (Figure 4.8A, right graph) and Panc02 cells (Figure 4.9A, right graph). This absence of response under HEPES/MES buffering confirms that this intracellular acidification is dependent on bicarbonate transport.

With the aim to assess if this overall reduction of pH_i had an impact on cell metabolism and, subsequently, on TME conditions, pH_e measurements were performed, finding that T1-44 reduced H^+ production in both 1.0 and 5.0 µM treatments in a dose-dependent fashion in Panc-1 and Panc02 cells (Figure 4.8B and Figure 4.9B, upper rows) under physiological buffering. This reduction persisted only for 5.0 µM T1-44 when Panc-1 and Panc02 (Figure 4.8B and Figure 4.9B, lower rows) were maintained under NVB. To observe if T1-44 treatment altered cell respiration mechanisms, parallel O_2 consumption measurements were analysed, observing a consistent reduction in both cell lines when treated with T1-44 regardless of the buffering system that was employed (Figure 4.8C and Figure 4.9C).

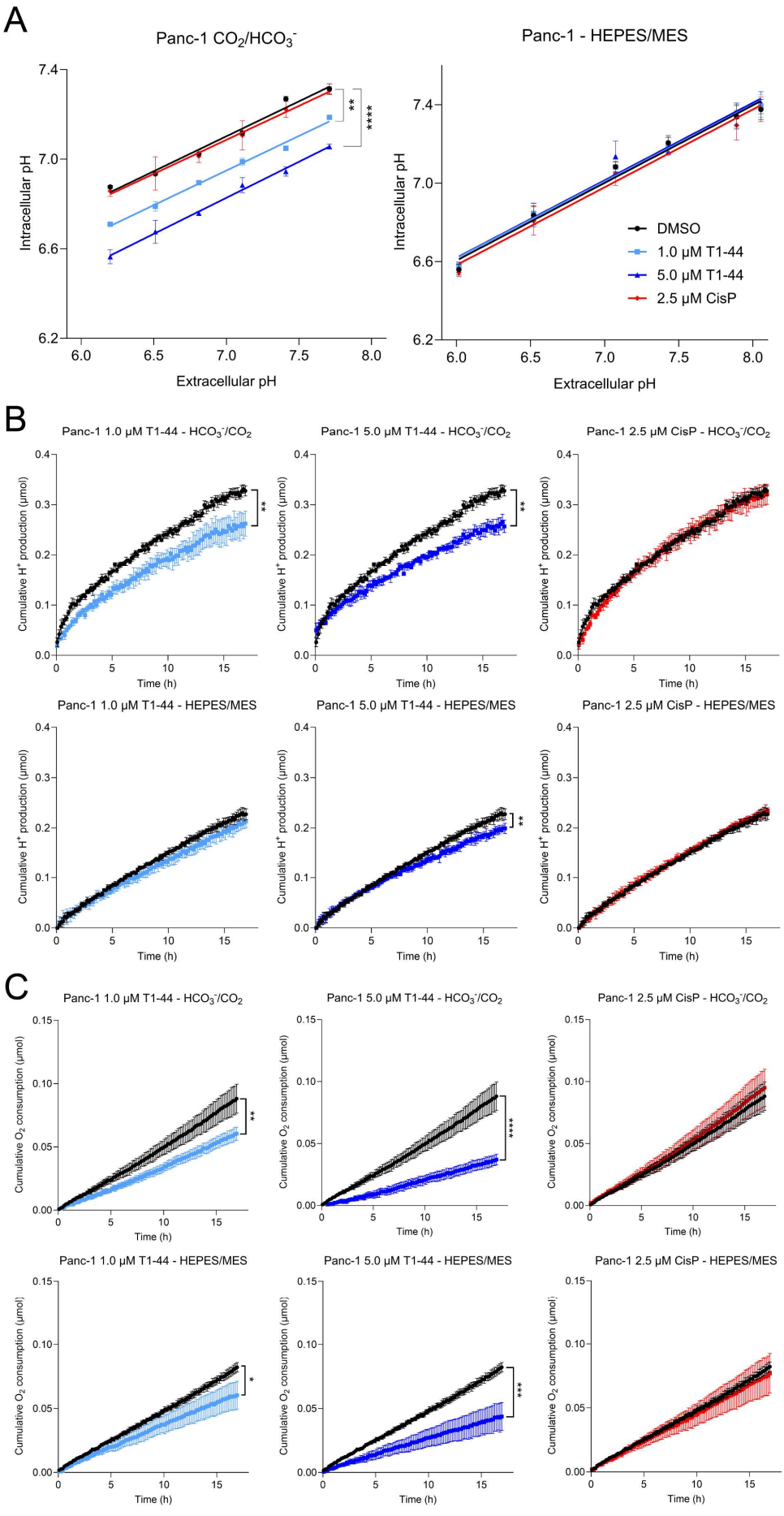
A
Panc-1 CO_2/HCO_3^-
Panc-1 - HEPES/MES
Intracellular pH
Extracellular pH
DMSO
1.0 μM T1-44
5.0 μM T1-44
2.5 μM CisP
B
Panc-1 1.0 μM T1-44 - HCO_3^-/CO_2
Panc-1 5.0 μM T1-44 - HCO_3^-/CO_2
Panc-1 2.5 μM CisP - HCO_3^-/CO_2
Panc-1 1.0 μM T1-44 - HEPES/MES
Panc-1 5.0 μM T1-44 - HEPES/MES
Panc-1 2.5 μM CisP - HEPES/MES
Cumulative H^+ production (μmol)
Time (h)
C
Panc-1 1.0 μM T1-44 - HCO_3^-/CO_2
Panc-1 5.0 μM T1-44 - HCO_3^-/CO_2
Panc-1 2.5 μM CisP - HCO_3^-/CO_2
Panc-1 1.0 μM T1-44 - HEPES/MES
Panc-1 5.0 μM T1-44 - HEPES/MES
Panc-1 2.5 μM CisP - HEPES/MES
Cumulative O_2 consumption (μmol)
Time (h)

Figure 4.8. PRMT5 inhibition alters pH dynamics and oxygen consumption in Panc-1 cells.

A. *Changes in intracellular pH measurements after 48-h treatments under CO_2/HCO_3^- (left) and HEPES/MES (right) buffering in parental Panc-1 cells. CisP was included as non-PRMT5 targeting control; n = 3 independent experiments performed in technical triplicates. Results are expressed as mean ± SEM; one-way ANOVA with Tukey's multiple comparisons; ** p < 0.001, **** p < 0.00001.* ***B.*** *Kinetic extracellular H^+ production measurements performed for 17 h in WT Panc-1 cells treated for 48 h with DMSO (black line), 1.0 μM T1-44 (light blue), 5.0 μM T1-44 (deep blue) and 2.5 μM CisP (red line). Measurements were performed using pH 7.4 low-capacity bicarbonate-based (upper row) and non-volatile (lower row) buffering under a humidified atmosphere at 37ºC, 0.5% CO_2 and 21% O_2; n = 3 independent experiments performed in technical triplicates. Results are expressed as mean ± SEM; one-way ANOVA with Tukey's multiple comparisons; ** p < 0.001.* ***C.*** *17-h oxygen consumption measurements for WT Panc-1 cells treated for 48 h with DMSO, T1-44 and CisP under physiological (upper row) and non-volatile (lower row) buffering; n = 3 independent experiments performed in technical triplicates. Results are expressed as mean ± SEM; one-way ANOVA with Tukey's multiple comparisons; * p < 0.05, ** p < 0.001, *** p < 0.0001, **** p < 0.00001.*

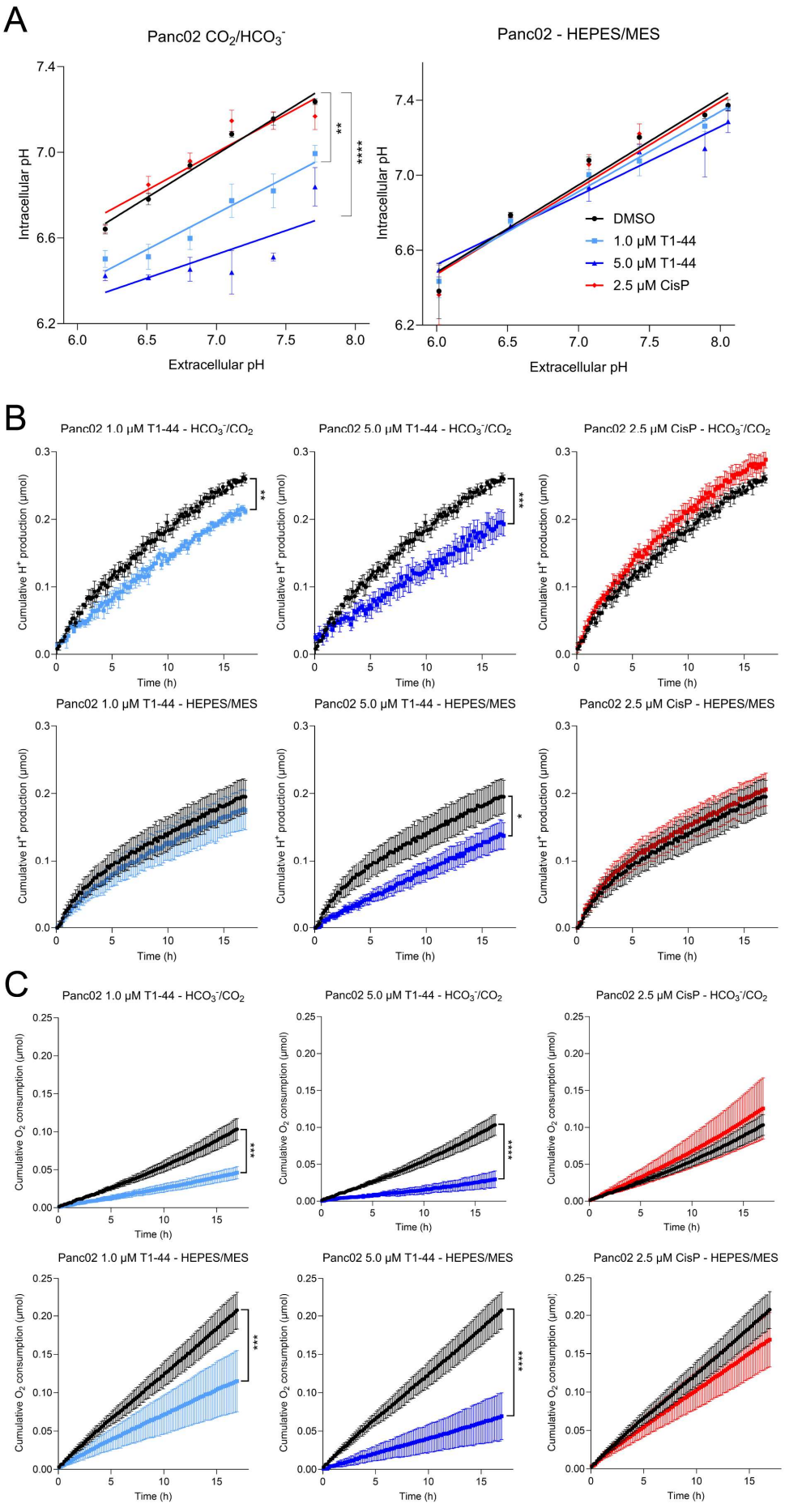
A
Panc02 CO_2/HCO_3^-
Panc02 - HEPES/MES
Intracellular pH
Extracellular pH
DMSO
1.0 μM T1-44
5.0 μM T1-44
2.5 μM CisP
B
Panc02 1.0 μM T1-44 - HCO_3^-/CO_2
Panc02 5.0 μM T1-44 - HCO_3^-/CO_2
Panc02 2.5 μM CisP - HCO_3^-/CO_2
Panc02 1.0 μM T1-44 - HEPES/MES
Panc02 5.0 μM T1-44 - HEPES/MES
Panc02 2.5 μM CisP - HEPES/MES
Cumulative H^+ production (μmol)
Time (h)
C
Cumulative O_2 consumption (μmol)
Time (h)

Figure 4.9. PRMT5 inhibition alters pH dynamics and oxygen consumption in Panc02 cells.

A. *Changes in intracellular pH measurements after 48-h treatments under CO_2/HCO_3^- (left) and HEPES/MES (right) buffering in parental Panc02 cells. CisP was included as non-PRMT5 targeting control; n = 3 independent experiments performed in technical triplicates. Results are expressed as mean ± SEM; one-way ANOVA with Tukey's multiple comparisons; ** p < 0.001, **** p < 0.00001.* ***B.*** *Kinetic extracellular H^+ production measurements performed for 17 h in WT Panc02 cells treated for 48 h with DMSO (black line), 1.0 μM T1-44 (light blue), 5.0 μM T1-44 (deep blue) and 2.5 μM CisP (red line). Measurements were performed using pH 7.4 low-capacity bicarbonate-based (upper row) and non-volatile (lower row) buffering under a humidified atmosphere at 37ºC, 0.5% CO_2 and 21% O_2; n = 3 independent experiments performed in technical triplicates. Results are expressed as mean ± SEM; one-way ANOVA with Tukey's multiple comparisons; * p < 0.05, ** p < 0.001, *** p < 0.0001.* ***C.*** *17-h oxygen consumption measurements for WT Panc02 cells treated for 48 h with DMSO, T1-44 and CisP under physiological (upper row) and non-volatile (lower row) buffering; n = 3 independent experiments performed in technical triplicates. Results are expressed as mean ± SEM; one-way ANOVA with Tukey's multiple comparisons; *** p < 0.0001, **** p < 0.00001.*

In general, PRMT5 inhibition reduced pH_i and increased pH_e in both PDAC cell lines under physiological buffering. Both T1-44 concentrations were capable to reduce O_2 consumption, being this activity independent of the buffering system.

These results confirm that T1-44 treatment impacts on pH dynamics, presumably because of the induced exon skipping of SLC4A7, as these effects were lost under bicarbonate-free conditions. In the following section, the involvement of SLC4A7 exon 25 skipping in both pH dynamics and O_2 consumption will be further evaluated, along with their implications on cell growth and the activity of basic conventional chemotherapeutics.

4.2.4. Skipping exon 25 of SLC4A7 affects pH dynamics, growth rate, and sensitivity to weakly-basic chemotherapeutics

To evaluate if the effects of T1-44 on pH dynamics can be attributed to SLC4A7 exon 25 splicing, two 2'-OMePS ASOs were designed as tools to induce this particular event. These oligonucleotides were named according to their targeted sequence within exon 25: SLC4A7 H/M25A (+27+48; represented graphically in Figure 4.10A) and (+58+79). The exon-skipping efficiency of both constructs was validated *in vitro* by transfecting Panc-1 and Panc02 cells with 200 nM ASO for 48 h, and testing full-length and Δ25 SLC4A7 expression using primers targeting exons 23 and 26. When the pixel density of full-length and Δ25 bands was compared, SLC4A7 H/M25A (+27+48; from now on identified as Δ25 ASO) showed the best exon-skipping performance by inducing 90% and 51% of Δ25 SLC4A7 in Panc-1 and Panc02, respectively (Figure 4.10B). This exon-skipping activity was further validated via qPCR, where Δ25 ASO led to a similar increase in SLC4A7 exon 25 skipping as T1-44 treatment (Figure 4.10C). In both experiments, a scrambled version of Δ25 ASO was used as a non-targeting control.

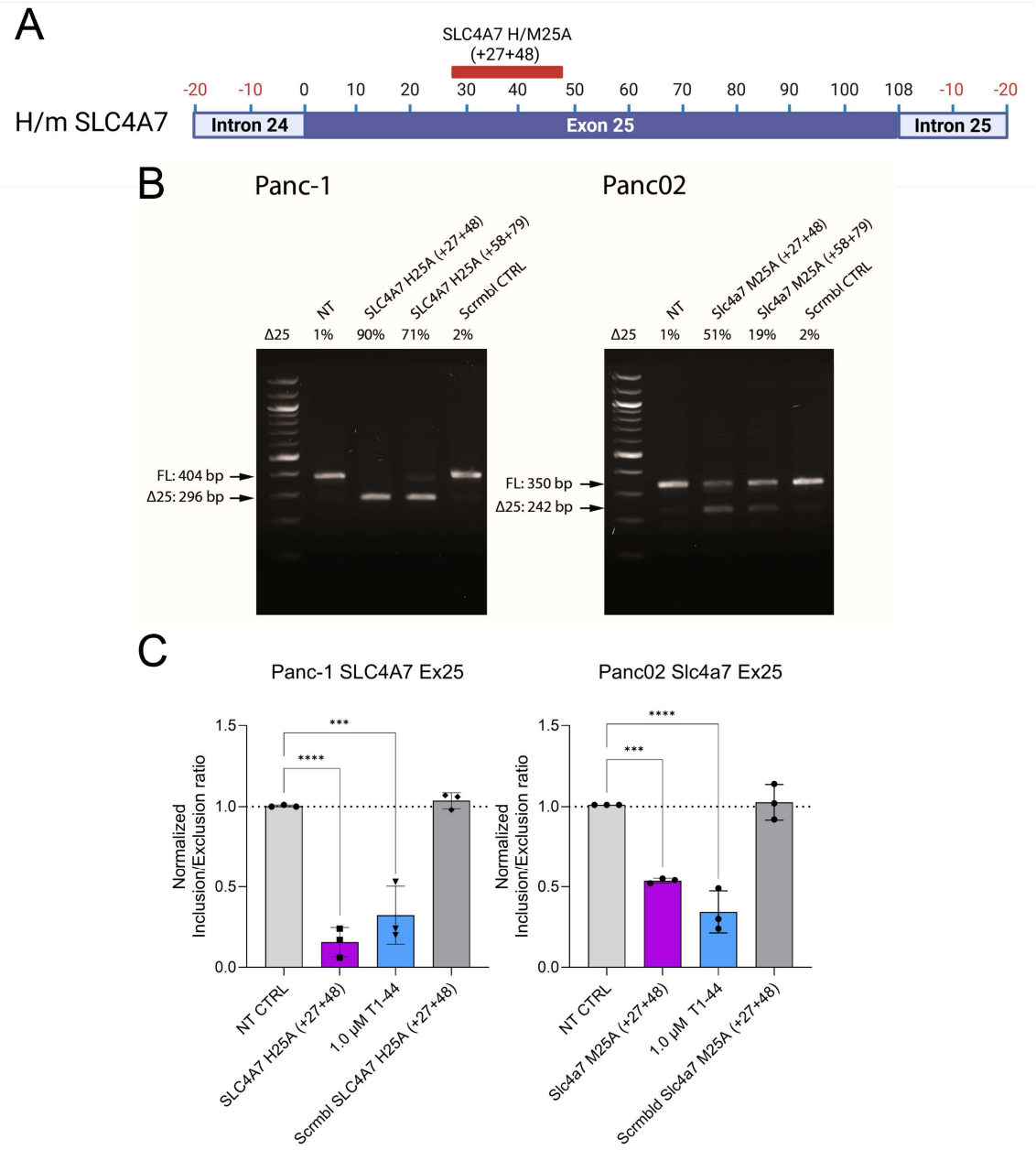

Figure 4.10. Design and validation of an ASO to induce SLC4A7 exon 25 skipping. ***A.*** *Diagram to represent the area targeted by the ASO H/M 25A (+27 +48) SLC4A7, which induces exon 25 skipping in both human and murine SLC4A7. Figure created in https://BioRender.com.* ***B.*** *Representative agarose gel to evaluate the exon-skipping activity of two SLC4A7-targeting ASO (namely SLC4A7 H/M25A (+27+48) and H/M25A (+58+79)) after transfecting Panc-1 and Panc02 cells for 48 h. Exon-skipping efficiency is expressed as percentage of the pixel density ratio between the full-length exon-including PCR product band (FL) and the skipped-exon 25 PCR product band (Δ25). As control conditions, non-transfected (NT) and non-targeting scrambled ASO (Scrmbl CTRL) treatments were included. n = 3 independent experiments.* ***C.*** *qPCR validation of Δ25 ASO (SLC4A7 H/M25A (+27+48)) exon-skipping activity found after treating Panc-1 and Panc02 cells with 200 nM Δ25 ASO or 1.0 μM T1-44 for 48 h. A scrambled ASO treatment was included as technical non-targeting control; n = 3 independent experiments performed in technical triplicates. Results are expressed as mean ± SD; one-way ANOVA with Tukey's multiple comparisons; *** p < 0.0001, **** p < 0.00001.*

After Δ25 ASO validation, its effects on pH dynamics were evaluated, finding that Δ25 ASO and T1-44 decreased pH_i in a similar fashion under physiological buffering. A comparable decrease was also observed with a Δ25 ASO + T1-44 combination treatment. However, this reduction was not statistically significant when compared with the single treatments (Figure 4.11A and Figure 4.11B, left graphs). As expected, the effects Δ25 ASO, T1-44 and Δ25 ASO + T1-44 were lost when HEPES/MES was used as a buffering system (Figure 4.11A and Figure 4.11B, right graphs).

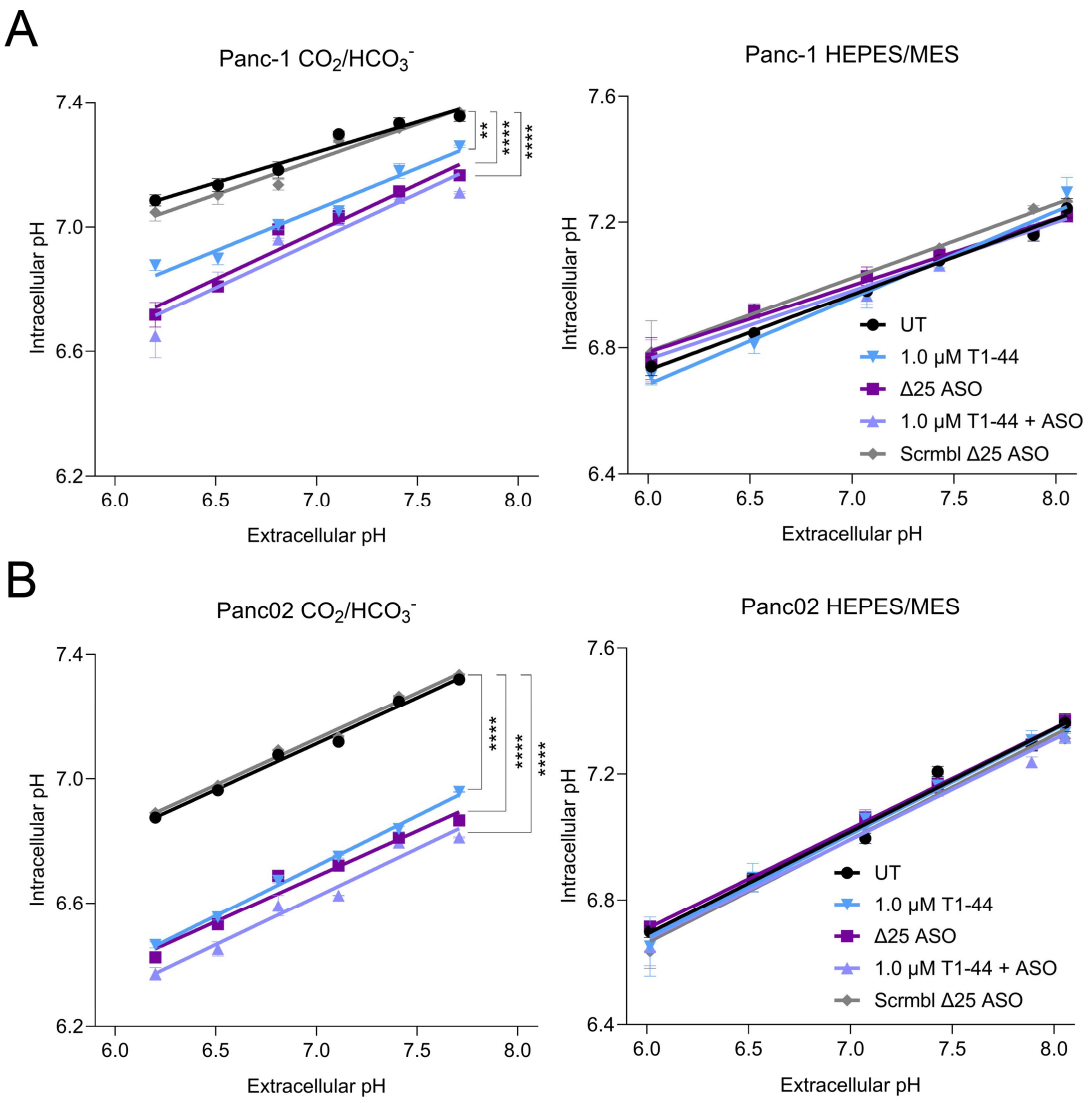

Figure 4.11. Effects of SLC4A7 exon 25 skipping in intracellular pH in Panc-1 and Panc02 cells.

*Intracellular pH measurements performed after 48-h treatments with Δ25 ASO, T1-44 and a combination of both agents under physiological (left) and non-volatile (right) buffering conditions in Panc-1 (**A**) and Panc02 (**B**) cells. A scrambled ASO treatment was included as technical non-targeting control; n = 3 independent experiments performed in technical triplicates. Results are expressed as mean ± SEM; one-way ANOVA with Tukey's multiple comparisons; ** p < 0.001, **** p < 0.00001.*

When the effects of Δ25 ASO on extracellular H^+ production (*i.e.* glycolytic metabolism) were tested, Δ25 ASO, T1-44 and Δ25 ASO + T1-44 under CO_2/HCO_3^- buffering elevated pH_e, indicating a decreased glycolytic metabolism (Figure 4.12). As expected, Δ25 ASO did not affect oxidative metabolism regardless of the buffering conditions, but T1-44 reduced O_2 consumption under both buffering systems (Figure 4.13).

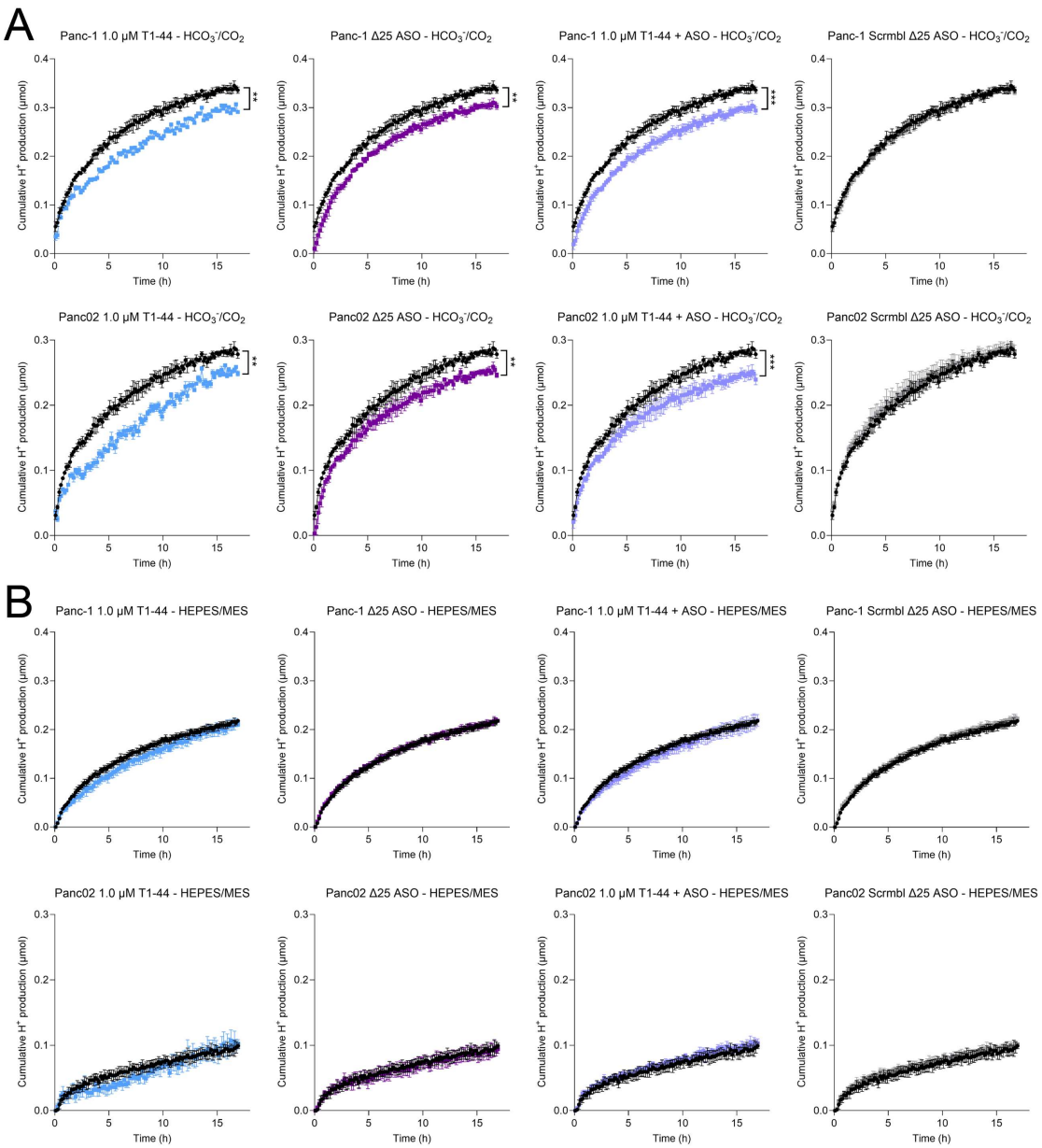

Figure 4.12. Effects of SLC4A7 exon 25 skipping in extracellular pH in Panc-1 and Panc02 cells.

*Kinetic extracellular H^+ production measurements performed for 17 h in WT Panc-1 (upper row) and Panc02 (lower row) cells treated for 48 h with empty transfection reagents (black line), 1.0 µM T1-44 (light blue), Δ25 ASO (deep purple), Δ25 ASO + T1-44 (light purple) and non-targeting scrambled ASO (grey line). Measurements were performed using pH 7.4 low-capacity (**A**) bicarbonate-based and (**B**) non-volatile buffering under a humidified atmosphere at 37ºC, 0.5% CO_2 and 21% O_2; n = 3 independent experiments performed in technical triplicates. Results are expressed as mean ± SEM; one-way ANOVA with Tukey's multiple comparisons; ** p < 0.001, *** p < 0.0001.*

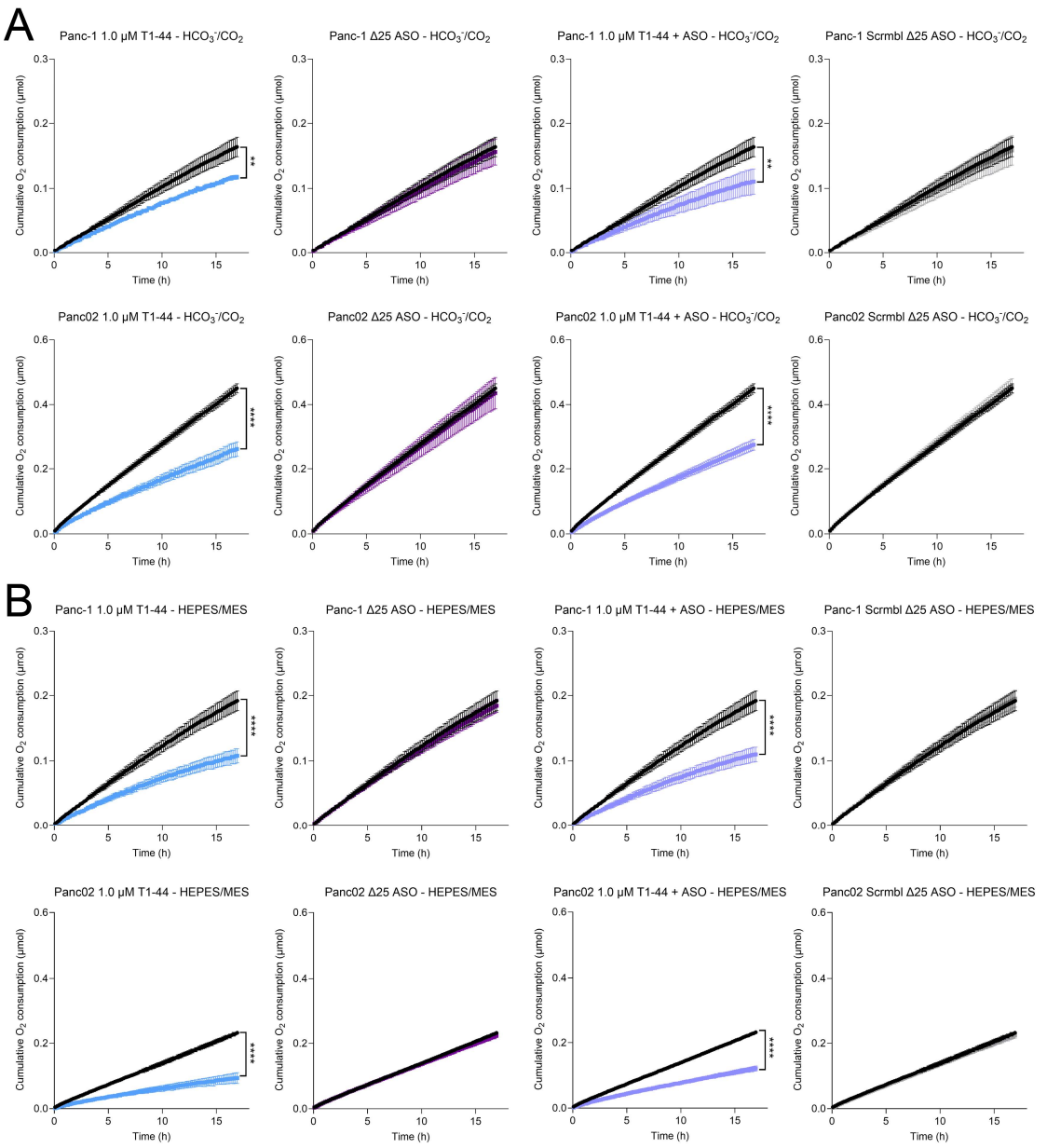

Figure 4.13. Effects of SLC4A7 exon 25 skipping in oxygen consumption in Panc-1 and Panc02 cells.

*Oxygen consumption measurements performed for 17 h in WT Panc-1 (upper row) and Panc02 (lower row) cells treated for 48 h with non-transfected, Δ25 ASO, T1-44, Δ25 ASO + T1-44 and scrambled ASO under (**A**) physiological and (**B**) non-volatile buffering; n = 3 independent experiments performed in technical triplicates. Results are expressed as mean ± SEM; one-way ANOVA with Tukey's multiple comparisons; ** p < 0.001, **** p < 0.00001.*

Once the characterization of the impact of Δ25 ASO on pH_i and oxidative and glycolytic metabolism was established, its impact on cell proliferation was assessed. Δ25 ASO treatment reduced cell growth, exerting significant effects after 48 and 96 h in Panc-1 and Panc02 cells, respectively (Figure 4.14).

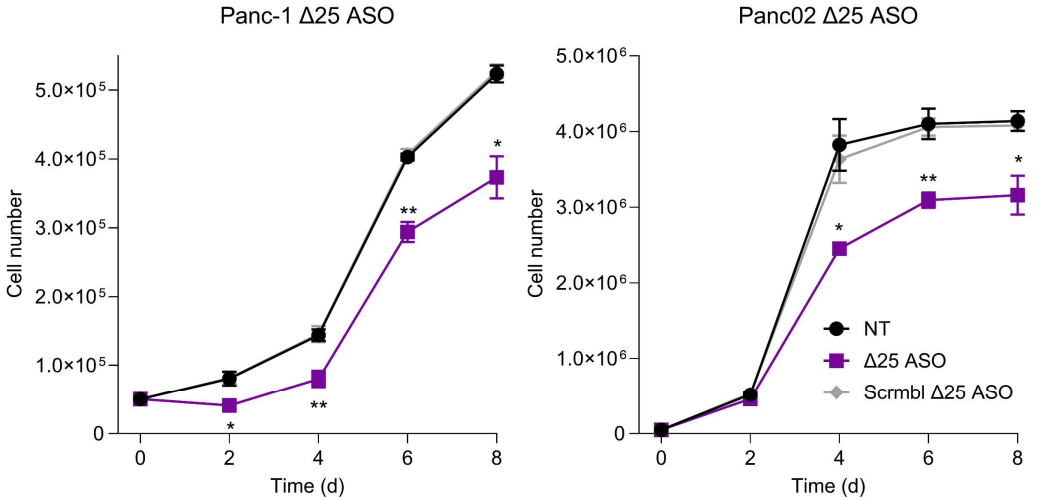

Figure 4.14. Effects of SLC4A7 exon 25 skipping in Panc-1 and Panc02 cell growth.

*Proliferation curves for WT Panc-1 (left) and Panc02 (right) cells treated and untreated with Δ25 ASO for 48 h under physiological buffering conditions. A scrambled version of Δ25 ASO was included as non-targeting control; n = 3 independent experiments performed in technical duplicates. Results are expressed as mean ± SD; two-way ANOVA with Tukey's multiple comparisons; * $p < 0.05$, ** $p < 0.001$.*

To evaluate if the increase in pH_e has functional impact in the uptake and subsequent activity of weakly-basic chemotherapeutics, combinatorial treatments using T1-44, Δ25 ASO and 100 nM doxorubicin (Dox; a weakly-basic drug that induces lipid peroxidation) were performed. Both T1-44 and Δ25 ASO enhanced the lipid peroxidation (expressed as reduction of the non-peroxidized/peroxidized ratio) induced by Dox, with no further increase when a triple combination was tested (Figure 4.15).

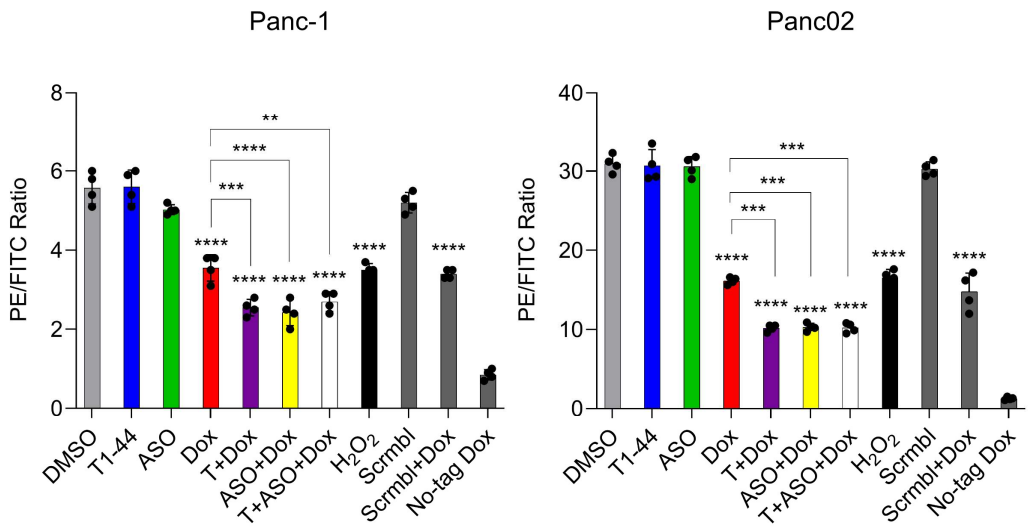

Figure 4.15. PRMT5 inhibition and SLC4A7 exon 25 skipping as potential enhancers of Dox effects in lipid peroxidation.

*Ratio between non-peroxidized (PE) and peroxidized (FITC) lipid signal obtained after treating parental Panc-1 (left) and Panc02 (right) cells for 48 h with 200 nM Δ25 ASO (ASO), 200 nM scrambled Δ25 ASO (Scrmbl), 1.0 μM T1-44 (T), 100 nM doxorubicin (Dox) or combinations of these agents under low-capacity bicarbonate buffering conditions. Dox and 250 μM H_2O_2 were included as positive controls for lipid peroxidation, and scrambled Δ25 ASO was included as non-targeting control; n = 4 independent experiments performed in technical duplicates. Results are expressed as mean ± SD; two-way ANOVA with Tukey's multiple comparisons; ** p < 0.001, *** p < 0.0001, **** p < 0.00001.*

In this section, validation results for a specific ASO to induce SLC4A7 exon 25 skipping and its effects on pH dynamics were provided. Skipping of the exon 25 of SLC4A7 induced a bicarbonate-dependant reduction in pH_i and an increase in pH_e without compromising oxygen consumption rates. As a result of the altered pH dynamics, the cell growth of both Panc-1 and Panc02 cells was reduced, Additionally, this elevated extracellular pH enhanced the lipid peroxidation activity of Dox.

However, the involvement of E2F1 status on these responses is yet to be clarified. SLC4A7, as a predicted E2F1 binder, might be regulated by the latter, and therefore have role on pH_i/pH_e balance observed in PDAC cells. The following

section will address these topics, establishing the relevance of E2F1 status on these effects.

4.2.5. E2F1 status influences the effects of SLC4A7 exon 25 skipping on cell growth and pH regulation

According to previous experiments, SLC4A7 was identified as a direct E2F1 target based on the presence of E2F1 binding motifs in its promoter region according to ChIP-seq datasets (UCSC Genome Browser and ContraV3), and it was found to be downregulated in Panc02 E2F1Cr cells *in vitro*. When SLC4A7 expression and exon 25 splicing analyses of Panc02 Cas9 and E2F1Cr tumour samples derived from C57BL/6 mice were performed, it was confirmed that the absence of E2F1 reduces SLC4A7 expression (Figure 4.16A, left graph), but also showed that this knock-out condition does not affect splicing of SLC4A7 exon 25 (Figure 4.16A, right graph).

To establish the role of E2F1 in SLC4A7-dependent pH balance and proliferation, Cas9 and E2F1Cr Panc-1 and Panc02 cells were subjected to treatments with Δ25 ASO. These experiments revealed that Δ25 ASO reduced the growth of Cas9 Panc-1 and Panc02 cells regardless of the medium pH (neutral = 7.4, or acidic = 6.2). However, these effects were lost when Δ25 ASO was used in E2F1Cr cells, restoring cell counts to numbers similar to those in non-transfected conditions, which were lower than their Cas9 counterparts under pH = 6.2 (Figure 4.16B). When the effects of Δ25 ASO treatment were studied in Cas9 and E2F1Cr

Panc-1 and Panc02 cells cultures under HEPES/MES buffering, no significant effects in cell growth were found for both E2F1Cr clones (Figure 4.16C).

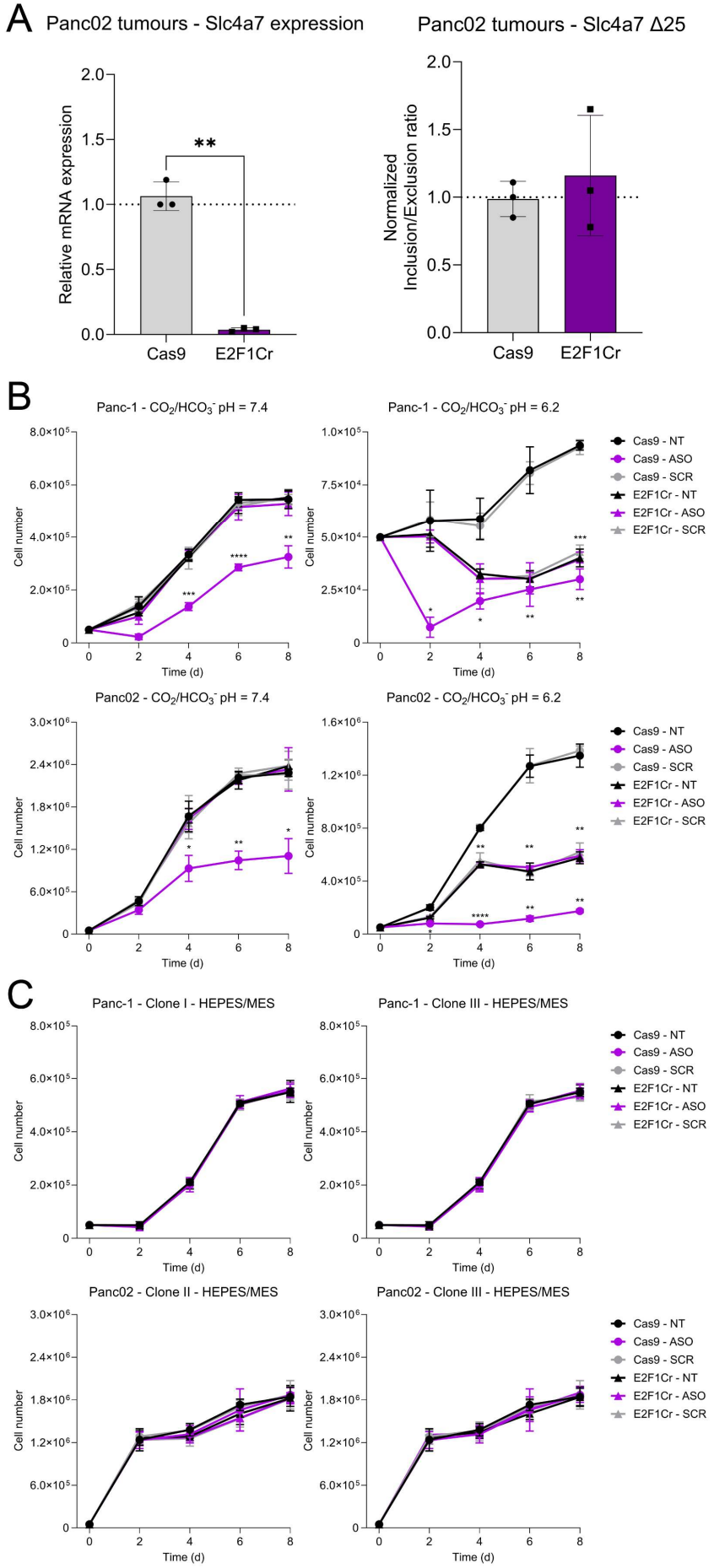
A
Panc02 tumours - Slc4a7 expression
Relative mRNA expression
Cas9
E2F1Cr
Panc02 tumours - Slc4a7 Δ25
Normalized Inclusion/Exclusion ratio
B
Panc-1 - CO2/HCO3- pH = 7.4
Panc-1 - CO2/HCO3- pH = 6.2
Panc02 - CO2/HCO3- pH = 7.4
Panc02 - CO2/HCO3- pH = 6.2
Cell number
Time (d)
Cas9 - NT
Cas9 - ASO
Cas9 - SCR
E2F1Cr - NT
E2F1Cr - ASO
E2F1Cr - SCR
C
Panc-1 - Clone I - HEPES/MES
Panc-1 - Clone III - HEPES/MES
Panc02 - Clone II - HEPES/MES
Panc02 - Clone III - HEPES/MES

Figure 4.16. E2F1 influences SLC4A7 expression and its effects on cell growth in Panc-1 and Panc02 cells.

A. *qPCR results representing the comparison between Cas9 and E2F1 KO Panc02 tumours in terms of Slc4a7 overall expression (left graph) and exon 25 skipping (right graph); n = 3 independent experiments performed in technical triplicates. Results are expressed as mean ± SD; two-tailed Student's t test comparisons; ** p < 0.001.* ***B.*** *Growth curves for Panc-1 (upper row) and Panc02 (lower row) Cas9 (●) /E2F1KO (▲) cells treated and untreated with Δ25 ASO for 48 h under physiological (pH = 7.4; left graphs) and acidic (pH = 6.2; right graphs) bicarbonate-based extracellular buffering; n = 3 independent experiments performed in technical duplicates. Results are expressed as mean ± SD; one-way ANOVA with Tukey's multiple comparisons; * p < 0.05, ** p < 0.001, *** p < 0.0001, **** p < 0.00001.* ***C.*** *Proliferation curves performed using the same experimental conditions, except for HEPES/MES as buffering condition; n = 3 independent experiments performed in technical duplicates.*

Following proliferation assessments, the functional implications of E2F1 status in pH dynamics were established. These experiments revealed that Δ25 ASO and T1-44 exerted similar pH_e increases in Panc02 Cas9 cells (Figure 4.17A, upper row) to those observed in the previous section in WT Panc02 cells under physiological buffering, but these effects on H^+ production were lost in E2F1Cr cells (Figure 4.17A, lower row). An analogous situation occurred when the buffering system was changed to HEPES/MES, observing that none of the treatments modified pH_e in neither Cas9 nor E2F1Cr Panc02 cells (Figure 4.17B).

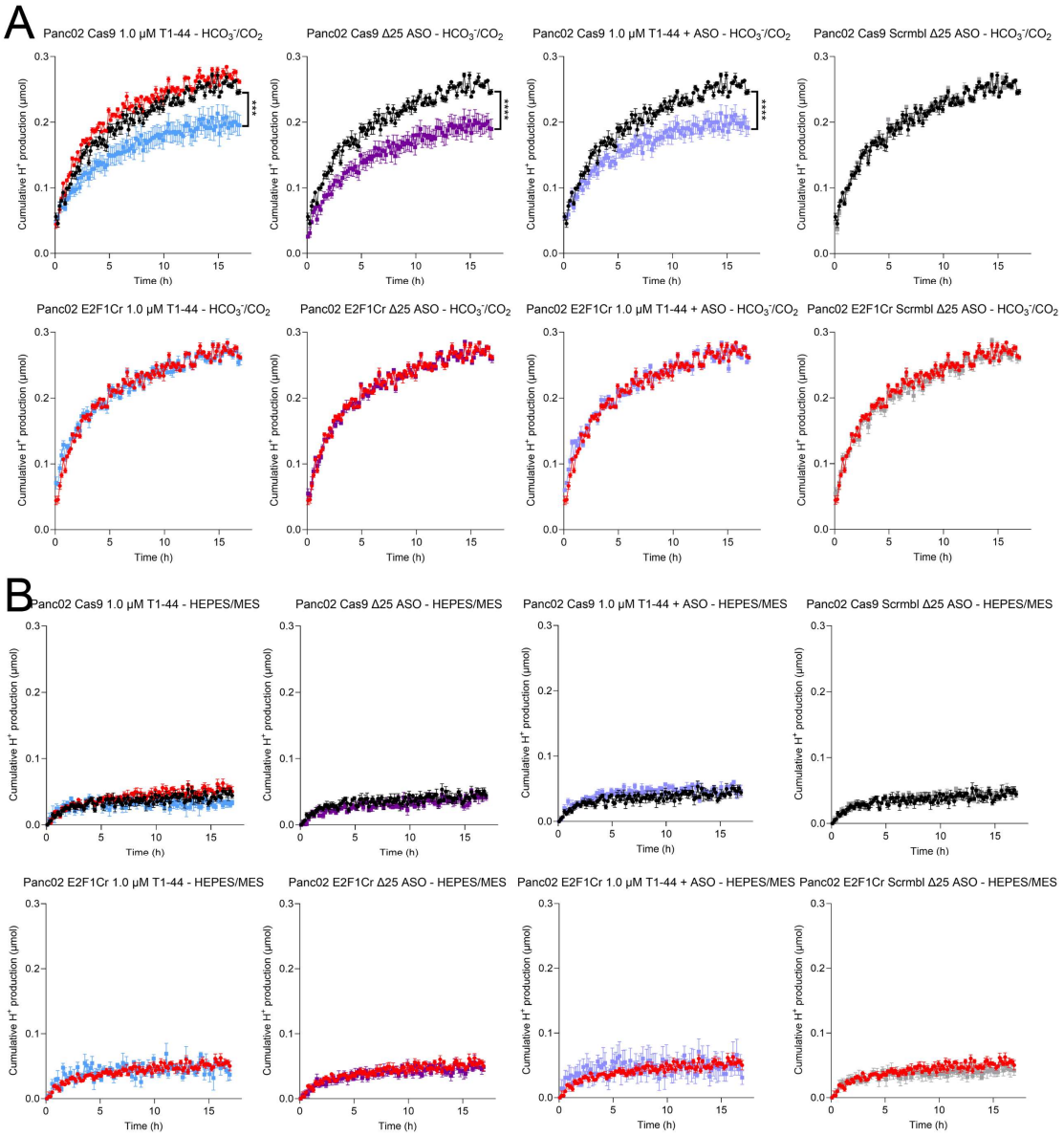

Figure 4.17. E2F1 influences SLC4A7 activity on extracellular pH regulation in Panc-1 and Panc02 cells.

*Kinetic extracellular H^+ production measurements performed for 17 h in Cas9 (upper row) and E2F1Cr (lower row) Panc02 cells treated for 48 h with empty transfection reagents (black and red line representing Cas9 and E2F1Cr cells, respectively), 1.0 µM T1-44 (light blue), Δ25 ASO (deep purple), Δ25 ASO + T1-44 (light purple) and non-targeting scrambled ASO (grey line). Measurements were performed using pH 7.4 low-capacity (**A**) bicarbonate-based and (**B**) non-volatile buffering under a humidified atmosphere at 37ºC, 0.5% CO_2 and 21% O_2. In the upper left corner graph, both non-transfected Cas9 and E2F1Cr conditions were included for the purpose of graphical comparison; n = 3 independent experiments performed in technical triplicates. Results are expressed as mean ± SEM; one-way ANOVA with Tukey's multiple comparisons; *** p < 0.0001, **** p < 0.00001.*

When the effects on O_2 consumption were evaluated, E2F1Cr Panc02 cells showed higher baseline levels than their Cas9 counterparts (Figure 4.18A, upper left corner graph). Regarding Δ25 ASO and T1-44 treatments, the former did not alter the oxidative metabolism rates of neither Cas9 and E2F1Cr Panc02 cells, but T1-44, both as single and combinatorial treatment, was the only condition capable to reduce O_2 consumption rates in both Cas9 and E2F1Cr Panc02 cells under both physiological (Figure 4.18A) and non-volatile (Figure 4.18B) buffering conditions.

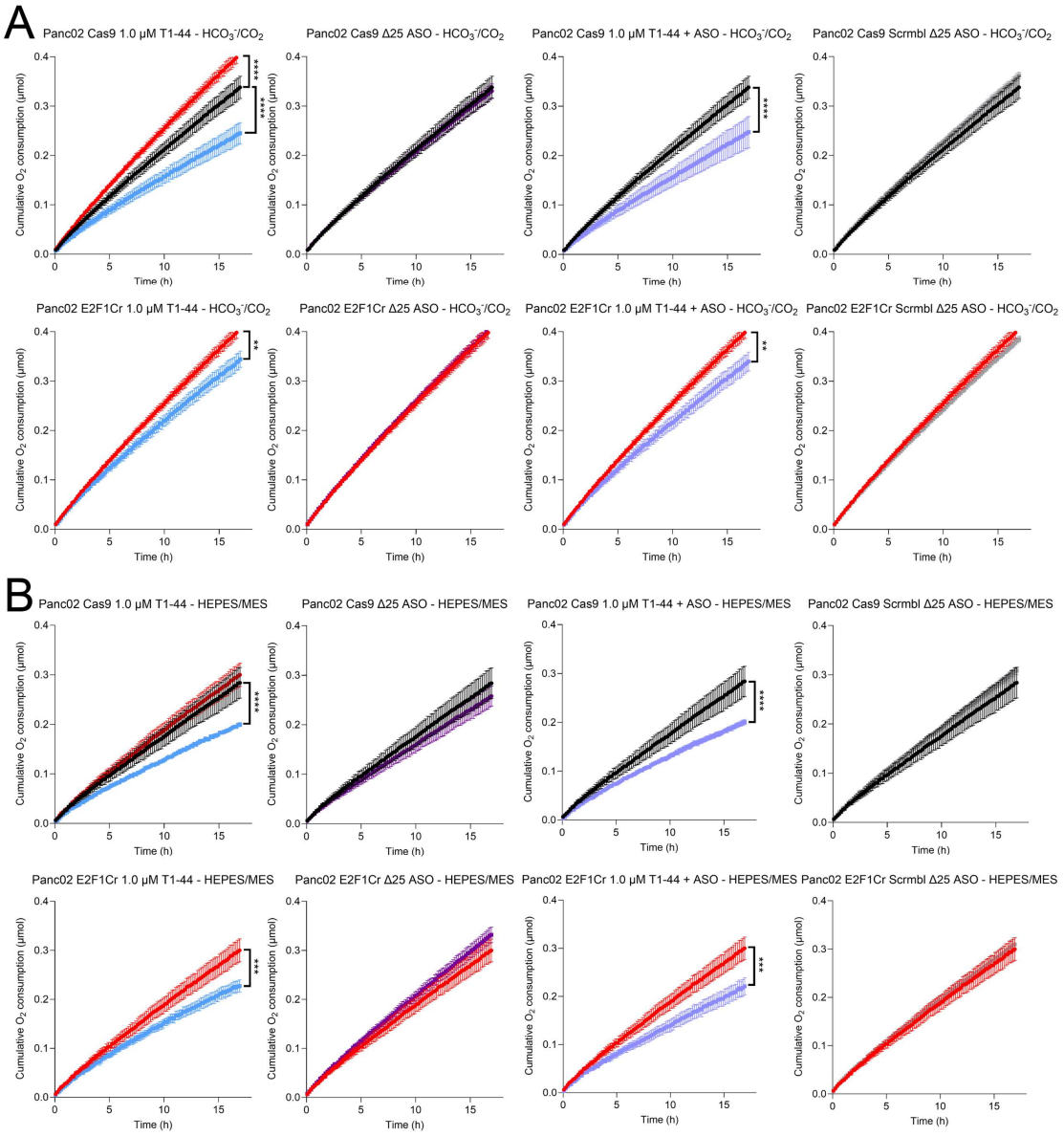

Figure 4.18. Effects of PRMT5 inhibition on oxygen consumption of Panc-1 and Panc02 cells are not dependent on E2F1 status.

*Oxygen consumption readings performed for 17 h in Cas9 (upper row) and E2F1Cr (lower row) Panc02 cells treated for 48 h with empty transfection reagents (black and red line representing Cas9 and E2F1Cr cells, respectively), 1.0 µM T1-44 (light blue), Δ25 ASO (deep purple), Δ25 ASO + T1-44 (light purple) and non-targeting scrambled ASO (grey line) under (**A**) physiological and (**B**) non-volatile buffering conditions. In the upper left corner graph, both non-transfected Cas9 and E2F1Cr conditions were included for the purpose of graphical comparison; n = 3 independent experiments performed in technical triplicates. Results are expressed as mean ± SEM; one-way ANOVA with Tukey's multiple comparisons; ** p < 0.001, *** p < 0.0001, **** p < 0.00001.*

In summary, as an E2F1 target, the expression of SLC4A7 is reduced in the absence of E2F1, while its exon 25 skipping levels remain unaffected. This reduction in SLC4A7 expression in E2F1Cr cells explains the lack of responsiveness to Δ25 ASO treatment, which leads to a loss of its effects on pH_i/pH_e dynamics and cell growth. These findings, along with those described in the previous sections, and their relevance in the microenvironmental regulation of PDAC cells will be discussed in the following section.

4.3. Discussion

After characterizing the effects of PRMT5 inhibition on cell cycle, cell growth, and the induction of apoptosis, a non-antiproliferative concentration of T1-44 was used to perform RNAseq experiments. These were conducted to evaluate the overall effects of this agent on gene and lncRNA expression. In general, and in accordance with previous reports (Barczak et al., 2023; Bate-Eya et al., 2025), T1-44 alters the expression level of several lncRNA transcripts, but its DEG profile is different than the ones observed for neuroblastoma and CRC. For example, T1-44 treatment up-regulated the expression of DANCR and MALAT1, and Gm15635 and EU59941 in the CRC cell lines HCT116 and CT26 (Barczak et al., 2023), but the expression levels of these lncRNA remained unchanged in the PDAC cell lines used in this thesis (Panc-1 and Panc02). These differences could be explained, in part, by the mutational profile of these cell lines (Maeng et al., 2025) and the inherent genetic variability between different types of cancer (Mahmoud et al., 2025). In line with this, PRMT5 inhibition reduced the expression of oncogenic lncRNAs like

NEAT1, a known overexpressed lncRNA in PDAC, breast and hepatocellular cancer that regulates the expression of the tumour suppressor microRNA miR-129-5p (Mahmoud et al., 2025). These findings highlight that the transcriptional effects of PRMT5 inhibition have the potential to be used altogether with other agents to improve antitumour response.

When *in silico* promoter analysis was performed on these DE lncRNA transcripts, a similar percentage of E2F1 binders than the ones observed for CRC was found for Panc-1 and Panc02 cells (Barczak et al., 2023). This information and the subsequent qPCR validation experiments performed for predicted E2F1 binders in Cas9 and E2F1Cr cell lines, confirm that the status of E2F1, a highly-deregulated transcription factor associated with poor prognosis in several malignancies including PDAC (Bertonnier-Brouty et al., 2024; Li et al., 2023), plays an important role in the transcriptional effects of PRMT5 inhibition.

Despite the fact that T1-44 modifies the expression of lncRNA transcripts, this does not provide any information about their translatability nor their MHC- I and/or MHC-II binding capacity (Lv et al., 2021). To address these issues, Ribo-seq and polysome enrichment analysis were performed on Panc02 cells, finding a group of potentially-translatable lncRNA transcripts which were identified in the polysomal fraction of T1-44-treated Panc02 cells. *In silico* analysis of these lncRNA sequences identified the presence of both conventional and alternative ORFs within them. The potential for translation of these lncRNA-derived peptides was demonstrated experimentally using a representative 9-mer, SAYCVPLYL, predicted as a strong H-2Db/Kb binder derived from a non-conventional ORF identified within

the 1700018L02Rik-201 sequence. This information, supported by previous findings where a poly-antigen string of lncRNA-derived peptides inserted in the adenoviral vector ChAdOx1 was capable to induce the immune response in CRC (Barczak et al., 2023), highlights the potential of these translatable lncRNA to be used as source of non-canonical peptides that could trigger IFNγ release by CD8+ cells, reverse MHC-I downregulation and therefore enhance PDAC immunogenicity, as has been demonstrated in previous reports (Baleeiro et al., 2022; Deng et al., 2021; Ely et al., 2025). This rationale led to the design of the ChAdOx1-PepLncP2 vaccine as tool to evaluate the immunogenic potential of these predicted lncRNA-derived peptides. However, this thesis followed an *in silico* pipeline that differs from standard the immunopeptidomics-based protocol used previously by our research group (Barczak et al., 2023), but similar immunoinformatic approaches have been successfully attempted for PDAC to perform a fast screening of cryptic antigens, despite the high rate of false-positive MHC-I binders reported for this type of pipelines (Borole and Rajan, 2024; Nilsson and Nielsen, 2024; Rojas et al., 2023). The evaluation of the ChAdOx1-PepLncP2 vaccine, and therefore, the potential of PRMT5 inhibition as a route to induce PDAC immunogenicity, is a topic that will be developed in the following chapter.

When the GO analysis results of Panc-1 and Panc02 cells treated with T1-44 are considered, several overrepresented terms associated with glycolysis and OXPHOS were found (*e.g.*, 'ATP biosynthetic process', 'pyruvate biosynthetic process', ´glycolytic process through glucose-6-phosphate', 'proton motive force-driven ATP synthesis', etc). These results were validated by testing the effects of T1-44 on pH dynamics and O_2 consumption, which revealed that PRMT5 inhibition

reduced of pH_i, likely because of a reduction of the activity of glycolytic enzymes, as shown in a report focused on the electrogenic bicarbonate transporter SLC4A4 (Cappellesso et al., 2022). This alteration of pH_i led to an increase in pH_e, and, in parallel, to a decreased oxygen consumption in Panc-1 and Panc02 cells. These data are consistent with previous reports for other PRMT5 inhibitors, such as JNJ-64619178 and the repurposed drug tadalafil, which attenuated aerobic glycolysis and cell proliferation of CRC and breast cancer cell lines (Shen et al., 2022; Yang et al., 2022). A similar effect of suppressed aerobic glycolysis was observed in PDAC with knocked-down PRMT5, which increased the activity of the tumour suppressor FBW7 and reduced cMyc activity (Qin et al., 2019). These effects of PRMT5 inhibition attenuating the pro-glycolytic features of PDAC (Chen et al., 2023), altogether with shifts in lipid metabolism, amino acid uptake and lactate secretion, which are relevant factors for PDAC survival (Daemen et al., 2015; Islam et al., 2022), should be able to improve the conditions within the TME to facilitate immune response. PDAC is characterized by an acidic TME with a dense desmoplastic stroma that reduces drug penetration and treatment efficacy (Islam et al., 2022; Li et al., 2022; Wang et al., 2021), promotes ECM remodelling (Czaplinska et al., 2023) and facilitates immunosuppression by reducing antigen presentation by myeloid DCs, and suppressing the function of NK and cytotoxic T cells (Cappellesso et al., 2022; Islam et al., 2022). Additionally, PDAC tumours are associated with increased regulatory T cell activity and tumour-associated macrophages (TAM) skewing towards anti-inflammatory phenotypes (Chang et al., 2022; Islam et al., 2022; Li et al., 2022; Wang et al., 2021; Wu et al., 2022; Yin et al., 2022).

After describing the functional effects of T1-44 on pH balance, and in line with the enrichment of GO terms associated with transporter activity (*e.g.*, 'positive ion transmembrane transport', 'regulation of anion transmembrane transport', 'glucose transmembrane transport', *etc*), an initial mechanism of action for this PRMT5 inhibitor was proposed: T1-44, via inducing changes in the activity or expression of SLC transporters involved in the uptake or extrusion of H^+, HCO_3^- and/or metabolites (*e.g.*, glucose, lactate, amino acids, etc), affects cell metabolism and TME conditions (Cho et al., 2025; Li et al., 2022). However, after confirming that the effects of PRMT5 on pH_i/pH_e balance were no longer apparent under NVB (*i.e.* HEPES/MES buffering), thus revealing a bicarbonate-dependent activity, NBCn1/SLC4A7, a bicarbonate uptake transporter associated with PDAC tumour survival and murine breast cancer growth and development (Lee et al., 2016; Li et al., 2022), appeared as a potential target regulated by PRMT5. Based on the literature, other representatives from the SLC4 transporter family have also been studied and considered as potential anti-cancer targets. For example, the HCO_3^- extruder SLC4A2, an anion exchanger which lysosomal degradation via mTORC1 inhibition has been proposed as a CRC adaptation mechanism to overcome the effects of acidic TME that hinders glycolytic rate and survival (Michl et al., 2023). Conversely, the electrogenic Na^+/HCO_3^- transporter NBCe1/SLC4A4, a highly-overexpressed carrier in PDAC closely related to SLC4A7, has been described as a relevant factor promoting intracellular alkalinization that facilitates tumour growth, glycolytic rate and lactate/H^+ extrusion via monocarboxylate transporters (MCT) (Cappellesso et al., 2022). These effects lead to a reduction in pH_e that inhibits mDC antigen presentation, CD8+ T cell activation, pro-

inflammatory TAM proliferation, and decreases PDAC response to immune checkpoint inhibitors (Cappellesso et al., 2022). All these effects were counteracted by SLC4A4 knockdown and non-specific inhibition by 4,4'-diisothiocyano-2,2'-stilbenedisulfonic acid (DIDS) (Benítez-Rangel et al., 2015; Cappellesso et al., 2022).

The choice of SLC4A7 as a downstream target of T1-44 activity is further supported by rMATS analysis and subsequent qPCR validation. This agent is capable of inducing a particular exon-skipping event, Δ25 SLC4A7, which has an impact in pH dynamics by the association of the skipping of exon 25, a 36-aa optional structural element from the C-terminus region known as cassette III, with a 3 to 5-fold reduction of the intrinsic Na^+/HCO_3^- uptake activity of SLC4A7 (Liu et al., 2013; Wang et al., 2022). To confirm that the effects of T1-44 in pH dynamics were associated with Δ25 SLC4A7 induction, an exon-skipping ASO was designed to trigger this specific event. After validation and quality control, the Δ25 ASO exerted similar pH_e increase and pH_i decrease effects as T1-44. Loss of effects under bicarbonate-free buffering conditions confirmed the likelihood that these effects were exerted by the activity of SLC4A7. Interestingly, no further changes in pH_i/pH_e were observed when combinatorial T1-44 + Δ25 ASO treatments were used. This could be explained by the saturation of SLC4A7 activity reduction, which was probably reached by individual treatments. Additionally, SLC4A7 is one of many transporters involved in pH regulation, so other carriers are likely to compensate to maintain pH dynamics favourable for tumour survival (Blaszczak et al., 2022; Wang et al., 2025). Additionally, no effects on O_2 consumption were found after Δ25 ASO treatment, which is consistent with previous gene enrichment analysis performed

in CRC cell lines that found no association between SLC4A7 and OXPHOS (Michl et al., 2022). In contrast, T1-44 treatments were capable of reducing O_2 consumption, which is in agreement with the OXPHOS-related terms found in the GO analysis. A similar study using the PRMT5 inhibitor JNJ-64619178 in cellular models of Merkel cell carcinoma also identified that PRMT5 regulates oxidative metabolism (Sevigny et al., 2025).

After confirming that Δ25 SLC4A7 plays a role in the mechanism by which T1-44 alters pH balance, the cellular implications of these changes were studied by testing cell growth and evaluating the lipid peroxidation effect in combination with the conventional chemotherapeutic doxorubicin. In general, Δ25 SLC4A7 reduced cell growth in both Panc-1 and Panc02 cells by impairing the activity of this bicarbonate transporter by the loss of functionally-relevant exon 25. This is consistent with previous findings in breast cancer and head and neck squamous cell carcinoma, where high SLC4A7 expression was associated with increased tumour cell growth and metastasis (Axelsen et al., 2024; Hu et al., 2023). Similarly, Axelsen *et al*. developed a monoclonal antibody designed to bind to the third extracellular loop of human SLC4A7 which hindered the growth of triple-negative breast cancer cells (Axelsen et al., 2024). When the effects of combinatorial treatments with Dox were analysed, an increase in the lipid peroxidation induced by this drug was found when it was combined with either T1-44 or Δ25 ASO. Triple Dox + T1-44 + Δ25 ASO treatments did not promote lipid peroxidation any further, supporting the claim of reaching maximal SLC4A7 activity reduction. This experiment provided further evidence that the modifications of pH_i/pH_e balance

induced by PRMT5 inhibition and Δ25 ASO are functionally relevant, and could increase the efficacy of weakly basic chemotherapeutics like Dox (Lee et al., 2023).

Lastly, the involvement of E2F1 in these responses was evaluated using Panc02 Cas9 and E2F1Cr cells. First, it was confirmed via qPCR in tumour samples that SLC4A7 acts as an E2F1 binder, showing that the overall expression of this bicarbonate transporter was reduced in E2F1Cr tumours, but the absence of E2F1 had no effects on SLC4A7 AS. Consequently, E2F1 loss hindered the exon-skipping activity of Δ25 ASO and cellular effects due to a reduction of the overall SLC4A7 transcript levels. A similar conclusion could be drawn to explain the lack of effects on pH balance on E2F1Cr cells. However, the O_2 consumption reduction after T1-44-containing treatments was maintained regardless of E2F1 status, highlighting that the effects of PRMT5 inhibition in this process are regulated by other factors. These experiments illustrate the involvement of E2F1 in PDAC cell survival, and how the deregulation of this transcription factor can be seen as a strategy of tumours to promote tumour survival via shifting expression and alternative splicing profiles.

In summary, the data described in this chapter indicate that PRMT5 inhibition exerts a two-pronged effect in PDAC cells: by inducing the expression of translatable lncRNA peptides, and by altering pH_i/pH_e dynamics via inducing the skipping of SLC4A7 exon 25. These effects depend, to a certain extent, on the status of E2F1, as can be observed in E2F1Cr models, which have impaired the lncRNA and SLC4A7 expression responses observed under PRMT5 inhibition. The impact of these *in vitro* findings in lncRNA expression and pH dynamics on PDAC immunogenicity will be described in the following chapter.

Chapter 5 : PRMT5 inhibition as a strategy to induce immunogenicity on *in vivo* PDAC models

5.1. Introduction

The limited efficacy of therapeutic agents against PDAC has been widely associated with the characteristics of its TME, a highly acidic microenvironment, with abundant ECM density and immunosuppressive cells like pro-inflammatory macrophages, MDSCs and regulatory T cells (Ju et al., 2024; Mundry et al., 2020; Musiu et al., 2024). For this reason, therapeutic strategies that aim to improve PDAC immune responsiveness by reversing some if its TME features have been proposed in the scientific literature.

For example, Zhang *et al*. used the intra-tumoral injection of a peptide-based hydrogel, which contained the bile pigment biliverdin and the thymic peptide thymopentin, reduced tumour growth and enhanced T cell infiltration in an orthotopic model of PDAC (Zhang et al., 2023a). Another example could be a combination treatment consisting of radiotherapy, the EGFR inhibitor cetuximab and ICP^{IL2ZA} (an NK- and monocyte-enriched cell extract activated with IL-2 and zoledronic acid), which decreased tumour volume and enhanced the infiltration and activation of T and NK cells in a syngeneic PDAC model expressing human EGFR (Rahman et al., 2025). Regarding PRMT5, the inhibitor EPZ-015866, in combination with anti-PD-L1 immunotherapy, reduced tumour weight and increased CD8 cell infiltration and activation in a lung cancer model (Hu et al., 2022). Another example

of this can be found in the case report by Leidner *et al.*, who proposed a therapeutic TCR approach based on the infusion of autologous T cells restricted to express human leukocyte antigen (HLA) allele HLA-C*08:02 TCR directed against KRASG12D (mutation present in ≈ 45% of PDAC cases). Using this approach, the authors obtained promising results in the regression of metastatic lung lesions in one patient, but the low prevalence of the HLA-C*08:02 allele restricted the applicability of this strategy to the general population (Leidner et al., 2022). Another therapeutic approach, proposed by Rojas et al., considered the use of a nanoparticle-based mRNA-lipoplex vaccine called autogene cevumeran containing *in silico*-predicted neoantigens that can be presented by both classes of MHC to treat patients submitted to pancreatic resection in combination with the anti-PD-L1 monoclonal antibody atezolizumab and modified FOLFIRINOX, which led to a 2-year-sustained T cell response that delayed PDAC recurrence in 8 out of 16 patients (Rojas et al., 2023).

Considering the relevance of the TME in PDAC, the precedents that PRMT5 inhibition has as an immunosensitizing agent in CRC (Barczak et al., 2023), and the potential that PRMT5 inhibition have demonstrated *in vitro* throughout this thesis, this chapter will focus on the immunogenicity evaluation of the lncRNA-derived peptides induced by T1-44, the *in vivo* assessment of the effects of PRMT5 inhibition in SLC4A7 exon 25 skipping and pH dynamics, and the implications that this might have in immune cell activation and infiltration.

5.2. Results

5.2.1. PepLncP2 peptides stimulate IFNγ release in C57BL/6 mice

To provide a general landscape of the immunogenic potential of the 28 *in silico*-predicted lncRNA-derived peptides contained in the PepLncP2 cassette, this string was cloned into a ChAdOx1 adenoviral vector. Then, C57BL/6 mice were immunized with the vaccine (Figure 5.1A). The capacity of the ChAdOx1-PepLncP2 vaccine to stimulate IFNγ secretion was tested via ELISpot on splenocytes treated with a pool of 28 PepLncP2 peptides, finding an increase in splenocyte stimulation (Figure 5.1B). This increase was substantially higher than the positive control PHA, which was capable to induce only a modest increase in IFNγ secretion. Additionally, ChAdOx1-PepLncP2 vaccination did not induce any changes in the body weight of the animals (Figure 5.1C, left graph) and was capable to promote IFNγ release when compared with the mice vaccinated with ChAdOx1-GFP (Figure 5.1C, right graph).

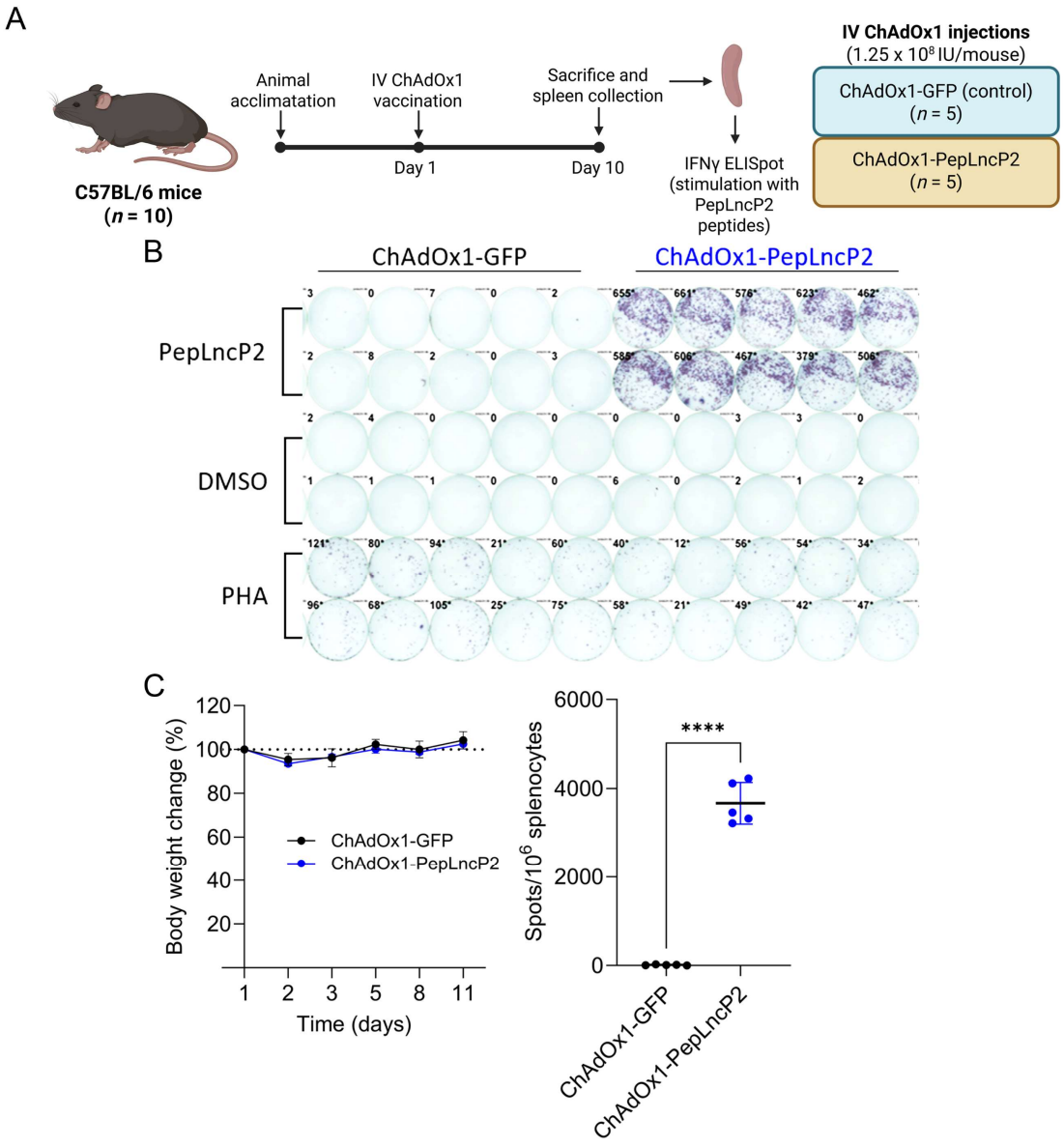

Figure 5.1. In silico-predicted lncRNA-derived peptides are capable to immunogenicity.

A. *Experimental design used for ELISpot experiments. Briefly, C57BL/6 mice were immunized with ChAdOx1-GFP or ChAdOx1-PepLncP2 vaccines (n = 5 mice per treatment). 9 days after vaccination, animals were culled and their splenocytes collected for ELISpot. Figure created in https://BioRender.com.* ***B.*** *IFNγ ELISpot plate obtained after stimulating splenocytes with a pool of the PepLncP2 peptides ('PepLncP2'). DMSO and PHA were included as negative and positive controls, respectively; n = 2 independent experiments.* ***C.*** *Relative body weight measurements (left graph) and IFNγ spots counts (right graph) obtained after treating C57BL/6 mice with ChAdOx1-GFP and ChAdOx1-PepLncP2 vaccines; n = 5 mice per treatment. Results are expressed as mean ± SD; two-tailed unpaired Student's t-test; **** p < 0.00001. These experiments were performed by Dr. Wiktoria Blaszczak.*

5.2.2. PRMT5 inhibition promotes Slc4a7 exon 25 skipping and modifies the pH of tumour microenvironment without compromising immune cell infiltration in C57BL/6 mice

As a way to establish if the effects of T1-44 in Panc02 cell growth and proliferation can also be observed *in vivo*, a model consisting in immunocompetent C57BL/6 mice bearing syngeneic Panc02 cells implanted subcutaneously received oral treatments with bicarbonate water, T1-44 and vehicle solution (*i.e.* 5.0% DMSO, 0.5% Tween 80 in water) for 16 days (Figure 5.2A). Initial assessments comparing all treatment groups showed that no differences were found for both tumour volume and body weight measurements during the entire length of the experiment (Figure 5.2B). However, when snap-frozen tumour samples were analysed, it was found that, in line with *in vitro* findings, none of the treatment conditions modified Slc4a7 expression (Figure 5.2C, left graph), but only T1-44 induced Slc4a7 exon 25 skipping (Figure 5.2C, right graph). These findings highlight that, despite T1-44 not showing antiproliferative effects *in vivo*, it is capable to promote Slc4a7 AS in a similar way as it was observed *in vitro*.

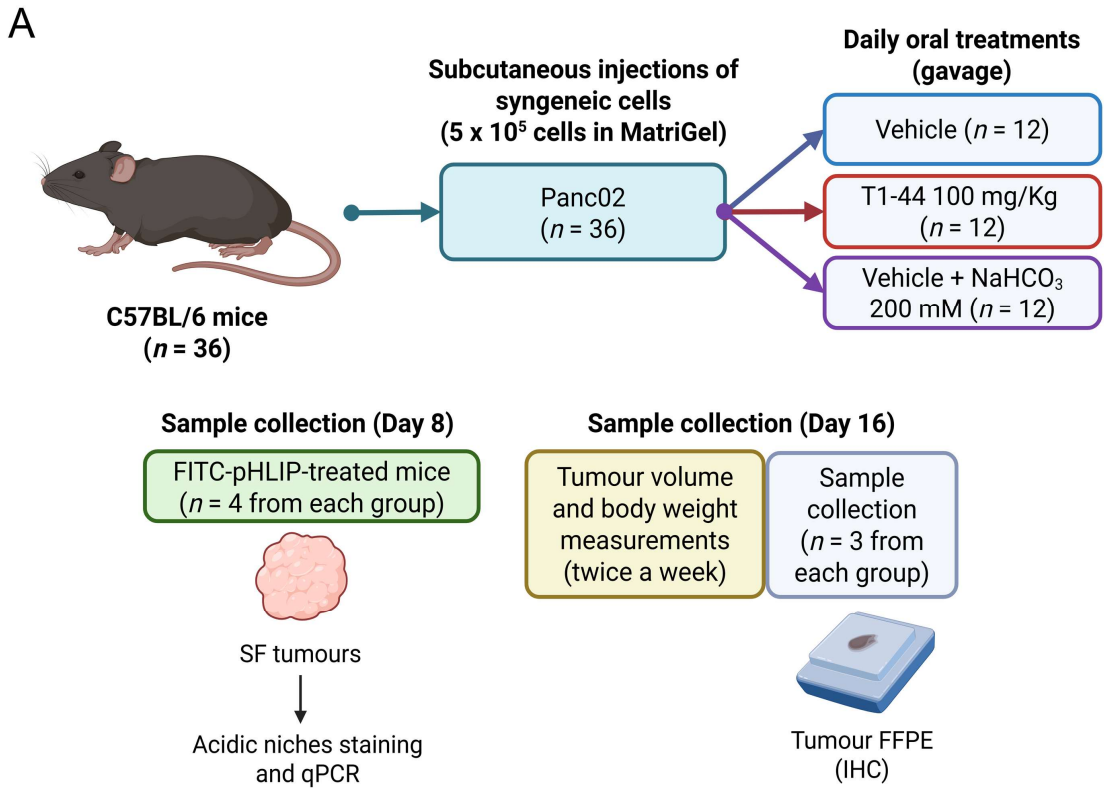
A
Subcutaneous injections of syngeneic cells (5 x 10⁵ cells in MatriGel)
Daily oral treatments (gavage)
Vehicle (n = 12)
T1-44 100 mg/Kg (n = 12)
Vehicle + NaHCO3 200 mM (n = 12)
Panc02 (n = 36)
C57BL/6 mice (n = 36)
Sample collection (Day 8)
FITC-pHLIP-treated mice (n = 4 from each group)
SF tumours
Acidic niches staining and qPCR
Sample collection (Day 16)
Tumour volume and body weight measurements (twice a week)
Sample collection (n = 3 from each group)
Tumour FFPE (IHC)

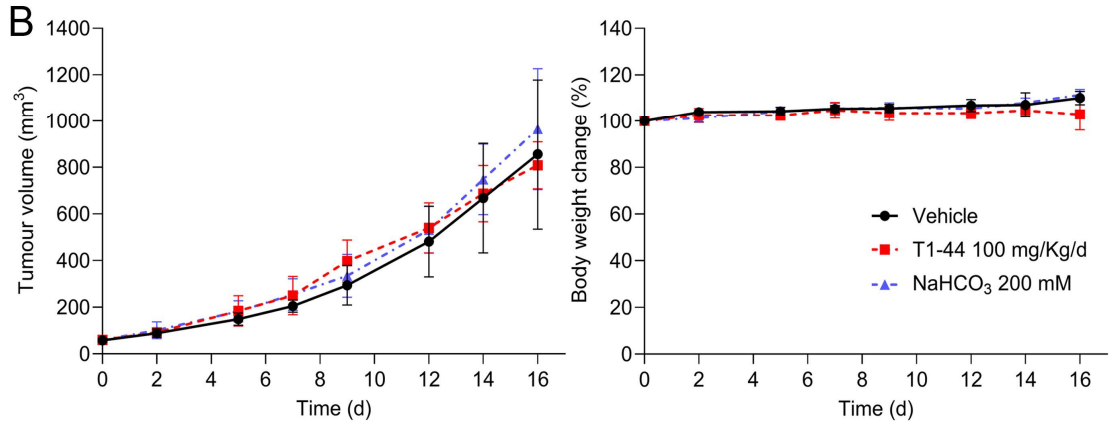
B
Tumour volume (mm3)
Time (d)
Body weight change (%)
Vehicle
T1-44 100 mg/Kg/d
NaHCO3 200 mM

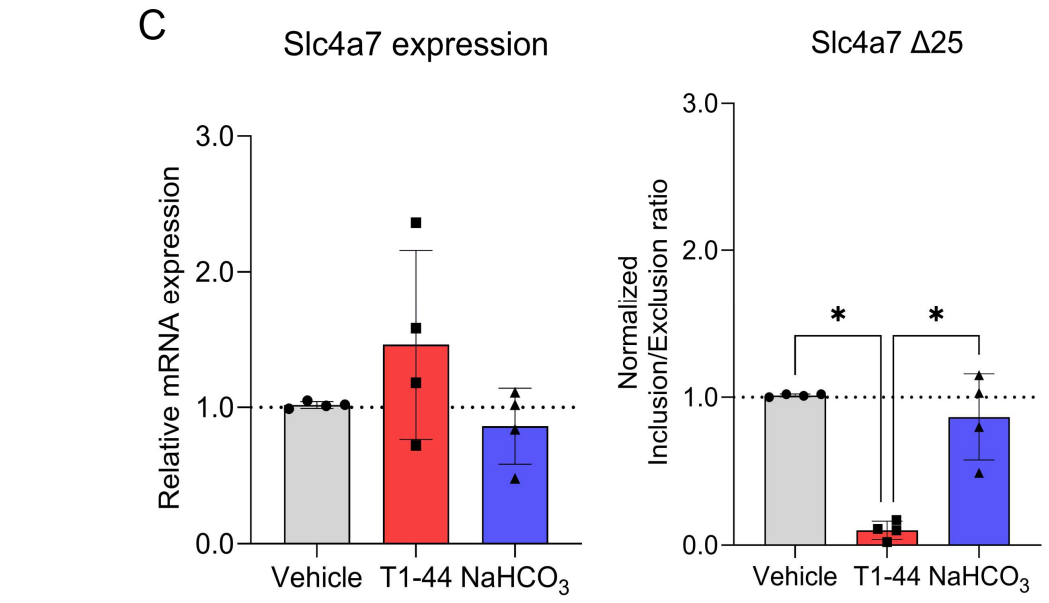
C
Slc4a7 expression
Slc4a7 Δ25
Relative mRNA expression
Normalized Inclusion/Exclusion ratio
Vehicle
T1-44
NaHCO3

Figure 5.2. PRMT5 inhibition is capable to promote Slc4a7 exon 25 skipping in vivo.

A. *Experimental design used for in vivo experiments. Briefly, C57BL/6 mice received subcutaneous injections of Panc02 cells and, after reaching a tumour volume between 50 and 150 mm^3, received daily oral treatments with vehicle (5% DMSO, 0.5% Tween 80 in water solution), T1-44 and ad libitum bicarbonate water (n = 12 mice per treatment group). After 8 days of treatment, 4 animals of each group were treated with a FITC-pHLIP probe and tumour samples were collected after culling. The rest of the animals were maintained until day 16, recording their body weight and tumour volume twice a week and collecting tumour FFPE samples by the experiment endpoint. Figure created in https://BioRender.com.* ***B.*** *Tumour volume (left graph) and body weight (right graph) measurements obtained after treating Panc02 tumour-bearing C57BL/6 mice with the aforementioned treatment conditions; n = 8 mice per treatment group. Results are expressed as mean ± SD; one-way ANOVA with Tukey's multiple comparisons.* ***C.*** *qPCR measurements performed on RNA extracts obtained from Panc02 tumour samples to quantify the relative effect of vehicle, T1-44 and $NaHCO_3$ treatment in Slc4a7 overall expression (left graph) and Slc4a7 exon 25 skipping (right graph); n = 4 mice per treatment group. Results are expressed as mean ± SD; one-way ANOVA with Tukey's multiple comparisons. * $p < 0.05$.*

However, to evaluate if the induction Slc4a7 exon 25 skipping promoted by T1-44 can have a functional impact in tumour acidity, immunofluorescence experiments using a FITC-pHLIP probe were considered. *In vitro* testing of this probe using Panc02 cells cultured at different pH conditions showed a progressive increase of the FITC signal when extracellular pH was reduced from 6.81 to 6.20 (Figure 5.3), validating the performance of this probe staining acidic niches.

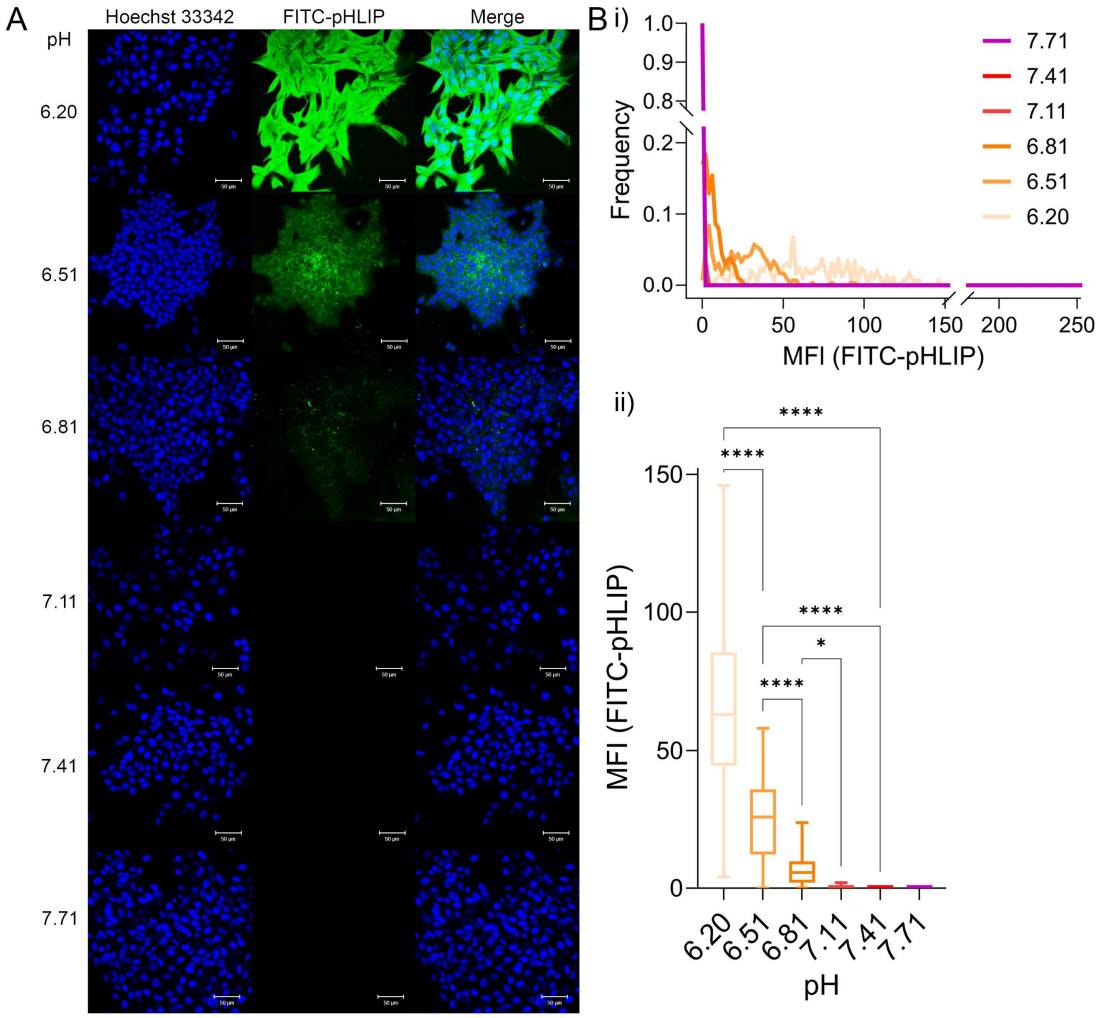

Figure 5.3. FITC-pHLIP probe is capable to detect acidic niches in Panc02 cells. ***A.*** *Representative immunofluorescence images of Panc02 cells cultured under different pH-adjusted bicarbonate-buffered sDMEM. Before mounting with antifade agent + Hoechst 33342, cells were treated for 20 min with a 10 µM FITC-pHLIP in DMSO solution; n = 3 independent experiments. Magnification: 40x, Scale bar: 50 µm.* ***B.*** *(i) Histograms and (ii) box and whiskers graphs detailing the distribution of the FITC-pHLIP signal intensity from Panc02 cells cultured under different pH conditions; n = 3 independent experiments. Results are expressed as box and whiskers representing the median and minimum to maximum MFI value range; one-way ANOVA with Tukey's multiple comparisons. * $p < 0.05$, **** $p < 0.00001$.*

When the tumour samples from mice treated with FITC-pHLIP were processed and analysed via immunofluorescence, an overall reduction of the FITC signal was observed for both T1-44 and bicarbonate water treatment (Figure 5.4).

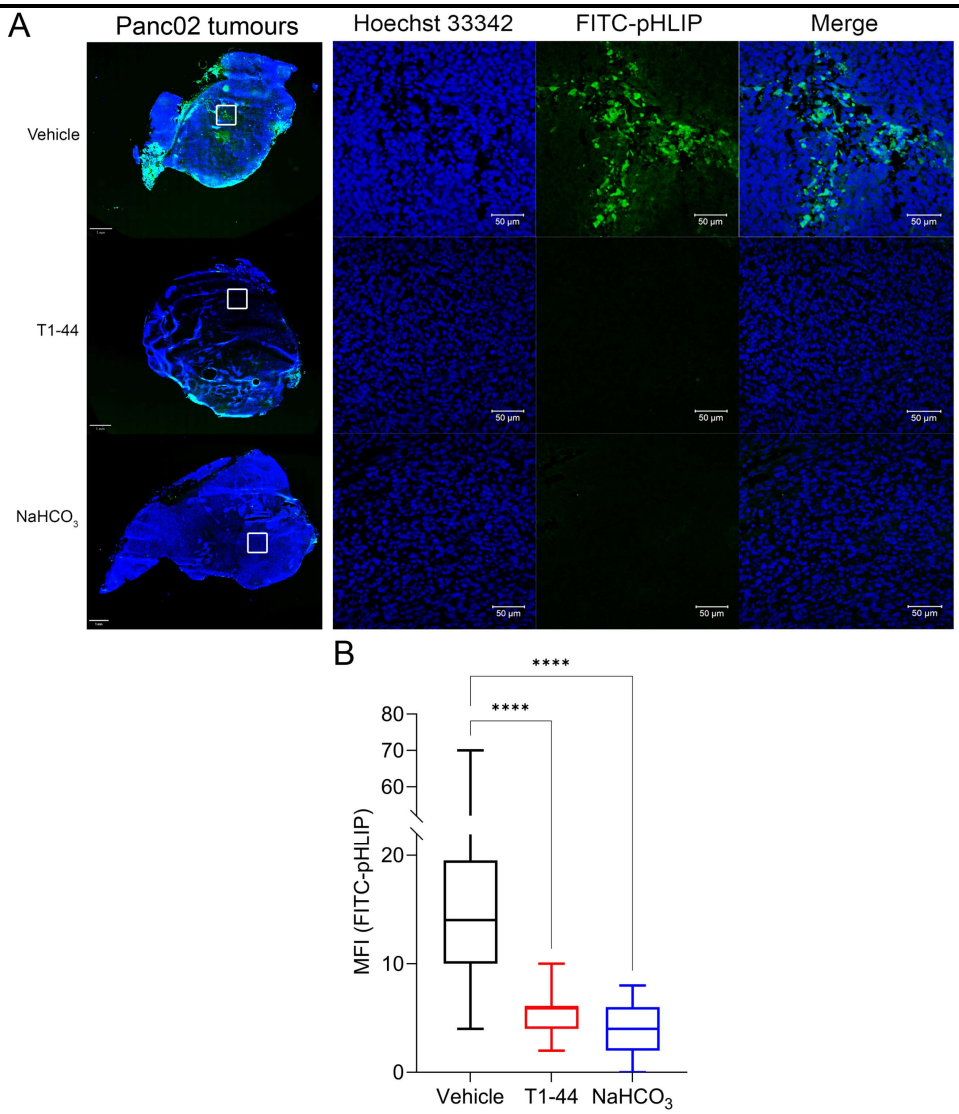

Figure 5.4. T1-44 reduces microenvironmental acidity in tumour samples. ***A.*** *Representative section scanning (left column) and confocal microscopy (right square) images of subcutaneous Panc02 tumours obtained from C57BL/6 mice treated with T1-44, bicarbonate water and vehicle solution, plus a FITC-pHLIP solution to detect acidic niches; n = 4. Magnification: 10x (section scanning) and 40x (confocal microscopy), Scale bar: 1 mm and 50 µm for scanning and confocal microscopy, respectively. White squares in the scanning microphotographs represent the area magnified for confocal microscopy.* ***B.*** *Distribution of the FITC-pHLIP fluorescent signal intensity obtained in tumour samples after treating mice with vehicle solution, T1-44 and bicarbonate water; n = 4 independent experiments. Results are expressed as box and whiskers representing the median and minimum to maximum MFI value range; one-way ANOVA with Tukey's multiple comparisons. **** $p < 0.00001$.*

Lastly, to evaluate if the microenvironmental effects of T1-44 in pH dynamics might induce immune cell activation or infiltration, immunohistochemistry experiments were performed. Despite confirming the presence of T1-44 pharmacological target by PRMT5 staining, and the activity of this drug by the suppression of the SDMe signal, none of treatments was capable to alter the infiltration of both CD4 and CD8 cells (Figure 5.5). However, PRMT5 inhibition slightly increased of GZMB staining, which is evidence of a slight increase in immune cell activity inside the tumour (Figure 5.5).

Overall, these experiments show that, in this particular *in vivo* model, T1-44 is capable to modify microenvironmental pH by inducing the skipping of Slc4a7 exon 25, and these changes do not affect CD4 and CD8 cells infiltration but induce GZMB release in tumour sites.

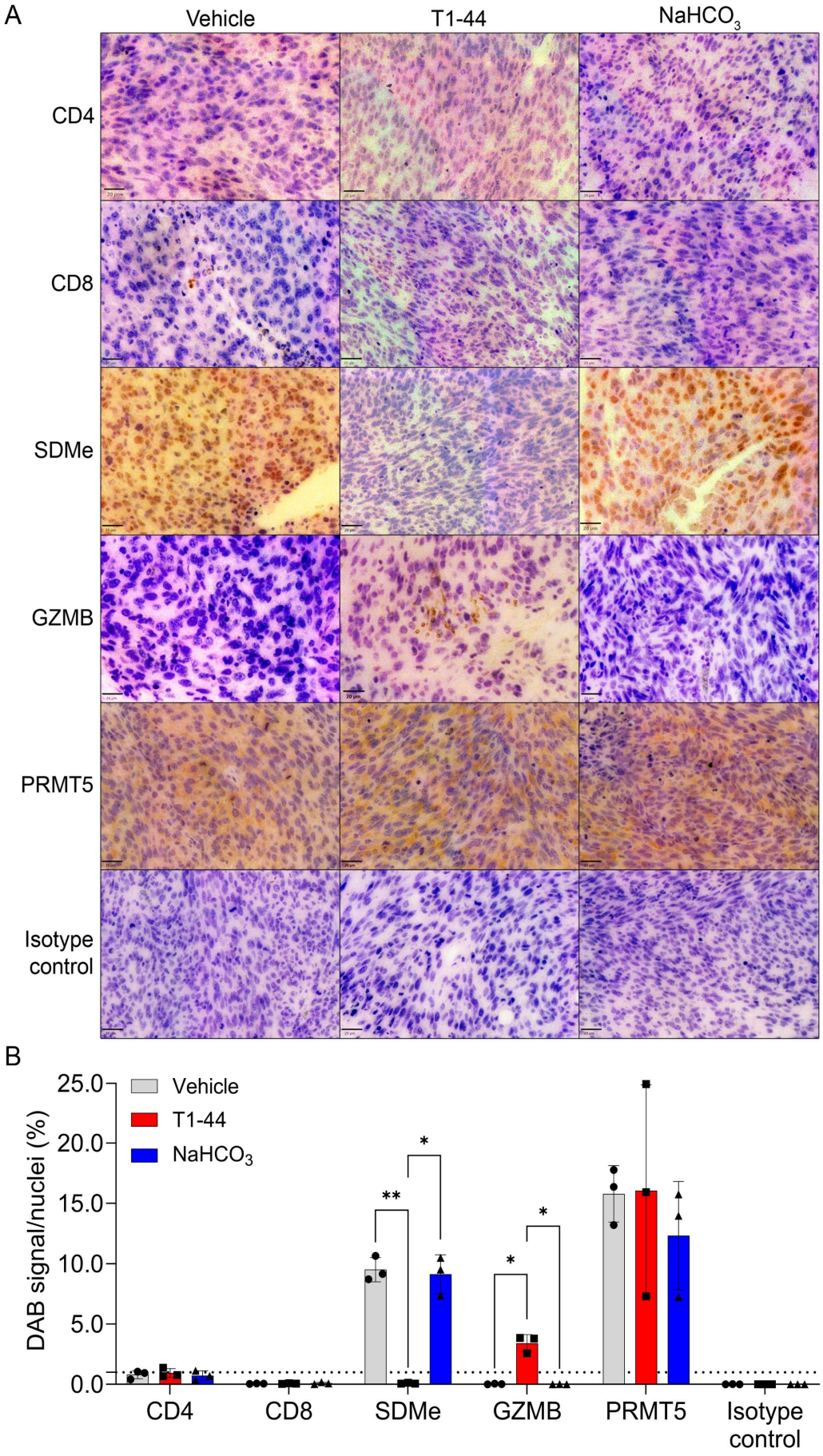
A
Vehicle
T1-44
NaHCO3
CD4
CD8
SDMe
GZMB
PRMT5
Isotype control
B
DAB signal/nuclei (%)
25.0
20.0
15.0
10.0
5.0
0.0
Vehicle
T1-44
NaHCO3
**
*
*
*
CD4
CD8
SDMe
GZMB
PRMT5
Isotype control

Figure 5.5. T1-44 treatment induces GZMB release, but it does not have any effects in CD4 and CD8 cells infiltration to tumour sites.
A. *Representative widefield microphotographs taken from tumour samples from C57BL/6 mice treated with T1-44, bicarbonate water and vehicle solution and stained with antibodies against CD4, CD8, SDMe, GZMB and PRMT5, and rabbit IgG isotype control; n = 3 independent experiments. Magnification: 40x, Scale bar: 20 µm.* ***B.*** *DAB pixel intensity analysis expressed as percentage of DAB signal/nuclei obtained for CD4, CD8, SDMe, GZMB, PRMT5 and rabbit IgG isotype control staining of tumour tissue samples treated with vehicle solution, T1-44 and bicarbonate water; n = 3 independent experiments using four images per replicate. Results are expressed as mean ± SD; two-way ANOVA with Geisser-Greenhouse corrections. * $p < 0.05$, ** $p < 0.01$.*

5.2.3. ChAdOx1-PepLncP2 treatment reduces tumour growth in C57BL/6 mice

With the purpose to evaluate the anti-tumour potential of the PepLncP2 cassette, tumour challenge experiments were carried out comparing C57BL/6 mice vaccinated with ChAdOx1-GFP and ChAdOx1-PepLncP2 (Figure 5.6A). After 25 days of tumour volume measurements, it was established that ChAdOx1-PepLncP2 was capable to reduce tumour growth when compared to ChAdOx1-GFP without compromising the body weight of the animals (Figure 5.6B). Subsequently, to demonstrate the immunogenic capacity of the ChAdOx1-PepLncP2 vaccine, IFNγ ELISpot was performed on splenocytes samples, finding that only the mice inoculated with ChAdOx1-PepLncP2 were capable to stimulate IFNγ secretion when splenocytes were treated with a pooled solution of the 28 PepLncP2 peptides (Figure 5.6C).

These experiments confirm that the immunogenic activity of the ChAdOx1-PepLncP2 vaccine is capable to compromise tumour growth in mice bearing subcutaneous Panc02 tumours.

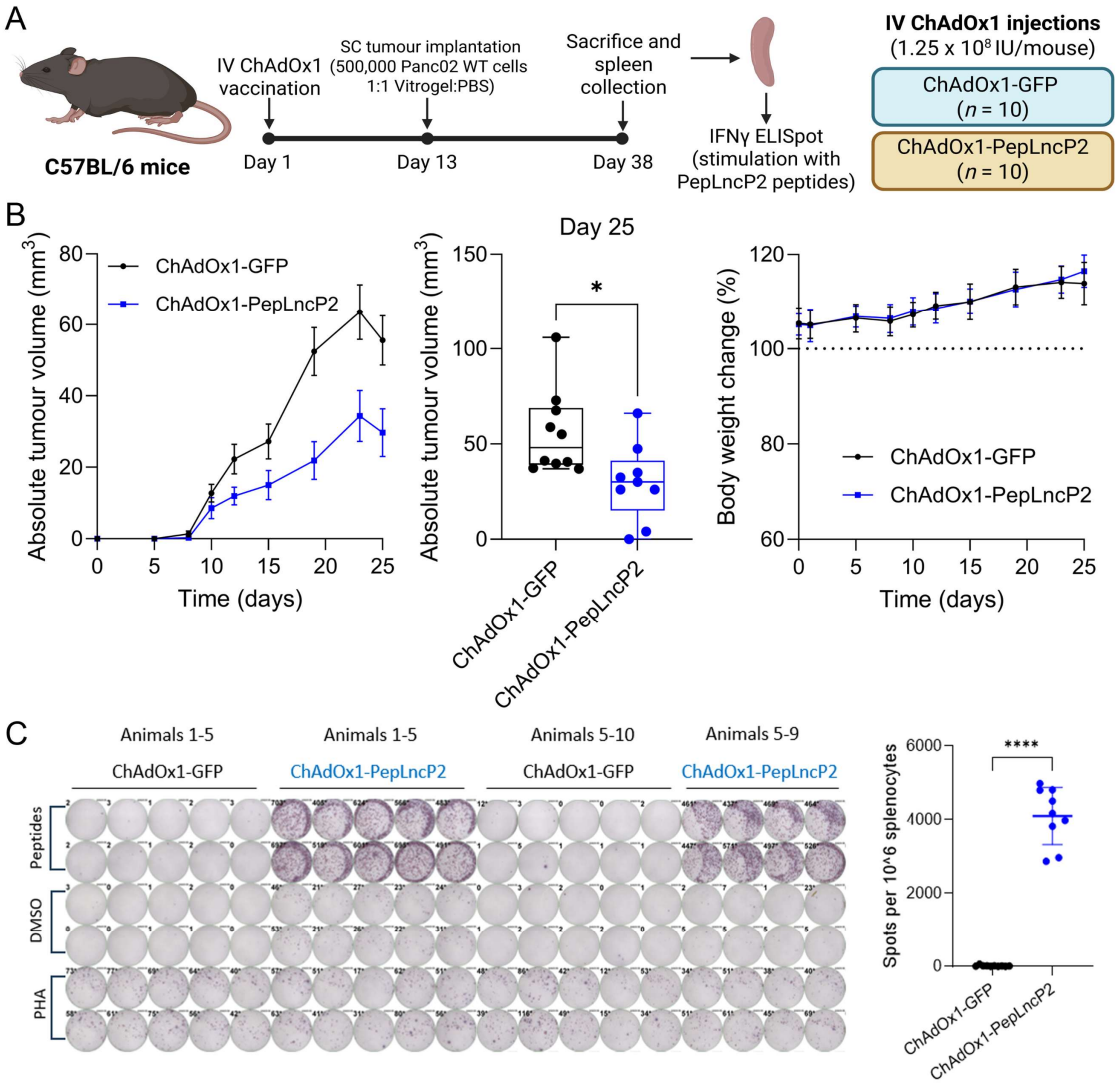

Figure 5.6. ChAdOx1-PepLncP2 vaccination decreases subcutaneous tumour growth in C57BL/6 mice.

A. *Design used for tumour challenge experiments. Briefly, C57BL/6 mice were inoculated with ChAdOx1-GFP or ChAdOx1-PepLncP2 vaccines (n = 10 mice per treatment). 12 days after vaccination, subcutaneous tumours were implanted in mice and tumour volume and body weight recordings were performed for 25 days, when animals were culled and their splenocytes collected for IFNγ ELISpot. Figure created in https://BioRender.com.* ***B.*** *Measurements of tumour volume throughout the experiment (left graph) and at day 25 (central graph), and body weight recordings (right graph) obtained when Panc02 tumours were implanted in C57BL/6 mice treated with ChAdOx1-GFP (n = 10) and ChAdOx1-PepLncP2 (n = 9) vaccines. Results are expressed as mean ± SEM (left graph), box and whiskers (central graph) and mean ± SD (right graph); two-tailed unpaired Student's t-test; * $p < 0.05$.* ***C.*** *IFNγ ELISpot plates (left graph) and IFNγ spots counts (right graph) obtained after stimulating splenocytes derived from mice treated with ChAdOx1-GFP (n = 10) and ChAdOx1-PepLncP2 (n = 9) with a pool of the PepLncP2 peptides ('Peptides'), DMSO and PHA. Results are expressed as mean ± SD; two-tailed unpaired Student's t-test; **** $p < 0.00001$. These experiments were performed by Dr. Wiktoria Blaszczak.*

5.3. Discussion

After confirming that T1-44 is capable to induce the expression of lncRNA-derived peptides and alter pH balance in PDAC cell lines, subsequent *in vivo* evaluations were needed to confirm these findings. As Initial approach to test the potential of PRMT5 inhibition as an immunosensitizer drug in PDAC, C57BL/6 mice were inoculated with ChAdOx1-PepLncP2. This vaccine contains a poly-antigen string of 28 lncRNA-derived peptides whose expression is induced by T1-44 and have been predicted *in silico* as strong MHC-I binders. As result, ChAdOx1-PepLnc2P vaccination significantly induced IFNγ release from splenocyte samples and reduced tumour growth. This effect can be associated with an enhancement of T cell activation (Wykes and Renia, 2017), a group of cells that constitutes about 20-35% of the population of splenocytes in C57BL/6 mice (Hensel et al., 2019), but this needs to be proven in future studies performing IHC analysis in tumour samples collected from mice treated with T1-44, ChAdOx1-PepLncP2 or combinatorial treatments.

This activation promoted by the PepLncP2 string goes in line with immunopeptidomics-based reports that propose that non-canonical antigens that bind to MHC-I, such as these lncRNA-derived peptides, are capable to enhance tumour immunogenicity and reduce tumour volume via T cell activation (Barczak et al., 2023; Ely et al., 2025).

Despite these *ex vivo* findings, acidic conditions pose a relevant challenge to immunotherapeutic agents, as the immune response is likely to be suppressed in the TME (Audero et al., 2023; du Toit-Thompson et al., 2025). PDAC acidosis

generates a highly immunosuppressive environment by promoting the selection of regulatory T cells, CAFs and immunosuppressive macrophages (Bräutigam et al., 2025; Falcomatà et al., 2023; Vaish et al., 2021; Victorasso Jardim Perassi et al., 2022), and inhibiting the effector function of CD8 cells (Wu et al., 2020b). Acidosis in PDAC TME also contributes to tumour survival by promoting metabolic adaptability and the use of fatty acids, acetate or glutamine as alternative oxidative substrates (Groessl et al., 2025; Ibanez and Feron, 2025).

The influence of microenvironmental factors in PDAC responsiveness to therapeutics may explain why single treatments with T1-44 did not compromise tumour growth nor stimulated the infiltration of CD4 and CD8 cells in subcutaneous Panc02 tumours. This absence of effects have also been reported in other *in vivo* PDAC studies using T1-44 (Hong et al., 2023) and EPZ-015666 (Wei et al., 2020) as PRMT5 inhibitors, but differs with the observations on *in vivo* CRC models, where T1-44 single treatment was capable to suppress tumour growth and promote CD4 and CD8 cell infiltration (Barczak et al., 2023), and MYCN-amplified neuroblastoma, where GSK3326593 treatment reduced tumour growth, improved survival rates and altered glutamine metabolism in *Th*-MYCN mice (Bojko et al., 2024).

Despite the fact that single treatments with T1-44 are ineffective against PDAC, several reports have proposed the use of PRMT5 inhibition as an effective combinatorial strategy, altogether with TGF-β inhibitors (Hong et al., 2023), KRAS inhibitors (Drizyte-Miller et al., 2025a; Schneider et al., 2025) and conventional chemotherapeutic agents, like gemcitabine (Feng et al., 2024; Wei et al., 2025) and paclitaxel (Wei et al., 2025), to improve PDAC responsiveness to treatment.

The aforementioned evidence, and the confirmation that T1-44 promotes SLC4A7 exon 25 skipping and suppressed acidic niches in FITC-pHLIP staining in Panc02 tumour samples, portray PRMT5 inhibition as a promising immunosensitizing strategy that could improve PDAC response to other therapeutic agents via improving TME conditions by inducing SLC4A7 AS, thus impacting in pH dynamics, and promoting the expression of immunogenic lncRNA-derived peptides.

Chapter 6 : Concluding remarks

The experiments described in this thesis have been focused on establishing the potential of PRMT5 inhibition as a strategy to enhance PDAC immunosensitivity. As initial characterization experiments, the selective PRMT5 inhibitor T1-44 was found capable to exert its known role suppressing SDMe without affecting cell viability nor altering the cell cycle and apoptosis profile of the PDAC cell lines Panc-1 and Panc02. In these initial experiments, a partial involvement of E2F1 was also described, showing that the loss of E2F1 was associated with a reduced sensitivity to PRMT5 inhibitors.

After these initial assessments, follow-up experiments using a T1-44 concentration that did not affect Panc-1 and Panc02 cell viability were made, finding that PRMT5 induced the expression of translatable lncRNAs and promoted the skipping of exon 25 of SLC4A7, a sodium/bicarbonate transporter. The induction of this particular AS event was associated with a bicarbonate-dependent change in the pH_i/pH_e balance of cells treated with both T1-44 and Δ25 ASO, an antisense oligonucleotide designed to induce this particular SLC4A7 exon-skipping event. In parallel, *in silico* predictions of the peptides translated from the lncRNAs overexpressed by T1-44 were made, choosing a series of 9-mers capable to bind to MHC-I to design the poly-antigen cassette PepLncP2. On the other hand, by using *in silico* approaches, E2F1 was identified as a regulator of the expression of several of the lncRNA whose expression was modified by PRMT5 inhibition. In addition, E2F1 also regulates the expression of SLC4A7, thus impacting on the effects of T1-44 and Δ25 ASO in pH dynamics in E2F1Cr cells.

Lastly, an evaluation of the efficacy of PRMT5 inhibition in syngeneic mouse models was performed. Here, it was found that a ChAdOx1-based vaccine containing PepLncP2 was capable to reduce tumour growth and stimulate IFNγ secretion, which illustrates that these lncRNA-derived peptides are capable to induce anticancer immunity. A similar induction of the activity of immune cells was found when an increased GZMB staining was observed in tumour samples treated with T1-44. However, PRMT5 inhibition did not have any effects on the infiltration of CD4 and CD8 cells. Similarly to the results observed *in vitro*, T1-44 also promoted SLC4A7 exon 25 skipping in tumour samples, and the impact of this agent in pH dynamics was subsequently confirmed by the loss of the FITC-pHLIP signal in tumour samples derived from mice treated with both T1-44 and $NaHCO_3$.

When the limitations and future perspectives of this work are analysed, the following points could be identified:

(i) The information describing the interaction between E2F1 and pH dynamics in PDAC is limited. Future mechanistic studies can be focused on considering if E2F1 modifies its role in gene expression and AS under low pH due to an increase in the protonation state of its histidine residues, thus impacting on E2F1 binding (Winiewska-Szajewska et al., 2024) and transcriptional regulation capacities that can contribute to PDAC metabolic adaptability and survival (Bertonnier-Brouty et al., 2024; Kisor et al., 2025).

(ii) The lack of *in situ* pH assessments limits the interpretability and scope of the pH dynamics results obtained *in vivo*, which were

focused only on acidic niches staining. Future studies can tackle this issue by using hyperpolarized ^{13}C bicarbonate (Mu et al., 2023) or ^{13}C pyruvate (Deen et al., 2023) magnetic resonance imaging, which can also offer additional evidence to associate the effects of PRMT5 inhibition in pH dynamics with its consequences in the balance between glycolytic and oxidative metabolism, a largely relevant topic in PDAC survival and metabolic adaptability (Chianese et al., 2026) that was only tangentially addressed in this thesis.

(iii) There is an absence of *in vivo* assessments of the impact of SLC4A7 and SLC4A7 Δ25 in pH dynamics and tumour growth. For this, *in vivo* experiments using nanoparticulated-Δ25 ASO formulations in more relevant syngeneic PDAC models, like C57BL/6 mice bearing KPC cells with or without KPC knock-outs, can be considered to confirm the relevance of SLC4A7 activity in PDAC survival.

(iv) The relevance of the proposed immunosensitizing effects of PRMT5 inhibition in terms of PDAC survival needs to be furtherly tested *in vivo*. For this, additional tumour challenge experiments involving ChAdOx1-PepLncP2 vaccination with T1-44 treatment and tumour volume measurements, T cell infiltration assessment and acidic niches staining could provide a clearer picture about the impact of T1-44 effects in tumour growth.

In summary, the experiments shown on this thesis provide *in vitro* and *in vivo* evidence to suggest that PRMT5 inhibition, via its interaction with E2F1, is a promising therapeutic strategy to increase PDAC immunosensitivity by altering pH

dynamics via inducing SLC4A7 AS, metabolic reprogramming and the expression of immunogenic lncRNA-peptides as can be observed in Figure 6.1.

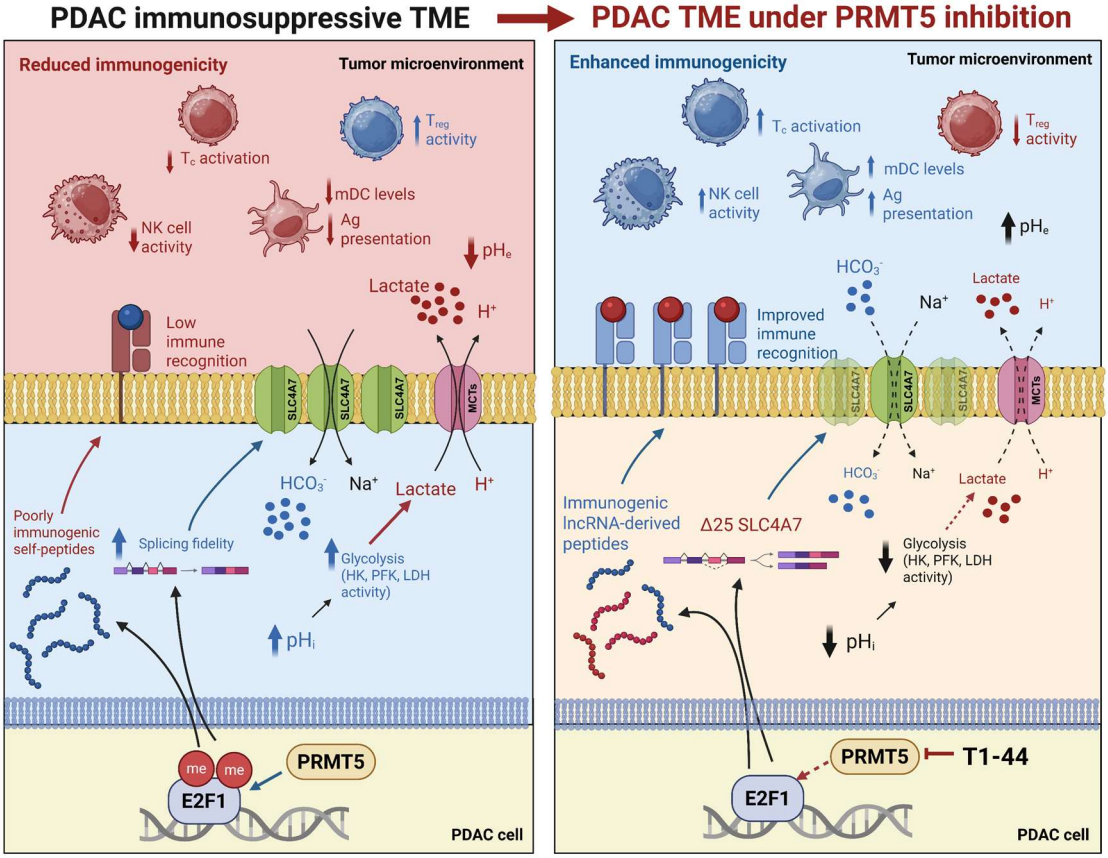

Figure 6.1. Proposed model of E2F1 and PRMT5 involvement regulating PDAC immunosensitivity via regulating the expression of lncRNA-derived peptides and pH dynamics.

In untreated conditions (left panel), E2F1 and PRMT5, frequently-deregulated proteins in PDAC, supress the expression of immunogenic lncRNA-derived peptides and regulate the activity of the bicarbonate transporter SLC4A7 by preserving its splicing fidelity. This enhancement of bicarbonate uptake is one of the factors that lead to an increase in the glycolytic rate of PDAC cells and subsequently augments H^+/lactate extrusion, contributing to the establishment of an acidic tumour microenvironment that impairs anti-tumour immune response and the efficacy of conventional chemotherapeutics. Under these circumstances, the PRMT5 inhibitor T1-44 (right panel) can be used as a dual immunosensitizing strategy that promotes the expression of immunogenic lncRNA-derived peptides and alters intra- and extracellular pH balance by promoting the skipping of SLC4A7 exon 25. Figure created in https://BioRender.com

References

Aartsma-Rus, A., A. Garanto, W. van Roon-Mom, E.M. McConnell, V. Suslovitch, W.X. Yan, J.K. Watts, and T.W. Yu. 2022. Consensus Guidelines for the Design and In Vitro Preclinical Efficacy Testing N-of-1 Exon Skipping Antisense Oligonucleotides. *Nucleic Acid Therapeutics*. 33:17-25.

Abe, Y., T. Sano, N. Otsuka, M. Ogawa, and N. Tanaka. 2024. PRMT5-mediated methylation of STAT3 is required for lung cancer stem cell maintenance and tumour growth. *Communications Biology*. 7:593.

Abe, Y., T. Sano, and N. Tanaka. 2023. The Role of PRMT5 in Immuno-Oncology. *Genes*. 14:678.

Agarwal, P., H. Qi, K. Munjal, J. Gai, A. Ferguson, R. Parkinson, J. Harrison, C. Rodriguez, R.A. Anders, E.D. Thompson, R. Burkhart, J. He, A. Narang, A.D. Jesus-Acosta, L. Zheng, E.M. Jaffee, B. George, D.A. Laheru, M. Yarchoan, and A. Osipov. 2023. Overall survival (OS) and pathologic response rate from a phase II clinical trial of neoadjuvant GVAX pancreas vaccine (with cyclophosphamide) in combination with nivolumab and stereotactic body radiation therapy (SBRT) followed by definitive resection for patients with borderline resectable pancreatic adenocarcinoma (BR-PDAC). *Journal of Clinical Oncology*. 41:e16309-e16309.

Alhowail, A.H., J. Bloemer, M. Majrashi, P.D. Pinky, S. Bhattacharya, Z. Yongli, D. Bhattacharya, M. Eggert, L. Woodie, M.A. Buabeid, N. Johnson, A. Broadwater, B. Smith, M. Dhanasekaran, R.D. Arnold, and V. Suppiramaniam. 2019. Doxorubicin-induced neurotoxicity is associated with acute alterations in synaptic plasticity, apoptosis, and lipid peroxidation. *Toxicology Mechanisms and Methods*. 29:457-466.

Andersen, H.B., R. Ialchina, S.F. Pedersen, and D. Czaplinska. 2021. Metabolic reprogramming by driver mutation-tumor microenvironment interplay in pancreatic cancer: new therapeutic targets. *Cancer and Metastasis Reviews*. 40:1093-1114.

Antonysamy, S., Z. Bonday, R.M. Campbell, B. Doyle, Z. Druzina, T. Gheyi, B. Han, L.N. Jungheim, Y. Qian, C. Rauch, M. Russell, J.M. Sauder, S.R. Wasserman, K. Weichert, F.S. Willard, A. Zhang, and S. Emtage. 2012. Crystal structure of the human PRMT5:MEP50 complex. *Proceedings of the National Academy of Sciences*. 109:17960-17965.

Audero, M.M., T.M.A. Carvalho, F.A. Ruffinatti, T. Loeck, M. Yassine, G. Chinigò, A. Folcher, V. Farfariello, S. Amadori, C. Vaghi, A. Schwab, S.J. Reshkin, R.A. Cardone, N. Prevarskaya, and A. Fiorio Pla. 2023. Acidic Growth Conditions Promote Epithelial-to-Mesenchymal Transition to Select More Aggressive PDAC Cell Phenotypes In Vitro. *Cancers*. 15:2572.

Aung-Htut, M.T., C.S. McIntosh, K.A. Ham, I.L. Pitout, L.L. Flynn, K. Greer, S. Fletcher, and S.D. Wilton. 2019. Systematic Approach to Developing Splice Modulating Antisense Oligonucleotides. *International Journal of Molecular Sciences*. 20:5030.

Axelsen, T.V., C. Olesen, D. Khan, A. Mohammadi, E.V. Bouzinova, C.J.F. Nielsen, M. Mele, K.R. Hauerslev, H.L. Pedersen, E. Balling, P. Vahl, T. Tramm, P.M. Christiansen, and E. Boedtkjer. 2024. Antibodies toward Na+,HCO3−-cotransporter NBCn1/SLC4A7 block net acid extrusion and cause pH-dependent growth inhibition and apoptosis in breast cancer. *British Journal of Cancer*. 130:1206-1220.

Baleeiro, R.B., C.J. Bouwens, P. Liu, C. Di Gioia, L.S.C. Dunmall, A. Nagano, R. Gangeswaran, C. Chelala, H.M. Kocher, N.R. Lemoine, and Y. Wang. 2022. MHC class II molecules on pancreatic cancer cells indicate a potential for neo-antigen-based immunotherapy. *OncoImmunology*. 11:2080329.

Banasavadi-Siddegowda, Y.K., A.M. Welker, M. An, X. Yang, W. Zhou, G. Shi, J. Imitola, C. Li, S. Hsu, J. Wang, M. Phelps, J. Zhang, C.E. Beattie, R. Baiocchi, and B. Kaur. 2018. PRMT5 as a druggable target for glioblastoma therapy. *Neuro Oncol*. 20:753-763.

Barczak, W., S.M. Carr, G. Liu, S. Munro, A. Nicastri, L.N. Lee, C. Hutchings, N. Ternette, P. Klenerman, A. Kanapin, A. Samsonova, and N.B. La Thangue. 2023. Long non-coding RNA-derived peptides are immunogenic and drive a potent anti-tumour response. *Nature Communications*. 14:1078.

Barczak, W., L. Jin, S.M. Carr, S. Munro, S. Ward, A. Kanapin, A. Samsonova, and N.B. La Thangue. 2020. PRMT5 promotes cancer cell migration and invasion through the E2F pathway. *Cell Death & Disease*. 11:572.

Barros, A.S., E.C. Costa, A.S. Nunes, D. de Melo-Diogo, and I.J. Correia. 2018. Comparative study of the therapeutic effect of Doxorubicin and Resveratrol combination on 2D and 3D (spheroids) cell culture models. *International Journal of Pharmaceutics*. 551:76-83.

Bate-Eya, L.T., G. Albayrak, S.M. Carr, A. Shrestha, A. Kanapin, A. Samsonova, and N.B. La Thangue. 2025. Sustained cancer-relevant alternative RNA splicing events driven by PRMT5 in high-risk neuroblastoma. *Molecular Oncology*. 19:741-763.

Bazan-Peregrino, M., R. Garcia-Carbonero, B. Laquente, R. Álvarez, A. Mato-Berciano, M. Gimenez-Alejandre, S. Morgado, A. Rodríguez-García, M.V. Maliandi, M.C. Riesco, R. Moreno, M.M. Ginestà, M. Perez-Carreras, J.B. Gornals, S. Prados, S. Perea, G. Capella, R. Alemany, R. Salazar, E. Blasi, C. Blasco, M. Cascallo, and M. Hidalgo. 2021. VCN-01 disrupts pancreatic cancer stroma and exerts antitumor effects. *Journal for ImmunoTherapy of Cancer*. 9:e003254.

Benítez-Rangel, E., M.C. López-Méndez, L. García, and A. Guerrero-Hernández. 2015. DIDS (4,4'-Diisothiocyanatostilbene-2,2'-disulfonate) directly inhibits caspase activity in HeLa cell lysates. *Cell Death Discovery*. 1:15037.

Bertonnier-Brouty, L., J. Andersson, T. Kaprio, J. Hagström, S. Bsharat, O. Asplund, G. Hatem, C. Haglund, H. Seppänen, R.B. Prasad, and I. Artner. 2024. E2F transcription factors promote tumorigenicity in pancreatic ductal adenocarcinoma. *Cancer Medicine*. 13:e7187.

Bilreiro, C., L. Andrade, I. Santiago, R.M. Marques, and C. Matos. 2024. Imaging of pancreatic ductal adenocarcinoma – An update for all stages of patient management. *European Journal of Radiology Open*. 12:100553.

Bischoff, J.R., D.H. Kirn, A. Williams, C. Heise, S. Horn, M. Muna, L. Ng, J.A. Nye, A. Sampson-Johannes, A. Fattaey, and F. McCormick. 1996. An Adenovirus Mutant That Replicates Selectively in p53- Deficient Human Tumor Cells. *Science*. 274:373-376.

Blackford, A.L., M.I. Canto, M. Dbouk, R.H. Hruban, B.W. Katona, A. Chak, R.E. Brand, S. Syngal, J. Farrell, F. Kastrinos, E.M. Stoffel, A. Rustgi, A.P. Klein, I. Kamel, E.K. Fishman, J. He, R. Burkhart, E.J. Shin, A.M. Lennon, and M. Goggins. 2024. Pancreatic Cancer Surveillance and Survival of High-Risk Individuals. *JAMA Oncology*. 10:1087-1096.

Blaszczak, W., Z. Tan, and P. Swietach. 2021. Cost-Effective Real-Time Metabolic Profiling of Cancer Cell Lines for Plate-Based Assays. *Chemosensors*. 9:139.

Blaszczak, W., B. White, and P. Swietach. 2024. Protocol for separating cancer cell subpopulations by metabolic activity using flow cytometry. *STAR Protoc*. 5:103105.

Blaszczak, W., H. Williams, and P. Swietach. 2022. Autoregulation of H+/lactate efflux prevents monocarboxylate transport (MCT) inhibitors from reducing glycolytic lactic acid production. *British Journal of Cancer*. 127:1365-1377.

Boedtkjer, E., and S.F. Pedersen. 2020. The Acidic Tumor Microenvironment as a Driver of Cancer. *Annual Review of Physiology*. 82:103-126.

Bogumil, D., A.H. Wu, D. Stram, J. Yang, C.-C. Tseng, L. Le Marchand, J. Wu, I. Cheng, and V.W. Setiawan. 2021. The association between ambient air pollutants and pancreatic cancer in the Multiethnic Cohort Study. *Environmental Research*. 202:111608.

Bojko, J., M. Kollareddy, M. Szemes, J. Bellamy, E. Poon, A. Moukachar, D. Legge, E.E. Vincent, N. Jones, S. Malik, A. Greenhough, A. Paterson, J.H. Park, K. Gallacher, L. Chesler, and K. Malik. 2024. Glutamine addiction is targetable via altering splicing of nutrient sensors and epitranscriptome regulators. *bioRxiv*:2024.2002.2028.582087.

Borole, P., and A. Rajan. 2024. Building trust in deep learning-based immune response predictors with interpretable explanations. *Communications Biology*. 7:279.

Bräutigam, K., K. Skok, K. Szymonski, C.V. Rift, and E. Karamitopoulou. 2025. Tumor immune microenvironment in pancreatic ductal adenocarcinoma revisited – Exploring the “Space”. *Cancer Letters*. 622:217699.

Bray, F., M. Laversanne, H. Sung, J. Ferlay, R.L. Siegel, I. Soerjomataram, and A. Jemal. 2024. Global cancer statistics 2022: GLOBOCAN estimates of incidence and mortality worldwide for 36 cancers in 185 countries. *CA Cancer J Clin*. 74:229-263.

Bustin, S.A., J.M. Ruijter, M.J.B. van den Hoff, M. Kubista, M.W. Pfaffl, G.L. Shipley, N. Tran, S. Rödiger, A. Untergasser, R. Mueller, T. Nolan, M. Milavec, M.J. Burns, J.F. Huggett, J. Vandesompele, and C.T. Wittwer. 2025. MIQE 2.0: Revision of the Minimum Information for Publication of Quantitative Real-Time PCR Experiments Guidelines. *Clinical Chemistry*. 71:634-651.

Byeon, S., T. du Toit-Thompson, J. Gillson, A.J. Gill, J.S. Samra, A. Mittal, and S. Sahni. 2023. Heterogeneous tumor microenvironment in pancreatic ductal adenocarcinoma: An emerging role of single-cell analysis. *Cancer Medicine*. 12:18020-18031.

Cao, L., C. Huang, D. Cui Zhou, Y. Hu, T.M. Lih, S.R. Savage, K. Krug, D.J. Clark, M. Schnaubelt, L. Chen, F. da Veiga Leprevost, R.V. Eguez, W. Yang, J. Pan, B. Wen, Y. Dou, W. Jiang, Y. Liao, Z. Shi, N.V. Terekhanova, S. Cao, R.J.-H. Lu, Y. Li, R. Liu, H. Zhu, P. Ronning, Y. Wu, M.A. Wyczalkowski, H. Easwaran, L. Danilova, A.S. Mer, S. Yoo, J.M. Wang, W. Liu, B. Haibe-Kains, M. Thiagarajan, S.D. Jewell, G. Hostetter, C.J. Newton, Q.K. Li, M.H. Roehrl, D. Fenyö, P. Wang, A.I. Nesvizhskii, D.R. Mani, G.S. Omenn, E.S. Boja, M. Mesri, A.I. Robles, H. Rodriguez, O.F. Bathe, D.W. Chan, R.H. Hruban, L. Ding, B. Zhang, H. Zhang, M. Amin, E. An, C. Ayad, T. Bauer, C. Birger, M.J. Birrer, S.M. Boca, W. Bocik, M. Borucki, S. Cai, S.A. Carr, S. Cerda, H. Chen, S. Chen, D. Chesla, A.M. Chinnaiyan, A. Colaprico, S. Cottingham, M. Derejska, S.M. Dhanasekaran, M.J. Domagalski, B.J. Druker, E. Duffy, M.A. Dyer, N.J. Edwards, M.J. Ellis, J. Eschbacher, A. Francis, J. Francis, S. Gabriel, N. Gabrovski, J. Gardner, G. Getz, M.A. Gillette, C.A. Goldthwaite, P. Grady, S. Guo, P. Hariharan, T. Hiltke, B. Hindenach, K.A. Hoadley, J. Huang, C.D. Jones, K.A. Ketchum, et al. 2021. Proteogenomic characterization of pancreatic ductal adenocarcinoma. *Cell*. 184:5031-5052.e5026.

Cappellesso, F., M.-P. Orban, N. Shirgaonkar, E. Berardi, J. Serneels, M.-A. Neveu, D. Di Molfetta, F. Piccapane, R. Caroppo, L. Debellis, T. Ostyn, N. Joudiou, L. Mignion, E. Richiardone, B.F. Jordan, B. Gallez, C. Corbet, T. Roskams, R. DasGupta, S. Tejpar, M. Di Matteo, D. Taverna, S.J. Reshkin, B. Topal, F. Virga, and M. Mazzone. 2022. Targeting the bicarbonate transporter SLC4A4 overcomes immunosuppression and immunotherapy resistance in pancreatic cancer. *Nature Cancer*. 3:1464-1483.

Chang, X., X. Liu, H. Wang, X. Yang, and Y. Gu. 2022. Glycolysis in the progression of pancreatic cancer. *Am J Cancer Res*. 12:861-872.

Chen, M., K. Cen, Y. Song, X. Zhang, Y.-C. Liou, P. Liu, J. Huang, J. Ruan, J. He, W. Ye, T. Wang, X. Huang, J. Yang, Y. Jia, X. Liang, P. Shen, Q. Wang, and T. Liang. 2023. NUSAP1-LDHA-Glycolysis-Lactate feedforward loop promotes Warburg effect and metastasis in pancreatic ductal adenocarcinoma. *Cancer Letters*. 567:216285.

Chen, W., F. Xie, T.Q. Luong, J. Chang, E. Lustigova, L.M. Matrisian, E.E. Shrader, and B.U. Wu. 2025. Identifying signs and symptoms of pancreatic cancer: a population-based study using electronic health records and natural language processing. *Pancreatology*. 25:1086-1094.

Chen, Y., C. Guo, X. Bai, S. Gao, Y. Shen, M. Zhang, J. Wu, R. Que, X. Li, T. Liang, and J. Wu. 2022. Randomized phase II trial of neoadjuvant chemotherapy with modified FOLFIRINOX versus modified FOLFIRINOX and PD-1 antibody for borderline resectable and locally advanced pancreatic cancer (the CISPD-4 study). *Journal of Clinical Oncology*. 40:562-562.

Chen, Y., X. Shao, X. Zhao, Y. Ji, X. Liu, P. Li, M. Zhang, and Q. Wang. 2021a. Targeting protein arginine methyltransferase 5 in cancers: Roles, inhibitors and mechanisms. *Biomedicine & Pharmacotherapy*. 144:112252.

Chen, Z., Y. Guo, D. Zhao, Q. Zou, F. Yu, L. Zhang, and L. Xu. 2021b. Comprehensive Analysis Revealed that CDKN2A is a Biomarker for Immune Infiltrates in Multiple Cancers. *Frontiers in Cell and Developmental Biology*. Volume 9 - 2021.

Cheng, R., F. Li, M. Zhang, X. Xia, J. Wu, X. Gao, H. Zhou, Z. Zhang, N. Huang, X. Yang, Y. Zhang, S. Shen, T. Kang, Z. Liu, F. Xiao, H. Yao, J. Xu, C. Yan, and N. Zhang. 2023. A novel protein RASON encoded by a lncRNA controls oncogenic RAS signaling in KRAS mutant cancers. *Cell Research*. 33:30-45.

Chianese, U., C. Papulino, G. Saggese, A. Ali, M. Ciotola, E. Lonardo, M. Cortese, G. Favale, A. Di Mauro, D. La Gioia, V. Golino, E. Sommella, P. Campiglia, R. Franco, F. Ciardiello, F. De Vita, V. Carafa, L. Altucci, and R. Benedetti. 2026. Glycolytic heterogeneity drives metabolic-targeted therapy in pancreatic ductal adenocarcinoma. *Signal Transduction and Targeted Therapy*. 11:25.

Chiba, S., Kenji Rowel Q. Lim, N. Sheri, S. Anwar, E. Erkut, Md Nur A. Shah, T. Aslesh, S. Woo, O. Sheikh, R. Maruyama, H. Takano, K. Kunitake, W. Duddy, Y. Okuno, Y. Aoki, and T. Yokota. 2021. eSkip-Finder: a machine learning-based web application and database to identify the optimal sequences of antisense oligonucleotides for exon skipping. *Nucleic Acids Research*. 49:W193-W198.

Chick, R.C., and T.M. Pawlik. 2024. Updates in Immunotherapy for Pancreatic Cancer. *Journal of Clinical Medicine*. 13:6419.

Cho, E.C., S. Zheng, S. Munro, G. Liu, S.M. Carr, J. Moehlenbrink, Y.C. Lu, L. Stimson, O. Khan, R. Konietzny, J. McGouran, A.S. Coutts, B. Kessler, D.J. Kerr, and N.B.L. Thangue. 2012. Arginine methylation controls growth regulation by E2F-1. *The EMBO Journal*. 31:1785-1797.

Cho, S.Y., H.S. Eun, J. Kim, Y.D. Ko, W.S. Rou, and J.S. Joo. 2025. The Solute Carrier Superfamily as Therapeutic Targets in Pancreatic Ductal Adenocarcinoma. *Genes*. 16:463.

Community, T.G. 2022. The Galaxy platform for accessible, reproducible and collaborative biomedical analyses: 2022 update. *Nucleic Acids Research*. 50:W345-W351.

Crowe, A.R., and W. Yue. 2019. Semi-quantitative Determination of Protein Expression Using Immunohistochemistry Staining and Analysis: An Integrated Protocol. *Bio-protocol*. 9:e3465.

Czaplinska, D., R. Ialchina, H.B. Andersen, J. Yao, A. Stigliani, J. Dannesboe, M. Flinck, X. Chen, J. Mitrega, S.P. Gnosa, O. Dmytriyeva, F. Alves, J. Napp, A. Sandelin, and S.F. Pedersen. 2023. Crosstalk between tumor acidosis, p53 and extracellular matrix regulates pancreatic cancer aggressiveness. *Int J Cancer*. 152:1210-1225.

Daemen, A., D. Peterson, N. Sahu, R. McCord, X. Du, B. Liu, K. Kowanetz, R. Hong, J. Moffat, M. Gao, A. Boudreau, R. Mroue, L. Corson, T. O'Brien, J. Qing, D. Sampath, M. Merchant, R. Yauch, G. Manning, J. Settleman, G. Hatzivassiliou, and M. Evangelista. 2015. Metabolite profiling stratifies pancreatic ductal adenocarcinomas into subtypes with distinct sensitivities to metabolic inhibitors. *Proceedings of the National Academy of Sciences*. 112:E4410-E4417.

Dardare, J., N. Martz, A. Witz, M. Betz, C. Michel, P. Gilson, J.-L. Merlin, A. Lambert, and A. Harle. 2026. Radiotherapy in the management of PDAC, from past to present. *Translational Oncology*. 63:102632.

Dayyani, F., T. Macarulla, A. Johnson, and Z.A. Wainberg. 2023. Second-line treatment options for patients with metastatic pancreatic ductal adenocarcinoma: A systematic literature review. *Cancer Treatment Reviews*. 113:102502.

Debiais, M., A. Tarabay, S. Blanchet-Deverly, G.M. Camilleri, A. Megherbi, L. Diebakate, M. Collin, A. Hollebecque, C. Smolenschi, M. Valéry, T. Pudlarz, A.C. Fuerea, V. Boige, M. Ducreux, and A. Boilève. 2026. Metastatic pancreatic adenocarcinoma: Real-world efficacy of first line treatment. *European Journal of Cancer*. 232:116160.

Deen, S.S., C. Rooney, A. Shinozaki, J. McGing, J.T. Grist, D.J. Tyler, E. Serrão, and F.A. Gallagher. 2023. Hyperpolarized Carbon 13 MRI: Clinical Applications and Future Directions in Oncology. *Radiology: Imaging Cancer*. 5:e230005.

Deng, Y., X. Xia, Y. Zhao, Z. Zhao, C. Martinez, W. Yin, J. Yao, Q. Hang, W. Wu, J. Zhang, Y. Yu, W. Xia, F. Yao, D. Zhao, Y. Sun, H. Ying, M.-C. Hung, and L. Ma. 2021. Glucocorticoid receptor regulates PD-L1 and MHC-I in pancreatic cancer cells to promote immune evasion and immunotherapy resistance. *Nature Communications*. 12:7041.

Dittrich, C., R. Königsberg, M. Mittlböck, K. Geissler, A. Sahmanovic-Hrgovcic, J. Pleiner-Duxneuner, M. Czejka, and P. Buchner. 2019. Phase Ib trial combining capecitabine, erlotinib and bevacizumab in pancreatic adenocarcinoma - REBECA trial. *Investigational New Drugs*. 37:127-138.

Driehuis, E., A. van Hoeck, K. Moore, S. Kolders, H.E. Francies, M.C. Gulersonmez, E.C.A. Stigter, B. Burgering, V. Geurts, A. Gracanin, G. Bounova, F.H. Morsink, R. Vries, S. Boj, J. van Es, G.J.A. Offerhaus, O. Kranenburg, M.J. Garnett, L. Wessels, E. Cuppen, L.A.A. Brosens, and H. Clevers. 2019. Pancreatic cancer organoids recapitulate disease and allow personalized drug screening. *Proceedings of the National Academy of Sciences*. 116:26580-26590.

Drizyte-Miller, K., L.D. Engstrom, J.A. Klomp, C.A. Stalnecker, A.G. Stamey, K.E. Taylor, M.K. Roach, R. Robb, L.M. Waters, A. Calinisan, S. Degan, W.H. Chang, X.M. Helu, D. Nguyen, E. Baldelli, M. Pierobon, E.F. Petricoin, D.M. Briere, J. Hallin, J.G. Christensen, K.L. Bryant, A.D. Cox, P. Olson, and C.J. Der. 2025a. Combination of the MTA-Cooperative PRMT5 Inhibitor BMS-986504 and KRAS Inhibitors Is an Effective Treatment Strategy for MTAP-Deleted KRAS-Mutant Pancreatic Cancer. *Cancer Res*. 85:3540-3557.

Drizyte-Miller, K., T. Talabi, A. Somasundaram, A.D. Cox, and C.J. Der. 2025b. KRAS: the Achilles' heel of pancreas cancer biology. *The Journal of Clinical Investigation*. 135.

du Toit-Thompson, T., L. Leck, J. Gillson, N. Pavlakis, A.J. Gill, J.S. Samra, A. Mittal, and S. Sahni. 2025. Overcoming therapy resistance in pancreatic cancer: challenges and emerging strategies. *Advanced Drug Delivery Reviews*. 224:115647.

Efthymiou, G., E. Lohmann, C. Montenegro, P. Kousteridou, P. Bertrand, J. Pereira, H.S. Carr, I. Ben-Sahra, C. Compare, I. Nemazanyy, G. Bidaut, P. Finetti, F. Bertucci, C. Lachaud, F. Guillaumond, R. Tomasini, and S. Vasseur. 2025. The

extracellular matrix drives guanylate production and protects pancreatic cancer cells from oxaliplatin-induced DNA damage. *Science Advances*. 11:eadu2276.

Ely, Z.A., Z.J. Kulstad, G. Gunaydin, S. Addepalli, E.K. Verzani, M. Casarrubios, K.R. Clauser, X. Wang, I.E. Lippincott, C. Louvet, T. Schmitt, K.S. Kapner, M.P. Agus, C.J. Hennessey, J.M. Cleary, S.R. Hadrup, S. Klaeger, J. Su, A.M. Jaeger, B.M. Wolpin, S. Raghavan, E.L. Smith, P.D. Greenberg, A.J. Aguirre, J.G. Abelin, S.A. Carr, T. Jacks, and W.A. Freed-Pastor. 2025. Pancreatic cancer–restricted cryptic antigens are targets for T cell recognition. *Science*. 388:eadk3487.

Falcomatà, C., S. Bärthel, G. Schneider, R. Rad, M. Schmidt-Supprian, and D. Saur. 2023. Context-Specific Determinants of the Immunosuppressive Tumor Microenvironment in Pancreatic Cancer. *Cancer Discovery*. 13:278-297.

Fang, Y.-T., W.-W. Yang, Y.-R. Niu, and Y.-K. Sun. 2023. Recent advances in targeted therapy for pancreatic adenocarcinoma. *World Journal of Gastrointestinal Oncology*. 15:571-595.

Fang, Z., M. Lin, C. Li, H. Liu, and C. Gong. 2020. A comprehensive review of the roles of E2F1 in colon cancer. *Am J Cancer Res*. 10:757-768.

Farhangnia, P., H. Khorramdelazad, H. Nickho, and A.-A. Delbandi. 2024. Current and future immunotherapeutic approaches in pancreatic cancer treatment. *Journal of Hematology & Oncology*. 17:40.

Fedoriw, A., S.R. Rajapurkar, S. O'Brien, S.V. Gerhart, L.H. Mitchell, N.D. Adams, N. Rioux, T. Lingaraj, S.A. Ribich, M.B. Pappalardi, N. Shah, J. Laraio, Y. Liu, M. Butticello, C.L. Carpenter, C. Creasy, S. Korenchuk, M.T. McCabe, C.F. McHugh, R. Nagarajan, C. Wagner, F. Zappacosta, R. Annan, N.O. Concha, R.A. Thomas, T.K. Hart, J.J. Smith, R.A. Copeland, M.P. Moyer, J. Campbell, K. Stickland, J. Mills, S. Jacques-O'Hagan, C. Allain, D. Johnston, A. Raimondi, M. Porter Scott, N. Waters, K. Swinger, A. Boriack-Sjodin, T. Riera, G. Shapiro, R. Chesworth, R.K. Prinjha, R.G. Kruger, O. Barbash, and H.P. Mohammad. 2019. Anti-tumor Activity of the Type I PRMT Inhibitor, GSK3368715, Synergizes with PRMT5 Inhibition through MTAP Loss. *Cancer Cell*. 36:100-114.e125.

Feng, M., Q. Jiao, Y. Ren, X. Liu, Z. Gao, Z. Li, Y. Wang, M. Zhao, and L. Bi. 2024. The interaction between UBR7 and PRMT5 drives PDAC resistance to gemcitabine by regulating glycolysis and immune microenvironment. *Cell Death Dis*. 15:758.

Festing, M.F.W. 2020. The “completely randomised” and the “randomised block” are the only experimental designs suitable for widespread use in pre-clinical research. *Scientific Reports*. 10:17577.

Force, U.P.S.T. 2019. Screening for Pancreatic Cancer: US Preventive Services Task Force Reaffirmation Recommendation Statement. *JAMA*. 322:438-444.

Fukahori, M., Y. Okabe, M. Shimokawa, T. Otsuka, F. Koga, Y. Ueda, J. Nakazawa, A. Komori, S. Otsu, S. Arima, A. Makiyama, H. Taguchi, T. Honda, T. Ushijima, K. Miwa, T. Shibuki, K. Nio, Y. Ide, N. Ureshino, T. Mizuta, K. Mitsugi, and T. Shirakawa. 2023. Efficacy of second-line chemotherapy after treatment with gemcitabine plus nab-paclitaxel or FOLFIRINOX in patients with metastatic pancreatic cancer. *Scientific Reports*. 13:19399.

Garcia-Carbonero, R., M. Bazan-Peregrino, M. Gil-Martín, R. Álvarez, T. Macarulla, M.C. Riesco-Martinez, H. Verdaguer, C. Guillén-Ponce, M. Farrera-Sal, R. Moreno, A. Mato-Berciano, M.V. Maliandi, S. Torres-Manjon, M. Costa, N. del Pozo, J. Martínez de Villarreal, F.X. Real, N. Vidal, G. Capella, R. Alemany, E. Blasi, C. Blasco, M. Cascalló, and R. Salazar. 2022. Phase I, multicenter, open-label study of intravenous VCN-01 oncolytic adenovirus with or without nab-paclitaxel plus gemcitabine in patients with advanced solid tumors. *Journal for ImmunoTherapy of Cancer*. 10:e003255.

Ge, L., H. Wang, X. Xu, Z. Zhou, J. He, W. Peng, F. Du, Y. Zhang, A. Gong, and M. Xu. 2020. PRMT5 promotes epithelial-mesenchymal transition via EGFR-β-catenin axis in pancreatic cancer cells. *Journal of Cellular and Molecular Medicine*. 24:1969-1979.

Gillespie, M.S., K. Chiang, G.L. Regan-Mochrie, S.-Y. Choi, C.M. Ward, D. Sahay, P. Garcia, R. Arnold, and C.C. Davies. 2025. PRMT5-regulated splicing of DNA repair genes drives chemoresistance in breast cancer stem cells. *Oncogene*. 44:862-876.

Glapiński, F., W. Zając, M. Fudalej, A. Deptała, A. Czerw, K. Sygit, R. Kozłowski, and A. Badowska-Kozakiewicz. 2025. The Role of the Tumor Microenvironment in Pancreatic Ductal Adenocarcinoma: Recent Advancements and Emerging Therapeutic Strategies. *Cancers*. 17:1599.

Gong, R., Y. Hu, Q. Yu, L. Fang, and H. Ren. 2023. Metabolic signatures in pancreatic ductal adenocarcinoma: diagnostic and therapeutic implications. *Journal of Pancreatology*. 6:185-195.

Graves, J.D., Y.-J. Lee, K. Liu, G. Li, F.-T. Lin, and W.-C. Lin. 2020. E2F1 sumoylation as a protective cellular mechanism in oxidative stress response. *Proceedings of the National Academy of Sciences*. 117:14958-14969.

Groessl, S., R. Kalis, M.T. Snaebjornsson, L. Wambach, J. Haider, F. Andersch, A. Schulze, W. Palm, and J. Zuber. 2025. Acidosis orchestrates adaptations of energy metabolism in tumors. *Science*. 390:eadp7603.

Gu, Z., W. Kong, X. Liu, L. Hu, Y. Zhou, Z. Liang, M. Zhang, D. Chen, F. Li, and W. Chen. 2025. Drug discovery targeting protein arginine methyltransferase 5 (PRMT5): an update. *Bioorganic & Medicinal Chemistry*. 128:118240.

Halbrook, C.J., C.A. Lyssiotis, M. Pasca di Magliano, and A. Maitra. 2023. Pancreatic cancer: Advances and challenges. *Cell*. 186:1729-1754.

Hallin, J., V. Bowcut, A. Calinisan, D.M. Briere, L. Hargis, L.D. Engstrom, J. Laguer, J. Medwid, D. Vanderpool, E. Lifset, D. Trinh, N. Hoffman, X. Wang, J. David Lawson, R.J. Gunn, C.R. Smith, N.C. Thomas, M. Martinson, A. Bergstrom, F. Sullivan, K. Bouhana, S. Winski, L. He, J. Fernandez-Banet, A. Pavlicek, J.R. Haling, L. Rahbaek, M.A. Marx, P. Olson, and J.G. Christensen. 2022. Anti-tumor efficacy of a potent and selective non-covalent KRASG12D inhibitor. *Nature Medicine*. 28:2171-2182.

Han, C., L. Sun, Q. Pan, Y. Sun, W. Wang, and Y. Chen. 2022. Polysome profiling followed by quantitative PCR for identifying potential micropeptide encoding long non-coding RNAs in suspension cell lines. *STAR Protocols*. 3:101037.

Hayashi, H., T. Higashi, T. Miyata, Y.-i. Yamashita, and H. Baba. 2021. Recent advances in precision medicine for pancreatic ductal adenocarcinoma. *Annals of Gastroenterological Surgery*. 5:457-466.

Hayat, U., P.S. Croce, A. Saadeh, K. Desai, J. Appiah, S. Khan, Y.I. Khan, K. Kumar, and A. Hanif. 2025. Current and Emerging Treatment Options for Pancreatic Cancer: A Comprehensive Review. *Journal of Clinical Medicine*. 14:1129.

He, L., G. Urrutia, and G. Lomberk. 2022. Inhibition of PRMT5 Disrupts Cell Cycle Progression and DNA Damage Signaling, Revealing a Potential Novel Combination Therapy for Pancreatic Cancer. *The FASEB Journal*. 36.

Hendi, M., B. Zhang, Y.-P. Mou, and X.-J. Cai. 2025. Importance of landscape exploration and progress in molecular therapies and precision medicine for

pancreatic ductal adenocarcinoma. *World Journal of Gastrointestinal Oncology*. 17:103337.

Henke, E., R. Nandigama, and S. Ergün. 2019. Extracellular Matrix in the Tumor Microenvironment and Its Impact on Cancer Therapy. *Front Mol Biosci*. 6:160.

Hensel, J.A., V. Khattar, R. Ashton, and S. Ponnazhagan. 2019. Characterization of immune cell subtypes in three commonly used mouse strains reveals gender and strain-specific variations. *Laboratory Investigation*. 99:93-106.

Ho, W.J., E.M. Jaffee, and L. Zheng. 2020. The tumour microenvironment in pancreatic cancer — clinical challenges and opportunities. *Nature Reviews Clinical Oncology*. 17:527-540.

Hong, E., W. Barczak, S. Park, J.S. Heo, A. Ooshima, S. Munro, C.P. Hong, J. Park, H. An, J.O. Park, S.H. Park, N.B. La Thangue, and S.-J. Kim. 2023. Combination treatment of T1-44, a PRMT5 inhibitor with Vactosertib, an inhibitor of TGF-β signaling, inhibits invasion and prolongs survival in a mouse model of pancreatic tumors. *Cell Death & Disease*. 14:93.

Hosonuma, M., and K. Yoshimura. 2023. Association between pH regulation of the tumor microenvironment and immunological state. *Front Oncol*. 13:1175563.

Hu, C., Y. Chen, X. Yin, R. Xu, C. Yin, C. Wang, and Y. Zhao. 2025. Pancreatic endocrine and exocrine signaling and crosstalk in physiological and pathological status. *Signal Transduction and Targeted Therapy*. 10:39.

Hu, J., G. Li, Z. Liu, H. Ma, W. Yuan, Z. Lu, D. Zhang, H. Ling, F. Zhang, Y. Liu, C. Liu, and Y. Qiu. 2023. Bicarbonate transporter SLC4A7 promotes EMT and metastasis of HNSCC by activating the PI3K/AKT/mTOR signaling pathway. *Molecular Carcinogenesis*. 62:628-640.

Hu, M., and X. Chen. 2024. A review of the known MTA-cooperative PRMT5 inhibitors. *RSC Advances*. 14:39653-39691.

Hu, R., B. Zhou, Z. Chen, S. Chen, N. Chen, L. Shen, H. Xiao, and Y. Zheng. 2022. PRMT5 Inhibition Promotes PD-L1 Expression and Immuno-Resistance in Lung Cancer. *Frontiers in Immunology*. Volume 12 - 2021.

Ibanez, S., and O. Feron. 2025. Tumor acidosis: Fusing mitochondrial dynamics and lipid metabolism. *Cell Metabolism*. 37:2298-2300.

IDEAYA-Biosciences. 2026. A Study of IDE892 as Monotherapy and Combination in MTAP-deleted Advanced Solid Tumors. Vol. 2026, ClinicalTrials.gov.

Ikezawa, K., M. Urabe, Y. Kai, R. Takada, H. Akita, S. Nagata, and K. Ohkawa. 2024. Comprehensive review of pancreatic acinar cell carcinoma: epidemiology, diagnosis, molecular features and treatment. *Jpn J Clin Oncol*. 54:271-281.

Ilic, I., and M. Ilic. 2022. International patterns in incidence and mortality trends of pancreatic cancer in the last three decades: A joinpoint regression analysis. *World J Gastroenterol*. 28:4698-4715.

Islam, M.M., A. Goertzen, P.K. Singh, and R. Saha. 2022. Exploring the metabolic landscape of pancreatic ductal adenocarcinoma cells using genome-scale metabolic modeling. *iScience*. 25:104483.

Jacobs, M.F., and E.M. Stoffel. 2024. Genetic and other risk factors for pancreatic ductal adenocarcinoma (PDAC). *Familial Cancer*. 23:221-232.

Jia, R., H.-Y. Si, M.-J. Fan, N. Zhang, G.-C. Deng, F.-F. Liu, L. Han, M.-M. Gou, Z.-L. Tan, X. Zhang, Y.-R. Wang, Y. Shi, Y.-Y. Zhang, Y.-S. Jia, Y.-Q. Wang, Q.-L. Han, Z.-K. Wang, and G.-H. Dai. 2025. First-line treatment with chemotherapy, surufatinib (an angio-immuno kinase inhibitor), and camrelizumab (an anti-PD-1 antibody) for locally advanced or metastatic pancreatic ductal adenocarcinoma: a phase Ib/II randomized study. *Signal Transduction and Targeted Therapy*. 10:339.

Ju, Y., D. Xu, M.-m. Liao, Y. Sun, W.-d. Bao, F. Yao, and L. Ma. 2024. Barriers and opportunities in pancreatic cancer immunotherapy. *npj Precision Oncology*. 8:199.

Julian, L.M., Y. Liu, C.A. Pakenham, D. Dugal-Tessier, V. Ruzhynsky, S. Bae, S.Y. Tsai, G. Leone, R.S. Slack, and A. Blais. 2016. Tissue-specific targeting of cell fate regulatory genes by E2f factors. *Cell Death & Differentiation*. 23:565-575.

Kane, S., A. Engelhart, J. Guadagno, A. Jones, I. Usoro, and E. Brutcher. 2020. Pancreatic Ductal Adenocarcinoma: Characteristics of Tumor Microenvironment and Barriers to Treatment. *J Adv Pract Oncol*. 11:693-698.

Kang, M.J., H.X. Li, Y. Gan, C. Fang, X.L. Yang, B. Li, and S. Su. 2024. Efficacy and safety of first-line chemotherapies for patients with advanced pancreatic ductal adenocarcinoma: A systematic review and network meta-analysis. *Heliyon*. 10:e27679.

Karamitopoulou, E. 2019. Tumour microenvironment of pancreatic cancer: immune landscape is dictated by molecular and histopathological features. *British Journal of Cancer*. 121:5-14.

Karp, N.A., and D. Fry. 2021. What is the optimum design for my animal experiment? *BMJ Open Sci*. 5:e100126.

Kay, E.J., and S. Zanivan. 2023. Bicarbonate transport as regulator of antitumour immunity in pancreatic cancer. *Molecular Oncology*. 17:541-544.

Kent, W.J., C.W. Sugnet, T.S. Furey, K.M. Roskin, T.H. Pringle, A.M. Zahler, and D. Haussler. 2002. The human genome browser at UCSC. *Genome Res*. 12:996-1006.

Kim, H., and Z.A. Ronai. 2020. PRMT5 function and targeting in cancer. *Cell Stress*. 4:199-215.

Kimura, H., A.P. Klein, R.H. Hruban, and N.J. Roberts. 2021. The Role of Inherited Pathogenic CDKN2A Variants in Susceptibility to Pancreatic Cancer. *Pancreas*. 50:1123-1130.

Kindler, H.L., D. Niedzwiecki, D. Hollis, S. Sutherland, D. Schrag, H. Hurwitz, F. Innocenti, M.F. Mulcahy, E. O'Reilly, T.F. Wozniak, J. Picus, P. Bhargava, R.J. Mayer, R.L. Schilsky, and R.M. Goldberg. 2010. Gemcitabine plus bevacizumab compared with gemcitabine plus placebo in patients with advanced pancreatic cancer: Phase III trial of the Cancer and Leukemia Group B (CALGB 80303). *Journal of Clinical Oncology*. 28:3617-3622.

Kisor, Kyle P., Diego G. Ruiz, Matthew P. Jacobson, and Diane L. Barber. 2025. A role for pH dynamics regulating transcription factor DNA-binding selectivity. *Nucleic Acids Research*. 53.

Kong, L.J., J.T. Chang, A.H. Bild, and J.R. Nevins. 2007. Compensation and specificity of function within the E2F family. *Oncogene*. 26:321-327.

Kreft, Ł., A. Soete, P. Hulpiau, A. Botzki, Y. Saeys, and P. De Bleser. 2017. ConTra v3: a tool to identify transcription factor binding sites across species, update 2017. *Nucleic Acids Research*. 45:W490-W494.

Kryukov, G.V., F.H. Wilson, J.R. Ruth, J. Paulk, A. Tsherniak, S.E. Marlow, F. Vazquez, B.A. Weir, M.E. Fitzgerald, M. Tanaka, C.M. Bielski, J.M. Scott, C. Dennis, G.S. Cowley, J.S. Boehm, D.E. Root, T.R. Golub, C.B. Clish, J.E. Bradner, W.C. Hahn, and L.A. Garraway. 2016. MTAP deletion confers enhanced dependency on the PRMT5 arginine methyltransferase in cancer cells. *Science*. 351:1214-1218.

Kumar, P., A. Nagarajan, and P.D. Uchil. 2018. Analysis of Cell Viability by the MTT Assay. *Cold Spring Harbor Protocols*. 2018:pdb.prot095505.

Landini, G., G. Martinelli, and F. Piccinini. 2020. Colour deconvolution: stain unmixing in histological imaging. *Bioinformatics*. 37:1485-1487.

Lee, J., M.-K. Choi, and I.-S. Song. 2023. Recent Advances in Doxorubicin Formulation to Enhance Pharmacokinetics and Tumor Targeting. *Pharmaceuticals*. 16:802.

Lee, J., J. Kim, and I. Hwang. 2025. Targeting PRMT5 in cancer: Mechanistic insights and clinical progress. *Biomedicine & Pharmacotherapy*. 193:118754.

Lee, S., T.V. Axelsen, A.P. Andersen, P. Vahl, S.F. Pedersen, and E. Boedtkjer. 2016. Disrupting Na+,HCO3−-cotransporter NBCn1 (Slc4a7) delays murine breast cancer development. *Oncogene*. 35:2112-2122.

Leidner, R., N.S. Silva, H. Huang, D. Sprott, C. Zheng, Y.-P. Shih, A. Leung, R. Payne, K. Sutcliffe, J. Cramer, S.A. Rosenberg, B.A. Fox, W.J. Urba, and E. Tran. 2022. Neoantigen T-Cell Receptor Gene Therapy in Pancreatic Cancer. *New England Journal of Medicine*. 386:2112-2119.

Li, B., Q. Zhang, C. Castaneda, and S. Cook. 2024. Targeted Therapies in Pancreatic Cancer: A New Era of Precision Medicine. *Biomedicines*. 12:2175.

Li, J., W. Bi, F. Lu, B. Pan, M. Xiong, L. Nasifu, Z. Nie, and B. He. 2023. Prognostic role of E2F1 gene expression in human cancer: a meta-analysis. *BMC Cancer*. 23:509.

Li, X., Y. Yang, B. Zhang, X. Lin, X. Fu, Y. An, Y. Zou, J.-X. Wang, Z. Wang, and T. Yu. 2022. Lactate metabolism in human health and disease. *Signal Transduction and Targeted Therapy*. 7:305.

Liaki, V., S. Barrambana, M. Kostopoulou, C.G. Lechuga, E. Zamorano-Dominguez, D. Acosta, L. Morales-Cacho, R. Álvarez, P. Sun, B. Rosas-Perez, R. Barrero, S. Jiménez-Parrado, A. López-García, M. San Roman, J.C. López-Gil, M. Drosten, B. Sainz, M. Musteanu, E. Caleiras, N. Dusetti, V. Poli, F. Sánchez-Bueno, C. Guerra, and M. Barbacid. 2025. A targeted combination therapy achieves effective pancreatic cancer regression and prevents tumor resistance. *Proceedings of the National Academy of Sciences*. 122:e2523039122.

Liang, Z., C. Wen, H. Jiang, S. Ma, and X. Liu. 2021. Protein Arginine Methyltransferase 5 Functions via Interacting Proteins. *Frontiers in Cell and Developmental Biology*. Volume 9 - 2021.

Lin, J., A.P. Rivadeneira, Y. Ye, C. Ryu, S. Parvin, K. Jang, S.M. Garraway, and I. Choi. 2024. Sodium Bicarbonate Decreases Alcohol Consumption in Mice. *International Journal of Molecular Sciences*. 25:5006.

Liu, M., J. Zhong, Z. Zeng, K. Huang, Z. Ye, S. Deng, H. Chen, F. Xu, Q. Li, and G. Zhao. 2019. Hypoxia-induced feedback of HIF-1α and lncRNA-CF129 contributes to pancreatic cancer progression through stabilization of p53 protein. *Theranostics*. 9:4795-4810.

Liu, Y., X. Qin, D.-K. Wang, Y.-M. Guo, H.S. Gill, N. Morris, M.D. Parker, L.-M. Chen, and W.F. Boron. 2013. Effects of optional structural elements, including two alternative amino termini and a new splicing cassette IV, on the function of the sodium–bicarbonate cotransporter NBCn1 (SLC4A7). *The Journal of Physiology*. 591:4983-5004.

Livak, K.J., and T.D. Schmittgen. 2001. Analysis of Relative Gene Expression Data Using Real-Time Quantitative PCR and the 2−ΔΔCT Method. *Methods*. 25:402-408.

Lockie, E.B., A. Sylivris, S. Pandanaboyana, J. Zalcberg, A. Skandarajah, and B.P. Loveday. 2025. Relationship between pancreatic cancer resection rate and survival at population level: systematic review. *BJS Open*. 9.

Lv, D., Z. Chang, Y. Cai, J. Li, L. Wang, Q. Jiang, K. Xu, N. Ding, X. Li, J. Xu, and Y. Li. 2021. TransLnc: a comprehensive resource for translatable lncRNAs extends immunopeptidome. *Nucleic Acids Research*. 50:D413-D420.

Lyu, S.I., K. Knipper, C. Fretter, E. Tzitzili, A.G. Simon, H. Alakus, A. Pamuk, C.J. Bruns, T. Schmidt, F.C. Popp, and A. Quaas. 2026. MTAP loss in gastrointestinal cancers is associated with CDKN2A deletion, poor prognosis in gastric carcinoma, and potential relevance for PRMT5-targeted therapy. *Scientific Reports*. 16:15061.

Maddalena, M., G. Mallel, N.B. Nataraj, M. Shreberk-Shaked, O. Hassin, S. Mukherjee, S. Arandkar, R. Rotkopf, A. Kapsack, G. Lambiase, B. Pellegrino, E. Ben-Isaac, O. Golani, Y. Addadi, E. Hajaj, R. Eilam, R. Straussman, Y. Yarden, M. Lotem, and M. Oren. 2021. TP53 missense mutations in PDAC are associated with enhanced fibrosis and an immunosuppressive microenvironment. *Proceedings of the National Academy of Sciences*. 118:e2025631118.

Madeira, F., M. Pearce, A.R.N. Tivey, P. Basutkar, J. Lee, O. Edbali, N. Madhusoodanan, A. Kolesnikov, and R. Lopez. 2022. Search and sequence analysis tools services from EMBL-EBI in 2022. *Nucleic Acids Research*. 50:W276-W279.

Maeng, J.E., J.-H. Kim, S.-C. Kim, W.-G. Yun, W. Kwon, Y. Han, D.-Y. Oh, S.H. Lee, J.-Y. Jang, and J.-L. Ku. 2025. Comprehensive molecular analysis of 26 newly established human pancreatic ductal adenocarcinoma cell lines reveals two clusters with variating drug sensitivities. *Cancer Cell International*. 25:53.

Mahat, D.B., H. Kumra, S.A. Castro, E. Metcalf, K. Nguyen, R. Morisue, W.W. Ho, I. Chen, B. Sullivan, L.H. Yim, A. Singh, J. Fu, S.K. Waterton, Y.-C. Cheng, E. Moiso, V.P. Chauhan, H.M. Silva, S. Spranger, R.K. Jain, and P.A. Sharp. 2025. Mutant p53 exploits enhancers to elevate immunosuppressive chemokine expression and impair immune checkpoint inhibitors in pancreatic cancer. *Immunity*. 58:1688-1705.e1689.

Mahmoud, H.S., N.A.-R. Eldesoky, O.G. Shaker, and A.A. El-Husseiny. 2025. The diagnostic value of LncRNA NEAT1 targeting miR-129-5p in pancreatic cancer patients. *Scientific Reports*. 15:27638.

Mai, T., M. Wang, Y. Qiu, W. Lu, H. Wu, S. Chen, P.J. Chiao, and P. Huang. 2026. KRASG12D mutation promotes pancreatic tumorigenesis by suppressing sirtuin three via the guanine nucleotide exchange factor RCC1. *Journal of Biological Chemistry*. 302:111057.

Maldonado, M.d.M., J. Schlom, and D.H. Hamilton. 2023. Blockade of tumor-derived colony-stimulating factor 1 (CSF1) promotes an immune-permissive tumor microenvironment. *Cancer Immunology, Immunotherapy*. 72:3349-3362.

Malla, M., Y. Sakr, G. Gupta, M. Akce, and B. El-Rayes. 2025. Emerging therapeutic advancements in pancreatic cancer: a contemporary review. *Discov Oncol*. 16:1885.

Manickavinayaham, S., R. Velez-Cruz, A.K. Biswas, J. Chen, R. Guo, and D.G. Johnson. 2020. The E2F1 transcription factor and RB tumor suppressor moonlight as DNA repair factors. *Cell Cycle*. 19:2260-2269.

Marjon, K., Michael J. Cameron, P. Quang, Michelle F. Clasquin, E. Mandley, K. Kunii, M. McVay, S. Choe, A. Kernytsky, S. Gross, Z. Konteatis, J. Murtie, Michelle L. Blake, J. Travins, M. Dorsch, Scott A. Biller, and Kevin M. Marks. 2016. MTAP Deletions in Cancer Create Vulnerability to Targeting of the MAT2A/PRMT5/RIOK1 Axis. *Cell Reports*. 15:574-587.

Marstrand-Daucé, L., D. Lorenzo, A. Chassac, P. Nicole, A. Couvelard, and C. Haumaitre. 2023. Acinar-to-Ductal Metaplasia (ADM): On the Road to Pancreatic Intraepithelial Neoplasia (PanIN) and Pancreatic Cancer. *International Journal of Molecular Sciences*. 24:9946.

Marzio, G., C. Wagener, M.I. Gutierrez, P. Cartwright, K. Helin, and M. Giacca. 2000. E2F Family Members Are Differentially Regulated by Reversible Acetylation *. *Journal of Biological Chemistry*. 275:10887-10892.

Mastrantoni, L., M. Chiaravalli, A. Spring, V. Beccia, A. Di Bello, C. Bagalà, M. Bensi, D. Barone, G. Trovato, G. Caira, G. Giordano, E. Bria, G. Tortora, and L. Salvatore. 2024. Comparison of first-line chemotherapy regimens in unresectable locally advanced or metastatic pancreatic cancer: a systematic review and Bayesian network meta-analysis. *The Lancet Oncology*. 25:1655-1665.

Mavrakis, K.J., E.R. McDonald, M.R. Schlabach, E. Billy, G.R. Hoffman, A. deWeck, D.A. Ruddy, K. Venkatesan, J. Yu, G. McAllister, M. Stump, R. deBeaumont, S. Ho, Y. Yue, Y. Liu, Y. Yan-Neale, G. Yang, F. Lin, H. Yin, H. Gao, D.R. Kipp, S. Zhao, J.T. McNamara, E.R. Sprague, B. Zheng, Y. Lin, Y.S. Cho, J. Gu, K. Crawford, D. Ciccone, A.C. Vitari, A. Lai, V. Capka, K. Hurov, J.A. Porter, J. Tallarico, C. Mickanin, E. Lees, R. Pagliarini, N. Keen, T. Schmelzle, F. Hofmann, F. Stegmeier, and W.R. Sellers. 2016. Disordered methionine

metabolism in MTAP/CDKN2A-deleted cancers leads to dependence on PRMT5. *Science*. 351:1208-1213.

Mello, S.S., B.M. Flowers, P.K. Mazur, J.J. Lee, F. Müller, S.K. Denny, S. Ferreira, K. Hanson, S.K. Kim, W.J. Greenleaf , L.D. Wood, and L.D. Attardi. 2023. Multifaceted role for p53 in pancreatic cancer suppression. *Proceedings of the National Academy of Sciences*. 120:e2211937120.

Michalak, N., and E. Małecka-Wojciesko. 2023. Modifiable Pancreatic Ductal Adenocarcinoma (PDAC) Risk Factors. *Journal of Clinical Medicine*. 12:4318.

Michl, J., S. Monterisi, B. White, W. Blaszczak, A. Hulikova, G. Abdullayeva, E. Bridges, Z. Yin, W.F. Bodmer, and P. Swietach. 2023. Acid-adapted cancer cells alkalinize their cytoplasm by degrading the acid-loading membrane transporter anion exchanger 2, SLC4A2. *Cell Reports*. 42:112601.

Michl, J., K.C. Park, and P. Swietach. 2019. Evidence-based guidelines for controlling pH in mammalian live-cell culture systems. *Communications Biology*. 2:144.

Michl, J., Y. Wang, S. Monterisi, W. Blaszczak, R. Beveridge, E.M. Bridges, J. Koth, W.F. Bodmer, and P. Swietach. 2022. CRISPR-Cas9 screen identifies oxidative phosphorylation as essential for cancer cell survival at low extracellular pH. *Cell Reports*. 38:110493.

Michl, J., B. White, S. Monterisi, W.F. Bodmer, and P. Swietach. 2024. Phenotypic screen of sixty-eight colorectal cancer cell lines identifies CEACAM6 and CEACAM5 as markers of acid resistance. *Proceedings of the National Academy of Sciences*. 121:e2319055121.

Miller, F.H., C. Lopes Vendrami, N.A. Hammond, P.K. Mittal, P. Nikolaidis, and A. Jawahar. 2023. Pancreatic Cancer and Its Mimics. *RadioGraphics*. 43:e230054.

Moghadamchargari, Z., J. Huddleston, M. Shirzadeh, X. Zheng, D.E. Clemmer, F. M. Raushel, D.H. Russell, and A. Laganowsky. 2019. Intrinsic GTPase Activity of K-RAS Monitored by Native Mass Spectrometry. *Biochemistry*. 58:3396-3405.

Moore, M.J., D. Goldstein, J. Hamm, A. Figer, J.R. Hecht, S. Gallinger, H.J. Au, P. Murawa, D. Walde, R.A. Wolff, D. Campos, R. Lim, K. Ding, G. Clark, T.

Voskoglou-Nomikos, M. Ptasynski, and W. Parulekar. 2023. Erlotinib Plus Gemcitabine Compared With Gemcitabine Alone in Patients With Advanced Pancreatic Cancer: A Phase III Trial of the National Cancer Institute of Canada Clinical Trials Group. *Journal of Clinical Oncology*. 41:4714-4720.

Morton, J.P., P. Timpson, S.A. Karim, R.A. Ridgway, D. Athineos, B. Doyle, N.B. Jamieson, K.A. Oien, A.M. Lowy, V.G. Brunton, M.C. Frame, T.R.J. Evans, and O.J. Sansom. 2010. Mutant p53 drives metastasis and overcomes growth arrest/senescence in pancreatic cancer. *Proceedings of the National Academy of Sciences*. 107:246-251.

Motolani, A., M. Martin, M. Sun, and T. Lu. 2021. The Structure and Functions of PRMT5 in Human Diseases. *Life*. 11:1074.

Mu, C., X. Liu, Y. Kim, A. Riselli, D.E. Korenchan, R.A. Bok, R. Delos Santos, R. Sriram, H. Qin, H. Nguyen, J.W. Gordon, J. Slater, P.E.Z. Larson, D.B. Vigneron, J. Kurhanewicz, D.M. Wilson, and R.R. Flavell. 2023. Clinically Translatable Hyperpolarized 13C Bicarbonate pH Imaging Method for Use in Prostate Cancer. *ACS Sensors*. 8:4042-4054.

Mulvaney, K.M. 2023. Early Clinical Success of MTA-Cooperative PRMT5 Inhibitors for the Treatment of CDKN2A/MTAP-Deleted Cancers. *Cancer Discovery*. 13:2310-2312.

Mundry, C.S., K.C. Eberle, P.K. Singh, M.A. Hollingsworth, and K. Mehla. 2020. Local and systemic immunosuppression in pancreatic cancer: Targeting the stalwarts in tumor's arsenal. *Biochimica et Biophysica Acta (BBA) - Reviews on Cancer*. 1874:188387.

Murimwa, G.Z., N.E. Williams, D. Alzhanova, A. Mohammadi, J.M. Westcott, F. Beato, R. Dai, L. Nivelo, F. Rossi, H.K. Fleming, A.F. Tassielli, Z. Yazgan, J.E. Toombs, J.B. Fleming, A.D. Singhi, C.G. Ethun, H. Huang, and R.A. Brekken. 2025. SMAD4 Deficiency Promotes Pancreatic Cancer Progression and Confers Susceptibility to TGFβ Inhibition. *Cancer Research*. 85:2987-2996.

Musher, B.L., S. Vasileiou, B.G. Smaglo, C.S. Robertson, M. Wu, T. Wang, A. Watanabe, M. Kuvalekar, Y. Velazquez, S. Ketkar, T.A. Doheyan, P.G. Papayanni, A. Shah, N. Lapteva, B.J. Grilley, G. Van Buren, P.D. Lulla, H.E. Heslop, C.M. Rooney, M.K. Brenner, and A.M. Leen. 2026. Autologous multiantigen-targeted T cell therapy for pancreatic cancer: a phase 1/2 trial. *Nature Medicine*. 32:258-269.

Musiu, C., F. Lupo, A. Agostini, G. Lionetto, M. Bevere, S. Paiella, C. Carbone, V. Corbo, S. Ugel, and F. De Sanctis. 2024. Cellular collusion: cracking the code of immunosuppression and chemo resistance in PDAC. *Front Immunol*. 15:1341079.

Nakajima, E.C., N. Drezner, X. Li, P.S. Mishra-Kalyani, Y. Liu, H. Zhao, Y. Bi, J. Liu, A. Rahman, E. Wearne, I. Ojofeitimi, L.T. Hotaki, D. Spillman, R. Pazdur, J.A. Beaver, and H. Singh. 2022. FDA Approval Summary: Sotorasib for KRAS G12C-Mutated Metastatic NSCLC. *Clin Cancer Res*. 28:1482-1486.

Ngoi, N., E.L. Scholefield, V. Parini, R.S.P. Huang, T. Janovitz, N. Danziger, M.A. Levy, S. Pant, M.M. Javle, J.S. Ross, and J.R. Ahnert. 2022. Genomic classification of clinically advanced pancreatic ductal adenocarcinoma (PDAC) based on methylthioadenosine phosphorylase (MTAP) genomic loss. *Journal of Clinical Oncology*. 40:604-604.

Nilsson, J.B., and M. Nielsen. 2024. The journey towards complete and accurate prediction of HLA antigen presentation. *ImmunoInformatics*. 13.

Norton, C., M.S. Shaw, Z. Rubnitz, J. Smith, H.P. Soares, C.D. Nevala-Plagemann, I. Garrido-Laguna, and V. Florou. 2025. KRAS Mutation Status and Treatment Outcomes in Patients With Metastatic Pancreatic Adenocarcinoma. *JAMA Network Open*. 8:e2453588-e2453588.

O'Reilly, E.M., Z.A. Wainberg, A.E. Hendifar, M.J. Borad, F. Pietrantonio, S. Pant, P. Hammel, C. Cremolini, G.A. Manji, P.E. Oberstein, I. Garrido-Laguna, C. Springfeld, N.S. Azad, M. Ueno, S.Y. Chui, Y. Zhang, H. Patel, Y. Lee, Z. Salman, and B.M. Wolpin. 2026. Daraxonrasib or Chemotherapy in Previously Treated Metastatic Pancreatic Cancer. *New England Journal of Medicine*. 395:325-337.

Orben, F., K. Lankes, C. Schneeweis, Z. Hassan, H. Jakubowsky, L. Krauß, F. Boniolo, C. Schneider, A. Schäfer, J. Murr, C. Schlag, B. Kong, R. Öllinger, C. Wang, G. Beyer, U.M. Mahajan, Y. Xue, J. Mayerle, R.M. Schmid, B. Kuster, R. Rad, C.J. Braun, M. Wirth, M. Reichert, D. Saur, and G. Schneider. 2022. Epigenetic drug screening defines a PRMT5 inhibitor–sensitive pancreatic cancer subtype. *JCI Insight*. 7.

Orth, M., P. Metzger, S. Gerum, J. Mayerle, G. Schneider, C. Belka, M. Schnurr, and K. Lauber. 2019. Pancreatic ductal adenocarcinoma: biological hallmarks, current status, and future perspectives of combined modality treatment approaches. *Radiation Oncology*. 14:141.

Ozturk, H., F. Seker-Polat, N. Abbaszadeh, Y. Kingham, S. Orsulic, and M. Adli. 2025. High PRMT5 levels, maintained by KEAP1 inhibition, drive chemoresistance in high-grade serous ovarian cancer. *The Journal of Clinical Investigation*. 135.

Palte, R.L., S.E. Schneider, M.D. Altman, R.P. Hayes, S. Kawamura, B.M. Lacey, M.S. Mansueto, M. Reutershan, P. Siliphaivanh, C. Sondey, H. Xu, Z. Xu, Y. Ye, and M.R. Machacek. 2020. Allosteric Modulation of Protein Arginine Methyltransferase 5 (PRMT5). *ACS Medicinal Chemistry Letters*. 11:1688-1693.

Pant, S., S. Kar, K.K. Lin, and E. Ahler. 2025. Frequency and incidence of oncogenic RAS mutations in patients with metastatic pancreatic ductal adenocarcinoma: Derived from the real-world evidence database Foundation Medicine Insights. *Journal of Clinical Oncology*. 43:777-777.

Park, W., A. Chawla, and E.M. O'Reilly. 2021. Pancreatic Cancer: A Review. *JAMA*. 326:851-862.

Pastore, F., N. Bhagwat, A. Pastore, A. Radzisheuskaya, A. Karzai, A. Krishnan, B. Li, R.L. Bowman, W. Xiao, A.D. Viny, A. Zouak, Y.C. Park, K.B. Cordner, S. Braunstein, J.L. Maag, A. Grego, J. Mehta, M. Wang, H. Lin, B.H. Durham, R.P. Koche, R.K. Rampal, K. Helin, P. Scherle, K. Vaddi, and R.L. Levine. 2020. PRMT5 Inhibition Modulates E2F1 Methylation and Gene-Regulatory Networks Leading to Therapeutic Efficacy in JAK2V617F-Mutant MPN. *Cancer Discovery*. 10:1742-1757.

Peduzzi, G., L. Archibugi, R. Farinella, R.P. de Leon Pisani, L. Vodickova, P. Vodicka, B. Kraja, J. Sainz, D. Bars-Cortina, N. Daniel, R. Silvestri, P. Uysal-Onganer, S. Landi, J. Dulińska-Litewka, A. Comandatore, D. Campa, D.J. Hughes, and C. Rizzato. 2025. The exposome and pancreatic cancer, lifestyle and environmental risk factors for PDAC. *Seminars in Cancer Biology*. 113:100-129.

Pethő, Z., K. Najder, S. Beel, B. Fels, I. Neumann, S. Schimmelpfennig, S. Sargin, M. Wolters, K. Grantins, E. Wardelmann, M. Mitkovski, A. Oeckinghaus, and A. Schwab. 2023. Acid-base homeostasis orchestrated by NHE1 defines the pancreatic stellate cell phenotype in pancreatic cancer. *JCI Insight*. 8.

Pian, L.-l., M.-h. Song, T.-f. Wang, L. Qi, T.-l. Peng, and K.-p. Xie. 2025. Identification and analysis of pancreatic intraepithelial neoplasia: opportunities and challenges. *Frontiers in Endocrinology*. Volume 15 - 2024.

Pilon-Thomas, S., K.N. Kodumudi, A.E. El-Kenawi, S. Russell, A.M. Weber, K. Luddy, M. Damaghi, J.W. Wojtkowiak, J.J. Mulé, A. Ibrahim-Hashim, and R.J. Gillies. 2016. Neutralization of Tumor Acidity Improves Antitumor Responses to Immunotherapy. *Cancer Research*. 76:1381-1390.

Prabhu, L., M. Martin, L. Chen, Ö. Demir, J. Jin, X. Huang, A. Motolani, M. Sun, G. Jiang, H. Nakshatri, M.L. Fishel, S. Sun, A. Safa, R.E. Amaro, M.R. Kelley, Y. Liu, Z.-Y. Zhang, and T. Lu. 2023. Inhibition of PRMT5 by market drugs as a novel cancer therapeutic avenue. *Genes & Diseases*. 10:267-283.

Principe, D.R., P.W. Underwood, S. Kumar, K.E. Timbers, R.M. Koch, J.G. Trevino, H.G. Munshi, and A. Rana. 2022. Loss of SMAD4 Is Associated With Poor Tumor Immunogenicity and Reduced PD-L1 Expression in Pancreatic Cancer. *Frontiers in Oncology*. Volume 12 - 2022.

Qin, Y., Q. Hu, J. Xu, S. Ji, W. Dai, W. Liu, W. Xu, Q. Sun, Z. Zhang, Q. Ni, B. Zhang, X. Yu, and X. Xu. 2019. PRMT5 enhances tumorigenicity and glycolysis in pancreatic cancer via the FBW7/cMyc axis. *Cell Communication and Signaling*. 17:30.

Radzisheuskaya, A., P.V. Shliaha, V. Grinev, E. Lorenzini, S. Kovalchuk, D. Shlyueva, V. Gorshkov, R.C. Hendrickson, O.N. Jensen, and K. Helin. 2019. PRMT5 methylome profiling uncovers a direct link to splicing regulation in acute myeloid leukemia. *Nat Struct Mol Biol*. 26:999-1012.

Rahman, M.M., A. Pennati, T. Atajanova, T. Debnath, R.H. Allawi, R.O. Meyers, T.J. Berg, Z. Gurel, N.V. Uboha, M.F. Bassetti, L. Mao, P.M. Sondel, R.J. Kimple, C.M. Capitini, Q.H. Sodji, J. Galipeau, and Z.S. Morris. 2025. Combined innate immune cell therapy, tumor-specific antibody, and radiation prompt antitumor response in pancreatic cancer models. *Science Advances*. 11:eadx2984.

Ran, F.A., P.D. Hsu, J. Wright, V. Agarwala, D.A. Scott, and F. Zhang. 2013. Genome engineering using the CRISPR-Cas9 system. *Nature Protocols*. 8:2281-2308.

Rawla, P., T. Sunkara, and V. Gaduputi. 2019. Epidemiology of Pancreatic Cancer: Global Trends, Etiology and Risk Factors. *World J Oncol*. 10:10-27.

Reiss, K.A., K.C. Soares, R.J. Torphy, and B. Gyawali. 2025. Treatment Innovations in Pancreatic Cancer: Putting Patient Priorities First. *American Society of Clinical Oncology Educational Book*. 45:e473204.

Reshetnyak, Y.K., L. Yao, S. Zheng, S. Kuznetsov, D.M. Engelman, and O.A. Andreev. 2011. Measuring Tumor Aggressiveness and Targeting Metastatic Lesions with Fluorescent pHLIP. *Molecular Imaging and Biology*. 13:1146-1156.

Reynisson, B., B. Alvarez, S. Paul, B. Peters, and M. Nielsen. 2020. NetMHCpan-4.1 and NetMHCIIpan-4.0: improved predictions of MHC antigen presentation by concurrent motif deconvolution and integration of MS MHC eluted ligand data. *Nucleic Acids Research*. 48:W449-W454.

Rojas, L.A., Z. Sethna, K.C. Soares, C. Olcese, N. Pang, E. Patterson, J. Lihm, N. Ceglia, P. Guasp, A. Chu, R. Yu, A.K. Chandra, T. Waters, J. Ruan, M. Amisaki, A. Zebboudj, Z. Odgerel, G. Payne, E. Derhovanessian, F. Müller, I. Rhee, M. Yadav, A. Dobrin, M. Sadelain, M. Łuksza, N. Cohen, L. Tang, O. Basturk, M. Gönen, S. Katz, R.K. Do, A.S. Epstein, P. Momtaz, W. Park, R. Sugarman, A.M. Varghese, E. Won, A. Desai, A.C. Wei, M.I. D'Angelica, T.P. Kingham, I. Mellman, T. Merghoub, J.D. Wolchok, U. Sahin, Ö. Türeci, B.D. Greenbaum, W.R. Jarnagin, J. Drebin, E.M. O'Reilly, and V.P. Balachandran. 2023. Personalized RNA neoantigen vaccines stimulate T cells in pancreatic cancer. *Nature*. 618:144-150.

Rolver, M.G., J. Camacho-Roda, Y. Dai, M. Flinck, R. Ialchina, J. Hindkær, R.T. Dyhr, A.N. Bodilsen, N.S. Prasad, J. Baldan, J. Yao, A. Sandelin, L. Arnes, and S.F. Pedersen. 2025. Tumor microenvironment acidosis favors pancreatic cancer stem cell properties and in vivo metastasis. *iScience*. 28:111956.

Rombel, I.T., K.F. Sykes, S. Rayner, and S.A. Johnston. 2002. ORF-FINDER: a vector for high-throughput gene identification. *Gene*. 282:33-41.

Roworth, A.P., S.M. Carr, G. Liu, W. Barczak, R.L. Miller, S. Munro, A. Kanapin, A. Samsonova, and N.B. La Thangue. 2019. Arginine methylation expands the regulatory mechanisms and extends the genomic landscape under E2F control. *Science Advances*. 5:eaaw4640.

Rozengurt, E., and G. Eibl. 2026. Pancreatic cancer: molecular pathogenesis and emerging therapeutic strategies. *Signal Transduction and Targeted Therapy*. 11:6.

Saarikettu, J., S. Lehmusvaara, M. Pesu, I. Junttila, J. Partanen, P. Sipilä, M. Poutanen, J. Yang, T. Haikarainen, and O. Silvennoinen. 2023. The RNA-binding protein Snd1/Tudor-SN regulates hypoxia-responsive gene expression. *FASEB BioAdvances*. 5:183-198.

Sarantis, P., E. Koustas, A. Papadimitropoulou, A.G. Papavassiliou, and M.V. Karamouzis. 2020. Pancreatic ductal adenocarcinoma: Treatment hurdles, tumor microenvironment and immunotherapy. *World Journal of Gastrointestinal Oncology*. 12:173-181.

Scarlato, E., S. Casalino, L. Mendo, A. Sordo, V. De Vita, E. San Lorenzo, A. Quinzii, C. Zecchetto, G. Butturini, and D. Melisi. 2025. Early-onset enriches the identification of actionable alterations in patients with KRAS wild-type pancreatic ductal adenocarcinoma. *ESMO Gastrointestinal Oncology*. 8:100179.

Schneider, C., V. Spielmann, C.J. Braun, and G. Schneider. 2025. PRMT5 inhibitors: Therapeutic potential in pancreatic cancer. *Translational Oncology*. 55:102366.

Sevigny, J.L., E.V. Proctor, H. Adams, E.R. MacDonald, W.K. Thomas, and J. Cheng. 2025. Protein arginine methyltransferase 5 sustains Tip60-EP400 complex via SRSF1 in Merkel cell carcinoma. *Life Science Alliance*. 8:e202503316.

Shen, Y., G. Gao, X. Yu, H. Kim, L. Wang, L. Xie, M. Schwarz, X. Chen, E. Guccione, J. Liu, M.T. Bedford, and J. Jin. 2020. Discovery of First-in-Class Protein Arginine Methyltransferase 5 (PRMT5) Degraders. *Journal of Medicinal Chemistry*. 63:9977-9989.

Shen, Y., P. Zhao, K. Dong, J. Wang, H. Li, M. Li, R. Li, S. Chen, Y. Shen, Z. Liu, M. Xie, P. Shen, and J. Zhang. 2022. Tadalafil increases the antitumor activity of 5-FU through inhibiting PRMT5-mediated glycolysis and cell proliferation in colorectal cancer. *Cancer & Metabolism*. 10:22.

Shen, Z., and C. Li. 2025. Targeting PRMT5: Current Inhibitors and Emerging Strategies for Therapeutic Intervention. *Processes*. 13:2878.

Sheng, M., R. Zhang, X. Ma, and H. Zhou. 2022. CT manifestations of childhood pancreatoblastoma. *World Journal of Pediatric Surgery*. 5:e000398.

Sherman, M.H., and G.L. Beatty. 2023. Tumor Microenvironment in Pancreatic Cancer Pathogenesis and Therapeutic Resistance. *Annu Rev Pathol*. 18:123-148.

Sherpally, D., and A. Manne. 2025. Advancing Immunotherapy in Pancreatic Cancer: A Brief Review of Emerging Adoptive Cell Therapies. *Cancers*. 17:589.

Shirmanova, M.V., I.N. Druzhkova, M.M. Lukina, V.V. Dudenkova, N.I. Ignatova, L.B. Snopova, V.I. Shcheslavskiy, V.V. Belousov, and E.V. Zagaynova. 2017. Chemotherapy with cisplatin: insights into intracellular pH and metabolic landscape of cancer cells in vitro and in vivo. *Scientific Reports*. 7:8911.

Siegel, R.L., K.D. Miller, and A. Jemal. 2019. Cancer statistics, 2019. *CA Cancer J Clin*. 69:7-34.

Sivapalan, L., H.M. Kocher, H. Ross-Adams, and C. Chelala. 2022. The molecular landscape of pancreatic ductal adenocarcinoma. *Pancreatology*. 22:925-936.

Škrha, P., A. Hořínek, J. Hajer, J. Potočková, P. Frič, J. Bureš, M. Anděl, and J. Škrha. 2025. Serum MicroRNA-196, -200 and -423 Improve Diagnostics and Differentiate Pancreatic Ductal Adenocarcinoma From Chronic Pancreatitis. *Physiol Res*. 74:837-847.

Sniegowski, T., D. Rajasekaran, S.R. Sennoune, S. Sunitha, F. Chen, M. Fokar, S. Kshirsagar, P.H. Reddy, K. Korac, M. Mahmud Syed, T. Sharker, V. Ganapathy, and Y.D. Bhutia. 2023. Amino acid transporter SLC38A5 is a tumor promoter and a novel therapeutic target for pancreatic cancer. *Scientific Reports*. 13:16863.

Sonbol, M.B., G.L. Mazza, L. Mi, T. Oliver, J. Starr, H. Gudmundsdottir, S.P. Cleary, T. Hobday, and T.R. Halfdanarson. 2022. Survival and Incidence Patterns of Pancreatic Neuroendocrine Tumors Over the Last 2 Decades: A SEER Database Analysis. *The Oncologist*. 27:573-578.

Song, P., and F. Yang. 2026. Protein arginine methyltransferase 5 as a novel therapeutic target in solid tumors. *Genes & Diseases*. 13:101796.

Stefanoudakis, D., M. Frountzas, D. Schizas, N.V. Michalopoulos, A. Drakaki, and K.G. Toutouzas. 2024. Significance of TP53, CDKN2A, SMAD4 and KRAS in Pancreatic Cancer. *Current Issues in Molecular Biology*. 46:2827-2844.

Stevens, C., and N.B. La Thangue. 2003. E2F and cell cycle control: a double-edged sword. *Archives of Biochemistry and Biophysics*. 412:157-169.

Stigliani, A., R. Ialchina, J. Yao, D. Czaplinska, Y. Dai, H.B. Andersen, S. Rennie, R. Andersson, S.F. Pedersen, and A. Sandelin. 2024. Adaptation to an acid microenvironment promotes pancreatic cancer organoid growth and drug resistance. *Cell Reports*. 43:114409.

Sun, L., M. Wang, Z. Lv, N. Yang, Y. Liu, S. Bao, W. Gong, and R.-M. Xu. 2011. Structural insights into protein arginine symmetric dimethylation by PRMT5. *Proceedings of the National Academy of Sciences*. 108:20538-20543.

Sun, M., Y. Ji, G. Zhang, Y. Li, F. Dong, and T. Wu. 2024. Posttranslational modifications of E2F family members in the physiological state and in cancer: Roles, mechanisms and therapeutic targets. *Biomedicine & Pharmacotherapy*. 178:117147.

Sun, Y., X. Jin, J. Meng, F. Guo, T. Chen, X. Zhao, H. Wu, and D. Ren. 2023. MST2 methylation by PRMT5 inhibits Hippo signaling and promotes pancreatic cancer progression. *The EMBO Journal*. 42:EMBJ2023114558.

Swietach, P., E. Boedtkjer, and S.F. Pedersen. 2023. How protons pave the way to aggressive cancers. *Nature Reviews Cancer*. 23:825-841.

Taieb, J., G.W. Prager, D. Melisi, C.B. Westphalen, N. D'Esquermes, A. Ferreras, A. Carrato, and T. Macarulla. 2020. First-line and second-line treatment of patients with metastatic pancreatic adenocarcinoma in routine clinical practice across Europe: a retrospective, observational chart review study. *ESMO Open*. 5.

Takikawa, T., K. Kikuta, S. Hamada, K. Kume, S. Miura, N. Yoshida, Y. Tanaka, R. Matsumoto, M. Ikeda, F. Kataoka, A. Sasaki, K. Nakagawa, M. Unno, and A. Masamune. 2022. Clinical features and prognostic impact of asymptomatic pancreatic cancer. *Scientific Reports*. 12:4262.

Tang, Y., G. Dai, Y. Yang, and H. Liu. 2023. GSG2 facilitates the progression of human breast cancer through MDM2-mediated ubiquitination of E2F1. *Journal of Translational Medicine*. 21.

Taylor, I.P., and J.A. Lopez. 2023. Oncolytic adenoviruses and the treatment of pancreatic cancer: a review of clinical trials. *Journal of Cancer Research and Clinical Oncology*. 149:8117-8129.

Timmer, F.E.F., B. Geboers, S. Nieuwenhuizen, M. Dijkstra, E.A.C. Schouten, R.S. Puijk, J.J.J. de Vries, M.P. van den Tol, A.M.E. Bruynzeel, M.M. Streppel, J.W. Wilmink, H.J. van der Vliet, M.R. Meijerink, H.J. Scheffer, and T.D. de Gruijl. 2021. Pancreatic Cancer and Immunotherapy: A Clinical Overview. *Cancers*. 13:4138.

Trovato, G., D. Rossini, A. Guidolin, Y.Y. Su, Y.S. Shan, N.J. Chiang, W.C. Chou, L.Y. Bai, C. Bagalà, M. Bensi, M. Niger, S. Marchesi, S.K. Garattini, A. Michelotti, A. Pretta, M. Scartozzi, C. Vivaldi, L. Bartalini, L. Procaccio, F. Bergamo, L. Antonuzzo, L.T. Chen, L. Salvatore, and G. Tortora. 2025. Second-line 5-FU plus nanoliposomal irinotecan versus FOLFOX/XELOX in metastatic pancreatic cancer after gemcitabine–nab-paclitaxel failure: a propensity score-matched analysis. *ESMO Open*. 10.

Tsanov, K.M., F.M. Barriga, Y.-J. Ho, D. Alonso-Curbelo, G. Livshits, S. Tian, R.P. Koche, T. Baslan, J. Simon, A.N. Wuest, J. Reyes, J. Park, W. Luan, J.E. Wilkinson, U. Bhanot, J. Ray-Kirton, I. Masilionis, N. Dimitrova, C.A. Iacobuzio-Donahue, R. Chaligné, D. Pe'er, J. Massagué, and S.W. Lowe. 2025. SMAD4 induces opposite effects on metastatic growth from pancreatic tumors depending on the organ of residence. *Nature Cancer*. 6:1839-1856.

Uniyal, P., V.K. Kashyap, T. Behl, D. Parashar, and R. Rawat. 2025. KRAS Mutations in Cancer: Understanding Signaling Pathways to Immune Regulation and the Potential of Immunotherapy. *Cancers*. 17:785.

Ushio, J., A. Kanno, E. Ikeda, K. Ando, H. Nagai, T. Miwata, Y. Kawasaki, Y. Tada, K. Yokoyama, N. Numao, K. Tamada, A.K. Lefor, and H. Yamamoto. 2021. Pancreatic Ductal Adenocarcinoma: Epidemiology and Risk Factors. *Diagnostics*. 11:562.

Vaish, U., T. Jain, A.C. Are, and V. Dudeja. 2021. Cancer-Associated Fibroblasts in Pancreatic Ductal Adenocarcinoma: An Update on Heterogeneity and Therapeutic Targeting. *International Journal of Molecular Sciences*. 22:13408.

Verkolf, E.M.M., E.N. Dekker, L.G. van der Geest, M.G. Besselink, B.A. Bonsing, M.J. Bruno, A.F. Sarasqueta, I.H.J.T. de Hingh, M.Y.V. Homs, N.B. Jamieson, V.E. de Meijer, M.F. van Velthuysen, J. Verheij, J. de Vos-Geelen, R.F. de Wilde, M. Doukas, and B.G. Koerkamp. 2025. 10-year survival after resection of pancreatic ductal adenocarcinoma with pathological re-examination of a nationwide cohort. *European Journal of Cancer*. 231:116099.

Victorasso Jardim Perassi, B., D. Abrahams, P. Irrera, C. Whelan, M. Beatty, S. Byrne, D. Longo, K. Gaspar, S. Pilon-Thomas, A. Ibrahim Hashim, C. Böhler, and R. Gillies. 2022. Targeting acidosis to improve immunotherapy in a pancreatic ductal adenocarcinoma model. *European Journal of Cancer*. 174:S90-S91.

Wainberg, Z.A., D. Melisi, T. Macarulla, R. Pazo Cid, S.R. Chandana, C. De La Fouchardière, A. Dean, I. Kiss, W.J. Lee, T.O. Goetze, E. Van Cutsem, A.S. Paulson, T. Bekaii-Saab, S. Pant, R.A. Hubner, Z. Xiao, H. Chen, F. Benzaghou, and E.M. O'Reilly. 2023. NALIRIFOX versus nab-paclitaxel and gemcitabine in treatment-naive patients with metastatic pancreatic ductal adenocarcinoma (NAPOLI 3): a randomised, open-label, phase 3 trial. *The Lancet*. 402:1272-1281.

Wang, G., H. Yao, Y. Gong, Z. Lu, R. Pang, Y. Li, Y. Yuan, H. Song, J. Liu, Y. Jin, Y. Ma, Y. Yang, H. Nie, G. Zhang, Z. Meng, Z. Zhou, X. Zhao, M. Qiu, Z. Zhao, K. Jiang, Q. Zeng, L. Guo, and Y. Yin. 2021. Metabolic detection and systems analyses of pancreatic ductal adenocarcinoma through machine learning, lipidomics, and multi-omics. *Science Advances*. 7:eabh2724.

Wang, J., A. Zahra, Y. Wang, and J. Wu. 2022. Understanding the Physiological Role of Electroneutral Na+-Coupled HCO3− Cotransporter and Its Therapeutic Implications. *Pharmaceuticals*. 15:1082.

Wang, W., H. R. Zhekova, K. Tsirulnikov, B.S. Dwadasi, E.G. Aparicio, R. Azimov, N. Abuladze, L. Kao, D. Acuna, D.P. Tieleman, Z.H. Zhou, A. Pushkin, and I. Kurtz. 2025. CryoEM and computational modeling structural insights into the pH regulator NBCn1. *Nature Communications*. 16:9932.

Wei, X., W.J. Kane, S.J. Adair, S. Nagdas, D. Liu, and T.W. Bauer. 2025. PRMT5 Identified as a Viable Target for Combination Therapy in Preclinical Models of Pancreatic Cancer. *Biomolecules*. 15:948.

Wei, X., J. Yang, S.J. Adair, H. Ozturk, C. Kuscu, K.Y. Lee, W.J. Kane, P.E. O'Hara, D. Liu, Y.M. Demirlenk, A.H. Habieb, E. Yilmaz, A. Dutta, T.W. Bauer, and M. Adli. 2020. Targeted CRISPR screening identifies PRMT5 as synthetic lethality combinatorial target with gemcitabine in pancreatic cancer cells. *Proceedings of the National Academy of Sciences*. 117:28068-28079.

Winiewska-Szajewska, M., D. Paprocki, E. Marzec, and J. Poznański. 2024. Effect of histidine protonation state on ligand binding at the ATP-binding site of human protein kinase CK2. *Scientific Reports*. 14:1463.

Wu, C., P. Yang, B. Liu, and Y. Tang. 2020a. Is there a CDKN2A-centric network in pancreatic ductal adenocarcinoma? *Onco Targets Ther*. 13:2551-2562.

Wu, H., V. Estrella, M. Beatty, D. Abrahams, A. El-Kenawi, S. Russell, A. Ibrahim-Hashim, D.L. Longo, Y.K. Reshetnyak, A. Moshnikova, O.A. Andreev, K. Luddy, M. Damaghi, K. Kodumudi, S.R. Pillai, P. Enriquez-Navas, S. Pilon-Thomas, P. Swietach, and R.J. Gillies. 2020b. T-cells produce acidic niches in lymph nodes to suppress their own effector functions. *Nature Communications*. 11:4113.

Wu, T.-C., C.-Y. Liao, W.-C. Lu, C.-R. Chang, F.-Y. Tsai, S.-S. Jiang, T.-H. Chen, K.M.-C. Lin, L.-T. Chen, and W.-S.W. Chang. 2022. Identification of distinct slow mode of reversible adaptation of pancreatic ductal adenocarcinoma to the prolonged acidic pH microenvironment. *Journal of Experimental & Clinical Cancer Research*. 41:137.

Wykes, M.N., and L. Renia. 2017. ELISPOT Assay to Measure Peptide-specific IFN-γ Production. *Bio Protoc*. 7:e2302.

Xiao, X., P. Huang, and X.-T. Xu. 2025. The choice of adjuvant radiotherapy in pancreatic cancer patients after up-front radical surgery. *PLOS ONE*. 20:e0317995.

Xie, C., J.-J. Ke, and F.-Q. Liu. 2025. Targeted and immunotherapy strategies in pancreatic ductal adenocarcinoma: Recent developments and insights. *Hepatobiliary & Pancreatic Diseases International*.

Xie, D., Q. Pei, J. Li, X. Wan, and T. Ye. 2021. Emerging Role of E2F Family in Cancer Stem Cells. *Frontiers in Oncology*. Volume 11 - 2021.

Xu, C., E. Jun, Y. Okugawa, Y. Toiyama, E. Borazanci, J. Bolton, A. Taketomi, S.C. Kim, D. Shang, D. Von Hoff, G. Zhang, and A. Goel. 2024. A Circulating Panel of circRNA Biomarkers for the Noninvasive and Early Detection of Pancreatic Ductal Adenocarcinoma. *Gastroenterology*. 166:178-190.e116.

Xu, J., Y. Li, Z. Li, W. Shao, J. Song, and J. Wei. 2022. Acidic Tumor Microenvironment Promotes Pancreatic Cancer through miR-451a/MEF2D Axis. *J Oncol*. 2022:3966386.

Yagublu, V., N. Caliskan, A.L. Lewis, R. Jesenofsky, L. Gasimova, J.M. Löhr, and M. Keese. 2013. Treatment of experimental pancreatic cancer by doxorubicin-, mitoxantrone-, and irinotecan-drug eluting beads. *Pancreatology*. 13:79-87.

Yamada, Y. 2020. Dimerization of Doxorubicin Causes Its Precipitation. *ACS Omega*. 5:33235-33241.

Yang, Z., T. Xiao, Z. Li, J. Zhang, and S. Chen. 2022. Novel Chemicals Derived from Tadalafil Exhibit PRMT5 Inhibition and Promising Activities against Breast Cancer. *International Journal of Molecular Sciences*. 23:4806.

Yao, H., L. Luo, R. Li, Y. Zhao, L. Zhang, M. Pešić, L. Cai, and L. Li. 2024. New insight into the role of SMAD4 mutation/deficiency in the prognosis and therapeutic resistance of pancreatic ductal adenocarcinomas. *Biochimica et Biophysica Acta (BBA) - Reviews on Cancer*. 1879:189220.

Yin, L., Y. Lu, C. Cao, Z. Lu, J. Wei, X. Zhu, J. Chen, F. Guo, M. Tu, C. Xi, K. Zhang, J. Wu, W. Gao, K. Jiang, Y. Miao, Q. Li, and Y. Peng. 2022. CA9-Related Acidic Microenvironment Mediates CD8+ T Cell Related Immunosuppression in Pancreatic Cancer. *Frontiers in Oncology*. Volume 11 - 2021.

Yousef, A., M. Yousef, S. Chowdhury, K. Abdilleh, M. Knafl, P. Edelkamp, K. Alfaro-Munoz, R. Chacko, J. Peterson, B.G. Smaglo, R.A. Wolff, S. Pant, M.S. Lee, J. Willis, M. Overman, S. Doss, L. Matrisian, M.W. Hurd, R. Snyder, M.H.G. Katz, H. Wang, A. Maitra, J.P. Shen, and D. Zhao. 2024. Impact of KRAS mutations and co-mutations on clinical outcomes in pancreatic ductal adenocarcinoma. *npj Precision Oncology*. 8:27.

Yuan, J., Y. Guo, and Y. Li. 2024. Diagnosis, treatment, and prognosis of adult pancreatoblastoma. *Cancer Med*. 13:e70132.

Zhang, B., K. Ohuchida, C. Tsutsumi, Y. Shimada, Y. Mochida, K. Oyama, C. Iwamoto, N. Sheng, S. Fei, K. Shindo, N. Ikenaga, K. Nakata, Y. Oda, and M. Nakamura. 2024. Dynamic glycolytic reprogramming effects on dendritic cells in pancreatic ductal adenocarcinoma. *Journal of Experimental & Clinical Cancer Research*. 43:271.

Zhang, W., S. Li, Y. Liu, R. Xing, Z. Jin, X. Yan, and H. Xue. 2023a. Immunosuppressive microenvironment improvement and treatment of aggressive malignancy pancreatic ductal adenocarcinoma based on local administration of injectable hydrogel. *Nano Today*. 50:101832.

Zhang, Z., H. Zhang, X. Liao, and H.-i. Tsai. 2023b. KRAS mutation: The booster of pancreatic ductal adenocarcinoma transformation and progression. *Frontiers in Cell and Developmental Biology*. Volume 11 - 2023.

Zheng, S., J. Moehlenbrink, Y.-C. Lu, L.-P. Zalmas, Cari A. Sagum, S. Carr, Joanna F. McGouran, L. Alexander, O. Fedorov, S. Munro, B. Kessler, Mark T. Bedford, Q. Yu, and Nicholas B. La Thangue. 2013. Arginine Methylation-Dependent Reader-Writer Interplay Governs Growth Control by E2F-1. *Molecular Cell*. 52:37-51.

Zhou, C., C. Yi, Y. Yi, W. Qin, Y. Yan, X. Dong, X. Zhang, Y. Huang, R. Zhang, J. Wei, D.W. Ali, M. Michalak, X.-Z. Chen, and J. Tang. 2020. LncRNA PVT1 promotes gemcitabine resistance of pancreatic cancer via activating Wnt/β-catenin and autophagy pathway through modulating the miR-619-5p/Pygo2 and miR-619-5p/ATG14 axes. *Molecular Cancer*. 19:118.

Zhou, J., W. Wen, Y. Xu, J. Yu, and D. Chen. 2026. Solute Carrier transporters in tumor metabolism and immune modulation: implications for therapy. *Journal of Translational Medicine*. 24:569.

Zhu, Y., B.L. Knolhoff, M.A. Meyer, T.M. Nywening, B.L. West, J. Luo, A. Wang-Gillam, S.P. Goedegebuure, D.C. Linehan, and D.G. DeNardo. 2014. CSF1/CSF1R Blockade Reprograms Tumor-Infiltrating Macrophages and Improves Response to T-cell Checkpoint Immunotherapy in Pancreatic Cancer Models. *Cancer Research*. 74:5057-5069.

Appendix I

List of differentially expressed genes after T1-44 treatment

Green and red squares in the log_2(FC) column represent overexpressed and downregulated genes (cutoff $|log_2FC| > 0.58$) obtained after treating Panc-1 and Panc02 cells with 1.0 μM T1-44 for 48 h, respectively.

- **Panc-1**

GeneID	Gene name	log_2(FC)	Adjusted *p* value
ENSG00000100697.17	DICER1	2.32917056	1.45613E-44
ENSG00000117360.13	PRPF3	2.05381559	9.71461E-17
ENSG00000221978.13	CCNL2	1.89827226	6.4992E-17
ENSG00000186891.14	TNFRSF18	1.67406858	4.33213E-11
ENSG00000179593.16	ALOX15B	1.5851291	1.22083E-18
ENSG00000143924.19	EML4	1.56034067	3.09383E-07
ENSG00000155846.17	PPARGC1B	1.48510181	6.10677E-08
ENSG00000163781.14	TOPBP1	1.46657287	1.47278E-07
ENSG00000253110.1	ENSG00000253110	1.45633199	1.50427E-06
ENSG00000096060.15	FKBP5	1.44683868	1.18853E-27
ENSG00000228559.2	ENSG00000228559	1.43723911	7.36928E-23
ENSG00000264125.1	ENSG00000264125	1.40344858	2.32644E-06
ENSG00000183034.13	OTOP2	1.34485648	7.18418E-06
ENSG00000159899.16	NPR2	1.28715481	6.71041E-13
ENSG00000242199.1	ENSG00000242199	1.23235402	2.30672E-14
ENSG00000160058.19	BSDC1	1.20221009	0.000130313
ENSG00000229522.1	LINC01523	1.20044839	2.37445E-05
ENSG00000289555.1	ENSG00000289555	1.16925175	0.000125228
ENSG00000163156.12	SCNM1	1.15591902	0.000165993
ENSG00000149131.17	SERPING1	1.15219251	4.53498E-05
ENSG00000237423.3	LINC01522	1.11388457	2.08046E-06
ENSG00000272161.1	ENSG00000272161	1.10991906	6.92999E-07
ENSG00000148843.15	PDCD11	1.10839978	0.000332037
ENSG00000234204.1	PIGPP2	1.09201152	2.22681E-06
ENSG00000114491.14	UMPS	1.04944084	1.92044E-31
ENSG00000109814.12	UGDH	1.04454032	6.04505E-05
ENSG00000234088.1	RPS15AP7	1.0336833	4.69322E-11
ENSG00000253457.3	SMIM18	1.03146956	1.15227E-07
ENSG00000266356.1	ENSG00000266356	1.03057471	4.91481E-05
ENSG00000213853.10	EMP2	1.02362078	0.001812809
ENSG00000158292.7	GPR153	1.01032941	0.001185328
ENSG00000139190.17	VAMP1	1.00940753	2.18683E-08
ENSG00000224870.9	MRPL20-AS1	1.00465826	0.002326754
ENSG00000031698.13	SARS1	1.00081777	4.19659E-09
ENSG00000139192.12	TAPBPL	0.99106453	0.001054425

ENSG00000250546.6	LINC02994	0.98907584	6.16834E-23
ENSG00000112739.17	PRPF4B	0.98818859	1.07163E-22
ENSG00000265981.1	MIR544B	0.98793247	4.41768E-12
ENSG00000205500.8	MAPRE3-AS1	0.98639851	0.002900102
ENSG00000125730.18	C3	0.98135237	0.000342001
ENSG00000230912.1	ENSG00000230912	0.97265997	0.003371411
ENSG00000180628.15	PCGF5	0.96958767	4.82699E-14
ENSG00000135916.16	ITM2C	0.96681215	1.19713E-05
ENSG00000136436.15	CALCOCO2	0.95433694	0.003807977
ENSG00000144567.11	RETREG2	0.94608203	0.004230775
ENSG00000198171.13	DDRGK1	0.93609315	0.00273841
ENSG00000277636.1	MIR8061	0.93409929	0.005116844
ENSG00000256350.1	ENSG00000256350	0.9283773	2.0507E-25
ENSG00000085978.22	ATG16L1	0.92709036	1.04975E-11
ENSG00000286493.1	ENSG00000286493	0.9217899	0.000434929
ENSG00000229859.10	PGA3	0.92082413	0.000356361
ENSG00000260236.2	PTPN23-DT	0.92042608	0.006255864
ENSG00000143318.13	CASQ1	0.91727956	0.00048974
ENSG00000290692.1	ENSG00000290692	0.91311344	0.005836358
ENSG00000263206.1	KYNUP3	0.91168835	0.006026349
ENSG00000223912.1	EEF1A1P36	0.9105173	8.12439E-11
ENSG00000149636.16	DSN1	0.9097885	3.77872E-32
ENSG00000120949.15	TNFRSF8	0.90661051	0.006779993
ENSG00000117984.15	CTSD	0.8986974	0.001782076
ENSG00000158578.21	ALAS2	0.88278762	0.009570783
ENSG00000288837.2	ENSG00000288837	0.88268019	0.003499457
ENSG00000204128.6	C2orf72	0.87112471	3.22778E-05
ENSG00000113790.11	EHHADH	0.86943443	6.83287E-05
ENSG00000133131.15	MORC4	0.86778771	8.05814E-05
ENSG00000254172.1	RNU5A-3P	0.86698948	2.417E-08
ENSG00000171522.6	PTGER4	0.85579379	1.54221E-10
ENSG00000163697.17	APBB2	0.85267953	4.73659E-11
ENSG00000176933.5	TOB2P1	0.84954987	0.009994739
ENSG00000099785.11	MARCHF2	0.8490429	1.0332E-12
ENSG00000262154.1	EIF1P4	0.84870077	0.00499939
ENSG00000119535.19	CSF3R	0.84771137	5.45607E-05
ENSG00000258513.1	ENSG00000258513	0.84230639	0.000172145
ENSG00000143570.19	SLC39A1	0.84116417	0.000165485
ENSG00000179751.7	SYCN	0.83906344	5.08863E-06
ENSG00000264115.1	MIR3180-4	0.83184835	0.000105517
ENSG00000013503.10	POLR3B	0.82965717	5.04553E-11
ENSG00000230284.1	ENSG00000230284	0.82949288	4.76072E-07
ENSG00000259482.2	RORA-AS2	0.79941942	0.008486403
ENSG00000268201.1	ENSG00000268201	0.79916958	6.33751E-05
ENSG00000178772.7	CPN2	0.7979562	1.32598E-05
ENSG00000249641.2	HOXC13-AS	0.79359569	0.001673808
ENSG00000163785.13	RYK	0.78376725	5.51426E-15
ENSG00000159210.10	SNF8	0.78319889	5.37582E-12

ENSG00000133226.19	SRRM1	0.78258065	1.10586E-08
ENSG00000276240.3	OR4E1	0.78161037	4.72681E-05
ENSG00000128536.16	CDHR3	0.78110765	0.000195826
ENSG00000226208.1	ENSG00000226208	0.77874882	1.18979E-10
ENSG00000130544.12	ZNF557	0.7764336	2.73052E-07
ENSG00000145526.12	CDH18	0.77474615	0.001674247
ENSG00000023171.20	GRAMD1B	0.77406498	1.22124E-05
ENSG00000139613.12	SMARCC2	0.76924402	1.04236E-07
ENSG00000204514.11	ZNF814	0.76270837	3.77444E-11
ENSG00000143164.16	DCAF6	0.76211037	5.0155E-06
ENSG00000101751.11	POLI	0.76059772	1.5531E-11
ENSG00000139354.11	GAS2L3	0.7585948	2.74477E-06
ENSG00000177721.5	ANXA2R	0.75338368	0.000183434
ENSG00000167721.11	TSR1	0.74973496	1.513E-10
ENSG00000149639.15	SOGA1	0.74808168	5.82598E-18
ENSG00000021826.18	CPS1	0.74559531	6.92076E-05
ENSG00000251637.6	LINC02754	0.74297217	8.42932E-09
ENSG00000263345.1	SGSM2-AS1	0.74058282	0.007616436
ENSG00000201846.1	RNA5SP166	0.74043928	0.005030961
ENSG00000158373.9	H2BC5	0.73707136	1.42888E-10
ENSG00000108262.16	GIT1	0.73476989	0.000142552
ENSG00000278685.4	IQCA1L	0.73348845	0.000939067
ENSG00000226752.10	CUTALP	0.73314314	0.003668794
ENSG00000112763.17	BTN2A1	0.71878893	3.23956E-09
ENSG00000171853.16	TRAPPC12	0.7176135	0.000446654
ENSG00000154485.5	MMP21	0.71406331	3.42316E-06
ENSG00000132359.16	RAP1GAP2	0.71273755	0.003468609
ENSG00000160712.13	IL6R	0.71250634	8.13837E-05
ENSG00000164081.13	TEX264	0.70770382	0.002683053
ENSG00000197265.9	GTF2E2	0.705285	0.001805048
ENSG00000149177.15	PTPRJ	0.69965642	3.06531E-09
ENSG00000260930.2	LINC01416	0.6993805	0.000246832
ENSG00000129744.3	ART1	0.69598873	0.00829559
ENSG00000114993.17	RTKN	0.68670446	5.53716E-09
ENSG00000229051.2	LINC01788	0.68561951	9.36421E-08
ENSG00000181754.7	AMIGO1	0.68337038	0.002484187
ENSG00000247271.9	ZBED5-AS1	0.68230592	0.001123361
ENSG00000116729.14	WLS	0.67819876	9.70981E-08
ENSG00000189195.15	BTBD8	0.6774217	0.002142026
ENSG00000257391.1	ENSG00000257391	0.6725317	4.38185E-10
ENSG00000174485.16	DENND4A	0.67093731	1.87201E-05
ENSG00000198691.14	ABCA4	0.66546825	7.54199E-07
ENSG00000081059.20	TCF7	0.66331083	1.35834E-06
ENSG00000254449.1	SF3A3P2	0.66179254	0.000634715
ENSG00000242259.9	C22orf39	0.66037854	5.37582E-12
ENSG00000150764.14	DIXDC1	0.65757234	3.33551E-06
ENSG00000266472.6	MRPS21	0.65743013	2.62682E-05
ENSG00000163644.15	PPM1K	0.65557001	4.40362E-07

ENSG00000113558.19	SKP1	0.65183849	7.12332E-11
ENSG00000230342.2	FANCD2P2	0.65124147	0.004260992
ENSG00000164744.14	SUN3	0.65074585	0.00896555
ENSG00000184831.14	APOO	0.64856152	0.005383232
ENSG00000166803.14	PCLAF	0.64836291	1.33381E-09
ENSG00000159398.16	CES5A	0.64707537	0.001959493
ENSG00000243022.1	MARK3P3	0.64486993	8.12994E-07
ENSG00000239880.1	RALBP1P1	0.64420052	2.19891E-05
ENSG00000086065.14	CHMP5	0.64350557	4.75595E-07
ENSG00000253376.2	ENSG00000253376	0.64194664	2.79907E-06
ENSG00000233924.1	RPSAP13	0.62952932	0.002753946
ENSG00000119729.12	RHOQ	0.62900131	1.03133E-07
ENSG00000151892.16	GFRA1	0.62624779	1.92685E-09
ENSG00000175061.20	SNHG29	0.62498626	0.000968054
ENSG00000211690.1	TRGJ1	0.62464095	9.85383E-05
ENSG00000168434.13	COG7	0.6230329	6.41337E-06
ENSG00000151665.13	PIGF	0.62205563	3.31129E-12
ENSG00000221933.3	OR2A25	0.62123147	0.000380927
ENSG00000146858.8	ZC3HAV1L	0.61674013	5.07475E-05
ENSG00000082213.18	C5orf22	0.61409461	1.4251E-08
ENSG00000157110.16	RBPMS	0.61270427	0.000529888
ENSG00000124802.12	EEF1E1	0.60966697	0.00475841
ENSG00000274528.1	ENSG00000274528	0.60922391	7.73669E-05
ENSG00000006715.16	VPS41	0.60834511	4.28822E-05
ENSG00000189050.16	RNFT1	0.60015682	0.002353709
ENSG00000137393.10	RNF144B	0.59704444	0.000725956
ENSG00000263624.1	ENSG00000263624	0.59412263	0.000456345
ENSG00000112186.13	CAP2	0.59408733	1.97926E-09
ENSG00000122025.15	FLT3	0.59300157	1.82776E-08
ENSG00000101444.13	AHCY	0.59249949	1.4713E-07
ENSG00000173692.14	PSMD1	0.59068974	0.000744548
ENSG00000287977.1	ENSG00000287977	0.58960618	6.41337E-06
ENSG00000167965.18	MLST8	0.58733225	0.002577814
ENSG00000253872.1	ENSG00000253872	0.58592249	0.006003456
ENSG00000256968.1	SNRPEP2	0.58561978	2.68164E-05
ENSG00000166822.13	TMEM170A	0.58506152	1.15642E-05
ENSG00000107104.21	KANK1	0.58405517	5.38838E-09
ENSG00000234592.1	TJAP1P1	0.58196742	1.34112E-08
ENSG00000104365.16	IKBKB	0.58184464	0.001088885
ENSG00000267327.2	ENSG00000267327	0.58109252	0.003337996
ENSG00000132535.22	DLG4	-0.58100881	6.32638E-10
ENSG00000130822.16	PNCK	-0.58155987	6.78381E-12
ENSG00000131759.18	RARA	-0.58175784	4.82244E-11
ENSG00000252534.1	Y_RNA	-0.58276825	0.006255864
ENSG00000174791.11	RIN1	-0.58296706	4.90001E-07
ENSG00000185924.7	RTN4RL1	-0.58332949	0.001943793
ENSG00000088888.18	MAVS	-0.58431187	3.80069E-07
ENSG00000168056.18	LTBP3	-0.58432448	1.10475E-09

ENSG00000137812.21	KNL1	-0.5853935	1.24672E-07
ENSG00000083720.13	OXCT1	-0.58572733	1.38463E-05
ENSG00000142611.17	PRDM16	-0.58622741	0.004981943
ENSG00000075568.17	TMEM131	-0.58661386	0.001987989
ENSG00000233872.1	TOR1BP1	-0.58931135	2.03052E-06
ENSG00000279136.1	ENSG00000279136	-0.59040487	0.001905793
ENSG00000196531.14	NACA	-0.59065354	0.000364088
ENSG00000165271.17	NOL6	-0.59073369	5.16706E-10
ENSG00000015285.12	WAS	-0.59117759	0.000406463
ENSG00000174996.12	KLC2	-0.59157311	1.42888E-10
ENSG00000204179.11	PTPN20	-0.59158978	0.006350969
ENSG00000160050.16	CCDC28B	-0.59303491	0.000896405
ENSG00000161860.8	SYCE2	-0.59350981	3.87378E-08
ENSG00000110025.13	SNX15	-0.59376315	0.001066499
ENSG00000112659.14	CUL9	-0.59443689	0.007529119
ENSG00000101222.12	SPEF1	-0.59579693	1.94907E-07
ENSG00000089159.17	PXN	-0.59640183	0.002282507
ENSG00000099864.18	PALM	-0.59877318	0.000114388
ENSG00000288531.1	ENSG00000288531	-0.60030964	0.009597627
ENSG00000157823.17	AP3S2	-0.6019155	3.80949E-06
ENSG00000233585.2	ACAA2P1	-0.60433542	6.81278E-06
ENSG00000008710.20	PKD1	-0.60517298	2.11823E-09
ENSG00000128872.10	TMOD2	-0.60536304	0.00315168
ENSG00000186638.17	KIF24	-0.60633093	6.94851E-09
ENSG00000063127.16	SLC6A16	-0.60833667	0.003455561
ENSG00000196262.15	PPIA	-0.60861127	3.65675E-08
ENSG00000104879.5	CKM	-0.60937802	0.000137011
ENSG00000124469.12	CEACAM8	-0.60960168	0.005051911
ENSG00000116251.11	RPL22	-0.60977986	6.22457E-05
ENSG00000187051.9	RPS19BP1	-0.60990854	0.00570519
ENSG00000197272.2	IL27	-0.6100385	0.000652494
ENSG00000105427.10	CNFN	-0.61073808	0.009338071
ENSG00000130702.15	LAMA5	-0.61229197	7.97447E-08
ENSG00000215915.10	ATAD3C	-0.61503385	2.0924E-06
ENSG00000137073.24	UBAP2	-0.61505823	4.71108E-13
ENSG00000170484.10	KRT74	-0.61526486	2.6304E-07
ENSG00000185522.9	LMNTD2	-0.61557851	0.000777607
ENSG00000160051.12	IQCC	-0.61617587	0.009333567
ENSG00000174903.16	RAB1B	-0.61617925	1.76985E-06
ENSG00000166959.8	MS4A8	-0.61646055	1.14254E-05
ENSG00000075240.17	GRAMD4	-0.61708202	0.000366965
ENSG00000124440.16	HIF3A	-0.61793887	2.38632E-05
ENSG00000197785.14	ATAD3A	-0.61831237	0.0001944
ENSG00000182327.8	GLTPD2	-0.62009644	1.18565E-05
ENSG00000206417.8	H1-10-AS1	-0.62016061	1.35154E-08
ENSG00000092470.12	WDR76	-0.62020544	0.00275488
ENSG00000162571.14	TTLL10	-0.6213808	0.00498442
ENSG00000011132.12	APBA3	-0.62138156	7.06322E-06

ENSG00000082458.12	DLG3	-0.62180027	1.02297E-14
ENSG00000131389.18	SLC6A6	-0.62348945	6.34751E-05
ENSG00000134369.16	NAV1	-0.62353785	3.3586E-16
ENSG00000105376.5	ICAM5	-0.62355383	1.10529E-05
ENSG00000164880.16	INTS1	-0.62427374	9.35365E-07
ENSG00000167272.11	POP5	-0.62468614	1.43361E-09
ENSG00000177731.16	FLII	-0.62599421	0.000132353
ENSG00000234371.6	RPSAP31	-0.62720506	4.62579E-07
ENSG00000275484.1	ENSG00000275484	-0.62729872	1.1899E-05
ENSG00000197376.3	ENSG00000197376	-0.6278654	8.81401E-07
ENSG00000167220.12	HDHD2	-0.62901871	5.0586E-06
ENSG00000280402.1	ENSG00000280402	-0.63024615	0.002827129
ENSG00000103342.13	GSPT1	-0.63186225	1.64441E-05
ENSG00000167281.20	RBFOX3	-0.63236313	4.38512E-09
ENSG00000198700.10	IPO9	-0.63309021	1.12767E-05
ENSG00000065989.16	PDE4A	-0.63315962	1.74319E-06
ENSG00000132692.19	BCAN	-0.63330157	2.14373E-06
ENSG00000103510.20	KAT8	-0.63364651	1.01281E-09
ENSG00000172613.8	RAD9A	-0.63373689	2.08005E-10
ENSG00000239576.1	COX6CP14	-0.63553396	0.004867401
ENSG00000149527.18	PLCH2	-0.63565572	0.000175649
ENSG00000146197.9	SCUBE3	-0.63617059	0.000703838
ENSG00000289494.2	ENSG00000289494	-0.63655028	0.000161681
ENSG00000099624.8	ATP5F1D	-0.63758152	2.54879E-10
ENSG00000106635.8	BCL7B	-0.63885179	9.9933E-06
ENSG00000140992.19	PDPK1	-0.63917607	0.000426312
ENSG00000196329.12	GIMAP5	-0.64006888	3.37219E-05
ENSG00000167578.18	RAB4B	-0.64023574	1.57E-06
ENSG00000160870.15	CYP3A7	-0.64035236	0.00023315
ENSG00000130707.18	ASS1	-0.64164368	2.292E-05
ENSG00000089154.11	GCN1	-0.64187579	2.04114E-06
ENSG00000173548.9	SNX33	-0.64296321	1.15247E-05
ENSG00000099331.14	MYO9B	-0.64328688	2.10306E-06
ENSG00000160117.16	ANKLE1	-0.64376202	0.000379371
ENSG00000270747.1	S100A11P9	-0.64470585	5.75988E-05
ENSG00000129451.12	KLK10	-0.64559531	0.000164783
ENSG00000243789.11	JMJD7	-0.64566034	0.003676094
ENSG00000155980.13	KIF5A	-0.64595931	0.009362275
ENSG00000289857.1	ENSG00000289857	-0.65157281	0.003231722
ENSG00000103319.12	EEF2K	-0.65182291	0.004475462
ENSG00000164967.10	RPP25L	-0.65238273	2.22845E-07
ENSG00000176022.7	B3GALT6	-0.65557536	0.006397926
ENSG00000260053.2	ABCB10P4	-0.65611452	0.003532069
ENSG00000227163.2	ENSG00000227163	-0.66225478	2.93796E-06
ENSG00000100299.18	ARSA	-0.66310284	0.002964004
ENSG00000099797.15	TECR	-0.66389196	2.6304E-07
ENSG00000109805.10	NCAPG	-0.66580618	0.000899375
ENSG00000177156.11	TALDO1	-0.66626564	7.46447E-18

ENSG00000010810.18	FYN	-0.66656373	0.000697749
ENSG00000160087.21	UBE2J2	-0.667026	5.60475E-13
ENSG00000100167.21	SEPTIN3	-0.66786683	5.14747E-15
ENSG00000107186.17	MPDZ	-0.66811116	2.3142E-08
ENSG00000185361.9	TNFAIP8L1	-0.66859934	2.78881E-06
ENSG00000187741.16	FANCA	-0.66953985	1.03814E-08
ENSG00000065268.11	WDR18	-0.6697567	9.6354E-11
ENSG00000279080.1	ENSG00000279080	-0.67023714	8.2347E-06
ENSG00000242137.1	RPL11P5	-0.67317142	1.15085E-05
ENSG00000161640.15	SIGLEC11	-0.67351519	0.00250035
ENSG00000089486.17	CDIP1	-0.67406251	7.10478E-11
ENSG00000161328.11	LRRC56	-0.67686634	0.000344185
ENSG00000153898.13	MCOLN2	-0.67919656	9.74297E-07
ENSG00000099821.14	POLRMT	-0.68095591	6.66732E-12
ENSG00000278133.1	ENSG00000278133	-0.68107272	1.03736E-08
ENSG00000114062.22	UBE3A	-0.68236429	5.04653E-08
ENSG00000135094.11	SDS	-0.68256338	0.000253364
ENSG00000275052.5	PPP4R3B	-0.68363718	0.002214512
ENSG00000103145.11	HCFC1R1	-0.68983592	3.36272E-14
ENSG00000103260.9	METRN	-0.69028404	8.84901E-08
ENSG00000289689.1	ENSG00000289689	-0.69049859	6.15146E-06
ENSG00000237738.1	RNF216-IT1	-0.6912578	1.45773E-05
ENSG00000066056.14	TIE1	-0.69140405	8.99193E-07
ENSG00000168874.13	ATOH8	-0.6927319	4.74056E-11
ENSG00000177732.9	SOX12	-0.69335715	7.90214E-07
ENSG00000127948.17	POR	-0.69437796	6.22457E-05
ENSG00000243710.8	CFAP57	-0.69506051	7.42208E-05
ENSG00000090554.13	FLT3LG	-0.69665952	4.828E-05
ENSG00000188176.12	SMTNL2	-0.69745845	0.000418701
ENSG00000119559.17	C19orf25	-0.70159643	1.75982E-09
ENSG00000011007.13	ELOA	-0.70210737	4.98909E-05
ENSG00000166825.15	ANPEP	-0.70335832	3.11717E-08
ENSG00000131398.15	KCNC3	-0.70412889	1.22346E-05
ENSG00000184007.22	PTP4A2	-0.70485579	0.003715368
ENSG00000229976.2	ENSG00000229976	-0.70563113	4.828E-05
ENSG00000122756.15	CNTFR	-0.71173558	0.004910538
ENSG00000214063.12	TSPAN4	-0.71186043	3.31569E-14
ENSG00000184908.20	CLCNKB	-0.71188735	2.54991E-11
ENSG00000289560.2	ENSG00000289560	-0.71455529	0.000110187
ENSG00000123472.13	ATPAF1	-0.71543821	0.004285055
ENSG00000242485.6	MRPL20	-0.7162488	2.04114E-06
ENSG00000157570.12	TSPAN18	-0.71664726	0.00963277
ENSG00000170486.11	KRT72	-0.71751413	3.70483E-06
ENSG00000141959.17	PFKL	-0.71786405	0.000556205
ENSG00000185519.9	FAM131C	-0.71798927	7.81887E-05
ENSG00000102221.14	JADE3	-0.71940638	2.80374E-16
ENSG00000188706.13	ZDHHC9	-0.72159489	0.003143013
ENSG00000116871.16	MAP7D1	-0.72185279	1.07387E-09

ENSG00000230404.1	ENSG00000230404	-0.72818413	0.000291692
ENSG00000172890.13	NADSYN1	-0.72869072	0.005999575
ENSG00000151914.22	DST	-0.72927358	0.00373217
ENSG00000008300.17	CELSR3	-0.73125038	1.64398E-20
ENSG00000163257.11	DCAF16	-0.73126677	3.25897E-07
ENSG00000115255.12	REEP6	-0.73233484	6.85576E-06
ENSG00000168397.17	ATG4B	-0.73291396	2.23863E-16
ENSG00000103254.10	ANTKMT	-0.73394202	1.18979E-10
ENSG00000126522.17	ASL	-0.734211	0.004409869
ENSG00000137038.8	DMAC1	-0.73502766	1.66858E-06
ENSG00000167216.19	KATNAL2	-0.73619118	1.32598E-05
ENSG00000100726.15	TELO2	-0.73737803	4.60245E-15
ENSG00000287934.1	ENSG00000287934	-0.73859388	0.000148451
ENSG00000017483.16	SLC38A5	-0.73956601	1.2227E-08
ENSG00000254004.7	ZNF260	-0.74037392	9.69058E-05
ENSG00000233603.1	JTBP1	-0.7422358	0.002276998
ENSG00000284678.1	LINC02811	-0.74279793	0.008245286
ENSG00000235421.1	ENSG00000235421	-0.74339086	8.2514E-05
ENSG00000107130.10	NCS1	-0.74486971	0.000223185
ENSG00000168393.13	DTYMK	-0.74549957	3.0785E-09
ENSG00000255468.7	B4GAT1-DT	-0.75044836	0.000754252
ENSG00000183044.12	ABAT	-0.75116628	8.32956E-08
ENSG00000254454.2	RCC2P6	-0.75385325	1.80972E-07
ENSG00000185955.5	SPACDR	-0.75746094	1.07661E-05
ENSG00000160075.12	SSU72	-0.7596627	1.24108E-06
ENSG00000289731.1	FAM153B	-0.76022232	3.41668E-10
ENSG00000198326.10	TMEM239	-0.76171227	1.4713E-07
ENSG00000272341.1	ENSG00000272341	-0.76209048	0.009362275
ENSG00000130720.13	FIBCD1	-0.7624145	2.2901E-08
ENSG00000160305.18	DIP2A	-0.76300688	0.007970058
ENSG00000181404.18	WASHC1	-0.76451721	3.49807E-08
ENSG00000115694.15	STK25	-0.76568936	9.67983E-10
ENSG00000010256.11	UQCRC1	-0.76639322	0.007589674
ENSG00000284719.3	ENSG00000284719	-0.76645818	0.000109564
ENSG00000177337.10	DLGAP1-AS1	-0.76651797	0.000383421
ENSG00000279243.3	LINC02736	-0.76774248	1.22103E-12
ENSG00000272405.1	ENSG00000272405	-0.76836748	3.47566E-16
ENSG00000230368.2	FAM41C	-0.76985531	0.003858771
ENSG00000157933.11	SKI	-0.77042547	0.00275488
ENSG00000125734.16	GPR108	-0.77085965	2.79249E-12
ENSG00000198400.14	NTRK1	-0.77193339	0.000722072
ENSG00000133313.15	CNDP2	-0.77254181	0.001634503
ENSG00000068745.15	IP6K2	-0.77393388	1.64104E-07
ENSG00000137161.18	CNPY3	-0.77466588	2.50745E-06
ENSG00000265927.1	ENSG00000265927	-0.77507976	0.005132996
ENSG00000187535.14	IFT140	-0.77715105	5.37582E-12
ENSG00000287356.1	ENSG00000287356	-0.7776787	0.000439991
ENSG00000246851.1	ENSG00000246851	-0.7785952	0.002541624

ENSG00000078687.18	TNRC6C	-0.78087968	1.68354E-05
ENSG00000166908.18	PIP4K2C	-0.78287647	0.005263899
ENSG00000251322.11	SHANK3	-0.78346284	4.69198E-18
ENSG00000151176.8	PLBD2	-0.786504	0.000502992
ENSG00000160803.8	UBQLN4	-0.78660082	3.83445E-06
ENSG00000277363.5	SRCIN1	-0.78757814	1.27679E-23
ENSG00000157827.20	FMNL2	-0.78767056	0.00275488
ENSG00000137135.18	ARHGEF39	-0.79023962	5.13631E-13
ENSG00000025434.19	NR1H3	-0.79372233	3.60002E-12
ENSG00000177352.10	CCDC71	-0.79420267	7.27393E-05
ENSG00000067842.19	ATP2B3	-0.79555331	5.32483E-23
ENSG00000135114.14	OASL	-0.7956862	7.44919E-07
ENSG00000266578.2	ENSG00000266578	-0.79642504	9.13093E-05
ENSG00000255410.2	ENSG00000255410	-0.79655025	4.37625E-16
ENSG00000187147.18	RNF220	-0.79662537	0.000555851
ENSG00000229953.1	BCAN-AS2	-0.80186383	1.28402E-07
ENSG00000177963.15	RIC8A	-0.80501422	3.98859E-24
ENSG00000176383.9	B3GNT4	-0.80882734	0.001335574
ENSG00000160055.20	TMEM234	-0.8090964	0.004106891
ENSG00000131652.14	THOC6	-0.81063992	2.9328E-10
ENSG00000154930.15	ACSS1	-0.81124993	0.003124337
ENSG00000184697.7	CLDN6	-0.81359017	0.00047313
ENSG00000168395.16	ING5	-0.81383029	1.79074E-10
ENSG00000286931.3	ENSG00000286931	-0.81456783	0.000105453
ENSG00000165338.17	HECTD2	-0.81642524	1.26724E-09
ENSG00000162069.16	BICDL2	-0.8172017	2.6304E-07
ENSG00000291299.2	ENSG00000291299	-0.81800065	2.2485E-07
ENSG00000279980.1	GABARAPL3	-0.81836151	6.21613E-20
ENSG00000112658.8	SRF	-0.81956922	1.03722E-06
ENSG00000178233.18	TMEM151B	-0.82028284	0.000100585
ENSG00000101057.16	MYBL2	-0.82587309	2.25138E-06
ENSG00000120063.10	GNA13	-0.83050712	4.90919E-10
ENSG00000280381.1	ENSG00000280381	-0.83165004	5.24973E-07
ENSG00000262075.3	DKFZP434A062	-0.8351157	0.001124643
ENSG00000258115.1	ENSG00000258115	-0.83533711	0.004171604
ENSG00000143816.8	WNT9A	-0.83661221	2.07893E-12
ENSG00000132635.17	PCED1A	-0.83824741	1.55018E-05
ENSG00000272068.1	BCAN-AS1	-0.84002626	1.57167E-25
ENSG00000052344.16	PRSS8	-0.84149339	6.17158E-07
ENSG00000180900.20	SCRIB	-0.84207452	2.54583E-06
ENSG00000231924.10	PSG1	-0.84514284	0.000105517
ENSG00000166897.16	ELFN2	-0.84944494	1.89141E-08
ENSG00000239552.2	HOXB-AS2	-0.85161974	1.74268E-09
ENSG00000107566.14	ERLIN1	-0.8534007	1.34017E-09
ENSG00000070371.16	CLTCL1	-0.85372729	1.62416E-05
ENSG00000136634.7	IL10	-0.85428582	2.30672E-14
ENSG00000004534.15	RBM6	-0.85460575	6.57796E-05
ENSG00000159720.13	ATP6V0D1	-0.85508075	0.000195826

ENSG00000125877.13	ITPA	-0.86002518	1.42576E-08
ENSG00000072818.12	ACAP1	-0.86072793	3.63491E-10
ENSG00000221990.5	EXOC3-AS1	-0.86143772	0.002719324
ENSG00000163001.12	CFAP36	-0.86222439	3.5795E-08
ENSG00000268041.3	ERFL	-0.86334648	3.52485E-05
ENSG00000267922.1	ENSG00000267922	-0.86587756	0.000652904
ENSG00000215187.13	FAM166B	-0.8672503	0.007335309
ENSG00000271781.1	ENSG00000271781	-0.86892887	0.004813203
ENSG00000151348.16	EXT2	-0.86901516	0.001397961
ENSG00000068078.20	FGFR3	-0.87120201	0.000454781
ENSG00000138035.15	PNPT1	-0.87210107	2.35666E-05
ENSG00000054938.17	CHRDL2	-0.87381795	3.1339E-09
ENSG00000232771.2	PPP1R26P5	-0.87658205	1.12423E-06
ENSG00000063180.9	CA11	-0.87738992	0.000345491
ENSG00000006327.14	TNFRSF12A	-0.87799519	6.4992E-17
ENSG00000112877.8	CEP72	-0.88000859	8.97288E-08
ENSG00000138175.9	ARL3	-0.88120243	1.33336E-07
ENSG00000229931.3	ATXN1-AS1	-0.88134572	0.000955044
ENSG00000118640.11	VAMP8	-0.8830547	1.54302E-06
ENSG00000086967.10	MYBPC2	-0.88381605	5.50276E-23
ENSG00000173540.14	GMPPB	-0.88407758	1.06227E-14
ENSG00000167920.12	KRT10-AS1	-0.88615389	6.27454E-05
ENSG00000131165.16	CHMP1A	-0.89027004	5.00075E-07
ENSG00000184916.9	JAG2	-0.89249554	7.63853E-16
ENSG00000105705.16	SUGP1	-0.89471281	1.32563E-14
ENSG00000132507.18	EIF5A	-0.89519892	1.07373E-09
ENSG00000146221.10	TCTE1	-0.89560105	0.000141263
ENSG00000166986.15	MARS1	-0.89743361	7.42708E-18
ENSG00000262919.8	CCNQ	-0.89898026	1.61386E-19
ENSG00000225911.1	ENSG00000225911	-0.90534961	2.02587E-06
ENSG00000095917.14	TPSD1	-0.90764697	5.75055E-06
ENSG00000101181.18	MTG2	-0.90766276	2.62644E-10
ENSG00000167771.6	RCOR2	-0.91226175	0.001156294
ENSG00000182272.12	B4GALNT4	-0.91301469	1.28699E-13
ENSG00000265902.1	MIR4696	-0.91355124	8.53989E-07
ENSG00000105255.11	FSD1	-0.91515816	4.50081E-10
ENSG00000161643.13	SIGLEC16	-0.92071618	1.63453E-07
ENSG00000171443.7	ZNF524	-0.93490943	2.46395E-17
ENSG00000110955.9	ATP5F1B	-0.93631959	2.09685E-14
ENSG00000288730.1	ENSG00000288730	-0.93865255	3.27982E-06
ENSG00000291039.1	ENSG00000291039	-0.93954364	0.00298473
ENSG00000130829.18	DUSP9	-0.94220467	3.07532E-19
ENSG00000145214.14	DGKQ	-0.94386397	9.9933E-06
ENSG00000112033.14	PPARD	-0.94678196	1.18954E-06
ENSG00000291133.1	ENSG00000291133	-0.9516803	0.00248476
ENSG00000228709.3	LINC02575	-0.9521182	7.29691E-13
ENSG00000197847.12	SLC22A20P	-0.95540914	2.56335E-12
ENSG00000177225.17	GATD1	-0.96228345	3.62766E-30

ENSG00000269504.3	ENSG00000269504	-0.96412931	6.55666E-05
ENSG00000233527.10	ZNF529-AS1	-0.96446388	3.32287E-15
ENSG00000183397.6	TEKTIP1	-0.96615362	0.001152376
ENSG00000170689.10	HOXB9	-0.97065496	1.62539E-13
ENSG00000102898.13	NUTF2	-0.97074941	0.00023316
ENSG00000179950.15	PUF60	-0.97296857	4.6637E-19
ENSG00000186174.13	BCL9L	-0.97332849	1.27374E-21
ENSG00000121774.18	KHDRBS1	-0.97577994	0.001930566
ENSG00000290756.1	ENSG00000290756	-0.97603036	2.02397E-09
ENSG00000261221.4	ZNF865	-0.97775679	9.09971E-14
ENSG00000291147.1	ENSG00000291147	-0.97838352	1.01281E-09
ENSG00000014257.17	ACP3	-0.98808071	2.96369E-05
ENSG00000203362.2	POLH-AS1	-0.99172444	9.40908E-08
ENSG00000205116.4	TMEM88B	-0.99382136	8.32956E-08
ENSG00000175115.13	PACS1	-0.99447033	9.06065E-12
ENSG00000226777.9	FAM30A	-1.00344817	1.07937E-19
ENSG00000197838.5	CYP2A13	-1.00486829	5.31903E-10
ENSG00000267197.1	ENSG00000267197	-1.00879719	3.73584E-05
ENSG00000235098.9	ANKRD65	-1.0095128	7.4935E-16
ENSG00000179094.16	PER1	-1.01665234	3.80069E-07
ENSG00000116014.10	KISS1R	-1.01677319	0.001044309
ENSG00000162341.18	TPCN2	-1.0180378	3.64492E-11
ENSG00000075702.19	WDR62	-1.01866307	0.000657726
ENSG00000198858.10	R3HDM4	-1.02025701	3.64704E-23
ENSG00000165478.8	HEPACAM	-1.02144065	0.001930566
ENSG00000137692.12	DCUN1D5	-1.02348677	0.000652494
ENSG00000224387.1	ENSG00000224387	-1.02421496	0.000239487
ENSG00000130005.13	GAMT	-1.02447945	1.15547E-21
ENSG00000225285.1	LINC01770	-1.02526453	5.97051E-08
ENSG00000101868.13	POLA1	-1.02601176	3.42316E-06
ENSG00000288901.1	ENSG00000288901	-1.02829034	7.88975E-09
ENSG00000177106.17	EPS8L2	-1.02872143	8.03983E-22
ENSG00000260460.1	ENSG00000260460	-1.02936736	4.56675E-07
ENSG00000185507.21	IRF7	-1.03340141	2.05212E-15
ENSG00000254533.1	ENSG00000254533	-1.03569105	4.35967E-14
ENSG00000204991.11	SPIRE2	-1.03636743	5.81785E-09
ENSG00000269392.1	ENSG00000269392	-1.04066818	0.000342001
ENSG00000186020.13	ZNF529	-1.04267486	9.01887E-17
ENSG00000163354.15	DCST2	-1.04813761	1.83831E-23
ENSG00000152056.18	AP1S3	-1.0482832	1.13881E-05
ENSG00000263574.2	ENSG00000263574	-1.05259654	8.81401E-07
ENSG00000157992.12	KRTCAP3	-1.05549731	1.95306E-05
ENSG00000130988.13	RGN	-1.06471835	2.59728E-22
ENSG00000278803.3	PWWP4	-1.06965912	2.6021E-47
ENSG00000105258.9	POLR2I	-1.0719425	8.54383E-07
ENSG00000188981.11	MSANTD1	-1.07328275	7.04113E-05
ENSG00000164068.16	RNF123	-1.07333726	1.66434E-37
ENSG00000197446.9	CYP2F1	-1.07345974	1.40967E-08

ENSG00000164053.22	ATRIP	-1.07407412	6.48774E-09
ENSG00000185818.8	NAT8L	-1.07594384	7.10161E-19
ENSG00000140044.13	JDP2	-1.07671921	5.07311E-22
ENSG00000105193.9	RPS16	-1.07701372	1.43885E-51
ENSG00000262343.1	ENSG00000262343	-1.08355238	8.14754E-12
ENSG00000260182.1	ENSG00000260182	-1.08999517	1.46937E-05
ENSG00000235267.1	ENSG00000235267	-1.09311047	6.71505E-11
ENSG00000289452.1	ENSG00000289452	-1.09882786	3.6516E-06
ENSG00000130821.17	SLC6A8	-1.1004819	1.98588E-21
ENSG00000262370.7	ENSG00000262370	-1.10441401	1.14344E-18
ENSG00000234200.2	ENSG00000234200	-1.10719307	4.02161E-05
ENSG00000188760.11	TMEM198	-1.11104477	3.36124E-06
ENSG00000092054.13	MYH7	-1.11150433	1.31809E-19
ENSG00000269404.7	SPIB	-1.12215322	3.78276E-10
ENSG00000127578.7	WFIKKN1	-1.12690622	1.04252E-17
ENSG00000063176.16	SPHK2	-1.12901309	1.33381E-09
ENSG00000103335.22	PIEZO1	-1.13448312	1.00931E-29
ENSG00000285873.1	ENSG00000285873	-1.14370124	1.05151E-16
ENSG00000138002.16	IFT172	-1.15085071	9.79584E-40
ENSG00000243581.1	RPS29P25	-1.15167173	4.96814E-07
ENSG00000139641.13	ESYT1	-1.15253669	2.92955E-23
ENSG00000110448.11	CD5	-1.15487591	1.27941E-18
ENSG00000179148.10	ALOXE3	-1.17594458	4.25696E-32
ENSG00000124006.15	OBSL1	-1.17920427	3.02676E-15
ENSG00000063177.13	RPL18	-1.18074812	4.92821E-07
ENSG00000184207.9	PGP	-1.18171057	1.6244E-11
ENSG00000108691.10	CCL2	-1.18230964	1.01392E-05
ENSG00000260121.1	ENSG00000260121	-1.18474329	1.76241E-10
ENSG00000119973.6	PRLHR	-1.18667574	1.48042E-08
ENSG00000244253.1	RPS29P24	-1.18815358	1.48259E-05
ENSG00000136731.13	UGGT1	-1.1944255	1.38353E-09
ENSG00000075711.21	DLG1	-1.19838447	2.98198E-06
ENSG00000104953.20	TLE6	-1.20175183	1.18207E-05
ENSG00000141293.16	SKAP1	-1.21002001	1.52841E-26
ENSG00000224888.4	ENSG00000224888	-1.21330232	4.03593E-06
ENSG00000142233.14	NTN5	-1.21616606	4.82244E-11
ENSG00000167967.16	E4F1	-1.21866383	3.55137E-18
ENSG00000167513.9	CDT1	-1.21976746	1.37559E-13
ENSG00000105516.11	DBP	-1.22480825	8.67735E-12
ENSG00000174915.12	PTDSS2	-1.22750012	7.28963E-46
ENSG00000179855.9	GIPC3	-1.24022988	4.18723E-08
ENSG00000225697.13	SLC26A6	-1.25065763	2.96531E-05
ENSG00000228794.12	LINC01128	-1.27892612	2.9169E-18
ENSG00000185101.13	ANO9	-1.28659104	3.31129E-12
ENSG00000167749.12	KLK4	-1.29960452	1.22021E-14
ENSG00000258657.5	ENSG00000258657	-1.3020046	1.57167E-25
ENSG00000131634.14	TMEM204	-1.30574918	4.2655E-12
ENSG00000221739.1	MIR1203	-1.30633613	1.7975E-36

ENSG00000188976.11	NOC2L	-1.3216986	4.44114E-14
ENSG00000168936.11	TMEM129	-1.32212825	4.16694E-21
ENSG00000203325.3	ENSG00000203325	-1.34631479	3.48643E-07
ENSG00000131471.7	AOC3	-1.3495013	6.51877E-11
ENSG00000198681.7	MAGEA1	-1.36606512	1.9869E-20
ENSG00000239701.1	ENSG00000239701	-1.37728954	2.7688E-16
ENSG00000198517.10	MAFK	-1.40767672	3.29956E-32
ENSG00000187642.10	PERM1	-1.42764834	3.38852E-29
ENSG00000064687.13	ABCA7	-1.45589644	1.62431E-30
ENSG00000164855.16	TMEM184A	-1.45852896	9.34314E-14
ENSG00000086015.23	MAST2	-1.46676864	3.78914E-61
ENSG00000091536.20	MYO15A	-1.47504493	1.11265E-61
ENSG00000142102.16	PGGHG	-1.53942029	5.74351E-33
ENSG00000263571.3	ENSG00000263571	-1.56814882	1.6323E-63
ENSG00000264791.1	ENSG00000264791	-1.56966299	1.6232E-56
ENSG00000124702.19	KLHDC3	-1.68630381	4.13428E-37
ENSG00000112640.16	PPP2R5D	-1.69439364	1.13094E-44
ENSG00000124733.5	MEA1	-1.71286619	7.00839E-24
ENSG00000261156.6	LINC01989	-1.77431043	1.16454E-41

- **Panc02**

GeneID	Gene name	$\log_2$(FC)	Adjusted *p* value
ENSMUSG00000020890.12	Gucy2e	2.17881837	1.63593E-49
ENSMUSG00000087147.2	Gm14228	2.03640463	3.18468E-51
ENSMUSG00000028763.19	Hspg2	2.00174036	3.91438E-67
ENSMUSG00000094035.4	Ldlrad2	1.91412394	1.16532E-35
ENSMUSG00000111250.2	Gm47818	1.86543475	2.718E-105
ENSMUSG00000082456.2	Gm11598	1.76435063	2.13813E-23
ENSMUSG00000101451.2	Gm29430	1.60245787	4.956E-23
ENSMUSG00000024220.15	Zfp523	1.59713396	3.4325E-134
ENSMUSG00002075611.1	Gm56344	1.50030029	1.33567E-39
ENSMUSG00000043432.8	Leng9	1.41268491	4.4576E-49
ENSMUSG00000006057.16	Atp5g1	1.39403551	5.56301E-11
ENSMUSG00000032059.14	Alg9	1.35066093	1.13326E-39
ENSMUSG00000057133.15	Chd6	1.34200476	6.58105E-10
ENSMUSG00000035778.18	Ggta1	1.31743104	2.61216E-79
ENSMUSG00000030064.17	Frmd4b	1.31689349	1.04992E-06
ENSMUSG00000112545.3	1300014J16Rik	1.30806972	1.08382E-08
ENSMUSG00000021400.9	Wrnip1	1.23840191	3.40649E-13
ENSMUSG00000086539.9	Gm16759	1.21907622	1.18056E-17
ENSMUSG00000023064.5	Sncg	1.20967564	2.49069E-13
ENSMUSG00000017697.4	Ada	1.20915508	1.20386E-06
ENSMUSG00000033295.15	Ptprf	1.19907458	1.69885E-12
ENSMUSG00000036986.17	Pml	1.19419863	1.30761E-12
ENSMUSG00000055730.17	Ces2a	1.19071729	7.69635E-06

ENSMUSG00000020299.7	4930524B15Rik	1.15661267	2.33861E-05
ENSMUSG00000014039.19	Prdm15	1.14472556	7.18817E-06
ENSMUSG00000066368.2	Actl11	1.13739862	2.90623E-05
ENSMUSG00000022892.12	App	1.1362342	4.0688E-12
ENSMUSG00000118367.2	Gm50277	1.10288776	3.59641E-11
ENSMUSG00000050538.9	B230217C12Rik	1.1023088	6.77943E-05
ENSMUSG00000106108.2	Gm43221	1.09823376	1.11596E-23
ENSMUSG00000040339.11	Fam102b	1.09678492	1.07137E-22
ENSMUSG00000100151.2	Gm28382	1.08494515	1.4574E-46
ENSMUSG00000042406.9	Atf4	1.06361997	9.7943E-05
ENSMUSG00000041684.12	Bivm	1.04729106	2.52232E-15
ENSMUSG00000101958.2	Gm19085	1.0449563	9.20876E-09
ENSMUSG00000071001.5	Hrct1	1.03465913	0.00014184
ENSMUSG00000111545.2	Gm18015	1.02527584	0.000246587
ENSMUSG00000026414.14	Tnnt2	1.02518839	4.41611E-67
ENSMUSG00000026536.10	Ifi211	1.02420928	0.000199126
ENSMUSG00000031085.17	Acte1	1.02238563	1.35409E-07
ENSMUSG00000047767.18	Atg16l2	1.01743245	5.01947E-06
ENSMUSG00000106447.2	Gm42957	1.01630023	0.000213949
ENSMUSG00000090210.8	Itga10	1.00854377	4.12741E-06
ENSMUSG00000052417.7	Or2t6	1.00772392	0.00030453
ENSMUSG00000110110.2	Gm30978	1.00401523	3.23587E-05
ENSMUSG00000058743.7	Kcnj14	1.00090278	1.30103E-40
ENSMUSG00000051314.12	Ffar2	0.9971333	0.000324918
ENSMUSG00000039126.11	Prune2	0.99319015	3.08115E-06
ENSMUSG00000051048.18	P4ha3	0.99267484	2.06657E-05
ENSMUSG00000039860.20	Srrm3	0.98630896	0.000453538
ENSMUSG00000026843.16	Fubp3	0.98260012	2.73682E-07
ENSMUSG00000049588.14	Ccdc69	0.97984528	3.6168E-10
ENSMUSG00000004789.11	Dlst	0.97836607	1.55893E-05
ENSMUSG00000025878.17	Uimc1	0.97834943	8.67023E-05
ENSMUSG00000043286.13	Pnpla1	0.97722858	4.00329E-56
ENSMUSG00000059013.13	Sh2d3c	0.97665471	7.76196E-43
ENSMUSG00000018659.13	Pnpo	0.96978033	0.000476723
ENSMUSG00000062169.14	Cnih4	0.96416854	2.0615E-65
ENSMUSG00000038677.15	Scube3	0.96288928	0.000480318
ENSMUSG00000003575.14	Crtc1	0.96249802	4.57186E-13
ENSMUSG00000024646.15	Cyb5a	0.95836025	6.99994E-28
ENSMUSG00000025576.18	Rbfox3	0.95754149	5.31706E-25
ENSMUSG00000095174.3	Gm20069	0.95379094	8.92987E-05
ENSMUSG00000086798.2	Gm16222	0.94896136	0.000308696
ENSMUSG00000030341.18	Tnfrsf1a	0.93753681	0.000885912
ENSMUSG00000084257.2	Gm11597	0.93294629	2.61709E-10
ENSMUSG00000028106.14	Rprd2	0.93184789	2.62181E-06
ENSMUSG00000032041.16	Tirap	0.92162453	1.56843E-08
ENSMUSG00000081423.2	Gm12882	0.90702488	1.38513E-16
ENSMUSG00000038733.15	Wdr26	0.89920361	7.69828E-30
ENSMUSG00000035262.6	Amh	0.89906629	5.00785E-23

ENSMUSG00000116141.2	Gm49495	0.89491622	2.99337E-09
ENSMUSG00000026353.10	Ubxn4	0.89438327	0.001789438
ENSMUSG00000029681.13	Bcl7b	0.88745082	0.000986864
ENSMUSG00000017631.20	Abr	0.88446334	0.000219255
ENSMUSG00000028884.15	Rpa2	0.88161946	2.28392E-10
ENSMUSG00000028759.14	Hp1bp3	0.87608626	1.33181E-10
ENSMUSG00000070644.14	Etnk2	0.87236425	6.27852E-16
ENSMUSG00000060615.6	Ang4	0.86910476	0.001339873
ENSMUSG00000120747.1	ENSMUSG00000120747	0.86194987	0.002746662
ENSMUSG00000024039.16	Cbs	0.8609707	1.46216E-13
ENSMUSG00000005625.16	Psmd4	0.86026237	1.59645E-06
ENSMUSG00000096856.8	Gm10778	0.8575013	0.001749604
ENSMUSG00000022032.15	Scara5	0.85626477	3.79727E-22
ENSMUSG00000051518.9	Rps19bp1	0.85454478	7.00807E-05
ENSMUSG00000018581.16	Dnah11	0.85284149	3.63525E-25
ENSMUSG00000020216.14	Jsrp1	0.85227499	3.49897E-17
ENSMUSG00000111316.2	Gm47344	0.8490945	0.002317296
ENSMUSG00000082097.2	Gm14039	0.844429	0.001126928
ENSMUSG00000089829.3	Gm16565	0.84257414	0.001339873
ENSMUSG00000062712.4	Or2j6	0.84177057	0.002277939
ENSMUSG00000026271.16	Gpr35	0.83920938	4.25181E-10
ENSMUSG00000002076.13	Hsf2bp	0.83767346	0.000128307
ENSMUSG00000109251.2	E230032D23Rik	0.83615768	0.001878758
ENSMUSG00000103099.2	Gm6074	0.83574889	0.002403026
ENSMUSG00000115545.2	Gm48908	0.83505339	0.000562631
ENSMUSG00000029763.18	Exoc4	0.83081949	8.5418E-14
ENSMUSG00000116560.2	Gm2808	0.83077634	2.87303E-31
ENSMUSG00000108697.2	4930486N12Rik	0.82944601	1.58055E-06
ENSMUSG00000110529.2	Gm45694	0.82912003	8.98175E-14
ENSMUSG00000113635.2	Gm48816	0.82570749	0.004183609
ENSMUSG00000024128.14	Sbp	0.82422188	2.32388E-08
ENSMUSG00000113634.2	Gm36756	0.82353023	0.003084424
ENSMUSG00000070645.6	Ren1	0.8207422	1.26443E-07
ENSMUSG00000074892.10	B3galt5	0.82019649	0.000391685
ENSMUSG00000107341.2	1700065J11Rik	0.81846817	0.004915949
ENSMUSG00000120409.1	ENSMUSG00000120409	0.81359482	0.005229232
ENSMUSG00000031090.15	Nadsyn1	0.81198207	0.001295852
ENSMUSG00000051550.11	Zfp579	0.81061822	0.000602839
ENSMUSG00000038600.13	Atp6v0a4	0.80093766	0.005544021
ENSMUSG00000034413.15	Neurl1b	0.80088032	4.91763E-05
ENSMUSG00000110656.2	Gm20735	0.79903314	0.005954754
ENSMUSG00000005251.16	Ripk4	0.79900617	0.0054509
ENSMUSG00000033253.19	Szt2	0.79876132	1.79637E-18
ENSMUSG00000021486.8	Prelid1	0.7931347	1.67029E-05
ENSMUSG00000026700.5	Tnfsf4	0.79185894	0.005873899
ENSMUSG00000110017.2	Gm45237	0.79102156	0.005866575
ENSMUSG00000033799.11	Tasor2	0.78958034	0.00076867
ENSMUSG00000099241.3	Gvin-ps2	0.78104947	3.17911E-06

ENSMUSG00000024212.10	Mllt1	0.78103239	0.005971618
ENSMUSG00000022884.17	Eif4a2	0.77658568	1.75892E-05
ENSMUSG00000044951.18	Mylk4	0.77423403	0.007680677
ENSMUSG00000028211.12	Trp53inp1	0.76599525	1.93122E-23
ENSMUSG00002076631.1	Gm54824	0.76595695	0.001850227
ENSMUSG00000037254.19	Itih2	0.76368349	0.005018298
ENSMUSG00000039804.16	Ncoa5	0.75861673	3.51278E-17
ENSMUSG00000062203.16	Gspt1	0.75649509	0.008857611
ENSMUSG00000022037.16	Clu	0.75557324	4.33889E-06
ENSMUSG00000106262.2	Gm43375	0.75357387	3.76198E-11
ENSMUSG00000032294.18	Pkm	0.75170705	1.93044E-10
ENSMUSG00000042613.10	Pbxip1	0.75097133	3.92695E-12
ENSMUSG00000039771.14	Polr2j	0.74637217	7.62392E-06
ENSMUSG00000115231.2	4930402D18Rik	0.74386015	0.000476723
ENSMUSG00000025872.6	Thoc3	0.74361342	4.49308E-19
ENSMUSG00000010751.16	Tnfrsf22	0.74331813	0.003575085
ENSMUSG00000020868.16	Xylt2	0.74235701	3.10363E-07
ENSMUSG00000047415.13	Gpr68	0.73703475	8.60223E-14
ENSMUSG00000003992.16	Ssbp2	0.73465022	8.69263E-08
ENSMUSG00000037846.19	Rtkn2	0.72985431	7.27904E-05
ENSMUSG00000085860.3	2410003L11Rik	0.72859177	9.48179E-06
ENSMUSG00000009621.19	Vav2	0.72763829	3.22356E-06
ENSMUSG00000117768.3	8030456M14Rik	0.72736028	5.43448E-12
ENSMUSG00000085836.2	Gm13074	0.72196044	0.004052266
ENSMUSG00000039347.8	Atp6v0e2	0.72168974	0.006492696
ENSMUSG00000068117.11	Mei1	0.71518181	2.01828E-12
ENSMUSG00000025006.19	Sorbs1	0.70974546	0.000116094
ENSMUSG00000113159.2	Gm48771	0.7094715	7.60477E-07
ENSMUSG00000083707.2	Gm13592	0.70823334	9.46969E-06
ENSMUSG00000050097.7	Ces2b	0.70625525	1.36885E-08
ENSMUSG00000120872.1	ENSMUSG00000120872	0.70624019	0.001279524
ENSMUSG00000070056.7	Mfhas1	0.70366295	0.000363424
ENSMUSG00002075812.1	Gm55252	0.70216014	0.001589849
ENSMUSG00000026921.21	Egfl7	0.7019336	0.00347893
ENSMUSG00000108449.3	Gm44507	0.70028923	0.000259478
ENSMUSG00000024913.17	Lrp5	0.69387029	0.000220633
ENSMUSG00000030780.16	Rusf1	0.69330787	0.007793888
ENSMUSG00000032988.5	Slc16a8	0.69145439	1.17839E-12
ENSMUSG00000113615.2	Gm47150	0.69133741	0.000788375
ENSMUSG00000034463.5	Scara3	0.68753025	1.1555E-15
ENSMUSG00000102649.2	Gm38021	0.68275742	0.008519416
ENSMUSG00000037300.20	Ttc13	0.68247798	0.002211836
ENSMUSG00000085589.8	A430078I02Rik	0.68076616	0.00460802
ENSMUSG00000045350.16	Fam186a	0.67792949	4.006E-06
ENSMUSG00000030000.11	Add2	0.67576685	0.00020544
ENSMUSG00000017969.14	Ptgis	0.67332874	5.22075E-08
ENSMUSG00000048772.16	Tmem53	0.67017224	7.27904E-05
ENSMUSG00000044086.9	Lmod3	0.66968943	7.24697E-17

ENSMUSG00000096370.9	Gm21992	0.6693425	0.00022145
ENSMUSG00000021114.10	Atp6v1d	0.66869728	3.34089E-11
ENSMUSG00000039908.15	Slc26a11	0.66774324	1.05507E-05
ENSMUSG00000033420.13	Antxr1	0.66704977	4.62464E-13
ENSMUSG00000036073.19	Galt	0.66687739	3.19162E-07
ENSMUSG00000117263.2	Gm35290	0.66637328	7.82771E-06
ENSMUSG00000026620.12	Mark1	0.66621629	0.009360498
ENSMUSG00000002342.18	Tmem161a	0.6645145	0.000341674
ENSMUSG00000021185.17	Dglucy	0.66183142	2.26351E-11
ENSMUSG00000034345.15	Gtf2h5	0.66146471	0.000849205
ENSMUSG00000051067.9	Lingo3	0.65796251	1.30361E-17
ENSMUSG00000059248.14	Septin9	0.65376652	1.18266E-17
ENSMUSG00000006462.8	A530013C23Rik	0.65295628	6.82823E-09
ENSMUSG00000042817.16	Flt3	0.65183111	2.20275E-07
ENSMUSG00000039813.15	Tbc1d2	0.65158146	1.6784E-08
ENSMUSG00000047824.14	Pygo2	0.64799727	9.62978E-15
ENSMUSG00000076903.2	Traj26	0.64734873	3.99806E-09
ENSMUSG00000021190.15	Lgmn	0.64707235	1.57051E-13
ENSMUSG00000022771.18	Ppil2	0.64336799	1.22597E-12
ENSMUSG00000077202.3	Gm25612	0.64331203	0.005854189
ENSMUSG00000034872.7	Gipc3	0.64262212	4.60229E-20
ENSMUSG00000052446.18	Zfp961	0.64214553	4.72901E-11
ENSMUSG00000106290.2	Gm43429	0.64075005	0.000148864
ENSMUSG00000116120.2	Eif2s3x-ps1	0.63965361	0.002399889
ENSMUSG00000006392.17	Med8	0.63560527	0.000792628
ENSMUSG00000022487.15	Gtsf1	0.63498362	0.000215825
ENSMUSG00000086050.2	Gm16045	0.63314747	7.78889E-20
ENSMUSG00000030433.16	Sbk2	0.63144411	0.000495832
ENSMUSG00000020232.18	Hmg20b	0.63101466	1.5869E-20
ENSMUSG00000112021.2	Gm30346	0.62596079	0.001071334
ENSMUSG00000037731.6	Themis2	0.62582883	7.69864E-05
ENSMUSG00000084766.2	Gm12714	0.62566635	4.86022E-05
ENSMUSG00000112989.2	Gm48143	0.62538301	1.77605E-06
ENSMUSG00000030703.9	Gdpd3	0.62499499	9.29873E-05
ENSMUSG00000034105.10	Meak7	0.62417909	0.001439946
ENSMUSG00000026814.17	Eng	0.62337308	4.91514E-10
ENSMUSG00000030536.11	Iqgap1	0.62090201	6.21688E-24
ENSMUSG00000112991.2	Gm36635	0.62080192	4.90635E-16
ENSMUSG00000078580.4	E430018J23Rik	0.61863358	1.30498E-16
ENSMUSG00000082353.2	Vmn1r-ps1	0.61850106	8.43478E-14
ENSMUSG00000027889.18	Ampd2	0.6180155	1.05954E-06
ENSMUSG00000024735.14	Prpf19	0.61409153	2.73682E-07
ENSMUSG00000020755.10	Sap30bp	0.61280881	1.64047E-10
ENSMUSG00000043336.15	Filip1l	0.61065329	1.04715E-15
ENSMUSG00000095409.2	Gm13043	0.60917138	6.71334E-10
ENSMUSG00000022881.16	Rfc4	0.60885243	0.007516893
ENSMUSG00000002496.11	Tsc2	0.60869316	0.001732221
ENSMUSG00000028479.19	Gne	0.60811052	4.31338E-16

ENSMUSG00000108321.2	Gm44649	0.60773613	0.00326616
ENSMUSG00000042148.9	Cox10	0.60539573	0.000346163
ENSMUSG00000108006.2	Gm44418	0.60463342	0.00045519
ENSMUSG00000027208.15	Fgf7	0.60296897	1.20716E-08
ENSMUSG00000110197.2	Gm45444	0.60281917	2.56237E-07
ENSMUSG00000061048.9	Cdh3	0.59899302	0.005056295
ENSMUSG00000015749.13	Anp32e	0.5980206	3.83664E-08
ENSMUSG00000046314.17	Stxbp6	0.59617739	0.001405122
ENSMUSG00000001870.17	Ltbp1	0.59432892	6.88643E-08
ENSMUSG00000059119.10	Nap1l4	0.5941558	1.92782E-16
ENSMUSG00000097039.10	Pvt1	0.59349492	0.000486264
ENSMUSG00000005267.14	Zfp287	0.5906895	1.65137E-11
ENSMUSG00000112711.2	Gm32552	0.59027072	1.02002E-06
ENSMUSG00000086920.2	Gm12207	0.5901026	0.009299717
ENSMUSG00000085748.2	Gm12280	0.58984723	0.0081825
ENSMUSG00000030877.12	Mfsd13b	0.5893518	0.000344382
ENSMUSG00000035711.6	Dok3	0.58773165	7.36195E-06
ENSMUSG00000022964.15	Tmem50b	0.58410024	4.44808E-06
ENSMUSG00000048794.15	Cfap100	0.58367096	2.65561E-05
ENSMUSG00000003269.19	Cyth2	0.58272684	3.58644E-11
ENSMUSG00000058620.6	Adra2b	0.58229218	6.12973E-09
ENSMUSG00000083064.2	Gm7785	0.5820743	0.004166853
ENSMUSG00000030527.16	Crtc3	0.58192446	4.69501E-10
ENSMUSG00000025237.17	Parp6	0.58186317	8.77409E-08
ENSMUSG00000052087.15	Rgs14	0.58142597	2.22207E-10
ENSMUSG00000018752.20	Tnfsfm13	0.58036641	3.19071E-09
ENSMUSG00000015247.11	Nipsnap3b	-0.58132652	2.12897E-06
ENSMUSG00000020260.10	Pofut2	-0.58168052	1.05968E-10
ENSMUSG00000078249.6	Hmga1b	-0.58170095	2.95329E-08
ENSMUSG00000034108.7	Ccs	-0.58207413	0.003336911
ENSMUSG00000085823.9	Gm13012	-0.58240342	0.003637397
ENSMUSG00000034066.14	Farp2	-0.58358214	2.0028E-12
ENSMUSG00000055866.10	Per2	-0.58560402	2.64119E-07
ENSMUSG00000101464.2	Gm7436	-0.58847814	0.001339873
ENSMUSG00000027315.14	Spint1	-0.58948351	0.002503004
ENSMUSG00000040247.7	Tbc1d10c	-0.59142354	0.000124956
ENSMUSG00000028309.15	Rnf20	-0.59220853	1.93888E-14
ENSMUSG00000025610.8	Map3k7cl	-0.59254494	0.004665095
ENSMUSG00000053684.9	Kics2	-0.59264627	1.31134E-08
ENSMUSG00000110644.2	Gm7390	-0.59395848	3.02233E-09
ENSMUSG00000056153.16	Socs6	-0.59693394	2.32388E-08
ENSMUSG00000046679.17	C87436	-0.60019487	2.33861E-05
ENSMUSG00000039704.9	Lmbrd2	-0.60075069	1.53345E-09
ENSMUSG00000025352.7	Gdf11	-0.60513401	2.34585E-05
ENSMUSG00000035638.15	Muc20	-0.60580272	1.32346E-10
ENSMUSG00000007415.16	Gatad1	-0.60812202	1.89875E-09
ENSMUSG00000086443.2	4933421A08Rik	-0.6095996	1.24037E-05
ENSMUSG00000040473.16	Cfap69	-0.60972297	5.2632E-09

ENSMUSG00000035498.11	Cdcp1	-0.60976021	5.30137E-05
ENSMUSG00000063354.8	Slc39a4	-0.6106083	3.00932E-11
ENSMUSG00000085502.3	Gm12320	-0.61166382	3.35041E-12
ENSMUSG00000001155.14	Ftcd	-0.61667033	1.35373E-05
ENSMUSG00000018500.3	Adora2b	-0.61725256	0.000537787
ENSMUSG00000083618.2	Gm11771	-0.61929961	3.70581E-06
ENSMUSG00000118170.2	Gm30094	-0.61951773	0.000653514
ENSMUSG00000105516.5	Gm36823	-0.62012684	0.000389643
ENSMUSG00000110094.2	Gm45326	-0.62080584	0.000338739
ENSMUSG00000026646.17	Suv39h2	-0.6219481	0.00115597
ENSMUSG00000106214.2	Gm43426	-0.62219858	0.005023157
ENSMUSG00000112630.3	Gm36908	-0.62230183	0.001291903
ENSMUSG00000015405.16	Ace2	-0.6233813	2.35706E-05
ENSMUSG00000094622.4	Gm3055	-0.62413263	0.006837951
ENSMUSG00000060376.8	Bckdha	-0.62453421	0.001615608
ENSMUSG00000029438.10	Bcl7a	-0.62649924	2.21724E-10
ENSMUSG00000022415.13	Syngr1	-0.62735698	0.000653514
ENSMUSG00000036921.3	Tex46	-0.62832825	8.16992E-09
ENSMUSG00000020982.10	Nemf	-0.63100991	1.51571E-05
ENSMUSG00000104406.2	Gm38014	-0.63246122	0.001002236
ENSMUSG00000027778.16	Ift80	-0.63288299	1.05624E-05
ENSMUSG00000000303.13	Cdh1	-0.63574385	6.05502E-05
ENSMUSG00000097529.2	Rp31-ps19	-0.63590844	0.007533036
ENSMUSG00000083054.2	Gm12986	-0.63858376	4.95237E-08
ENSMUSG00000042167.7	Tent2	-0.63907091	0.009907474
ENSMUSG00000022246.15	Rai14	-0.63915527	1.7526E-20
ENSMUSG00000064348.1	mt-Tn	-0.64169398	4.69501E-10
ENSMUSG00000114749.2	Gm48442	-0.64190131	0.000454032
ENSMUSG00000116091.2	Gm49479	-0.64362609	0.007483755
ENSMUSG00000097256.2	Gm26769	-0.64588436	6.17871E-14
ENSMUSG00000059834.13	Sclt1	-0.64615225	0.000929314
ENSMUSG00000071753.14	Cdr1os	-0.64629059	1.63063E-05
ENSMUSG00000027204.14	Fbn1	-0.64650952	0.003097132
ENSMUSG00000097750.3	Gm4673	-0.64976242	6.69887E-06
ENSMUSG00000028223.9	Decr1	-0.65012856	0.00015154
ENSMUSG00000021003.11	Galc	-0.65127783	7.56386E-17
ENSMUSG00000071769.12	Rhox3h	-0.6534129	0.004117983
ENSMUSG00000047466.11	8030462N17Rik	-0.65436009	1.02002E-06
ENSMUSG00000052131.8	Akr1b7	-0.65594903	0.000273743
ENSMUSG00000021111.16	Papola	-0.65805834	1.07407E-07
ENSMUSG00000026478.15	Lamc1	-0.65929115	0.007884393
ENSMUSG00000028557.11	Rnf11	-0.66041653	0.001523622
ENSMUSG00000012017.5	Scarf2	-0.66383385	4.84833E-07
ENSMUSG00000120347.1	ENSMUSG00000120347	-0.66512969	0.000167519
ENSMUSG00000023067.15	Cdkn1a	-0.66537075	0.006881346
ENSMUSG00000028461.13	Ccdc107	-0.66605765	6.20884E-10
ENSMUSG00000117792.2	4930588A03Rik	-0.66621529	0.002399889
ENSMUSG00000033054.8	Npat	-0.66872224	0.000351245

ENSMUSG00000028438.17	Kif24	-0.67225333	1.039E-08
ENSMUSG00000062604.12	Srpk2	-0.6727851	1.33363E-12
ENSMUSG00000081520.2	Gm16200	-0.67331033	0.003908624
ENSMUSG00000007655.17	Cav1	-0.67495757	5.86958E-20
ENSMUSG00000030830.19	Itgal	-0.67705775	4.37611E-05
ENSMUSG00000088575.3	Gm24537	-0.68044583	0.004352594
ENSMUSG00000085920.2	Gm12951	-0.68125837	0.002983968
ENSMUSG00000081733.2	Gm12852	-0.68289367	3.76297E-05
ENSMUSG00000022550.19	Adck5	-0.68366079	1.64631E-05
ENSMUSG00000004936.9	Map2k1	-0.68627049	0.000233689
ENSMUSG00000028292.15	Rars2	-0.68685526	1.02145E-09
ENSMUSG00000040746.16	Rnf167	-0.68850614	4.03173E-05
ENSMUSG00000033386.11	Frrs1	-0.6885063	0.001001971
ENSMUSG00000025512.16	Chid1	-0.68955458	1.30702E-15
ENSMUSG00000025873.17	Faf2	-0.68955625	1.27951E-07
ENSMUSG00000048647.10	Exd1	-0.69006938	1.68696E-05
ENSMUSG00000035595.7	Fam174c	-0.69017887	0.000377939
ENSMUSG00000031430.9	Vsig1	-0.69020901	4.94496E-05
ENSMUSG00000023066.11	Rttn	-0.69083279	0.000918401
ENSMUSG00000024251.11	Thada	-0.69087503	9.62375E-12
ENSMUSG00000020694.18	Tlk2	-0.69102101	8.9759E-06
ENSMUSG00000031812.17	Map1lc3b	-0.69203509	0.003949954
ENSMUSG00000031557.17	Plekha2	-0.69323045	0.000157379
ENSMUSG00000064349.1	mt-Tc	-0.69515605	0.000210181
ENSMUSG00000045193.14	Cirbp	-0.70013177	1.01468E-06
ENSMUSG00000017049.5	Ccdc70	-0.70041225	0.000700416
ENSMUSG00000025450.5	Gm9752	-0.70246762	0.000231604
ENSMUSG00000017291.14	Taok1	-0.70266545	9.10468E-10
ENSMUSG00000047989.12	Ino80c	-0.70404292	7.05508E-05
ENSMUSG00000105973.2	Gm42881	-0.70590307	0.008484331
ENSMUSG00000039382.13	Wdr45	-0.70694011	0.001280244
ENSMUSG00000035297.15	Cops4	-0.70906656	8.58661E-05
ENSMUSG00000059479.8	B3gnt8	-0.71018216	0.00015541
ENSMUSG00000034488.15	Edil3	-0.71070662	0.009843034
ENSMUSG00000024668.9	Sdhaf2	-0.71100192	8.92987E-05
ENSMUSG00000004994.13	Ccdc130	-0.71131394	0.000608323
ENSMUSG00000035860.10	Cdhr3	-0.71219756	0.005545893
ENSMUSG00000054920.13	Klhl5	-0.71272908	0.000608323
ENSMUSG00000111160.2	Gm48855	-0.71316402	1.91333E-10
ENSMUSG00000032224.16	Fam81a	-0.7132421	6.06456E-19
ENSMUSG00000031467.11	Agpat5	-0.71398184	6.83245E-06
ENSMUSG00000086389.2	Gm15998	-0.71553515	2.56775E-05
ENSMUSG00000027737.11	Slc7a11	-0.71598582	2.09361E-05
ENSMUSG00000095677.3	Dynlt1f	-0.71603134	0.008580162
ENSMUSG00000030515.10	Tarsl2	-0.7168175	1.08812E-19
ENSMUSG00000022211.10	Carmil3	-0.71941382	3.49443E-23
ENSMUSG00000005220.11	Corin	-0.72007548	1.25101E-05
ENSMUSG00000031828.10	Klhl36	-0.72078254	5.08393E-05

ENSMUSG00000096992.4	Gm26788	-0.72234454	0.000484411
ENSMUSG00000050732.10	Vamp8	-0.72248057	7.39795E-11
ENSMUSG00000001911.17	Nfix	-0.72422108	1.10994E-06
ENSMUSG00000031196.14	F8	-0.72593634	7.93295E-28
ENSMUSG00000055978.6	Fut2	-0.72598549	0.000828542
ENSMUSG00000107497.2	Gm44957	-0.72640717	0.003277627
ENSMUSG00000103781.2	Gm37523	-0.72938034	9.32866E-12
ENSMUSG00000104031.2	Gm17771	-0.73287432	4.6044E-32
ENSMUSG00000024566.11	Atp9b	-0.738099	3.03331E-06
ENSMUSG00000021809.11	Nudt13	-0.73991259	9.48179E-06
ENSMUSG00000033948.4	Zswim5	-0.74406741	0.008934024
ENSMUSG00000110400.2	Gm45416	-0.74461005	8.19544E-10
ENSMUSG00000042499.14	Hoxd11	-0.74628402	0.00011061
ENSMUSG00000029104.16	Htt	-0.74707429	6.61321E-05
ENSMUSG00000028381.9	Ugcg	-0.74848015	9.93324E-18
ENSMUSG00000004056.16	Akt2	-0.74859784	2.98319E-08
ENSMUSG00000040713.13	Creg1	-0.75506344	0.00052305
ENSMUSG00000031932.15	Gpr83	-0.75530257	1.47502E-09
ENSMUSG00000025405.10	Inhbc	-0.75563164	4.69428E-10
ENSMUSG00000100658.3	F730311O21Rik	-0.75587616	0.001465151
ENSMUSG00000115090.2	Gm49016	-0.75891622	0.000154832
ENSMUSG00000028032.14	Papss1	-0.7589341	3.37288E-09
ENSMUSG00000025130.12	P4hb	-0.75962256	2.13569E-09
ENSMUSG00000024614.8	Tmx3	-0.75985446	3.28065E-06
ENSMUSG00000049176.17	Frmpd4	-0.76678148	1.94159E-07
ENSMUSG00000115009.2	G930009F23Rik	-0.77176911	0.008496669
ENSMUSG00000033762.9	Recql4	-0.77198044	2.53192E-10
ENSMUSG00000058794.13	Nfe2	-0.77386676	0.000862827
ENSMUSG00000002279.20	Lmf1	-0.77393234	4.62559E-20
ENSMUSG00000020080.9	Hkdc1	-0.77778567	2.30631E-08
ENSMUSG00000120809.1	ENSMUSG00000120809	-0.77798913	0.004425173
ENSMUSG00000032425.16	Zfp949	-0.77895646	2.94775E-11
ENSMUSG00000115432.2	D130009I18Rik	-0.7792189	8.63967E-07
ENSMUSG00000073791.14	Efcab7	-0.78023576	0.000218824
ENSMUSG00000108912.2	E230020D15Rik	-0.78394877	8.12334E-14
ENSMUSG00000027217.14	Tspan18	-0.78399394	0.007027755
ENSMUSG00000025221.17	Kcnip2	-0.78409414	2.09463E-06
ENSMUSG00000061286.8	Exosc5	-0.78466835	1.00041E-21
ENSMUSG00000120234.1	ENSMUSG00000120234	-0.78481843	5.02059E-08
ENSMUSG00000031697.13	Orc6	-0.7848994	0.000407647
ENSMUSG00000009907.18	Vps4b	-0.78511617	9.44455E-07
ENSMUSG00000050410.16	Tcf19	-0.78540263	9.14978E-12
ENSMUSG00000025220.9	Oga	-0.78807658	1.26657E-26
ENSMUSG00000028556.16	Dock7	-0.78827039	4.10347E-11
ENSMUSG00000051235.11	Gen1	-0.78959124	4.72196E-15
ENSMUSG00000074916.6	Chst14	-0.78987798	3.98635E-05
ENSMUSG00000018171.10	Vmp1	-0.79444746	6.61412E-09
ENSMUSG00000028453.11	Fancg	-0.79951098	8.6341E-05

ENSMUSG00000024912.7	Fosl1	-0.80062156	0.005980904
ENSMUSG00000025766.15	D3Ertd751e	-0.80171415	0.005479404
ENSMUSG00000113020.2	Gm48063	-0.80389191	5.42848E-12
ENSMUSG00000042801.6	Or6c2b	-0.80570375	2.27064E-11
ENSMUSG00000089745.2	1810008B01Rik	-0.80882456	6.36469E-11
ENSMUSG00000026961.7	Lrrc26	-0.82205979	2.27998E-08
ENSMUSG00000111525.2	Gm47082	-0.82251326	3.35148E-11
ENSMUSG00000097571.11	Jpx	-0.83196597	0.000367007
ENSMUSG00000084965.2	Gm13857	-0.83426057	2.41119E-07
ENSMUSG00000031558.16	Slit2	-0.83881794	0.000467631
ENSMUSG00000116579.2	Gm49701	-0.84369102	0.0035174
ENSMUSG00000064337.1	mt-Rnr1	-0.84694957	1.21824E-05
ENSMUSG00000039270.10	Megf9	-0.84695844	2.31078E-05
ENSMUSG00000056536.15	Pign	-0.84890157	4.7369E-05
ENSMUSG00000092210.2	A930009A15Rik	-0.84913125	0.00046533
ENSMUSG00000051832.8	E230016K23Rik	-0.85177016	0.001001971
ENSMUSG00000040860.17	Crocc	-0.8536208	2.97108E-06
ENSMUSG00000035506.17	Slc12a8	-0.85513715	2.07483E-06
ENSMUSG00000121209.1	ENSMUSG00000121209	-0.85759047	0.002798096
ENSMUSG00000051952.6	Or7c19	-0.85851181	0.000257218
ENSMUSG00000114895.2	4930579J19Rik	-0.86198208	0.000167806
ENSMUSG00000092230.2	Gm18889	-0.87321335	0.001416286
ENSMUSG00000113537.2	Gm48807	-0.87831059	2.02741E-05
ENSMUSG00000073529.10	F830208F22Rik	-0.8844503	1.87615E-06
ENSMUSG00000027301.8	Oxt	-0.886205	4.47611E-05
ENSMUSG00000047284.15	Neurl4	-0.89234082	2.4283E-24
ENSMUSG00002076448.1	Gm55071	-0.89393196	0.000460375
ENSMUSG00000044034.12	Npb	-0.89451832	0.00146378
ENSMUSG00000081819.2	Gm12722	-0.8982716	0.001090141
ENSMUSG00000063971.8	Krt88	-0.89855284	9.2743E-05
ENSMUSG00000029286.13	Enam	-0.90329189	6.49217E-06
ENSMUSG00000035448.10	Ccr3	-0.91263146	5.70071E-07
ENSMUSG00000000058.7	Cav2	-0.91350192	3.25566E-20
ENSMUSG00000008932.11	Slc1a7	-0.91468091	1.0783E-06
ENSMUSG00000028217.12	Cdh17	-0.91611525	1.15294E-34
ENSMUSG00000044544.5	4921513I03Rik	-0.91717981	0.000443617
ENSMUSG00000110245.2	Gm20100	-0.92196048	2.04547E-08
ENSMUSG00000117628.2	Gm50012	-0.92249882	0.000322869
ENSMUSG00000028013.17	Ppa2	-0.92251672	1.80306E-06
ENSMUSG00000028039.12	Efna3	-0.9238661	2.49892E-10
ENSMUSG00000112419.2	Gm9044	-0.92449424	6.9564E-06
ENSMUSG00000097404.3	Gm10814	-0.9293075	2.43521E-16
ENSMUSG00000071324.12	Armc2	-0.93168537	0.001038911
ENSMUSG00000014599.11	Csf1	-0.93639036	4.32429E-25
ENSMUSG00000064369.1	mt-Te	-0.94181868	0.000201358
ENSMUSG00000032410.14	Xrn1	-0.94259014	3.57144E-10
ENSMUSG00000078681.11	Tm2d3	-0.94447658	5.02655E-12
ENSMUSG00000023911.13	Flywch2	-0.94944363	0.000101921

ENSMUSG00000028344.13	Invs	-0.95264446	3.0709E-16
ENSMUSG00000026275.14	Ppp1r7	-0.95300177	6.70544E-16
ENSMUSG00000045165.7	AI467606	-0.95891276	6.90617E-06
ENSMUSG00000071112.13	Spx	-0.96357319	1.02966E-06
ENSMUSG00000079852.5	Klra4	-0.97413471	4.69668E-09
ENSMUSG00000045794.4	Lkaaear1	-0.97420433	1.29356E-06
ENSMUSG00000019899.18	Lama2	-0.97823681	4.98344E-10
ENSMUSG00000116011.2	Gm49501	-0.98250351	0.000345956
ENSMUSG00000086624.2	Gm16130	-0.9903404	0.000295399
ENSMUSG00000039648.15	Kyat1	-0.99470121	1.03012E-06
ENSMUSG00000046434.17	Hnrnpa1	-0.99535663	8.21351E-13
ENSMUSG00000118670.1	Muc19	-0.99664062	2.3236E-11
ENSMUSG00000082315.3	Gm16523	-1.00014199	6.11444E-08
ENSMUSG00000025702.16	Marchf8	-1.00861037	2.00385E-05
ENSMUSG00000086719.2	Gm16275	-1.01753235	1.91559E-13
ENSMUSG00000038668.15	Lpar1	-1.02286007	1.82039E-07
ENSMUSG00000103189.2	Gm37092	-1.02583815	2.37294E-27
ENSMUSG00000120130.1	ENSMUSG00000120130	-1.02998857	5.94639E-17
ENSMUSG00000014444.18	Piezo1	-1.03259567	1.88367E-17
ENSMUSG00000021681.9	Aggf1	-1.03395243	1.65621E-06
ENSMUSG00000022209.13	Dhrs2	-1.03530864	0.000166954
ENSMUSG00000104044.2	Gm37566	-1.05615088	1.7052E-05
ENSMUSG00000085347.3	Hk1os	-1.06480681	1.55314E-05
ENSMUSG00000028229.12	Rmdn1	-1.07394053	1.40966E-06
ENSMUSG00000083736.2	Gm6039	-1.07903917	9.49259E-09
ENSMUSG00000018341.13	Il12rb2	-1.08178627	9.20876E-09
ENSMUSG00000047193.17	Dync2h1	-1.08843861	6.43579E-16
ENSMUSG00000121089.1	ENSMUSG00000121089	-1.09076343	3.03605E-05
ENSMUSG00000027012.16	Dync1i2	-1.11467942	5.95336E-12
ENSMUSG00000022621.17	Rabl2	-1.12141884	8.60223E-14
ENSMUSG00000091475.6	Cerox1	-1.15837519	2.16751E-30
ENSMUSG00000120552.1	ENSMUSG00000120552	-1.16672778	1.90007E-05
ENSMUSG00000059540.16	Tcea2	-1.18634632	3.7218E-12
ENSMUSG00000064339.1	mt-Rnr2	-1.18870258	2.22221E-09
ENSMUSG00000047237.14	Fbxw21	-1.1934251	7.25564E-09
ENSMUSG00000047878.14	A4galt	-1.20254138	4.33301E-09
ENSMUSG00000053929.19	Cyhr1	-1.21324503	3.60709E-13
ENSMUSG00000004371.16	Il11	-1.2208121	2.56335E-09
ENSMUSG00000082841.2	Gm12994	-1.22946647	1.52229E-08
ENSMUSG00000061950.18	Ppp4r1	-1.24479279	8.10523E-25
ENSMUSG00000086844.3	B230206H07Rik	-1.30724802	1.072E-08
ENSMUSG00000030792.9	Dkkl1	-1.32276235	3.9144E-38
ENSMUSG00000022231.11	Sema5a	-1.32915614	1.39531E-37
ENSMUSG00000052565.8	H1f3	-1.33661681	8.36799E-77
ENSMUSG00000049044.17	Rapgef4	-1.33940191	1.50556E-17
ENSMUSG00000096971.4	4930556M19Rik	-1.35868258	4.0531E-07
ENSMUSG00000034220.8	Gpc1	-1.37781943	1.32233E-10
ENSMUSG00000006471.19	Ndor1	-1.42444741	1.14836E-09

ENSMUSG00000097050.2	Gm9918	-1.45234971	2.91462E-11
ENSMUSG00000023232.18	Serinc2	-1.52989398	1.62463E-85
ENSMUSG00000097616.9	1110019D14Rik	-1.58070476	6.35104E-13
ENSMUSG00000108276.3	Gm36640	-1.6197672	5.56847E-21
ENSMUSG00000020888.17	Dvl2	-1.62133069	4.04272E-17
ENSMUSG00000007867.10	Ift43	-1.72639089	4.29612E-15
ENSMUSG00000002297.17	Dbf4	-1.74537657	5.56847E-21
ENSMUSG00000092518.10	Garin5b	-1.75252496	8.98175E-14
ENSMUSG00000045665.6	Mfsd5	-1.82786154	1.97843E-21
ENSMUSG00000024176.11	Sox8	-1.84892891	4.09478E-39
ENSMUSG00000117309.2	Gm49960	-1.88217993	1.37997E-14
ENSMUSG00000006469.14	Slc34a3	-2.10583875	3.78457E-31
ENSMUSG00000040380.15	Cbln3	-2.34317056	6.3564E-52

Appendix II

Diagram and sequence of the ChAdOx1-PepLncP2 vaccine

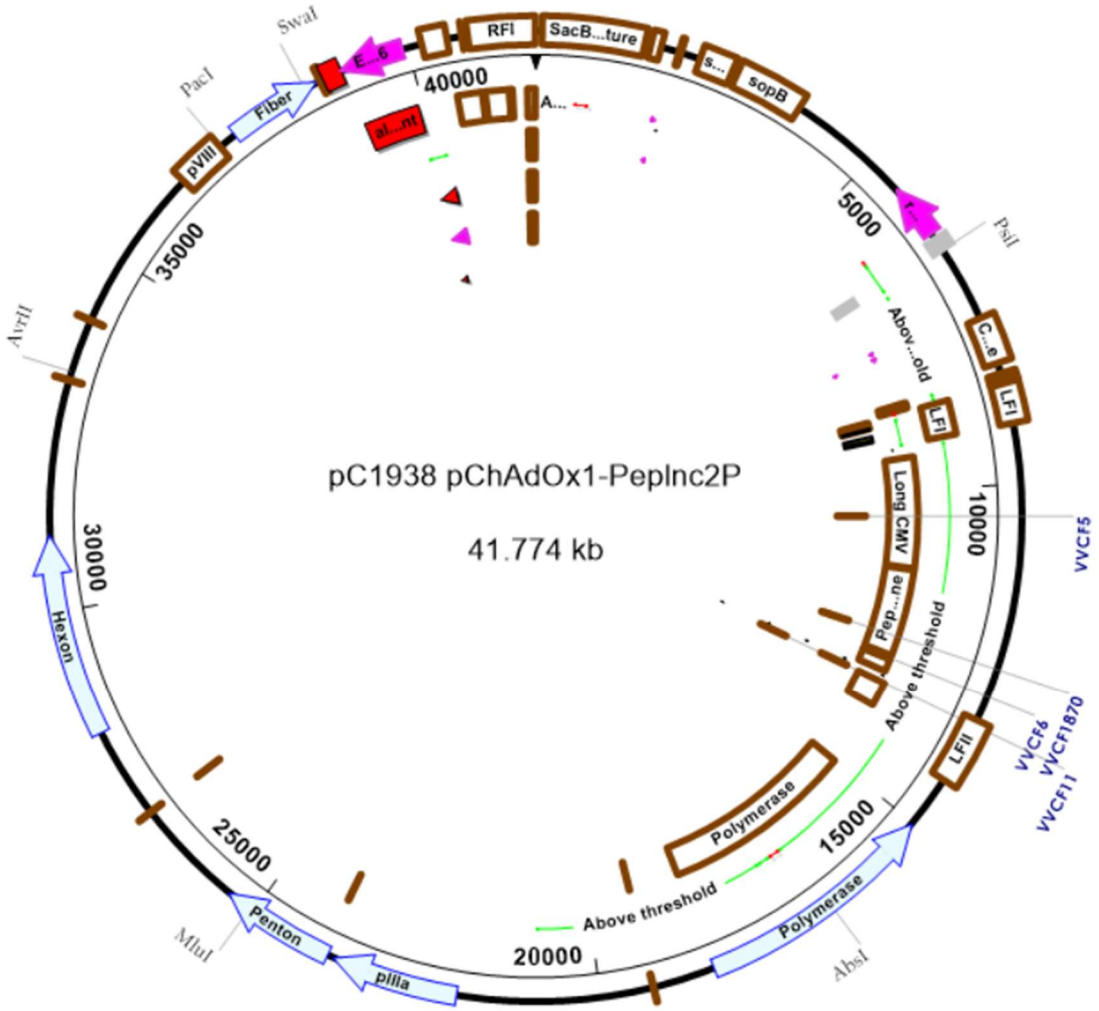

This procedure was performed by the Viral Vector Core Facility (Pandemic Sciences Institute, University of Oxford) using the GeneArt algorithm (Thermo Fisher) for nucleotide sequence optimization.

Detailed PepLncP2 sequence:

Legend:

- Kozak sequence
- TPA sequence
- **START AND STOP CODONS**
- Flanking sequences for PepLncP2 lncRNA-derived peptides
- PepLncP2 lncRNA-DERIVED PEPTIDE SEQUENCE

1. **DNA sequence:**

GCCACC**ATG**GACGCTATGAAGCGCGGACTGTGTTGCGTGCTGCTGCTTTGTGGCGC
CGTGTTTGTGTCTGCCAGCCAAGAGATCCACGCCAGATTCCGGCGGctgcacagaccaT
CTGCTCCTCTGCATCCTACACCTCTGagcagcaccagaaggctgaggcctAGCGCTTTCAGC
CCTGTGGACAACCTGgctcctagaagcgatctgctgcccAGCGCCTTCTCTCCACATTTCCTG
CTGctgcaaggccctgaggaactgcctAGCGCCTATTGCGTGCCACTGTACCTGgaagccagcg
aggaaatcatgagcAGCGGCTTCGGCATGCTGAGCCACCTGgacagaagagagatcgagaacgg
cAGCAGCCCTGAGATCTGGCTGTCCATGctgaagaacctgttctacttcctgACCATCTTCGGC
AACTTTACCATCATCaccatcagccgggtgtcctacaccACACAGTACAAGATCATCCACCAGA
TCgccagccaccagctgctgatgtccAGCACCTTCCAGATGTTCGTGCTGATCctgcctcggcgggt
gtacaacagcACCAGCTTCCACCTGAACTACACCCTGtgctttgtgcacgagctgatcaacGCCA
GCTTCGACATTGGCGCCAGCCTGagcgctagaacacaccctgcctgtATCAGCCTGTTCCTG
CGGCAAGAACTGgtggctcccatccagaacaaggtgTCCAGCGGCGTGCTGTTCAACGCCC
TGacacaggtggccaagtccagcacaGTGTCTCCCGTGGTCAACATCCTGCTGgtgcctgaacag
cctatggccagcTCTGCCCTGGAATTCTGCCAGAAGATGggcgctcccagaacactgacatggTC
CTCCGGCAGCTTCCAGACACCTCTGgccgatcctgacaaccctcctgtgTACAGCCTGAAGC
GGTTCCTGAACATCctgacactgctgggcagagccagaAGCGCCCTGAGCTTTAGTCAGAGC
GTGtgcgtgtcctttccaacaccagccGCTTCTCTGCTGCTCCTGAGCAACCTGagaaggctgga
agaagtggccgccACAGCCGCCTCTCACTCTCATAATCTGcctctcgtgggcttctacgtgtccGC
CATCATCCATCTGCACGTGACCCTGatgcagatcgcctggaagatcgtgGTGTCTCCACTGCA
CCCTATCCTGTTCtggaccagcctgaaagtgggcaccGTGCAGCCTCAGTTTGGAGCCCAACT
GcatctgcccagactgtttctgaagTCCAGCTTCAGCTCCTGGATGCACCTGggaagagagaagct
ggcctctcagATCTCCCTGAAGCTGCTGGCTAGCCTGatcctgtgtagcgtgcccggaacaatgAG
CCCTCTGCTGATTCTGCGGCTGaactgctgcctgtggacctgccacTCTAGCATCTGGCCCTTT
CTGCACCTGgtgtctttctgcctgtttaccgacGTGCAGCTGACCCTGCTGTCCCACTTTctgacc
ttcatc**TGATGA**

2. **Protein sequence:**

MDAMKRGLCCVLLLCGAVFVSASQEIHARFRRLHRPSAPLHPTPLSSTRRLRPSAFSPVD
NLAPRSDLLPSAFSPHFLLLQGPEELPSAYCVPLYLEASEEIMSSGFGMLSHLDRREIENG
SSPEIWLSMLKNLFYFLTIFGNFTIITISRVSYTTQYKIIHQIASHQLLMSSTFQMFVLILPRRV
YNSTSFHLNYTLCFVHELINASFDIGASLSARTHPACISLFLRQELVAPIQNKVSSGVLFNA
LTQVAKSSTVSPVVNILLVPEQPMASSALEFCQKMGAPRTLTWSSGSFQTPLADPDNPPV
YSLKRFLNILTLLGRARSALSFSQSVCVSFPTPAASLLLLSNLRRLEEVAATAASHSHNLPLV
GFYVSAIIHLHVTLMQIAWKIVVSPLHPILFWTSLKVGTVQPQFGAQLHLPRLFLKSSFSS
WMHLGREKLASQISLKLLASLILCSVPGTMSPLLILRLNCCLWTCHSSIWPFLHLVSFCLF
TDVQLTLLSHFLTFI--